Investigation into steady state and stability behavior of natural circulation systems operating with supercritical fluids

by

MANISH SHARMA

A dissertation submitted in partial fulfillment of the requirement for the degree of

Doctor of Philosophy in Engineering

Supervised by

Prof. YUTAKA ASAKO

September 2014

Department of Mechanical Engineering,

Graduate School of Science and Engineering,

TOKYO METROPOLITAN UNIVERSITY

1-1 Minami-Osawa Hachioji-shi 192-0397

Tokyo, JAPAN

This thesis is dedicated to my beloved father

Late Shri Som Raj Sharma

and

My spiritual Guruji

His Holiness Sri Sri Ravi Shankar

Their blessings are always with me

Abstract

Supercritical Water Reactor (SCWR) is one of the next generation (Generation-IV) reactor concept. Supercritical water is being considered as a coolant in SCWRs on account of its potential to offer high thermal efficiency, compact size, elimination of steam generator, separator, dryer and recirculation system making it economically competitive. Several SCWR designs with forced circulation of primary coolant have been proposed in the past, however most of Generation-IV designs are generally not expected to be available for commercial construction before 2030. Supercritical water natural circulation loops are capable of generating density gradients comparable to two-phase natural circulation loops. Hence, natural circulation is also considered as a viable option of heat removal in SCWRs. Safety is a key issue in the design of advanced reactors and considerable emphasis is given on passive safety. Cooling a reactor at full power with natural instead of forced circulation is generally considered as an enhancement of passive safety. Hence, the behavior of steady state natural circulation with supercritical fluids is of interest for a number of new reactor systems. Besides stable steady state, operation with unstable natural circulation is undesirable. Since supercritical water (SCW) experiences steep change in its thermodynamic and transport properties (particularly density) near the pseudo-critical temperature region, supercritical water reactors may be susceptible to

density wave instability. Due to drastic change in SCW properties, the heat transfer behavior is also quite different from sub-critical convective heat transfer.

The experimental studies on natural circulation with supercritical fluids is very limitedly available in open literature and details of stability of supercritical water natural circulation have not been revealed yet. Elucidation of such phenomenon and development of numerical codes are required. Hence, to gain an insight in to the steady state, stability and heat transfer behavior of natural circulation systems operating with supercritical fluids a test facility named Supercritical Pressure Natural Circulation Loop (SPNCL) has been set up at Bhabha Atomic Research Centre (BARC), India. In this research work, steady state and stability experiments were conducted with supercritical carbon dioxide as well as supercritical water in SPNCL. Two independent stability codes, one based on linear analysis (SUCLIN) and other based on non-linear analysis (NOLSTA) were developed and used to simulate the steady state and stability behavior of SPNCL and other test facilities available in literature for both open and closed loop boundary conditions. The studies revealed that instability was observed for a very narrow window of power near the pseudo-critical temperature range of operation. Experimental instability data could only be simulated with the developed codes by including pipe wall thermal capacitance models which is very important for stability analysis of natural circulation at supercritical

conditions (for both open and closed loop boundary conditions).

Journal publications from dissertation:

i) **Manish Sharma**, P.K. Vijayan, D.S. Pilkhwal, D. Saha and R.K. Sinha," Steady state and linear stability analysis of a supercritical water natural circulation loop", Nuclear Engineering and Design 240 (2010) 588–597. (Corresponding to Chapter 2)

ii) **Manish Sharma**, P.K. Vijayan, D.S. Pilkhwal, D. Saha and R.K. Sinha, "Linear and non-linear stability analysis of a supercritical natural circulation loop", ASME Journal of Engineering for Gas Turbines and Power, October 2010, Vol. 132/ 102904-1. (Corresponding to Chapter 3)

iii) **Manish Sharma**, D.S. Pilkhwal, P.K. Vijayan D. Saha and R.K. Sinha," Steady state behaviour of Natural Circulation loops operating with supercritical fluids for open and closed loop boundary conditions", Heat transfer Engineering Journal, 33(9):1-12,2012. (Corresponding to Chapter 4)

iv) **Manish Sharma**, P.K. Vijayan, D.S. Pilkhwal and Yutaka Asako, "Steady state and stability characteristics of Natural Circulation loops operating with carbon dioxide at supercritical pressures for open and closed loop boundary conditions", Nuclear Engineering and Design 265 (2013) 737–754. (Corresponding to Chapter 5)

v) **Manish Sharma**, P.K. Vijayan, D.S. Pilkhwal and Yutaka Asako, " Natural convective flow and heat transfer studies for supercritical water in a rectangular circulation loop", Nuclear Engineering and Design, 273 (2014) 304-320. (Corresponding to Chapter 6)

Acknowledgement

I owe it all to almighty god for granting me wisdom, health and strength to undertake this research task and enabling me to its completion. First, I would like to thank my wife Ritu for her personal support and great patience at all times. This thesis would have not been possible without help, support, guidance and patience of my guide Prof. Yutaka Asako (Professor, Department of Mechanical Engineering, Tokyo Metropolitan University). I am very much thankful to him for picking me up as a student at the crucial stage of my Ph.D. I am also extremely indebted to my home guide Prof. P.K. Vijayan (Director, Reactor Design & Development Group, BARC) for introducing me to the word 'flow instability' first in my life, not to mention his valuable advice and support throughout my Ph.D. programme. I would like to acknowledge financial and academic support provided by Japanese Society for Promotion of Science (JSPS) for this dissertation Ph. D. programme. I would also like to show my gratitude to my immediate superior Shri D.S. Pilkhwal (Head, Energy Engineering Section, BARC) for always encouraging me and bearing with me during my stays in Japan.

I am very grateful to my reviewers Prof. Hiroshi Mizunuma and Prof. Toshio Tagawa for their valuable and thought provoking comments. I would like to thank Shri S.S. Jana for providing his services for maintaining the loop instrumentation and all the operation staff

back home for leaving no stone unturned for carrying out experiments in the supercritical pressure natural circulation loop. I would also like to thank my lab colleagues in Japan for helping me unconditionally whenever needed.

Finally, but by no means least, thanks go to my mother, sister, mother-in-law and friends for their good wishes and also to my son Pratyush for giving me those playful moments during tough times.

Table of contents

List of tables

List of figures

Nomenclature

A	Cross-sectional flow area (m^2)
A_{htr}	Heat transfer area (m^2)
A_w	Cross-sectional area of pipe wall (m^2)
D	Hydraulic diameter (m)
c_p	Specific heat (J/(kg K))
C	Constant
d	diameter (m)
f	Friction factor
g	Acceleration due to gravity (m/s^2)
G	Mass flux ($kg/(m^2 s)$)
h	Heat transfer coefficient ($W/(m^2 K)$)
i	Enthalpy (J/kg)
k	Thermal conductivity (W/(m K))
K	Local loss coefficient
L	Length of a section (m)
L'	Length across bottom heated section, where differential pressure taps are provided (m)
n	Exponent
Nu	Nusselt number (hD/k)
p	Pressure (Pa)
Δp_h	Pressure drop measured by differential pressure taps installed across bottom horizontal heater section (Pa)
Pr	Prandtl No. ($\mu c_p/k$)
Pr'	Modified Prandtl No. $\left(\frac{i_w - i_b}{T_w - T_b}\ \frac{\mu_b}{k_b}\right)$
q'''	Heat given per unit volume of coolant (W/m^3)
q''	Heat flux (W/m^2)
Q	Heater Power (W)

Re	Reynolds number ($\rho uD/\mu$)
r_i	Heater inside radius (m)
r_o	Heater outside radius (m)
s	Stability parameter
t	Time (s)
Δt	Time increment (s)
T	Temperature (^{o}C or K)
u	Velocity (m/s)
U	Overall heat transfer coefficient (W/(m^2 K))
v	Specific Volume (m^3/kg)
w	Mass flow rate (kg/s)
x	Axial distance (m)
z	Elevation (m)

Greek symbols

ρ	Density (kg/m^3)
μ	Dynamic viscosity of fluid (Pa-s)
Φ	Inclination angle of the pipe with respect to vertical direction
τ	Residence time of fluid in differential length Δx $\left(\frac{-A\Delta x}{w_{ss}v_{ss}}\right)$, (s)
∞	Fully developed flow
Δ	differential

Subscripts

amb	ambient
av	average
b	Bulk fluid
c	Cooler
cold	Cold leg

h	Heater
hot	Hot leg
i	Inside
in	Heater inlet
j	Grid point at inlet face of control volume
j+1	Grid point at outlet face of control volume
m	thermally & hydro dynamically developing flow
min	minimum
o	Outside
out	Heater outlet
pc	pseudo-critical
s	secondary
ss	steady state
t	total
w	wall

Superscripts

n	Previous time step
n+1	Current time step

Chapter 1

Introduction

1.1 Background

Nuclear energy is the only non-greenhouse-gas emitting power source known to mankind which is possible to be deployed in large-scale. It has the potential to replace fossil fuels which are depleting day by day to meet the world energy demand and to reduce global warming.

To further enhance economic competitiveness and safety of existing nuclear reactors i.e. Boiling Water Reactors (BWRs), Pressurized water reactors (PWRs), Pressurized Heavy Water Reactors (PHWRs)/ Canadian Deuterium Uranium reactor (CANDU), Voda Voda Energo Reactors (VVERs), RBMK etc., several advanced designs of Nuclear Power Plants (NPPs) are being considered for future deployment. A group of 10 countries established the Generation-IV International Forum (GIF) to examine new design concepts in year 2000. Generation IV reactors (Gen IV) are a set of theoretical nuclear reactor designs currently being researched. Most of these designs are generally not expected to be available for commercial construction before 2030. Current reactors in operation around the world are generally considered second- or third-generation systems, with most of the first-generation systems having been retired some time ago. Evolution of nuclear reactors over various generations is summarized in figure 1-1. Among the large number of potential designs considered by GIF, six prominent concepts were selected by

participating countries to collaborate in relevant R&D work towards the design. The same are as follows –

Three of the design concepts are thermal neutron reactors

(a) Very-high-temperature reactor (VHTR)

(b) Molten-salt reactor (MSR)

(c) Supercritical-water-cooled reactor (SCWR)

Rest three of the design concepts are Fast neutron reactors

(d) Gas-cooled fast reactor (GFR)

(e) Sodium-cooled fast reactor (SFR)

(f) Lead-cooled fast reactor (LFR)

Among the six selected concept, Supercritical Water Reactor (SCWR) is one such concept which operates in the thermodynamic supercritical regime and can enhance the efficiency by as much as 50% compared to the current generation of NPPs. SCWR is the only concept that has directly evolved from the current generation of water-cooled NPPs. The term ‘supercritical fluid’ means any fluid at a temperature and pressure above its critical point (critical point for water indicated on T-S diagram in figure 1-2), where distinct liquid and gas phases don’t exist. Supercritical fluid can effuse through solids like gas and dissolve substances like a liquid. Carbon dioxide and water are most commonly used supercritical fluids in industry.

The critical point for water is-

Critical Temperature: 373.946 ^{o}C, Critical Pressure: 22.064 MPa

The critical point for carbon dioxide is-

Critical Temperature: 31.04 ^{o}C, Critical Pressure: 7.38 MPa

Research on supercritical water cooled reactors began in the late 1950s and continued till the early 1960's in the U.S. With the development and large-scale deployment of Light Water Reactors (LWRs) i.e. Boiling Water Reactors (BWRs) and Pressurized Water Reactors (PWRs), these projects were terminated although it was recognized that the SCWR designs could be economically more competitive. However, the realization in the 1990's that the improvement of economic competitiveness of LWRs over fossil fuelled power plants (FPPs) has reached a state of saturation triggered the development of economically competitive new reactor designs. This has revived the interest in SCWRs since the late 1990's. In general, the total thermal efficiency of a modern fossil fuelled thermal power plant with subcritical steam conditions is about 36–38%; with supercritical parameters about 45-50%. The highest total thermal efficiency achieved in today's thermal power industry is about 56–58% with the combined cycle of gas turbine – steam turbine. To improve the cycle efficiency to 43-48%, SCW NPPs would operate at higher operating parameters (i.e., pressures about 25 MPa and outlet temperatures up to 500°C - 625°C) than the current NPPs. Figure 1-2 compares the operating temperature-pressure conditions of current water-cooled NPPs (i.e. BWRs & PWRs) with SCWR. The major advantages of SCWRs are –

- High thermal efficiency of the order of 43 – 48 % as compared to 30 - 34% for LWR's/ Pressurized Heavy Water Reactors (PHWR's).

- Compact and simplified design. The supercritical steam can be directly sent to the turbine eliminating steam generator, separators, dryers and recirculation pumps.
- For same amount of thermal power the mass flow rate requirement is $1/4^{th}$ that of BWR's due to zero recirculation flow, reducing the number, capacity and size of required Primary Heat Transport (PHT) pumps.
- Elimination of Critical Heat Flux (CHF) phenomenon. CHF is a phenomenon where a heater/ fuel clad surface gets covered with a layer of vapors resulting in sudden and drastic deterioration of heat transfer resulting in excursion of heater wall temperature even beyond the melting point temperature of the heating element. Although, deterioration of heat transfer has been reported in literature for higher heat fluxes and lower mass fluxes of supercritical fluids, but it is very mild and gradual.
- Smaller containment due to lesser inventory as compared to BWRs.
- The balance of plant equipments are available from already operating Supercritical Fossil-fueled power plants and only inside core materials for SCWRs need to be developed.

1.2 Classification of SCWRs

Several new designs of SCWRs have already been proposed. SCWRs can be categorized according to the following bases: (a) neutron energy, (b) steam cycle, (c) construction type, (d) the circulation mode and (e) the coolant used.

1.2.1 Classification based on neutron energy

Based on neutron energy, nuclear reactors are generally classified as thermal and fast reactors. Both thermal neutron reactors as well as fast reactors have been proposed with supercritical water (SCW) as the coolant. However, most SCWRs studied are thermal neutron reactors and the design parameters of various thermal neutron SCWRs i.e. High Performance Light Water Reactor (HPLWR), B-500SKDI, United States Supercritical Water Reactor (US SCWR), Japanese Supercritical Water Reactor (JSCWR), Canadian SCWR etc. are compared in Table 1-1.

Table 1-1: A Comparison of thermal neutron SCWR design parameters

Parameters	Unit	Canadian SCWR CANDUal-X2[1]	Canadian SCWR CANDU-X NC[2]	B-500SKDI[3]	HPLWR[4]	JSCWR[5]	US SCWR[6]
Country	**–**	Canada	Canada	Russia	EU	Japan	US
Reactor type	**–**	PT	PT	Integral	RPV	RPV	RPV
spectrum	**–**	Thermal	Thermal	Thermal	Thermal	Thermal	Thermal
Power thermal	**MW**	2540	930	1350	2300	4039	3575
linear max/ave	**kW/m**			-	35/14, 8, 4.5	-/13.5	39/19.2
Thermal eff.	**%**	48	40	38.1	43.5	42.7	45
Pressure	**MPa**	25	25	23.6	25	25	25
T_{in} coolant	**ºC**	350	350	365	280	290	280
T_{out} coolant	**ºC**	625	430	381.1	500	510	500
Flow rate	kg/s	1320	820	2470	1179	2105	1843
Active core height	**m**	5.0	-	-	4.2	4.2	4.27
Equiv. core diameter	**m**	~5.5	-	-	3.8	3.34	3.93
Fuel	**–**	Pu-Th	-	UO_2	UO_2	UO_2	UO_2
Cladding material	**–**	SS	-	SS/ Zr alloy	316SS	310SS	SS
D_{rod}	**mm**	12.4	-	9.1	8	7	10.2
Pitch	**mm**	vary	-	-	9.44		11.2
T_{max} cladding	**ºC**	850	-	425	620	700	
Moderator	**–**	D_2O	-	-	H_2O	H_2O	H_2O

[1,2] Bushby et al. (2000); [3] Silin et al. (1993); [4] Heusener (2000); [5] Ishiwatari et al.(2009); [6] Zhao et al. (2005)

The Supercritical Fast Reactor (SCFR) system has been studied by the Babcock and Wilcox Company in the 1960's. It may be noted that breeding is possible with SCW cooling in a tight-lattice core (Oka et al. (1994)). An example is the 1100 MWe SCFR-D studied by Oka et al. (1994) and Kitoh et al. (2000). They also showed that the efficiency of the SCFR with a core outlet temperature of 431 ^{o}C at 25 MPa matches that of a FPP operating at 24.2 MPa and 566 ^{o}C basically due to the low boiler efficiency in FPPs. Besides improving the thermal efficiency, the design also results in significant reduction in the size of the reactor pressure vessel and containment vessel compared to a BWR. Table 1-2 compares the design parameters of various supercritical fast reactors.

Table 1-2: A Comparison of supercritical fast neutron reactors design parameters

Parameter	Unit	SCFR[1]	B&W[2]	SCFR-D[3,1]	SCFR-H[4,1]
Country	**-**	Japan	Japan	Japan	Japan
Power	**MWe**	1245	980	1508	1728
Th. Power	**MWth**	3000	2326	3640	3893
Power density	**MW/m^3**		447	199	144
Efficiency	**%**	41.5	42.2	41.5	44.4
T_{CI}	**^{o}C**	310	-	310	280
T_{CO}	**^{o}C**	431	538	431	526
Core flow	**kg/s**	2048	3214	2485	1694
Pressure	**MPa**	25.0	25.3	25.0	25.0
Fuel material	**MOX**	MOX	MOX	MOX	MOX
Fuel rod o.d.	**mm**	8.8	5.84	8.8	8.8
Linear Power	**kW/m**	40	54.8	41	38.5
Fuel clad material	**SS**	SS	19-9DL SS	SS	Ni-alloy/Inconel
Burnup	**MWd/kg**	77.7	48	77	45
Clad surface temperature	**-**	-	-	448	-
Breeding ratio	-	-	1.11	-	-

[1] Kitoh, Koshizuka and Oka (2001); [2] Oka (2000); [3] Oka et al. (1994); [4] Oka and Koshizuka (2000)

1.2.2 Classification based on steam cycle

Based on the steam cycle employed, the SCWRs can be categorized into direct cycle and indirect cycle types. Besides these two, dual cycle SCWRs have also been studied.

Direct cycle SCWRs: These are also known as Once-Through SCWRs. Since the supercritical steam can be directly sent to the turbine therefore the steam generator, steam separator, dryer and recirculation system of a direct cycle BWR are not required (Figure 1-3a). Hence the direct cycle SCWR is economically more competitive than the indirect cycle concept. This is also the most popular SCWR concept. To our knowledge, the water moderated and supercritical steam cooled SCWR proposed by the Westinghouse Corporation in the late 1950's is the earliest concept in this category. Typical examples of direct cycle SCWRs are the high performance light water reactor (HPLWR) (being pursued by the European Union), Japanese Supercritical Water Reactor (JSCWR), United States Supercritical Water Reactor (US-SCWR). The reactor pressure vessel and control rods of a direct cycle SCWR resembles that of a PWR while the containment and emergency core cooling systems are similar to a BWR with the balance of plant similar to that of a Fossil fueled Power Plant (FPP).

Indirect cycle SCWRs: The indirect cycle SCWR has a primary system with steam generators and a secondary coolant that passes through the turbine (Figure 1-3b). The primary system is similar to that in a PWR and the secondary and the balance of plant is similar to the FPP. Typical example is natural circulation based CANada Deuterium Uranium pressure tube type reactor called CANDU-X NC.

Dual cycle SCWRs: Dual cycle SCWRs generate part of their power in the direct cycle mode and the rest in the indirect cycle mode. In this concept, the supercritical fluid from the core first goes through a Very High Pressure (VHP) turbine and the exhaust from the

turbine is the heat source for an indirect cycle plant similar to the conventional PWRs or PHWRs (Figure 1-3c). Typical example is CANDUal-X2.

1.2.3 Classification based on the construction type

Based on the construction type, SCWRs can be classified as

a) Integral type
b) Pressure vessel type (RPV) and
c) Pressure tube type (PT)

Integral type: In this type, the entire primary system is encased in a vessel. A typical example is the 500 MWe light water integral reactor B-500SKDI design (Figure 1-4a) with natural circulation of the coolant proposed by Silin et al. (1993).

Pressure vessel type: Here the entire core is encased in a pressure vessel with the inlet and outlet piping connecting it with the rest of the system (Figure 1-4b). Reactor pressure vessel design is similar to that of a PWR with the subcritical water entering it and supercritical water leaving the vessel. Typical examples are HPLWR, JSCWR, US-SCWR and the SCFR-D.

Pressure tube type SCWRs: In this design, the core is made up of pressure tubes similar to a FPP (Figure 1-4c). The SC-CANDU designs being pursued by AECL conform to this type i.e. CANDUal-X2, CANDU-X NC.

1.2.4: Classification based on the circulation mode

Based on the coolant circulation mode, SCWRs can be classified as natural and forced circulation reactors.

Natural circulation SCWRs: The density change in SCWRs is comparable to that in BWRs. Further, the thermal expansion coefficient of SCW is significantly large in the near critical region, natural circulation SCWRs operate best in this region. Typical examples of NC concepts are the CANDU-X NC and the Russian BF-500SKDI.

Forced circulation SCWRs: In this concept, pumps are used to circulate the primary coolant. Typical examples of forced circulation SCWRs are HPLWR, JSCWR, US-SCWR.

To our knowledge, the only other fluid proposed to be used in Supercritical fluid reactor is carbon dioxide, Tom and Hauptmann, 1979 and Driscoll and Hejzlar, 2004. The main advantage of using supercritical CO_2 is that the design pressure is significantly low. By locating the pumps in the single-phase subcritical region, significant saving in pumping cost is obtained compared to gas cooled reactors employing CO_2.

1.3 Thermal hydraulic design challenges

Having reviewed the various proposed design concepts let us see some technological challenges in SCWR design. There are many challenges in design of SCWRs like materials to be used inside the core i.e. material of fuel clad and materials for pressure tubes & insulating liners (in pressure tube type of designs). The pressure tube type of

design can be considered to be of direct relevance to Indian nuclear programme in view of the mastery achieved over this technology in several decades. However, here we will only restrict to thermal hydraulic challenges in design of SCWRs as given below.

1.3.1 Flow stability

Due to supercritical operating conditions in SCWR, thermodynamic and transport properties of water change significantly as its temperature approaches the pseudo-critical temperature, where distinction between liquid and vapor phases disappear. The heat capacity increase dramatically, however thermal conductivity, density, and viscosity reduce significantly near the pseudo-critical temperature at constant pressure as shown in figure 1-5a & 1-5b. Pseudo-critical temperature is the temperature corresponding to maximum specific heat of the supercritical fluid at a given pressure as shown in figure 1-5a. However, the specific heat again reduces beyond pseudo-critical temperature.

Some of these changes are similar in magnitude to those encountered during boiling with phase change. It may be noted that there is no phase transition i.e. two phases don't co-exist as fluid temperature crosses the pseudo-critical point. It means the 'liquid' like fluid gradually changes over a range of temperature near pseudo-critical temperature in to a 'gas' like fluid.

Single phase sub-critical natural circulation (where Boussinesq approximation is used for calculating buoyancy force term in momentum equation) had been the subject of several previous investigations. For example, Keller (1966) theoretically studied a rectangular natural circulation loop with point heat source and sink located at the center of the bottom

and top horizontal sections respectively. He predicted unidirectional periodic flow. Welander (1967) proposed a mechanism for the instability based on the growth of small amplitude oscillations. Chen (1985) showed that the aspect ratio (height/ width) plays an important role on the stability of a rectangular loop. In Chen's work, the loop considered had the entire bottom horizontal pipe heated and the entire top horizontal pipe cooled. His predictions showed that the loop became unstable as the aspect ratio approached unity. Theoretical predictions using the linear analysis by Vijayan et al. (1992) showed that the unstable region shifted to higher Grashof numbers by increasing the length-to-diameter ratio (Lt/D) of rectangular loops. These predictions were made for a rectangular loop with heater and cooler centrally located at the bottom and top horizontal sections respectively. Experiments by Creveling et al. (1975) showed for the first time the occurrence of the instability for single phase subcritical ordinary fluids albeit in a toroidal loop. The mechanism for the instability was observed to be that proposed by Welander. Subsequent experimental work by Gorman et al. (1986) in the toroidal loop of Creveling observed three different chaotic flow regimes: a globally chaotic regime whose essential features can be described by a one-dimensional cusp-shaped map, a subcritical regime in which the flow can be either chaotic or steady, and a transient regime in which the flow remains chaotic for a time and then decays into a steady flow. The earliest experimental work in a rectangular loop with vertical heater and cooler by Holman and Boggs (1960) did not study the instability. Subsequent studies in rectangular loops by Huang–Zelaya (1988), Misale et al. (1991), Bernier– Baliga (1992) and Ho et al. (1997) also concentrated on the steady state behavior. Vijayan et al. (1992) observed instability for the first time in a rectangular loop while experimenting with uniform diameter loops. The observed

instability behavior involved repetitive flow reversals and the nature of the oscillatory behavior could be numerically simulated Vijayan et al. (1995) with a fine nodalization. With a low diffusion scheme Ambrosini and Ferreri (2003) could predict the instability with a much coarser nodalization. Vijayan et al. (1992) also observed a conditionally stable (hysteresis) regime in which the flow can be steady or oscillatory depending on the heat addition path followed in the experiment. However, instability studies on subcritical single phase flow is of little importance in a reactor scenario, because no instability is observed during single phase forced circulation of coolant at reactor full power operation or even during reactor shutdown when most water cooled reactors use single phase natural circulation for decay heat removal. This is due to larger frictional resistance owing to longer lengths of the reactor pipes.

However similar to BWR's, SCWR core will experience large density changes across the core i.e. 770 kg/m^3 to 90 kg/m^3 and therefore may be susceptible to flow instabilities similar those observed in BWRs (Boure et al., 1973 & Van Bragt & Van Der Hagen, 1998) such as density wave instability and coupled neutronic-thermal hydraulic instability. State of art reviews on thermal-hydraulic instabilities that may occur in boiling two phase flow systems are provided in Bergles, 1976, Ishii 1976, Fukuda & Kobori, 1979 and Yadigaroglu, 1978. The reviews suggest following types of instabilities possible in boiling two phase systems-

i) Instability arising from steady state characteristics of the system-

a) Flow excursion or Ledinegg type instability

b) Flow pattern transition, Geysering, flashing etc.

ii) Instability arising from dynamic nature of the system-

a) Density wave instability

b) Acoustic instability

c) Thermal oscillations

However, the most commonly encountered instability in BWR is coupled neutronic density wave instability which is also expected in SCWRs. Some authors have also predicted ledinegg type of instability in SCWRs but the same is obtained at very low core inlet temperatures which are very much lower and far from operating conditions envisaged in SCWR channel (Ambrosini (2007); Chatoorgoon (2013).

As discussed earlier, supercritical water natural circulation loops are capable of generating density gradients comparable to two-phase natural circulation loops. Hence, natural circulation is also considered as a viable option of heat removal in supercritical water cooled reactors (Silin et al., 1993; Bushby et al., 2000). Safety is a key issue in the design of advanced reactors and considerable emphasis is given on passive safety. Cooling a reactor at full power with natural instead of forced circulation is generally considered as enhancement of passive safety. Natural circulation can also be used for passive decay heat removal after reactor shutdown. Hence, the behaviour of steady state natural circulation with supercritical fluids is of interest for a number of new reactor systems. Besides stable steady state, operation with unstable flow is undesirable as it can lead to power oscillations in natural circulation or forced circulation based SCWRs. However, natural circulation mode of cooling is more prone to instability as the energy equation and driving force term in momentum equation are strongly coupled. Moreover,

it can also cause mechanical vibration of components and failure of control systems. Since supercritical water or any other supercritical fluid experiences drastic change in its thermo-physical properties (e.g. density) in the pseudo-critical region, supercritical water reactors may be susceptible to density wave instability. Frequency domain linear stability analysis of supercritical water cooled reactors has been done by Yi et al. (2004) and Tian et al. (2012). Hou et al. (2011) did a linear and non-linear analysis of parallel channel within the Supercritical Water Reactor (SCWR) core and compared the results.

The literature reveals only very few experimental studies on natural circulation with supercritical fluids. Harden and Boggs et al. (1964) conducted studies on Freon loop near critical region. High and low frequency oscillations were observed when bulk fluid temperature approached pseudo-critical temperature. Adelt and Mikielewicz (1981) performed studies on 4m high loop with carbon dioxide (CO_2). As the fluid was heated through pseudo-critical point, pressure oscillations were observed for a particular test but the study mainly focused upon heat transfer rather than stability. Lomperski et al. (2004) have reported experiments in a two meter high natural circulation loop with carbon dioxide at supercritical pressure. The loop was operated in a base case configuration that maximized flow rates and in a second configuration having an orifice in the hot leg. No flow instabilities were observed in these tests as the fluid was heated through thermodynamic pseudo-critical point. Yoshikawa et al. (2005) have studied the performance of a closed natural circulation loop operating with supercritical CO_2. The performance of the loop was determined by measuring flow velocities of CO_2 which could be correlated to Grashof number, Prandtl number and dimensionless effective density difference. No flow instability has been reported during the experiments. In a

very recent study, T'Joen and Rhode (2012) conducted stability experiments with artificial neutronic feedback in scaled natural circulation driven HPLWR (High Performance Light Water Reactor) facility named Delight maintaining the inlet temperature constant (i.e. with open loop boundary conditions). They used Freon R23 at 5.7 MPa as the scaling fluid. The decay ratios and frequencies of the riser inlet temperature oscillations were measured. They found that for a single inlet temperature the system undergoes two transitions as the power is increased. At low power the system is stable and becomes unstable as the power is increased, but on further increasing the power the system stabilizes. They also found a threshold inlet temperature above which no instability is observed. Xiong et al. (2012) have carried out experiments on flow instability in two parallel channels with supercritical water. They did a parametric study which shows that flow becomes more stable by increasing the pressure or decreasing the inlet temperature in the range of experiments conducted.

Various researchers have investigated theoretically the stability in supercritical fluid natural circulation loops and heated channels. Zuber (1966) did an extensive review and the first in-depth analytical study of the various instability modes of supercritical fluid flow. He considered flow in a straight pipe in a once through system and concluded that supercritical flow instability would be similar to two-phase flow instability, possessing both the excursive and oscillatory types. Literature reveals linear approach which is mostly done in frequency domain and non-linear approach which is carried out in time domain for studying of stability of natural circulation systems/ heated channels operating with supercritical fluids. Chatoorgoon (2001) considered a constant area rectangular natural circulation open loop with horizontal heater & horizontal cooler and did the

steady state and non-linear stability predictions with supercritical water as the working fluid. The threshold of instability has been judged to be the peak of steady-state mass flow rate versus power curve. Jain and Corradini (2006) did the linear stability analysis of supercritical water natural circulation loop. Their results suggest that the instability behaviour of supercritical natural circulation loop is not strictly related to the peak of the steady-state flow rate versus power curve. Ambrosini and Sharabi (2008) has developed non-dimensional stability parameters for supercritical fluids which are independent of system pressure and operating fluid and are similar to that used for stability analysis of two phase systems. They also generated stability maps for heated channel in term of non-dimensional parameters using linear analysis as well as nonlinear system code RELAP5/MOD3.3 (Scientech, 1999) which were found to be in good agreement. Ortega Gomez et al. (2008) studied a uniformly heated channel with supercritical water using linear as well as non-linear codes. They also developed a set of non-dimensional stability parameters similar to those of two phase systems but are not exactly same as those of Ambrosini's. A few investigations were also conducted with supercritical CO_2 (which can be considered as good simulant fluid for water) using one dimensional non-linear stability codes (Chatoorgoon et al., 2005, Jain and Rizwan-uddin, 2008). Chen et al. (2010) numerically studied the effect of heat transfer on stability and transitions of supercritical CO_2 in a rectangular natural circulation loop using a two-dimensional model. They identified a second "pseudo-critical temperature", around 375 K for supercritical CO_2. Fluid-to-fluid modelling aspects have also been studied by Marcel et al. (2009) and found that a 77.5%/22.5% mixture of refrigerants R-32 & R-125 simulates the supercritical water (SCW) conditions in HPLWR. They also found that supercritical CO_2

cannot accurately simulate the HPLWR conditions with water. Sharabi et al. (2008) have used 3D-CFD code with different turbulence models for predicting unstable behaviour of heated channel with water at supercritical pressure which was also previously addressed by Ambrosini & Sharabi (2006) using both linear and non-linear codes. They found that details in the transient radial velocity distribution provided by CFD code does not significantly alter the prediction of the threshold of instability as compared to one-dimensional codes, thereby asserting the adequacy of one dimensional codes in predicting instability threshold at supercritical operating conditions.

1.3.2 Heat transfer

Moreover heat transfer characteristics of supercritical fluids under natural circulation conditions is also important. Since supercritical water (SCW) or any other supercritical fluid experiences drastic change in its thermodynamic and transport properties near the pseudo-critical temperature, the heat transfer behaviour is quite different from sub-critical convective heat transfer. Dramatic reduction in density near the pseudo-critical temperature results in strong buoyancy and acceleration effects across the flow cross-section causing unusual flow and heat transfer behaviour. Hence normal heat transfer correlations developed for turbulent flow of conventional fluids with small or moderate property variations like Dittus-Boelter (1930) correlation may not be applicable at supercritical conditions.

Several researchers in the past have carried out experimental investigation on forced convective heat transfer for SCW (Yamagata et al., 1972; Swenson et al., 1965) as well as supercritical carbon dioxide (Jackson et al., 2003; Fewster and Jackson, 2004).

Exhaustive literature search carried out for supercritical water and supercritical carbon dioxide (Pioro and Duffey, 2005; Duffey and Pioro, 2005) confirmed three heat transfer modes in supercritical pressure fluids: (1) so-called normal heat transfer, (2) improved heat transfer, characterized by higher-than-expected heat transfer coefficient (HTC) values than in the normal heat transfer regime and (3) deteriorated heat transfer, characterized by lower-than-expected HTC values than in the normal heat transfer regime. The expected HTC in the normal heat transfer regime is that calculated by Dittus-Boelter (1930) correlation. Improved heat transfer is observed at low heat fluxes & higher mass fluxes and deteriorated heat transfer is observed at higher heat fluxes & lower mass fluxes. In literature, there is still no unique definition for the onset of heat transfer deterioration. However, reduction in heat transfer coefficient is mild and gradual as compared to sudden and drastic increase in wall temperature (or sharp reduction in heat transfer coefficient) associated with boiling crisis at sub-critical pressure conditions. The difference of heating and cooling heat transfer coefficient has been studied theoretically by Dang and Hihara (2010) for laminar flow of supercritical carbon dioxide in miniature tubes.

1.4. Objectives of the study

The experimental studies on natural circulation with supercritical fluids are very limitedly available in open literature and details of stability of supercritical water natural circulation loop have not been revealed yet. Elucidation of such phenomenon and development of numerical codes are required. Hence, a test facility called Supercritical Pressure Natural Circulation Loop (SPNCL) has been set up at Bhabha Atomic Research Centre (BARC), India with the following objectives-

i) To gain an insight in to steady state and stability behavior of natural circulation systems operating with supercritical fluids.

ii) To develop in-house computer codes for investigating steady state and stability behavior of natural circulation systems operating with supercritical fluids.

iii) To validate in-house developed computer codes with the experimental data generated in SPNCL and that available from open literature.

iv) To generate experimental heat transfer data for natural circulation with supercritical fluids and comparing it with various heat transfer correlations available in literature (correlations are mostly available for forced circulation conditions).

1.5. Organization of the thesis

The thesis has been divided in to seven chapters–

Chapter 1 describes the advantages of Supercritical Water Reactors (SCWRs), their classifications and various thermal hydraulic challenges in the design of SCWRs. Considering the challenges, the objectives of the current research work have been defined.

Chapter 2 describes the formulations of the linear stability code (SUCLIN) developed for steady state and stability analysis of an open supercritical water natural circulation loop in frequency domain. The code has been qualitatively assessed against published results and has been extensively used for carrying out a detailed parametric study on steady state and stability behaviour of an open SPNCL. The peak of the steady state mass flow rate versus power curve for uniform diameter SPNCL is obtained at heater outlet temperature near the pseudo-critical value. The larger diameter loops are found to be more unstable in

terms of heater power compared to small diameter loops for supercritical water natural circulation. Beyond a specified value of heater inlet temperature no instability is observed and its value decreases with increase in loop diameter. These observations suggest that natural circulation systems operating with supercritical water can be designed for lower heater inlet temperatures and still not encounter instability whatever may be the power. Such systems can also take advantage of the large jump in enthalpy occurring across the pseudo-critical point.

Chapter 3 describes the formulations of the non-linear stability code (NOLSTA) developed for steady state and stability analysis of an open supercritical water natural circulation loop in time domain. The stability results generated by NOLSTA code has been compared with stability results obtained using linear code (SUCLIN) for open SPNCL and two codes are found to agree qualitatively. BARC also participated in the blind benchmark exercise coordinated by the University of Pisa in the frame of the IAEA Coordinated Research Programme (CRP) on Heat Transfer Behaviour and Thermo-hydraulics Codes Testing for SCWR. All the codes used by other participants including NOLSTA and SUCLIN qualitatively confirmed the following findings: Increase in outlet throttling results in increase in unstable zone of heated channels. Both oscillatory as well as excursive instabilities are possible in supercritical flows, the latter occurring at relatively low inlet temperature, in regions that would be hopefully of little interest to nuclear reactor operation. The general shape of the stability boundary in the N_{TPC} (Trans-Pseudo-Critical number) - N_{SPC} (Sub- Pseudo-Critical number) plane is same as predicted by all the codes.

Chapter 4 describes steady state natural circulation experiments conducted with carbon dioxide in Supercritical Pressure Natural Circulation Loop (SPNCL). NOLSTA code predicts the steady state natural circulation mass flow rates of closed SPNCL appreciably well (± 15%). For closed loop, the steady state flow behaviour of loop is found to be very sensitive to the empirical heat transfer correlation used for cooler primary side. The correlations evaluating thermal conductivity at wall temperatures/ pseudo-critical temperature for bulk fluid temperature exceeding the pseudo-critical temperature give a smoother reduction in flow as heater inlet temperature crosses the pseudo-critical temperature similar to that observed in the experiments.

Chapter 5 describes instability experiments conducted in SPNCL with carbon dioxide as working fluid. During experimentation with carbon dioxide, instability has been observed for a very narrow window of power near the pseudo-critical temperature for Horizontal Heater Horizontal Cooler (HHHC) orientation only and that too at lower secondary side chilled water flow rate i.e. 10-15 lpm. The predictions of NOLSTA code were only qualitatively matching with experimental instability data. However, consideration of pipe wall thermal capacitance predicts SPNCL to be completely stable, but reducing the thermal capacitance by 18% and neglecting the local losses the code is able to simulate limit cycle oscillations without flow reversal as observed during experiments. Modelling of thermal capacitance of pipe walls is strongly recommended for stability analysis of natural circulation at supercritical conditions (both open and closed loop boundary conditions) unlike two phase natural circulation loops.

Chapter 6 covers the steady state flow experiments conducted with supercritical water in SPNCL and same were compared with NOLSTA code predictions which are found to be in good agreement. During experimentation with water, instability was again observed for a very narrow window of power for HHHC orientation for operating pressure range of 22.1 to 22.9 MPa. However at, higher pressures no instability is observed. The reason for the same is higher thermal capacitance of fluid near pseudo-critical temperature at low pressures which cause enthalpy perturbations to generate very small fluid temperature perturbations only and hence fluid interaction with pipe wall or damping effect of wall becomes almost negligible. NOLSTA code along with pipe wall thermal capacitance model simulates the experimental instability data appreciably well. Scaling fluid for instability studies of supercritical fluids should take care of the ratio of thermal capacitance of the fluid and the wall near pseudo-critical temperature.

Chapter 7 summarizes the major findings and conclusions of the research work.

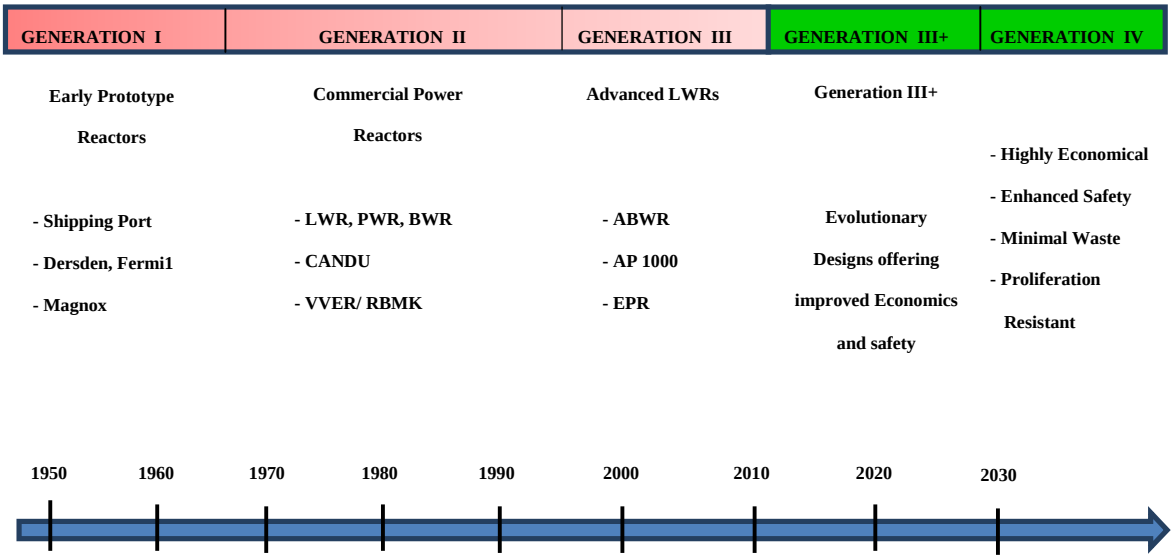

ABWR – Advanced Boiling Water Reactor, AP 1000 – Advanced Passive Pressurized Water Reactor,

EPR – European Pressurized Water Reactor

Figure 1-1: Evolution chart of nuclear reactors over various generations

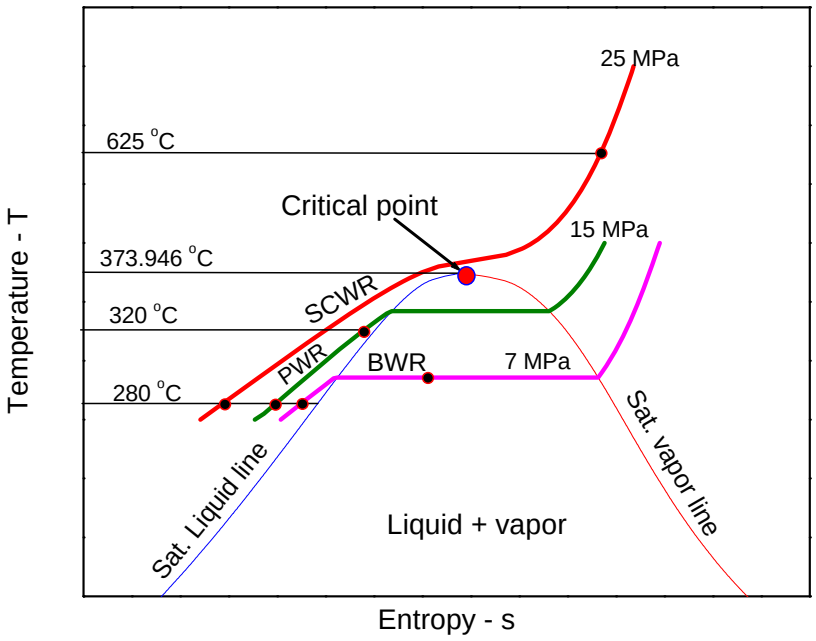

Figure 1-2: Comparison of the operating temperature-pressure conditions of currently operating BWRs / PWRs with SCWR

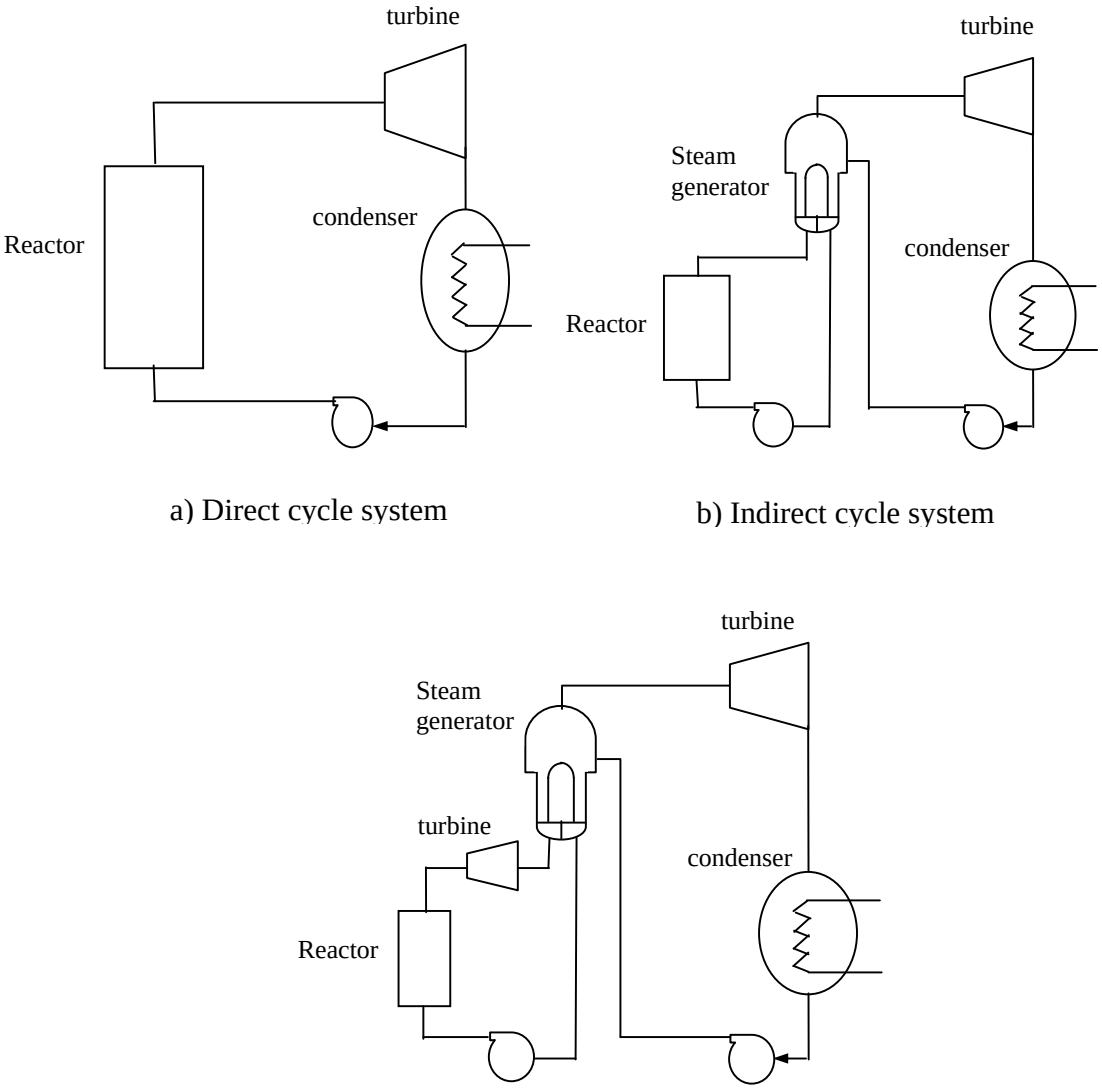

a) Direct cycle system

b) Indirect cycle system

c) Dual cycle system

Figure1-3: Categorization of SCWRs based on the steam cycle employed

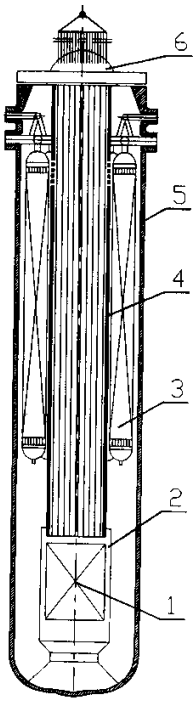

1 – reactor core
2 – core barrel
3 – steam generators
4 – guard tube block shroud
5 – reactor pressure vessel
6 – reactor closure head

Figure 1-4a: The BF500 SKDI integral reactor

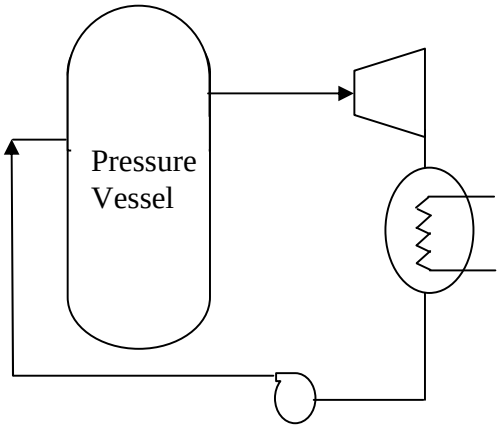

Figure 1-4b: Pressure vessel type SCWR

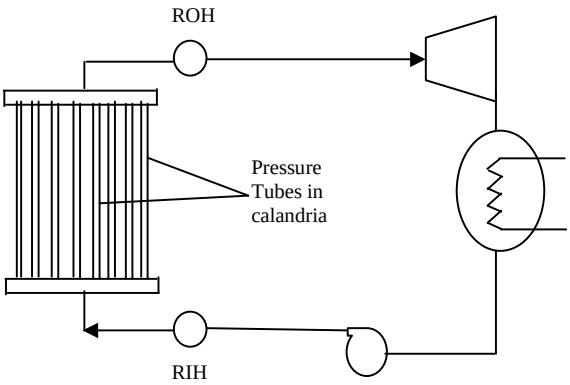

Figure 1-4c: Pressure tube type SCWR

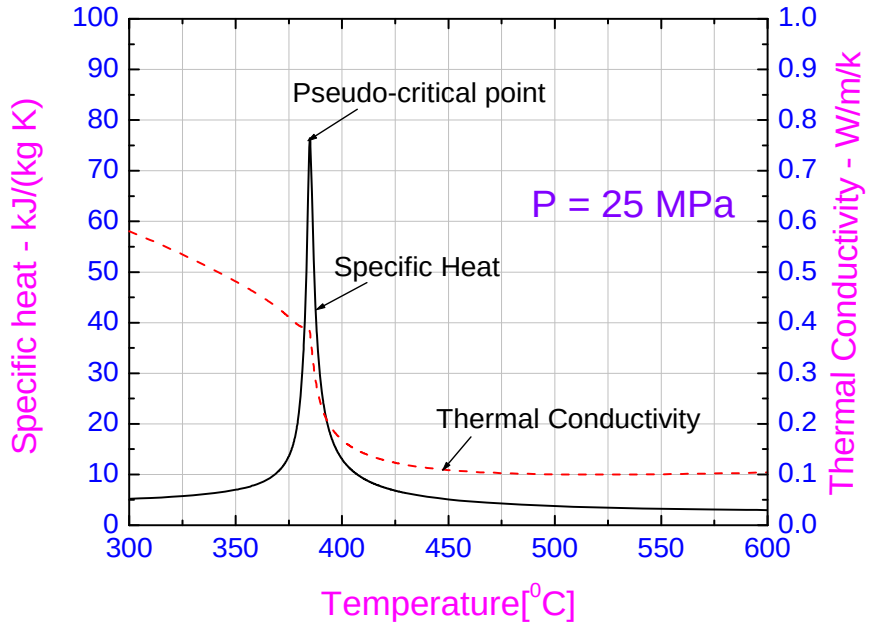

(a)

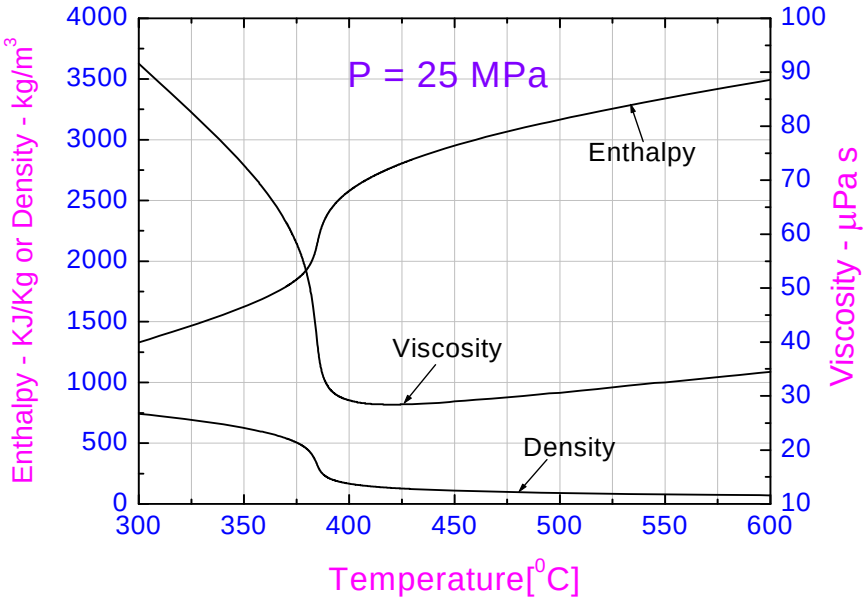

(b)

Figure 1-5: Thermodynamic and transport properties of supercritical water

Chapter 2

Development of steady state and linear stability model for natural circulation with supercritical fluids

2.1 Introduction

Literature reveals linear and non-linear approaches for studying stability of natural circulation (NC) systems operating with supercritical fluids. In the linear approach the time-dependent conservation equations of mass, momentum and energy are solved mostly in frequency domain. The non-linear equations are perturbed over the steady state operating point and linearized assuming the perturbation to be infinitesimally small. The linear stability analysis only predicts the threshold of instability but cannot predict the limit cycle oscillations; however, the approach is preferred considering the valuable reduction in computational time for generating a stability map. The non-linear approach solves the transient conservation equations in time domain. Usually, this approach is very time consuming, since the allowable time step may be very small and large number of cases need to be run to generate a stability map. Several researchers have developed linear stability codes for stability analysis of natural circulation systems/ heated channels operating with supercritical fluids (see Jain and Corradini (2006); Ambrosini and Sharabi (2008); Ortega Gomez et al. (2008)), however the complete methodology is not described. Hence, a linear stability code (SUCLIN) was developed for studying steady state and stability characteristics of natural circulation loop operating with supercritical water.

2.2 Code development for linear stability analysis

The geometry considered for the analysis is corresponding to a supercritical test facility set up in BARC (Bhabha Atomic Research Centre) to generate data for steady state, stability and heat transfer behavior of supercritical fluids under natural circulation conditions. The facility named Supercritical Pressure Natural Circulation Loop (SPNCL) is basically a uniform diameter rectangular loop which can operate with both supercritical water and supercritical carbon dioxide and the dimensions are shown in Figure 2-1. In one dimensional analysis the only co-ordinate x, runs around the loop with origin at the exit of the cooler. The open loop boundary conditions used by Chatoorgoon (2001) and Jain et al. (2006) have been considered where the inlet fluid temperature to cold leg/ heater is fixed irrespective of the heater power. For analysis of an open loop, whatever heat is supplied to the heater is rejected in the cooler keeping the heater inlet temperature constant that is heat rejection in the cooler is not evaluated based on calculation of overall heat transfer coefficient for cooler and temperature difference between primary and secondary fluid. The use of imposed cooling heat flux, instead of third order boundary condition, is something that is not very much close to the physics of a real loop. However, imposed cooling heat flux is taken in present analysis since it is consistent with previous works of Chatoorgoon (2001) and Jain et al (2006) who used the same boundary conditions. The open loop boundary conditions can be summarized as follows –

1) Inlet temperature to cold leg/ heater is constant.
2) Inlet pressure and outlet pressure are constant. However they should also be equal for natural circulation conditions.

Hence for open natural circulation loop analysis, inlet fluid temperature to the cold leg/ heater, loop operating pressure and the heater power are specified along with the entire geometry of the

loop (hydraulic diameter, flow area and length of each pipe). The governing continuity and momentum equations for one dimensional flow can be written as,

$$A\frac{\partial \rho}{\partial t}+\frac{\partial w}{\partial x}=0 \tag{2.1}$$

$$\frac{1}{A}\frac{\partial w}{\partial t}+\frac{1}{A^2}\frac{\partial}{\partial x}(w^2/\rho)+\rho g\cos\phi+\frac{w^2}{2\rho A^2}(\frac{f}{D}+K)+\frac{\partial p}{\partial x}=0 \tag{2.2}$$

where K is the local loss coefficient due to the presence of elbows, tees etc. The energy equation can be expressed as,

$$\frac{\partial(\rho i)}{\partial t}+\frac{1}{A}\frac{\partial(wi)}{\partial x}=\begin{cases} q_h''' \text{ or } -q_c''' & \text{for heater or cooler region,} \\ 0 & \text{adiabatic region.} \end{cases} \tag{2.3}$$

In addition an equation of state is required for the density and is given by

$$\rho = f(p,i) \tag{2.4}$$

The code development required supercritical water properties for which International Association for the properties of steam (IAPS), 1984 formulation (Haar et. al., 1984) has been used. The SCW properties have been compared with the National Institute of Standards and Technology (NIST) data base (http://webbook.nist.gov/chemistry/fluid/). Some typical comparisons have been shown in figures 2-2a, 2-2b & 2-2c.

The steady state solution, which is essential for performing the linear stability analysis, can be obtained by dropping the time derivatives from the above equations. These are

$$\frac{\partial w}{\partial x}=0 \tag{2.5}$$

$$\frac{1}{A^2}\frac{\partial}{\partial x}(w^2/\rho)+\rho g\cos\phi+\frac{w^2}{2\rho A^2}(\frac{f}{D}+K)+\frac{\partial p}{\partial x}=0 \tag{2.6}$$

$$\frac{1}{A}\frac{\partial(wi)}{\partial x} = \begin{cases} q_h''' \text{ or } -q_c''' & \text{for heater or cooler region,} \\ 0 & \text{adiabatic region.} \end{cases} \tag{2.7}$$

Equations (2.5) to (2.7) are solved together to obtain the steady state flow rate for a given power, pressure and inlet conditions as follows.

(i) Assume an initial steady state mass flow rate

(ii) With this mass flow rate, obtain the enthalpy in the heater region at any distance (x) as

$$i(x) = i_{in} + \frac{q_h''' Ax}{w} \tag{2.8}$$

Similarly, the enthalpy in the cooler region at any distance (x) can be calculated as

$$i(x) = i_{out} - \frac{q_c''' Ax}{w} \tag{2.9}$$

The enthalpy is constant in the adiabatic regions so that $i(x) = i_{in}$ from the cooler outlet to the heater inlet and $i(x) = i_{out}$ from heater outlet to the cooler inlet. The heater outlet enthalpy i_{out} can be calculated from equation (2.8) as

$$i_{out} = i_{in} + \frac{q_h''' AL_h}{w} \tag{2.10}$$

where, L_h is the total length of the heated region.

For steady state, the cooler inlet enthalpy will be i_{out} and cooler outlet enthalpy will be i_{in} since all heat added in heater will be removed in cooler. While the density at any axial distance is known from equation (2.4), the friction factor in the single-phase region (sub-critical or supercritical), is obtained from the local Reynolds number as follows.

$$f_{laminar} = 64/Re \quad \text{for laminar flow} \tag{2.11}$$

$$f_{turbulent} = 0.316/Re^{0.25} \quad \text{for turbulent flow} \tag{2.12}$$

and friction factor used in the calculations is selected as the maximum value calculated by the above two equations, i.e.

f = maximum of $(f_{laminar}, f_{turbulent})$ (2.13)

This has been done to avoid discontinuity in the friction factor value during transition from laminar to turbulent flow.

(iii) Equation (2.6) is then integrated over the whole length of the loop to evaluate the total pressure drop (Δp). For a natural circulation loop the total differential pressure (Δp) should be equal to zero. If not, an improved guess for steady state flow rate is made and the calculations are repeated from step (ii) till Δp becomes equal to zero.

2.2.1 Linear stability analysis

The conservation equations (2.1) to (2.3) can be rewritten by replacing density (ρ) with specific volume (v) as given below.

$$-\frac{A}{v^2}\frac{\partial v}{\partial t}+\frac{\partial w}{\partial x}=0 \tag{2.14}$$

$$\frac{1}{A}\frac{\partial w}{\partial t}+\frac{1}{A^2}\frac{\partial}{\partial x}(w^2 v)+\frac{\mathrm{g}}{v}\cos\phi+\frac{w^2 v}{2A^2}\left(\frac{f}{D}+K\right)+\frac{\partial p}{\partial x}=0 \tag{2.15}$$

The energy equation can be expressed as,

$$\frac{\partial(i/v)}{\partial t}+\frac{1}{A}\frac{\partial(wi)}{\partial x}=\begin{cases} q_h''' \text{ or } -q_c''' & \text{for heater or cooler region,} \\ 0 & \text{adiabatic region.} \end{cases} \tag{2.16}$$

The conservation equations (2.14) to (2.16) are perturbed by introducing small perturbations over the steady state as follows

$$w=w_{ss}+w';\ i=i_{ss}+i';\ p=p_{ss}+p';\ v=v_{ss}+v' \tag{2.17}$$

where $w'=\bar{w}(x)e^{st};\ i'=\bar{i}(x)e^{st};\ p'=\bar{p}(x)e^{st};\ v'=\bar{v}(x)e^{st}$ (2.18)

The perturbation in friction factor has been neglected in the present analysis, which is an acceptable approximation for rough pipes. In equation (2.18), $\bar{w}, \bar{i}, \bar{p}$ *and* $\bar{v}$ are the very small amplitudes of the perturbed flow rate, enthalpy, pressure and specific volume of coolant respectively and s is the stability parameter. With these substitutions, the perturbed conservation equations after linearization can be written as follows.

Perturbed continuity equation

$$\frac{d\bar{w}}{dx} = \frac{As}{v_{ss}^2}\ \bar{v} \tag{2.19}$$

Perturbed energy equation

$$\frac{d\bar{i}}{dx} + \left(\frac{As}{v_{ss} w_{ss}}\right)\bar{i} = \begin{cases} -\dfrac{\bar{w} q'''_{h,ss} A}{w_{ss}^2} \quad or \quad \dfrac{\bar{w} q'''_{c,ss} A}{w_{ss}^2} & \text{heater/cooler region} \\ 0 & \text{adiabatic region} \end{cases} \tag{2.20}$$

Perturbed momentum equation

$$\frac{d\bar{p}}{dx} + \bar{w}\left(\frac{s}{A} + \frac{w_{ss} v_{ss}}{A^2}\left(\frac{f}{D} + K\right)\right) + \bar{v}\left[\frac{w_{ss}^2}{2A^2}\left(\frac{f}{D} + K\right) - \frac{g}{v_{ss}^2} + \frac{2s w_{ss}}{A v_{ss}}\right] + \frac{w_{ss}^2}{A^2}\frac{d\bar{v}}{dx} = 0 \tag{2.21}$$

The equation of state has been obtained as a polynomial by least square fit between specific volume (v) and enthalpy (i) for water at 25 MPa pressure for temperature range of 280 ^{o}C - 1000 ^{o}C as given below.

$$v = a_0 + a_1 i + a_2 i^2 + a_3 i^3 + a_4 i^4 + a_5 i^5 + a_6 i^6 \tag{2.22}$$

The polynomial has been compared with actual specific volume data in figure 2-3. The coefficients a_0 to a_6 are also shown in figure 2-3. The amplitude of perturbation in specific volume ($\bar{v}$) is considered only as a function of amplitude of perturbation in enthalpy ($\bar{i}$) and

contribution of amplitude of pressure perturbation ($\bar{p}$) in $\bar{v}$ has been neglected because significant contribution to $\bar{v}$ comes from $\bar{i}$. The same can be expressed as given below

$$\bar{v} = c1_{ss}\ \bar{i} \tag{2.23}$$

where

$$c1_{ss} = \left(\frac{\partial v}{\partial i}\right)_p = a_1 + 2a_2 i_{ss} + 3a_3 i^2_{ss} + 4a_4 i^3_{ss} + 5a_5 i_{ss}^4 + 6a_6 i_{ss}^5 \tag{2.24}$$

2.2.2 Solution procedure

The differential equations (2.19) to (2.21) have been solved analytically to obtain perturbed amplitude of pressure drop $\Delta\bar{p}_i$, where *i* stands for individual components e.g. heater, adiabatic hot leg, cooler and adiabatic cold leg in a supercritical pressure natural circulation loop (SPNCL).

Adiabatic components:

The perturbed energy equation (2.20) is integrated over length Δx which can be expressed as

$$\bar{i} = \bar{i}_{in}\ e^{-\tau s} \tag{2.25}$$

where, τ is the residence time of fluid in length Δx, $\tau = \dfrac{-A\Delta x}{w_{ss} v_{ss}}$ (2.26)

For integrating perturbed continuity equation (2.19) over length Δx the same can be expressed as

$$\frac{d\bar{w}}{dx} = \frac{As}{v_{ss}^2}\ c1_{ss}\,\bar{i} \tag{2.27}$$

Integrating above equation gives

$$\bar{w} = \bar{w}_{in} + \frac{w_{ss}}{v_{ss}} c1_{ss}\ \bar{i}_{in}\left[1 - e^{-\tau s}\right] \tag{2.28}$$

Using equations (2.25) and (2.28), the perturbed pressure drop over length Δx can be calculated by integrating equation (2.21) as expressed below

$$\Delta \bar{p} = -\left[\frac{s}{A} + \frac{fw_{ss}v_{ss}}{DA^2}\right]\left[\bar{w}_{in}\Delta x + \frac{w_{ss}}{v_{ss}} c1_{ss}\bar{i}_{in}\left(\Delta x + \frac{w_{ss}v_{ss}}{As}(\mathrm{e}^{-\tau s} - 1)\right)\right] + \left[\frac{fw_{ss}^2}{2DA^2} - \frac{\mathrm{g}}{v_{ss}^2} + \frac{2w_{ss}s}{Av_{ss}}\right] c1_{ss}\bar{i}_{in}\frac{w_{ss}v_{ss}}{As}(\mathrm{e}^{-\tau s} - 1) - \frac{w_{ss}^2}{A^2} c1_{ss}\bar{i}_{in}(\mathrm{e}^{-\tau s} - 1) \tag{2.29}$$

Non-adiabatic components:

The perturbed energy equation (2.20) is integrated which can be expressed as

$$\bar{i} = B\mathrm{e}^{r_1 x} + C\mathrm{e}^{r_2 x} \tag{2.30}$$

where

$$B = \frac{\bar{i}_{in}\left[r_2 + \frac{As}{w_{ss}v_{ss}}\right] + \frac{q_{hss}A}{w_{ss}^2}\bar{w}_{in}}{r_2 - r_1} \tag{2.31}$$

$$C = \bar{i}_{in} - B \tag{2.32}$$

$$r_1 = \left[-m_1 + \left(m_1^2 - 4m_2\right)^{0.5}\right]/2, \tag{2.33}$$

$$r_2 = \left[-m_1 - \left(m_1^2 - 4m_2\right)^{0.5}\right]/2 \tag{2.34}$$

and

$$m_1 = \left[\frac{As}{w_{ss}v_{ss,av}}\right], \tag{2.35}$$

$$m_2 = \left[\frac{q_{hss}A^2 sc1_{ss,av}}{w_{ss}^2 v_{ss,av}^2}\right] \tag{2.36}$$

The perturbed continuity equation (2.19) is integrated which can be expressed as

$$\bar{w} = \bar{w}_{in} + \frac{As}{v_{ss,av}^2} c1_{ss,av} \left[\frac{B}{r_1} \left(e^{r_1 \Delta x} - 1 \right) + \frac{C}{r_2} \left(e^{r_2 \Delta x} - 1 \right) \right] \tag{2.37}$$

Using equations (2.30) and (2.37), the perturbed pressure drop over length Δx can be calculated by integrating equation (2.21) as expressed below

$$\begin{aligned} \Delta \bar{p} = -\left[\frac{s}{A} + \frac{f w_{ss} v_{ss,av}}{DA^2} \right] \left[\bar{w}_{in} \Delta x + \frac{As}{v_{ss,av}^2} c1_{ss,av} \left[\frac{B}{r_1^2} \left(e^{r_1 \Delta x} - 1 \right) - \frac{B}{r_1} \Delta x + \frac{C}{r_2^2} \left(e^{r_2 \Delta x} - 1 \right) - \frac{C}{r_2} \Delta x \right] \right] + \\ c1_{ss,av} \left[\frac{f w_{ss}^2}{2DA^2} - \frac{g}{v_{ss,av}^2} + \frac{2 w_{ss} s}{A v_{ss,av}} \right] \left[\frac{B}{r_1} \left(e^{r_1 \Delta x} - 1 \right) + \frac{C}{r_2} \left(e^{r_2 \Delta x} - 1 \right) \right] - \frac{w_{ss}^2}{A^2} c1_{ss,av} \left[B \left(e^{r_1 \Delta x} - 1 \right) + C \left(e^{r_2 \Delta x} - 1 \right) \right] \end{aligned} \tag{2.38}$$

The boundary conditions used are

$$\bar{i}_{in} = 0 \text{ and } \sum \Delta \bar{p}_i = 0 \tag{2.39}$$

The characteristic equation can be written as

$$Y(s) = \Sigma \Delta \bar{p}_i = 0, \tag{2.40}$$

where, s is the stability parameter which is a complex number.

Regula-falsi method is employed to find out the roots of the complex characteristic equation. If the real part for any of the roots is > 0 then the loop is unstable and if real part of all of the roots is < 0 then loop is stable. If real part of the any of roots is ≈ 0 and real part of all the other roots are ≤ 0 then the loop is neutrally stable.

Instead of looking for the roots of the characteristic equation the stability maps were obtained by using Nyquist plots. The Nyquist plot is obtained by substituting s=ib in $\sum \Delta \bar{p}_i$ (LHS of equation 2.39) where angular frequency (b) is increased in positive steps starting from zero value to get the values of perturbed pressure drop which are plotted on the real-imaginary plane. If the

trajectory encircles origin the loop operating condition is unstable, if the trajectory does not encircle origin the loop operating condition is stable. If the trajectory passes through origin the loop operating condition is neutrally stable. All neutrally stable points are joined to obtain the stability map.

2.2.3 Qualitative assessment of the code

2.2.3.1 Chatoorgoon's loop geometry with SCW

The steady state mass flow rate as a function of power at 25 MPa and heater inlet temperature of 350^{o}C, has been generated using SUCLIN code for the loop geometry available in Chatoorgoon (2001). The geometric details of the loop and the steady state results are shown in figure 2-4a and figure 2-4b respectively. The peak steady state flow rate is obtained at a power of 3.75 MW. Chatoorgoon proposed that the threshold of instability is the power corresponding to peak flow. He used a nonlinear code (SPORTS) which shows the threshold of instability as 4.5 MW for the same loop geometry at 25 MPa pressure and 350^{o}C heater inlet temperature. The SUCLIN code has also been used to predict the threshold of instability which shows the threshold of instability as 4.2 MW. The Nyquist plots for the same are shown in figure 2-5. The difference can be attributed to the stability assessments made with different techniques and assumptions.

The threshold of instability identified by Nyquist plot was also checked by identifying the complex dominant roots of the characteristic equation 2.39 for Chatoorgoon's loop at 25 MPa and 350^{o}C heater inlet temperature which are given in Table 2-1. It can be seen that at 4.2 MW power the dominant root has almost zero real part indicating a neutrally stable case.

Table 2-1: Dominant roots of characteristic equation for Chatoorgoon's loop at 25 MPa and 350^{o}C heater inlet temperature

Power (MW)	Dominant Root's Real part (*a*)	Dominant Root's Imaginary part / Angular Frequency (*b*)	Remark
4.0	-0.0147	0.8928	Stable
4.2	-0.00051	0.9052	Neutrally stable
4.5	0.0192	0.9193	Unstable

The stability map of Chatoorgoon's loop plotted in figure 2-6 indicates that lower threshold power of instability increase only mildly (3.9 to 4.9 MW), whereas upper threshold of instability reduces significantly (9.75 to 5.4 MW) with increase in heater inlet temperature from 300 ^{o}C to 364^{o}C . The ratio of lower threshold power of instability and power corresponding to peak steady state natural circulation flow rate at a specified heater inlet temperature for different heater inlet temperatures have been plotted in figure 2-7. The figure shows the lower threshold power of instability to be within -30% to +50% of the power corresponding to peak flow for heater inlet temperature varying from 300^{o}C to 364^{o}C. For heater inlet temperature above 365^{o}C no instability is observed although peak steady state flows occur at 2.9 MW and 2.3 MW for heater inlet temperatures of 370^{o}C and 380^{o}C respectively.

2.2.3.2 University of Wisconsin (UW)-Madison loop

UW-Madison loop is a SCW rectangular natural circulation loop having inside diameter, height, width and total length of 42.9 mm, 3m, 2m and 10 m respectively as given in Jain et al. (2006). The steady state characteristics of the loop predicted by SUCLIN code has been compared with

predictions available from Jain et al. (2006) in figure 2-8. The difference can be due to some local losses considered in Jain et al. which were not reported in the paper.

The linear stability analysis carried out by Jain et al. for UW-Madison loop was for heater inlet temperatures above 327^{o}C & up to 3 MW of power and no instability was observed. The higher power levels were not investigated since respective exit temperatures became so high that the heater wall material tolerance limit was exceeded. The stability map generated for the same loop by SUCLIN code is given in figure 2-9, which indicates that no instability is present in the loop for heater inlet temperature above 220^{o}C irrespective of the power. Thus the two results agree well. For generating this map only a new polynomial for equation of state has been fit for temperature range of 100-1000^{o}C at 25 MPa.

2.2.4 Steady state and stability analysis using SUCLIN code

After qualitative assessment, SUCLIN code has been extensively used for studying the effect of diameter, height, heater inlet temperature, pressure and local loss coefficients on steady state and stability behavior of Supercritical Pressure Natural Circulation Loop (SPNCL) operating with supercritical water shown in figure 2-1. The steady state characteristics have been predicted for various loop pipe diameters (i.e. 7 mm, 13.88 mm, 20.7 mm and 28 mm) with SCW (figure 2-10a & 2-10b). The steady state characteristics indicate that with initial increase in power the loop mass flow rate increases due to increase in buoyancy force caused by the large increase in the thermal expansion coefficient. Subsequently, flow decreases with power due to increased frictional pressure drop caused by a sharp reduction in density after the pseudo-critical temperature. The peak mass flow rates for 7 mm, 13.88 mm, 20.7 mm and 28 mm diameter loops with SCW operation at 25 MPa pressure are observed at heater outlet temperature of 389^{o}C,

390^{o}C, 390^{o}C and 390.6^{o}C respectively (pseudo-critical temperature of water at 25 MPa is 385^{o}C). The mass flow rate increases with pressure at high powers in friction dominant regime just as in two-phase Natural Circulation systems (Nayak et al., 1998) as shown in figure 2-11. The steady state natural circulation mass flow rate reduces significantly when heater inlet temperature exceeds the pseudo-critical temperature as shown in figure 2-12. This is attributed to the reduction in the buoyancy force resulting from the reduction in the thermal expansion coefficient as shown in figure 2-13. Moreover, when both the legs become supercritical the frictional resistance also increases dramatically resulting in larger flow reduction. Increasing the loop height increases the available buoyancy head and increases the natural circulation flow rate as shown in figure 2-14.

The heater outlet temperatures at which peak steady state mass flow rates are achieved for various heater inlet temperatures have been predicted for various geometrical parameters as shown in figure 2-15. It shows that with increase in heater inlet temperature the heater outlet temperature at which peak steady state flow rate is achieved also increases, but remains near the pseudo-critical temperature. A change in loop pipe diameter or loop height does not significantly affect the heater outlet temperature at which peak steady state flow rate is achieved. The local loss coefficients significantly affect the heater outlet temperature at which peak steady state flow rate is achieved as shown in figure 2-16. Local loss coefficient in the cold leg shifts the heater outlet temperature corresponding to peak flow much beyond the pseudo-critical temperature, whereas local loss coefficient in hot leg shifts it closer to pseudo-critical temperature.

The effect of loop pipe diameter on stability behavior of SPNCL is shown in figures 2-17a & 2-17b. Figure 2-17a shows that the power envelope of the unstable zone increases significantly with increase in loop pipe diameter just like in single-phase loops reported in Vijayan et al.

(2008). If one considers the heater outlet temperature for a fixed heater inlet temperature then instability is observed over a wide range of heater outlet temperature for smaller diameter loops. It can be observed that as the heater inlet temperature is increased, the lower threshold of instability increases slightly, whereas upper threshold of instability decreases significantly and beyond a specified value of heater inlet temperature no instability is observed. This value of heater inlet temperature beyond which instability is not observed decreases with increase in loop pipe diameter. This observation may be very useful in design of natural circulation based SCW cooled reactors because changing the heater inlet temperature does not significantly affect the lower threshold power of instability, hence heater inlet temperatures should be kept at values where no unstable zone is observed. This is possible without sacrificing the large jump in enthalpy occurring across the pseudo-critical point.

Increasing the loop height increases the SPNCL instability as shown in figure 2-18a & 2-18b. The effect of loop pressure on stability behavior of SPNCL is shown in figures 2-19a & 2-19b. Increasing the loop pressure shifts both power and heater outlet temperature maps slightly upwards, since the pseudo-critical temperature (at which maximum value of specific heat is observed) also increases with pressure. Whereas, pressure has a significant influence on stability of two phase natural circulation loops. Increasing the pressure stabilizes the two-phase loops (Nayak et al., 1998).

The effect of local losses on the stability behavior of SPNCL is shown in figures 2-20a & 2-20b. The loop stabilizes with local losses considered in cold or sub-critical leg and destabilizes with local losses considered in hot or supercritical leg which is similar to the behavior of two – phase natural circulation loops (Kyung et al., 1994).

Chatoorgoon (2001) postulated that threshold power of instability should be same as power corresponding to peak steady state natural circulation flow rate for a given heater inlet temperature. Hence, the effect of loop geometry on the ratio of lower threshold power of instability and power corresponding to peak steady state natural circulation flow rate at different heater inlet temperatures have been plotted in figure 2-21. The effect of local loss coefficient on the ratio of lower threshold power of instability and power corresponding to peak steady state natural circulation flow rate at different heater inlet temperatures have been plotted in figure 2-22. The ratio was found to be varying from 0.6 to 1.8 for some of the cases shown in figures 2-21 & 2-22 and as the ratio is not near unity, the postulation of Chatoorgoon (2001) is not correct as was also concluded by Jain and Corradini (2006).

2.3. Conclusions

The peak of the steady state mass flow rate versus power curve for uniform diameter supercritical water natural circulation is obtained at heater outlet temperature near the pseudo-critical value. A change in loop pipe diameter or loop height does not significantly affect the heater outlet temperature at which peak steady state flow rate is achieved. Local loss coefficient in the cold leg shifts the heater outlet temperature corresponding to peak flow much beyond the pseudo-critical temperature, whereas local loss coefficient in hot leg shifts it closer to pseudo-critical temperature. If the heater inlet temperature increases beyond the pseudo-critical temperature the steady state natural circulation mass flow rate reduces significantly. The steady state natural circulation flow rate increases with increase in pressure at higher powers in the friction dominant region just like two phase natural circulation loops.

In all the loops considered for stability analysis, it is observed that lower threshold power of instability increase only mildly whereas upper threshold of instability reduces significantly with increase in heater inlet temperature above 300^{o}C. The larger diameter loops are more unstable in terms of heater power compared to small diameter loops for supercritical water natural circulation, however smaller diameter loops are unstable over a wide range of heater outlet temperature for a fixed heater inlet temperature. Beyond a specified value of heater inlet temperature no instability is observed and its value decreases with increase in loop pipe diameter. These observations suggest that natural circulation systems operating with supercritical water can be designed for lower heater inlet temperatures and still not encounter instability whatever may be the power. Such systems can also take advantage of the large jump in enthalpy occurring across the pseudo-critical point. Increasing the loop height widens the SPNCL unstable zone. Increasing the loop pressure shifts the stability maps slightly upwards. Inducing local losses in cold leg improves the loop stability, whereas local losses in hot leg destabilize SPNCL. Lower stability threshold deviates as much as -40% to +80% from the power corresponding to peak steady state flow in some of the cases analyzed in this chapter. Hence, it can be concluded that lower stability threshold power of SPNCL is not strictly related to the peak of the steady state mass flow rate versus power curve. Moreover, for a particular heater inlet temperature the steady state mass flow rate peak may exist but instability may be altogether absent for that heater inlet temperature as can be observed for larger diameter loops.

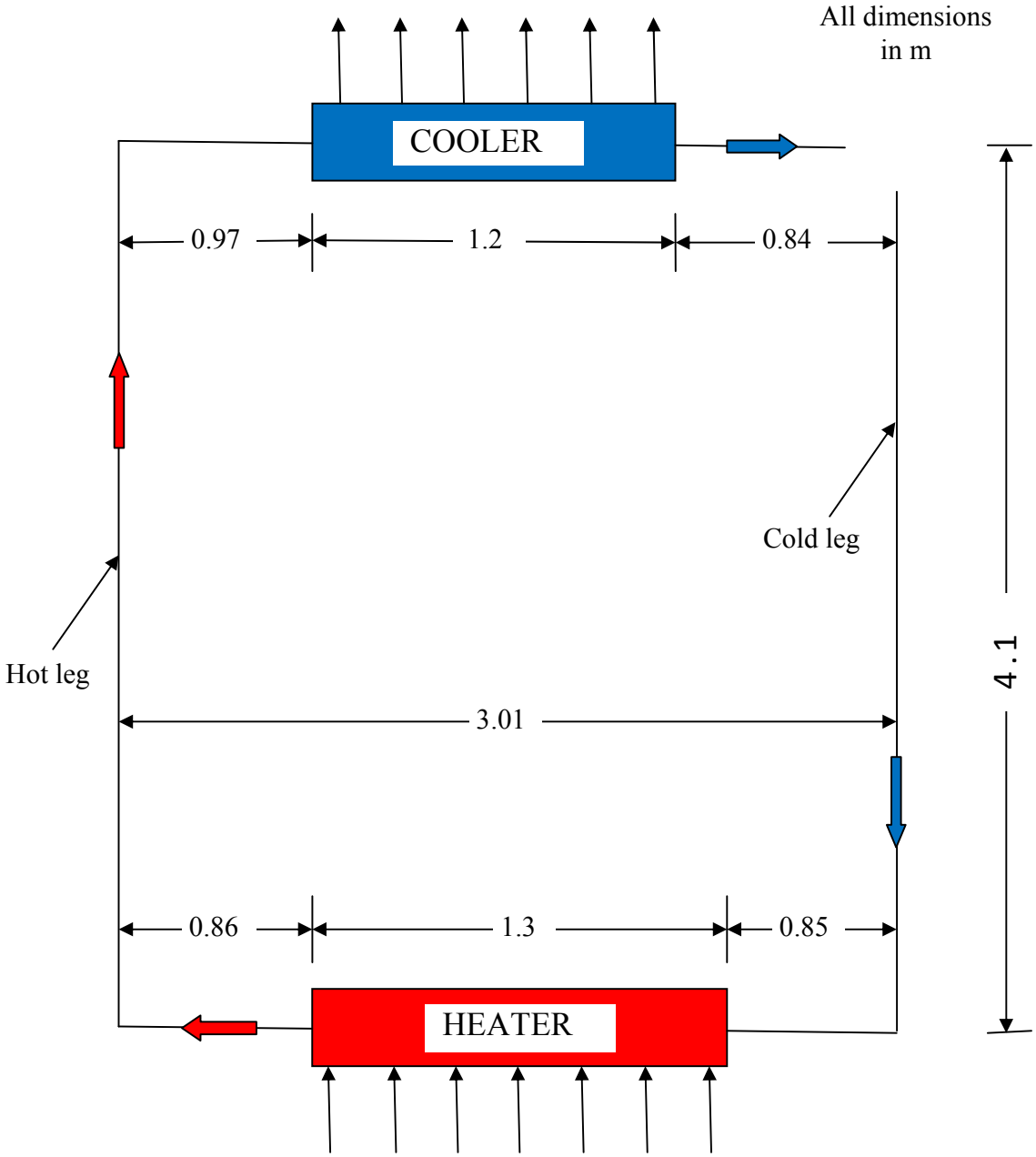

Figure 2-1: Simplified loop geometry considered for analysis

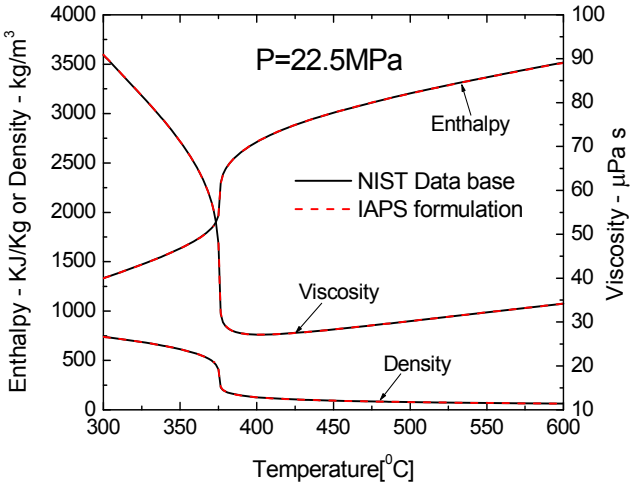

(a)

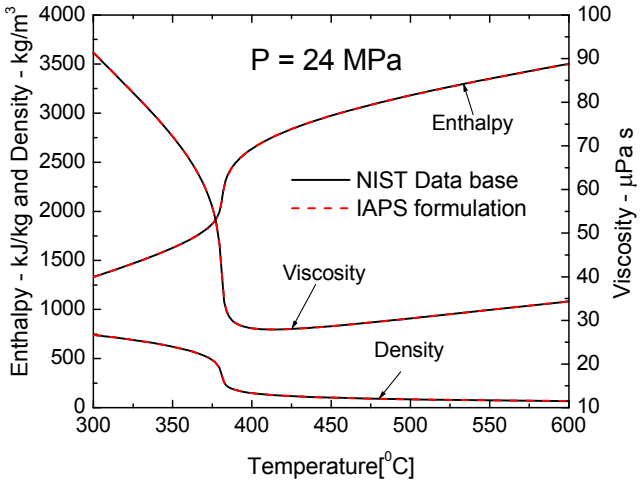

(b)

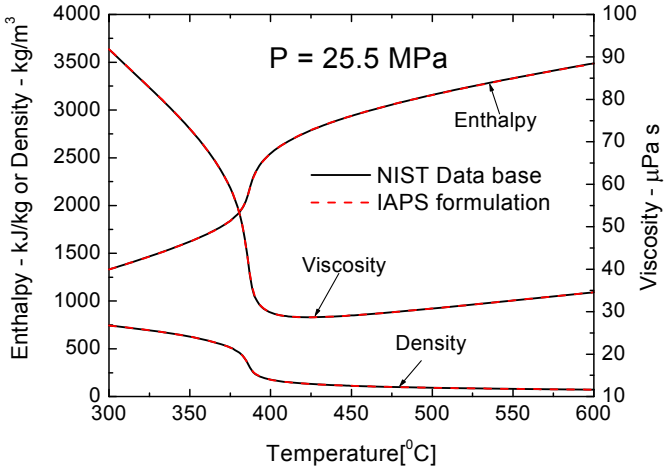

(c)

Figure 2-2: Comparison of supercritical water properties as predicted by IAPS formulations with NIST data base

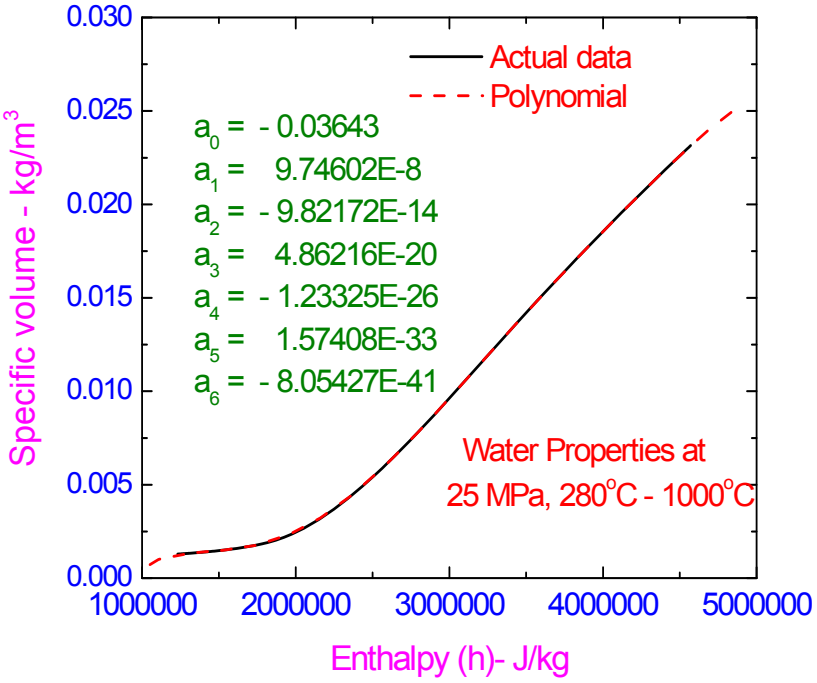

Figure 2-3: Polynomial for specific volume of supercritical water at 25 MPa

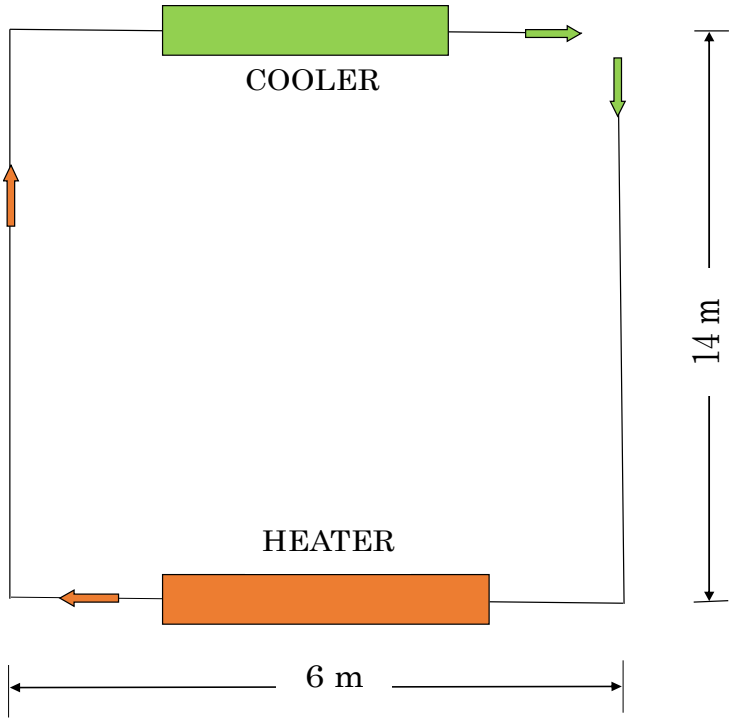

Figure 2-4a: Loop geometry in Chatoorgoon (2001)

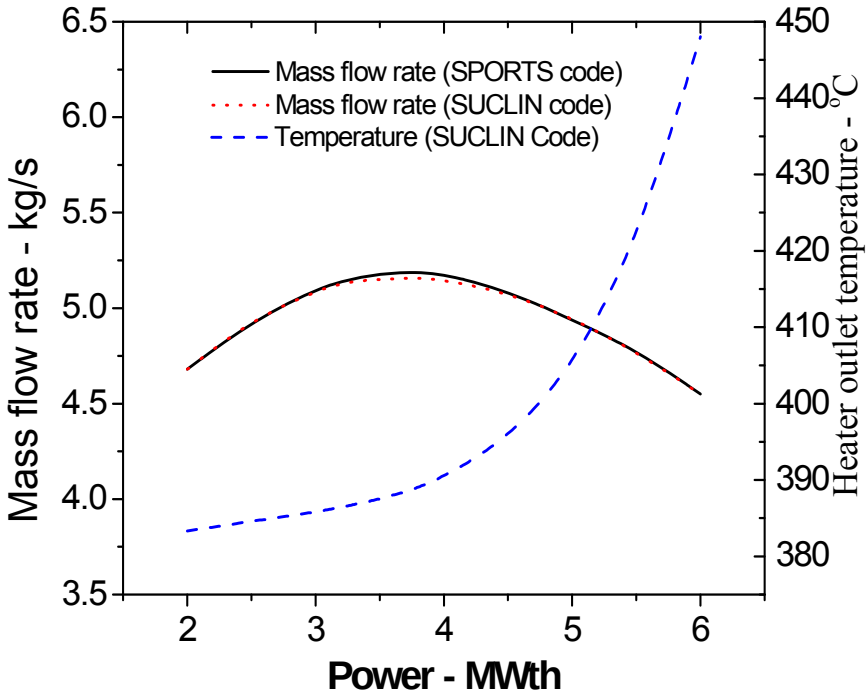

Figure 2-4b: Steady state natural circulation flow rate for Chatoorgoon's loop at 25 MPa and 350^{o} C heater inlet temperature

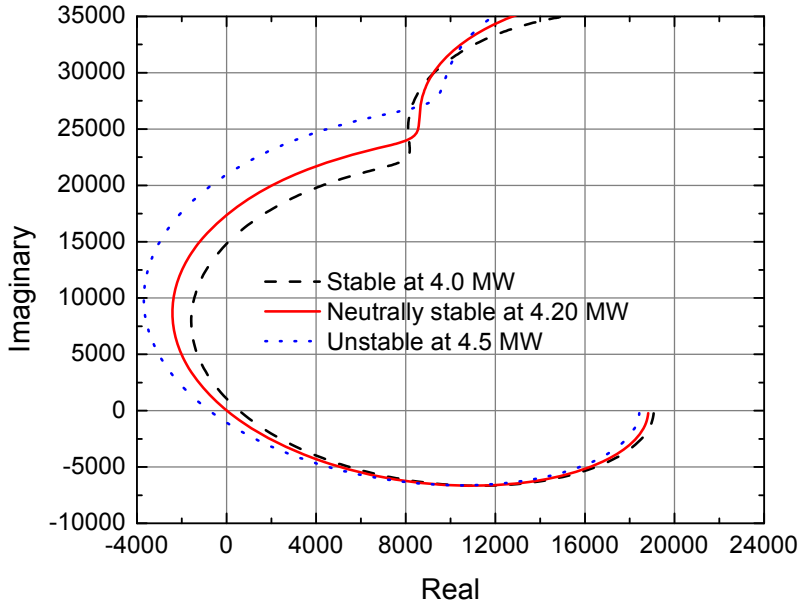

Figure 2-5: Nyquist plots for the Chatoorgoon's loop at 25 MPa and heater inlet temperature of 350^{o}C

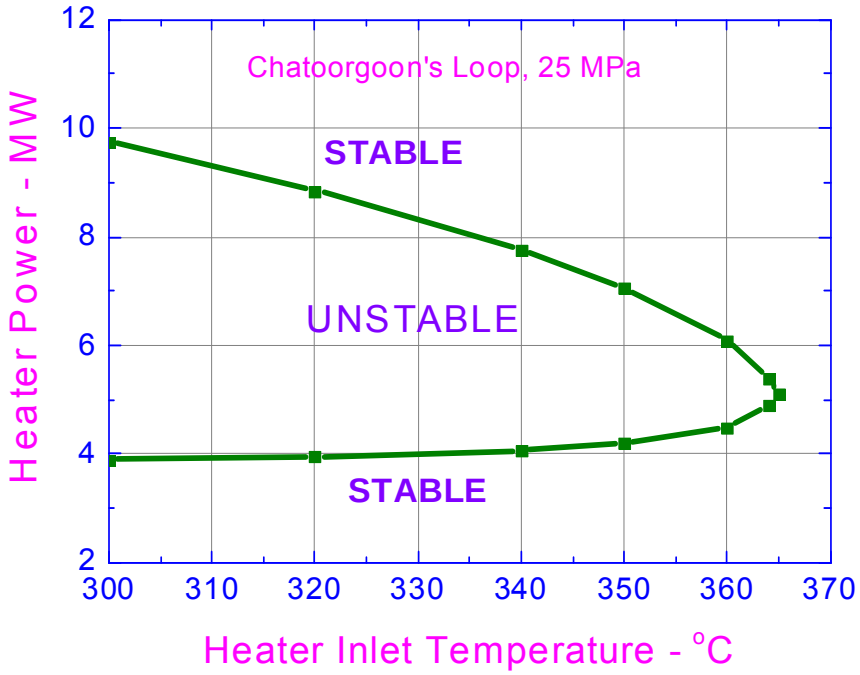

Figure 2-6: Stability map for Chatoorgoon's loop at 25 MPa predicted by SUCLIN code

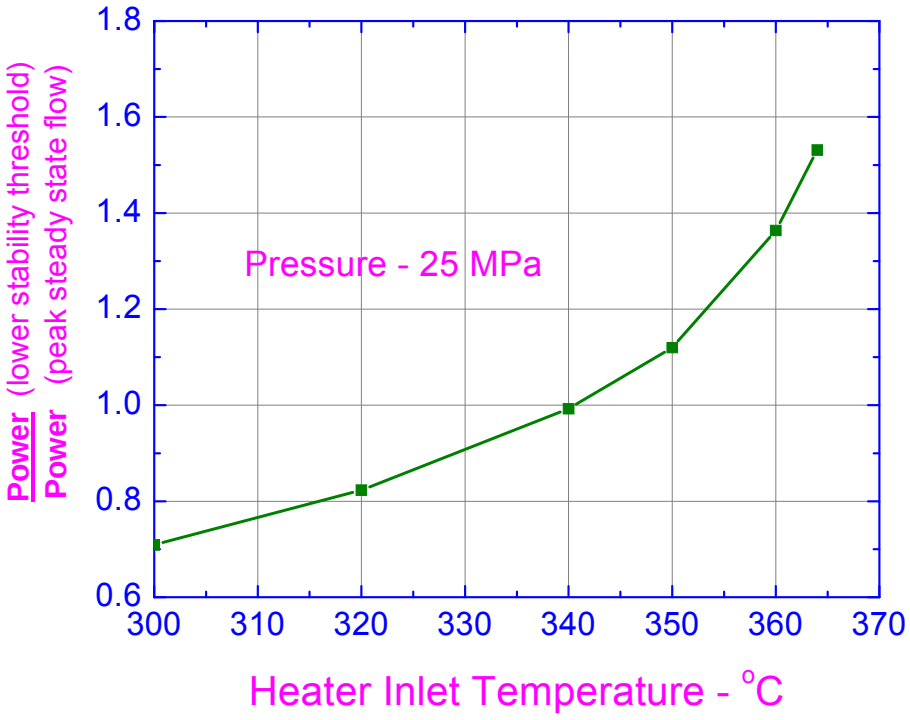

Figure 2-7: Comparison of lower threshold power of instability and power corresponding to peak flow for Chatoorgoon's loop.

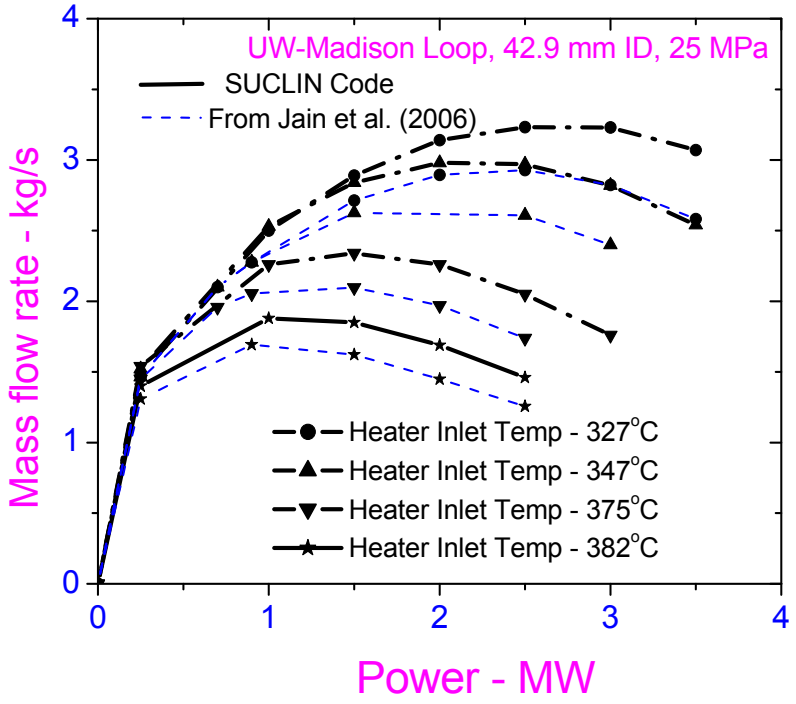

Figure 2-8: Steady state characteristics for UW- Madison loop predicted by SUCLIN code

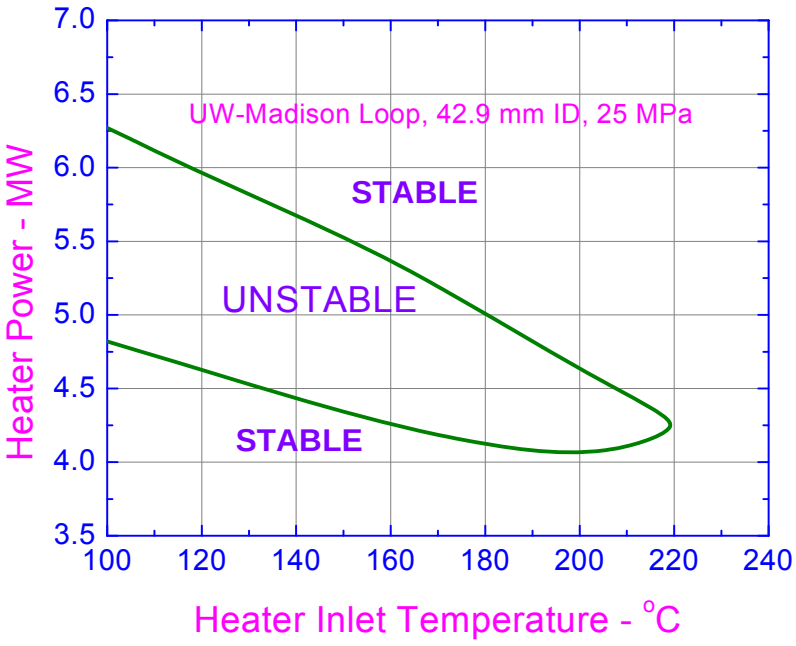

Figure 2-9: Stability map for UW- Madison loop predicted by SUCLIN code

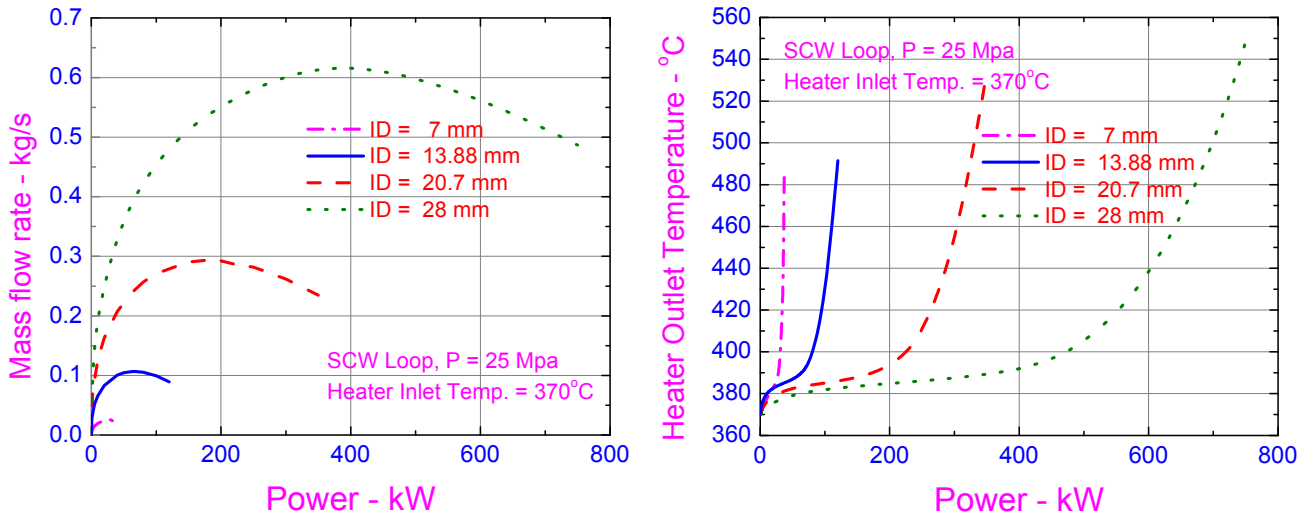

(a) (b)

Figure 2-10: Steady state characteristics for different diameter loops at 25 MPa and heater inlet temperature of 370°C.

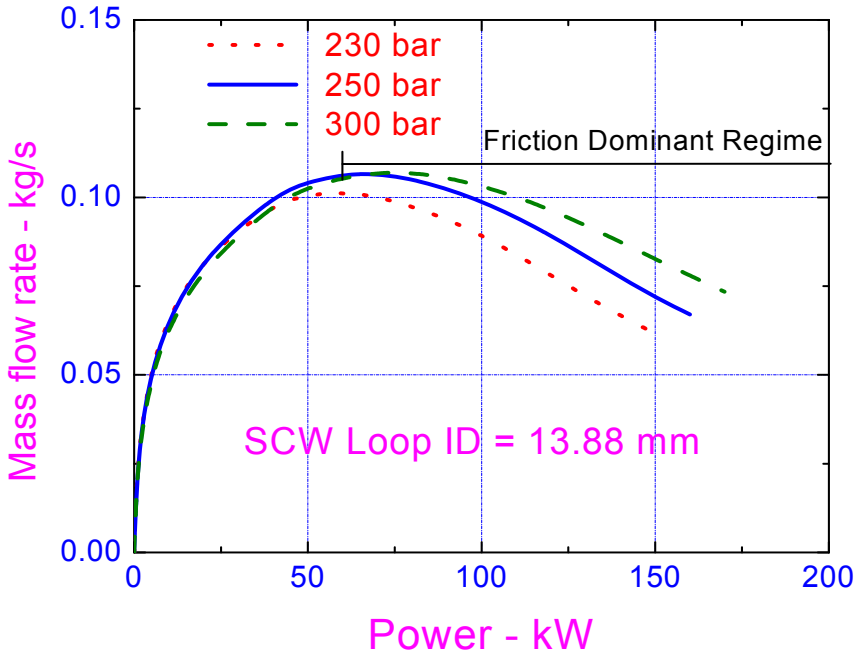

Figure 2-11: Effect of loop pressure on steady state mass flow rate at heater inlet temperature of 370°C

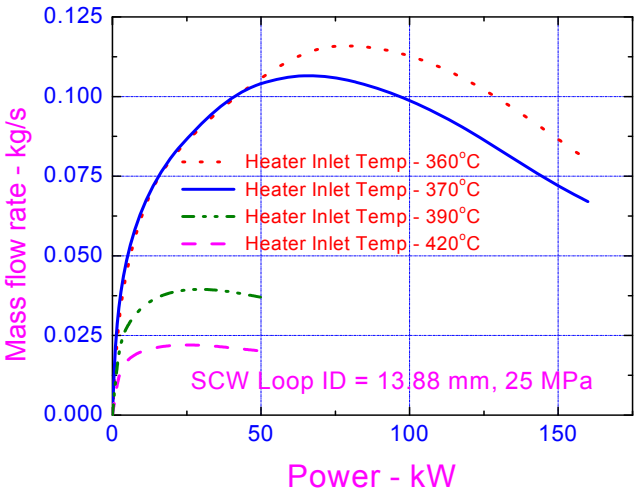

Figure 2-12: Effect of heater inlet temperature on steady state mass flow rate at 25 MPa.

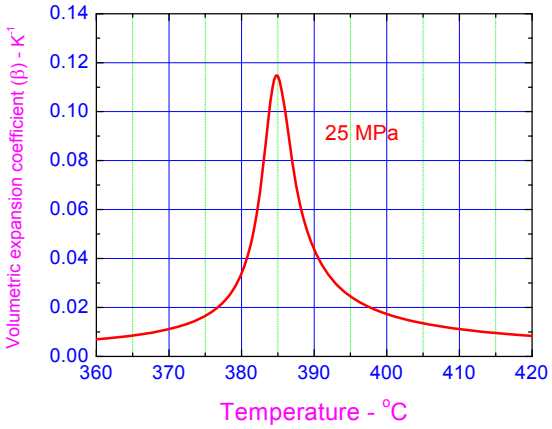

Figure 2-13: Variation of volumetric expansion coefficient with temperature for water

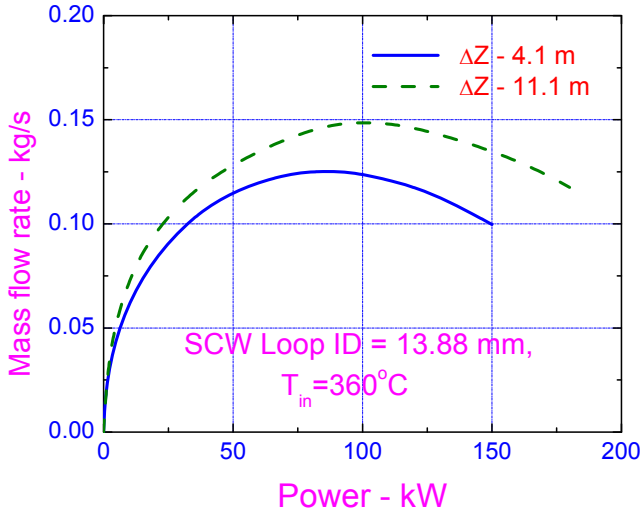

Figure 2-14: Effect of loop height on steady state mass flow rate at 25 MPa.

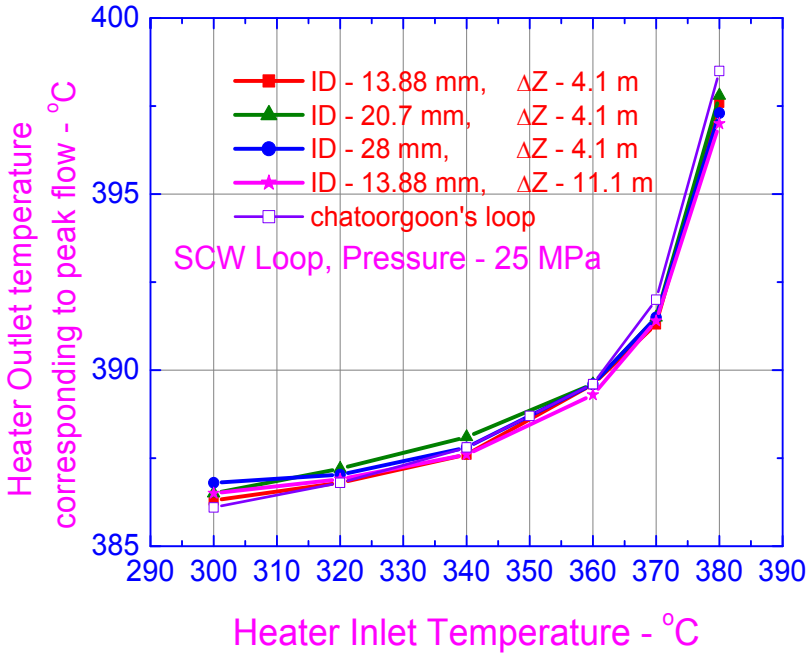

Figure 2-15: Effect of geometrical parameters on heater outlet temperature corresponding to peak flow

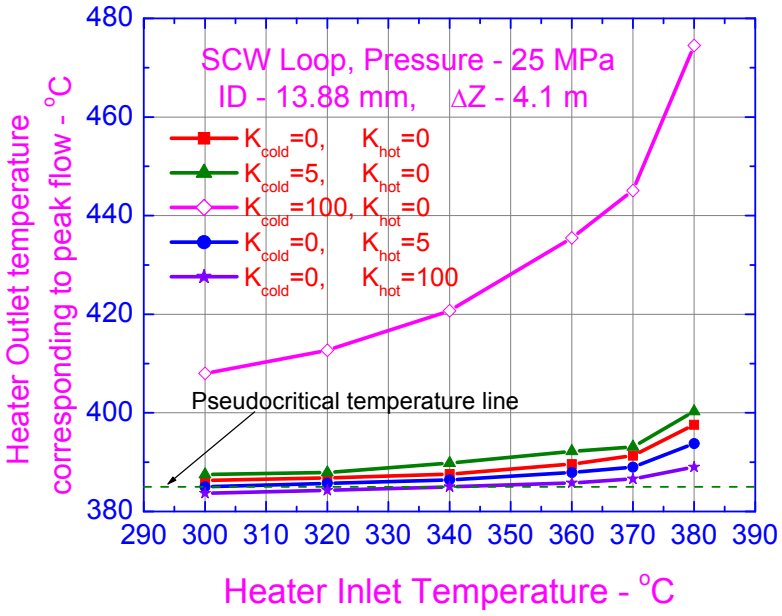

Figure 2-16: Effect of local loss coefficients on heater outlet temperature corresponding to peak flow

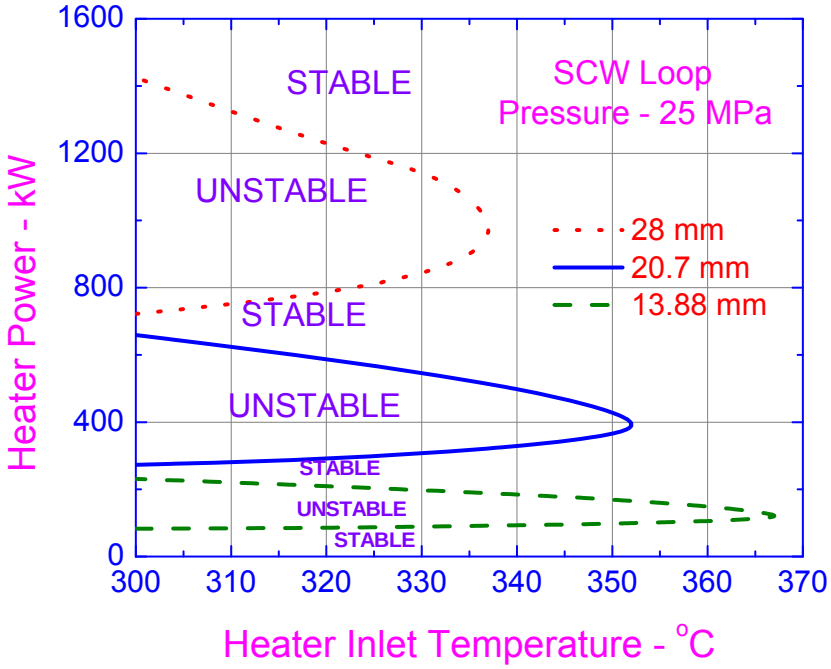

(a)

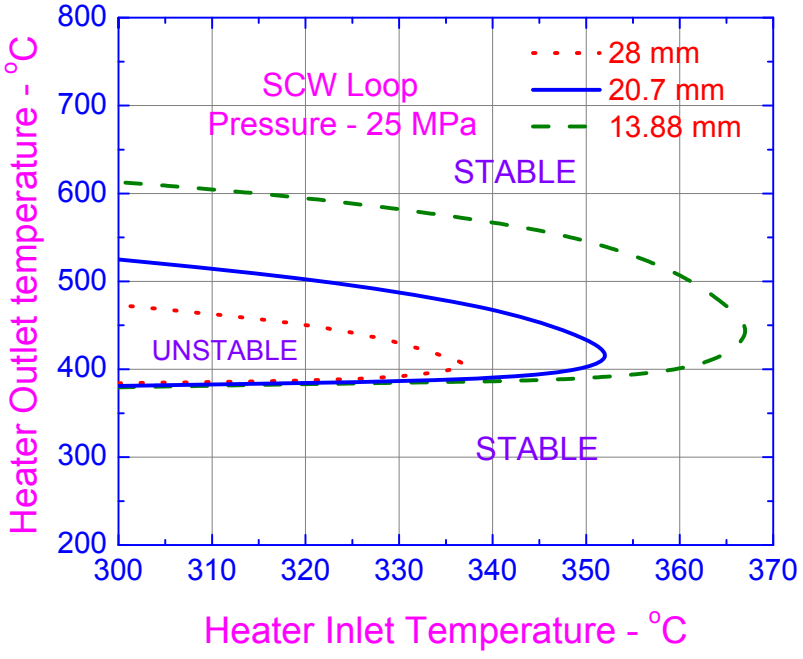

(b)

Figure 2-17: Effect of loop pipe diameter on stability behavior of SPNCL

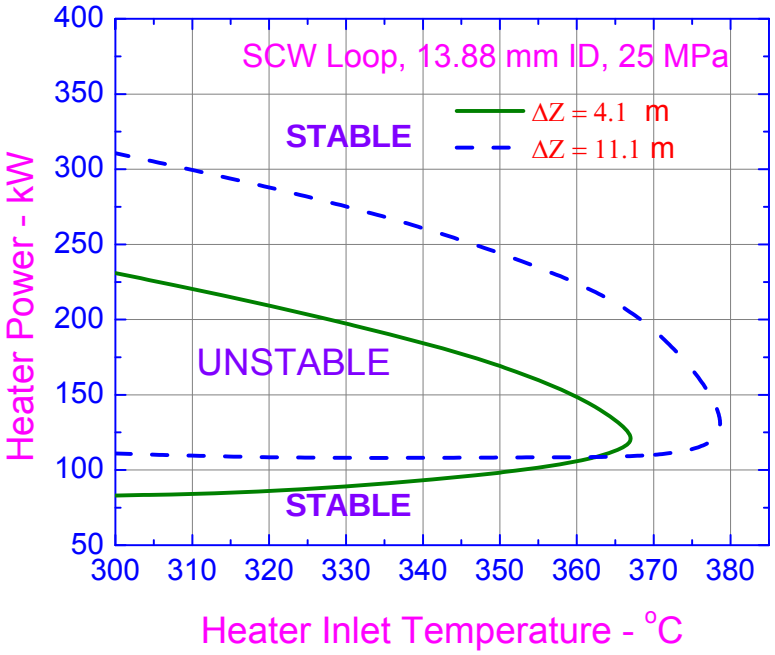

(a)

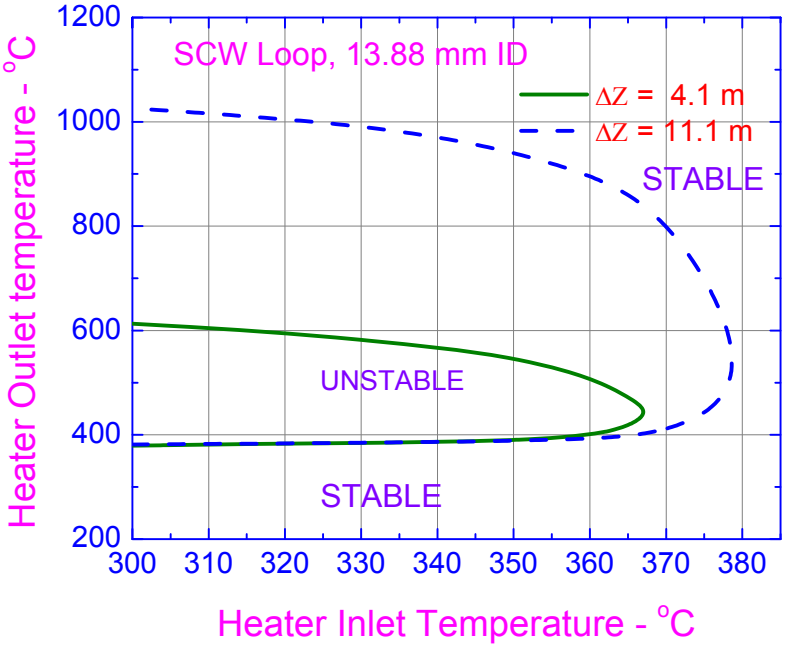

(b)

Figure 2-18: Effect of loop height on stability behavior of SPNCL

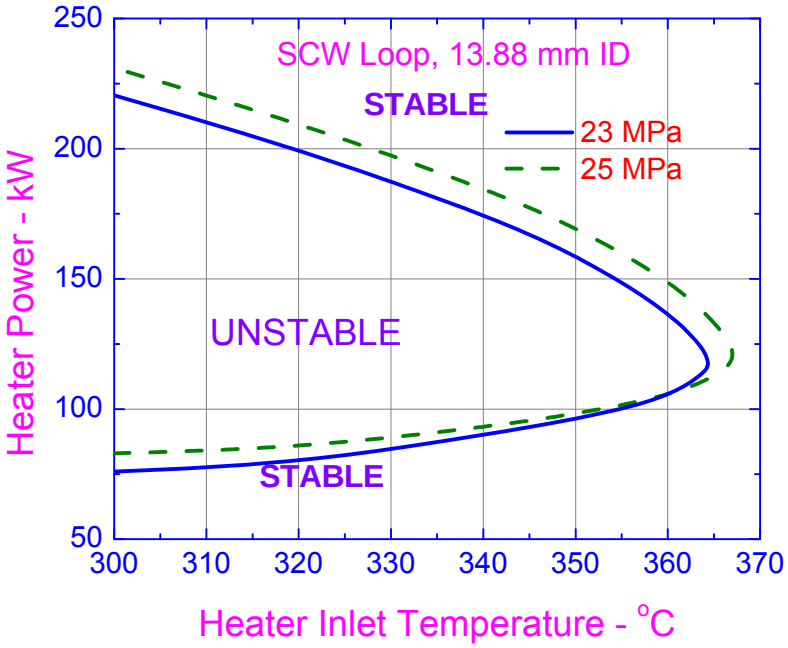

(a)

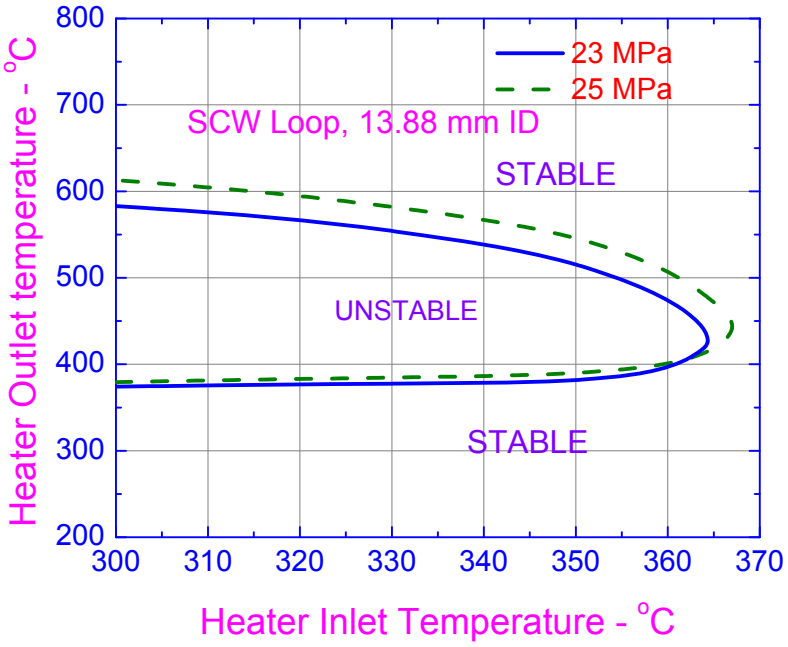

(b)

Figure 2-19: Effect of loop pressure on stability behavior of SPNCL

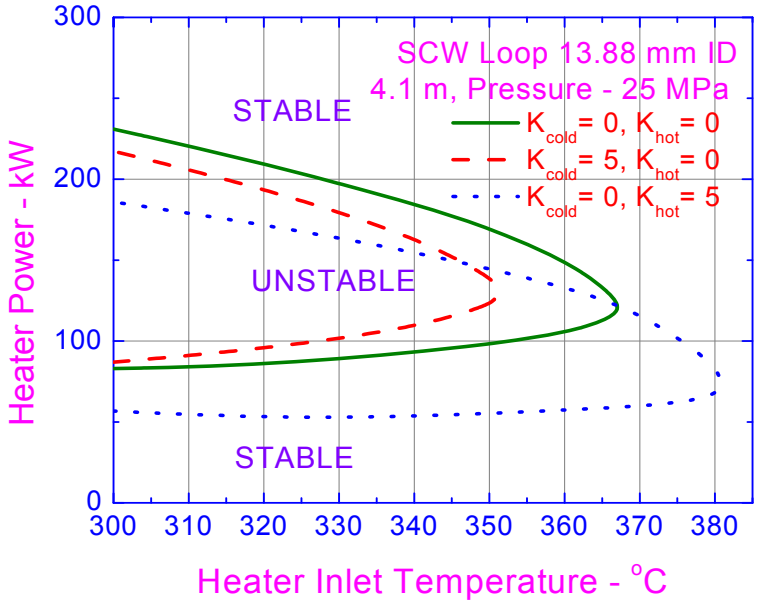

(a)

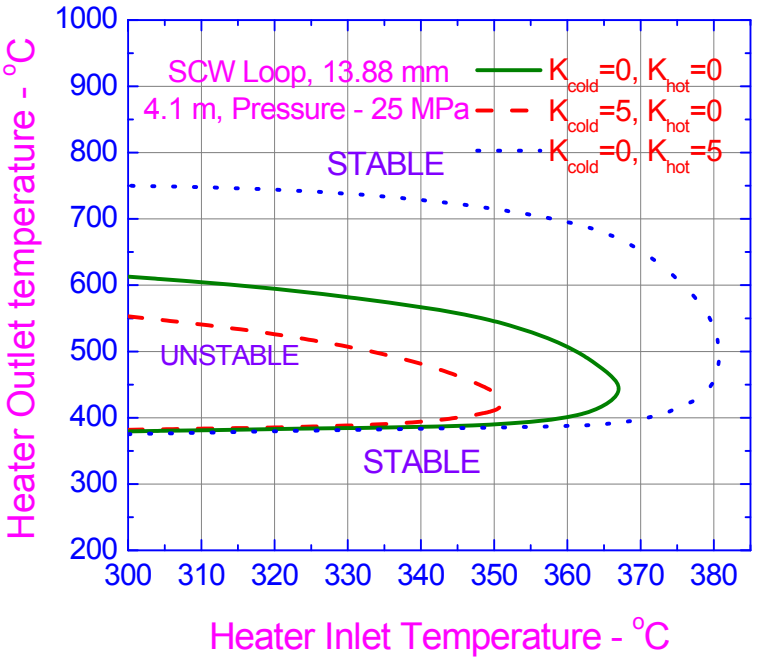

(b)

Figure 2-20: Effect of local losses on stability behavior of SPNCL

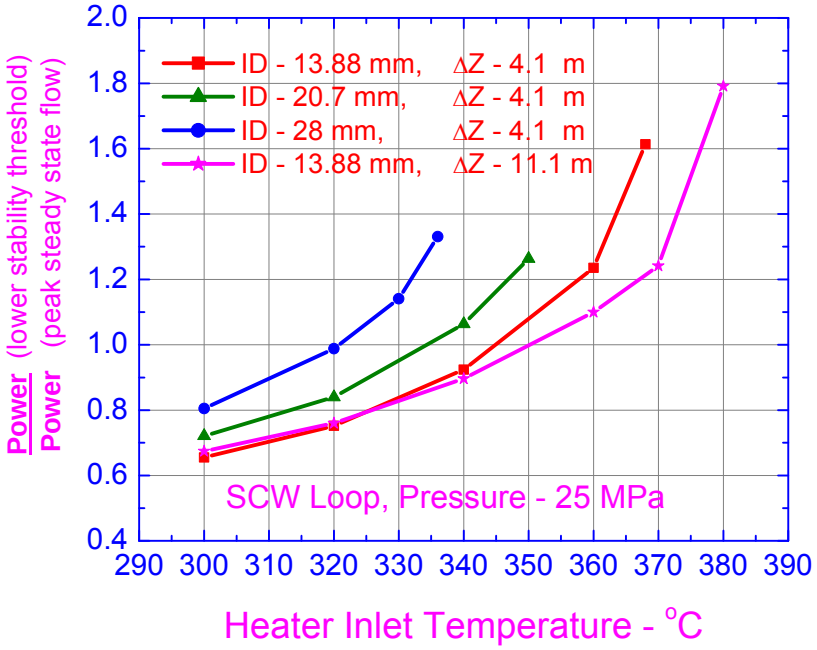

Figure 2-21: Effect of geometrical parameters on the ratio of lower threshold power of instability and power at peak flow for SPNCL.

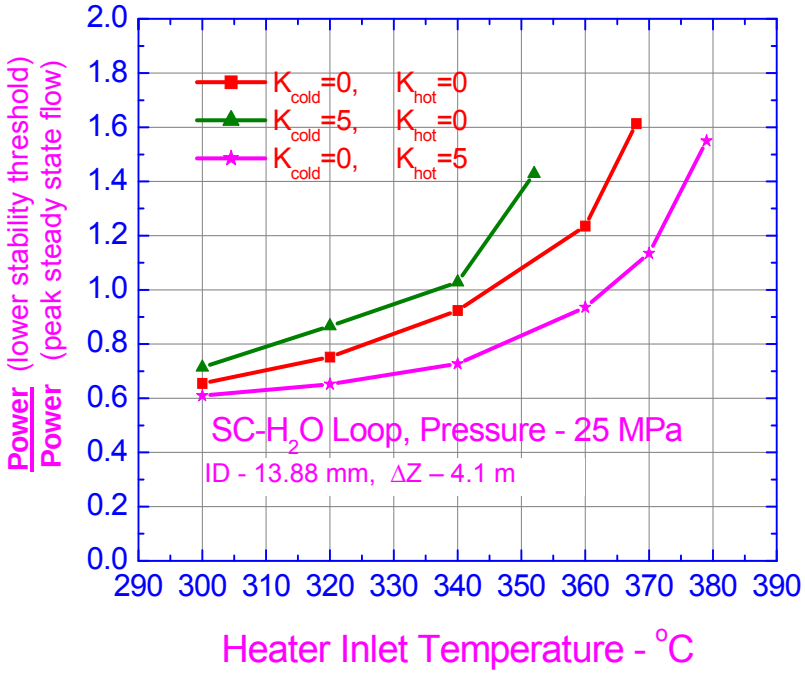

Figure 2-22: Effect of local losses on the ratio of lower threshold power of instability and power at peak flow for SPNCL.

Chapter 3

Non – linear thermal hydraulic stability code for natural circulation with supercritical fluids

3.1 Introduction

The equations for supercritical flow are highly non-linear and classical linear theroy can only be applied to linear system. A linear system can be constructed by linearizing the non-linear equations with the presumption that non-linear system will behave in a linear manner if the perturbation is small enough. The procedure can only tell if the initial small perturbation will grow or decay, but it cannot predict limit cycle oscillations as those will be governed by non-linear effects. Hence non-linear thermal hydraulic stability code was developed to study the transient response of the system in time domain. Non-linear approach relies on finite difference to approximate the partial derivatives and solving the resultant algebraic equations is time consuming, since large number of cases need to be run to generate a stability map, however, with ever increasing computational resources the time domain stability analysis has also become very popular. Several researchers have reported non-linear stability models for stability analysis of natural circulation systems/ heated channels operating with supercritical fluids (see Chatoorgoon (2001); Jain and Rizwan-uddin (2008);Ambrosini and Sharabi (2008); Ortega Gomez et al. (2008); Chen at al. (2010)).

3.2 Non-linear code development

A **NO**n-**L**inear **ST**ability **A**nalysis (NOLSTA) code has been developed for analyzing stability of natural circulation loops operating with supercritical fluids with open loop boundary conditions

as described in Chapter 2. In an open loop the inlet fluid temperature to heater is fixed irrespective of the heater power. For analysis of an open loop, whatever heat is supplied to the heater is rejected in the cooler keeping the heater inlet temperature constant. In this case, the operating pressure of the loop, inlet fluid temperature to the heater and the heater power are specified along with the entire geometry of the loop (hydraulic diameter, flow area and length of each pipe).

3.2.1 Governing equations

In one dimensional analysis the only co-ordinate *x*, runs around the loop with origin at the outlet of cooler. The governing continuity, momentum and energy equations for one dimensional flow can be written as,

Continuity:

$$\frac{\partial \rho}{\partial t}+\frac{\partial(\rho u)}{\partial x}=0 \tag{3.1}$$

Momentum:

$$\frac{\partial(\rho u)}{\partial t}+\frac{\partial(\rho u^2)}{\partial x}+\frac{\partial p}{\partial x}+\left(\frac{f}{D}+K\right)\frac{\rho u^2}{2}+\rho \mathrm{g}\cos\phi=0 \tag{3.2}$$

Energy:

$$\frac{\partial\left[\rho\left(i+\frac{u^2}{2}\right)\right]}{\partial t}+\frac{\partial\left[\rho u\left(i+\frac{u^2}{2}\right)\right]}{\partial x}+\rho u \mathrm{g}\cos\phi=q'''+\frac{\partial p}{\partial t} \tag{3.3}$$

In addition an equation of state is required for the density and is given by

$$\rho = f(p,i) \tag{3.4}$$

The set of mass, momentum and energy conservation equations is closed by equation of state for the supercritical fluid. The steady state solution can be obtained by dropping the time derivatives from the above equations. These are

$$\frac{\partial(\rho u)}{\partial x} = 0 \tag{3.5}$$

$$\frac{\partial(\rho u^2)}{\partial x} + \frac{\partial p}{\partial x} + \left(\frac{f}{D} + K\right)\frac{\rho u^2}{2} + \rho g \cos\phi = 0 \tag{3.6}$$

$$\frac{\partial\left[\rho u\left(i + \frac{u^2}{2}\right)\right]}{\partial x} + \rho u g \cos\phi = \begin{cases} q_h''' \text{ or } -q_c''' & \text{for heater or cooler region,} \\ 0 & \text{adiabatic region.} \end{cases} \tag{3.7}$$

Control volume discretization in space is employed to derive the difference equations for mass, momentum and energy conservation. In deriving the difference equations, the effect of integrating across a computational cell is analogous to averaging the field variables in that section and leads to better accuracy compared to first order difference schemes for the spatial derivatives (Dogan et al., 1983).

3.2.2 Discretization of governing equations for steady state solution

Integrating the steady state mass, momentum and energy equations (3.5, 3.6 and 3.7) across the control volume from *j* to *j*+1, where *j* & *j*+1 are grid points at inlet and outlet face of the control volume(as shown in figure 3-1), leads to following set of discretized equations:

Continuity:

$$(\rho u)_{j+1} = (\rho u)_j \tag{3.8}$$

Momentum:

$$p_{j+1} = p_j - \left(1 + \frac{1}{4}\left(\frac{f}{D}\Delta x + K\right)\right)(\rho u^2)_{j+1} + \left(1 - \frac{1}{4}\left(\frac{f}{D}\Delta x + K\right)\right)(\rho u^2)_j - \left(\frac{\rho_j + \rho_{j+1}}{2}\right) g\,\Delta z \qquad (3.9)$$

Energy:

$$\left(i_{j+1} + \frac{u_{j+1}^2}{2}\right) = \left(i_j + \frac{u_j^2}{2}\right) - g\Delta z + \frac{(q_h''' \text{ or } -q_c''')\,\Delta x}{(\rho u)_j} \quad \textit{for heater or cooler} \qquad (3.10)$$

Equation of state:

$$\rho_{j+1} = f(p_{j+1}, i_{j+1}) \qquad (3.11)$$

Boundary conditions for open loop:

(i) The heat coming from heater is rejected in the cooler which is imposed directly and this condition maintains heater inlet temperature constant.

(ii) The pressure at the inlet face of first control volume and that calculated by equation (3.9) for the outlet face of last control volume should be constant. However, for natural circulation conditions the two should be equal also (i.e. $\Sigma\Delta p = 0$).

While the density at any axial distance is known from equation (3.11), the friction factor in the single-phase region (sub-critical or supercritical), is obtained from the local Reynolds number as follows.

$$f_{la\,\min\,ar} = 64/Re \quad \text{for laminar flow} \qquad (3.12)$$

$$f_{turbulent} = 0.316/Re^{0.25} \quad \text{for turbulent flow} \qquad (3.13)$$

and friction factor used in the calculations is selected as the maximum value calculated by the above two equations, i.e.

$$f = \text{maximum of } (f_{laminar}, f_{turbulent}) \qquad (3.14)$$

This has been done to avoid discontinuity in the friction factor value during transition from laminar to turbulent flow.

3.2.3 Discretization for time dependent solution

Integrating time dependent conservation equations (3.1), (3.2) & (3.3) across the control volume from *j* to *j*+1 leads to following set of discretized equations:

Continuity:

$$(\rho u)_{j+1}^{n+1} = (\rho u)_{j}^{n+1} - \left(\rho_{j+1}^{n+1} - \rho_{j+1}^{n} + \rho_{j}^{n+1} - \rho_{j}^{n}\right)\frac{\Delta x}{2\,\Delta t} \tag{3.15}$$

Momentum:

$$p_{j+1}^{n+1} = p_{j}^{n+1} - \left(1 + \frac{1}{4}\left(\frac{f}{D}\Delta x + K\right)\right)(\rho u^2)_{j+1}^{n} + \left(1 - \frac{1}{4}\left(\frac{f}{D}\Delta x + K\right)\right)(\rho u^2)_{j}^{n} - \left(\frac{\rho_{j}^{n} + \rho_{j+1}^{n}}{2}\right) g\,\Delta z$$
$$- \left((\rho u)_{j+1}^{n+1} - (\rho u)_{j+1}^{n} + (\rho u)_{j}^{n+1} - (\rho u)_{j}^{n}\right)\frac{\Delta x}{2\,\Delta t} \tag{3.16}$$

Energy:

$$\left[i_{j+1}^{n+1} + \frac{\left(u_{j+1}^2\right)^{n+1}}{2}\right]\left((\rho u)_{j+1}^{n+1} + \frac{\Delta x}{2\,\Delta t}\rho_{j+1}^{n+1}\right) - \left[i_{j}^{n+1} + \frac{\left(u_{j}^2\right)^{n+1}}{2}\right](\rho u)_{j}^{n+1} + \left((\rho u)_{j+1}^{n+1} + (\rho u)_{j}^{n+1}\right)g\frac{\Delta z}{2} + T$$
$$= q'''\Delta x + \frac{\Delta x}{2\,\Delta t}\left(p_{j+1}^{n+1} + p_{j}^{n+1} - p_{j+1}^{n} - p_{j}^{n}\right) \tag{3.17}$$

where

$$T = \frac{\Delta x}{2\,\Delta t}\left[i_{j}^{n+1} + \frac{\left(u_{j}^2\right)^{n+1}}{2}\right]\rho_{j}^{n+1} - \frac{\Delta x}{2\,\Delta t}\left[\left(i_{j+1}^{n} + \frac{\left(u_{j+1}^2\right)^{n}}{2}\right)\rho_{j+1}^{n} + \left(i_{j}^{n} + \frac{\left(u_{j}^2\right)^{n}}{2}\right)\rho_{j}^{n}\right] \tag{3.18}$$

3.3 Stability analysis using NOLSTA code

To start with non-linear stability analysis a comparison of steady state results is mandatory. A comparison of steady state results for 13.88 mm ID loop (dimensions shown in Chapter 2, Figure

2-1) by NOLSTA and SUCLIN is given in Figure 3-2. The steady state results predicted by NOLSTA and SUCLIN are identical.

The non-linear stability analysis involves solution of steady –state equations for a given operating condition. The steady state solution is used as an initial condition for transient predictions. Then, difference equations have been solved in time domain to predict the transient response of the loop from the steady state. If the amplitude of flow oscillation increases with time then loop is unstable, if the amplitude of flow oscillation dies out with time and returns to the original steady state then the loop is stable and if flow continues to oscillate with the same amplitude then the loop is neutrally stable.

3.3.1 Sensitivity study

The stability analysis of SPNCL was carried out for open loop boundary conditions and stability threshold has been found to be sensitive to convergence value of loop pressure closure condition, the time step and grid size considered for analysis. Hence convergence value of loop pressure closure, time step and grid size independence test was carried out for SPNCL.

3.3.1.1 Effect of time step and grid size

To start with 1422 nodes were considered in the whole loop and time steps were changed to carry out the stability analysis of SPNCL at 100kW/ 25 Mpa with cold leg/ heater inlet temperature of 360 ^{o}C. It was observed that larger time steps (0.02 s) stabilized the predictions as shown in figure 3-3. On reducing the time step from 0.005 s to 0.0025s the predictions hardly change. Now considering 0.0025 as the time step the number of nodes were reduced to 284 and

then to 142, however, no change was observed in the results as shown in figure 3-4. Hence to save computational time the 142 nodes were finalized. Henceforth, 142 nodes and time step of 0.0025 s have been used for generating the stability results for SPNCL with open loop boundary conditions.

3.3.1.2 Effect of convergence value of loop pressure closure condition

For open loop natural circulation the pressure closure condition to be satisfied at any time step is $\Sigma\Delta p = 0$, where $\Sigma\Delta p$ is sum of pressure drop for all the components of the loop. The solution is converged if $\left|\sum \Delta p\right| \leq convergence\ value$. The stability predictions are found to be dependent on this convergence value as shown in figure 3-5. Unrealistic oscillations are predicted for convergence value of 100 Pa, whereas similar oscillations are predicted for 10 Pa and 1 Pa. Convergence value of 10 Pa has been considered for further analysis.

3.3.1.3 Prediction of stable, unstable and neutrally stable conditions

Considering above mentioned values of number of nodes (142), time step (0.0025s) and loop pressure closure convergence criterion (10 Pa) a typical stable (85kW), unstable (100kW) and neutrally stable (92kW) case was obtained at 25 MPa and 360^{o}C coldleg/heater inlet temperatureas shown in figure 3-6.

3.3.2 Stability analysis of SPNCL using NOLSTA code

The stability maps have been generated using NOLSTA code for 13.88 mm and 28 mm ID loops as shown in figures 3-7a &3-7b and figures 3-8a &3-8b respectively.

The NOLSTA code also predicts a lower as well as upper stability threshold for given heater inlet temperature but the upper threshold is predicted at high heater outlet temperatures and due to availability of Supercritical water (SCW) properties only up to 1000^{o}C the complete stability map at low heater inlet temperatures could not be generated. The NOLSTA code predicts larger unstable zone as compared to SUCLIN. The heater inlet temperature at which no instability is observed also reduces with increase in loop diameter. The results of NOLSTA and SUCLIN are matching qualitatively, but quantitatively there is a difference. Figures 3-9a &3-9b show the lower threshold of instability predicted by NOLSTA and SUCLIN for 13.88 mm and 28 mm ID loops respectively in greater detail. Both the results show that with increase in heater inlet temperature, the threshold heater outlet temperature at which instability occurs also increases and it is not always near the pseudo-critical temperature. Hence, it can be concluded that stability threshold of SPNCL is not confined to the near peak region of the steady state mass flow rate versus power curve as concluded in Jain et al. 2006 (since peak of steady mass flow rate versus power curve for SPNCL is at heater outlet temperature near the pseudo-critical temperature for both the inside diameters, see figure 2-10a & 2-10b).

3.4 Benchmarking of stability codes for supercritical fluids

Bhabha Atomic Research Centre (BARC) participated in the blind benchmark exercise coordinated by the University of Pisa in the frame of the IAEA Coordinated Research Programme (CRP) on Heat Transfer Behavior and Thermo-hydraulics Codes Testing for SCWR. The benchmarking activity was decided during the 1st Research Coordination Meeting of CRP held at Vienna, 22-25 July, 2008. Main objective of the benchmarking activity was to compare the results of linear and non-linear codes and models in the application to flow stability behavior

in a simple reference geometrical condition. The addressed problem involves a circular pipe with uniform heating along the axis and geometrical configuration is shown in Figure 3-10. It consists of a circular rough pipe with uniform cross section assumed to join two plena, mainly included to assign inlet and outlet conditions. The length is assumed to be 4.2672 m (14 ft) and the ID is 8.36 mm corresponding to a SCWR sub-channel. Uniform value of the roughness parameter, ε = 2.5×10^{-5} m, is assigned for the pipe wall. The boundary conditions involves:

1) Imposed inlet pressure(p_{in}) and imposed outlet pressure(p_{out}) such that p_{in} - p_{out} = 0.12 MPa. This means that flow is forced circulation.
2) Throttling at inlet i.e K_{in} = 20

The benchmark exercise was to be carried out for different outlet throttling conditions (K_{out} = 2, 5, 10, 20), different orientation i.e. vertical/ horizontal subchannel, different inlet pressures and different fluids i.e. water, carbon dioxide, ammonia and refrigerant R23. The exercise also addressed both dynamic (oscillatory) and static (excursive) instabilities. Eight institutes from different countries participated in the benchmark exercise as given in Table 3-1.

The reference data (which was not disclosed to the participants) was generated by the University of Pisa. The participants were requested to express the threshold of instability in terms of dimensionless numbers as specified below-

Sub - pseudo - critical number , $N_{SPC} = \frac{\beta_{pc}}{C_{p,pc}}(i_{pc} - i_{in})$, similar to subcooling number in two phase flow.

Trans-pseudo-critical number, $N_{TPC} = \frac{Q}{w_{in}} \frac{\beta_{pc}}{C_{p.pc}}$, similar to phase change number in two phase flow

Table 3-1: Participants in blind benchmark exercise conducted under IAEA Coordinated Research Programme (CRP).

ORGANISATION	**SCIENTISTS**
VTT, Valtion Teknillinen, Tutkimuskeskus, Finland	Markku Hänninen, Jorma Kurki
University of Manitoba and AECL, Canada	V. Chatoorgoon, S. Yeylaghi and L. Leung
BARC, Bhabha Atomic Research Centre, India	Manish Sharma,P.K. Vijayan, D.S. Pilkhwal and D. Saha,
JRC-IE, Petten, Netherlands	L. Ammirabile
Gidropress, Russia	Andrey N. Churkin
Gruppo di Ricerca Nucleare di San Piero a Grado Pisa, Italy and McMaster University, Canada	F. Fiori, D.R. Novog and A. Petruzzi

The above *sub-pseudo-critical* number and *trans-pseudo-critical* number introduced in Ambrosini and Sharabi (2006, 2008), were used respectively to specify inlet fluid thermodynamic conditions (e.g., inlet specific enthalpy) and for representing threshold power of instability respectively. BARC submitted results for water at 25 MPa inlet pressure with different outlet throttling conditions, different orientations and oscillatory/ excursive instability using both Linear code (SUCLIN) and Non-linear code (NOLSTA). The results were generated in

dimensional form by both the codes and later converted to dimensionless form. After benchmark exercise was over, University of PISA compiled a quick look report by Ambrosini, (2010) comparing results of different participants with reference data.

3.4.1 Benchmark results predicted by NOLSTA code

3.4.1.1 Vertical channel

The dimensional values of channel power, channel outlet temperature and steady state mass flow rate corresponding to threshold of instability are given in figure 3-11a, 3-11b& 3-11c respectively. The only data point corresponding to the threshold of excursive instability is observed at low value of channel inlet temperature and higher value of outlet throttling condition. The threshold power of instability reduces with increase of outlet loss coefficient thus making the channel more unstable as shown in figure 3-11a which is similar to observation for boiling natural circulation loop (Kyung et al., 1994). Higher outlet temperatures can be achieved in the channel for lower outlet loss coefficients without encountering instability as shown in figure 3-11b. The steady state mass flow rate corresponding to threshold of excursive instability shows a sudden increase as compared to mass flow rates corresponding to oscillatory instability as shown in figure 3-11c.

The threshold of excursive instability has been obtained by steady state conservation equations, where channel pressure drop characteristics and driving pressure drop are plotted with channel mass flow rate. If there are more than one point where the two curves intersect (indicating multiple steady state operating points), the system is prone to excursive instability also called as

Ledinegg instability.The typical case of excursive instability for vertical/ horizontal channel is shown in figure 3-12a & 3-12b respectively.

Figure 3-13, respresents the comparison of NOLSTA code results with reference stability boundaries in the N_{SPC}- N_{TPC} plane and same are found to closely matching. The lower lobe of the refernce data indicates threshold of oscillatoy instability and upper lobe indicates threshold of excursive instability.

3.4.1.2 Horizontal channel

The governing equations remain same for horizontal and vertical channel. Only the gravitational term (g) is made equal to zero in the momentum equation for horizontal channel. The threshold of oscillatory instability is same for vertical and horizontal channel, whereas, the horizontal channel is excursively more unstable as shown in figure 3-14 in the N_{SPC}- N_{TPC} plane**.**

3.4.2 Benchmark results predicted by SUCLIN code

The threshold of oscillatory instability has been judged by Nyquist criterion which states that if the Nyquist contour of transfer function Y(s) encircles the origin then the system is unstable, if it does not encircle origin then system is stable and if it passes through origin the system is neutrally stable or at the threshold of instability. The methodology of finding the threshold of excursive instability is same as described in section 3.4.1.1. SUCLIN code predictions have been compared with reference stability boundaries for vertical and horizontal channels in figures 3-15& 3-16 respectively. As observed for natural circulation in section 3.3.2, the SUCLIN code is

predicting a smaller unstable zone as compared to NOLSTA code/ reference data.This can be attributed to differences in the linear and non-linear analysis specified below

i) All the fluid properties are perturbed in non-linear analysis, whereas only enthalpy and specific volume perturbation is considered in linear stability analysis.

ii) Friction factor perturbation is not considered in linear stability analysis whereas non-linear analysis accounts for it.

iii) The perturbation induced in specific volume due to perturbation in enthalpy has been considered, whereas perturbation in specific volume due to perturbation in pressure has been neglected in linear analysis, whereas non-linear analysis accounts for both.

The results reported by other participants also showed some deviations from the reference data, however all submissions confirmed the following findings

- Increase in outlet throttling results in increase in unstable zone of heated channels (a well-known fact for two phase flow in heated channels);
- The presence of oscillating as well as excursive instabilities, the latter occurring at relatively low inlet temperature, in regions that would be hopefully of little interest to nuclear reactor operation;
- The general shape of the stability boundary in the NTPC-NSPC plane.

3.5 Conclusions

The non-linear stability analysis code (NOLSTA) also confirms that larger diameter loops are more unstable in terms of heater power compared to small diameter loops and beyond a specified value of heater inlet temperature no instability is observed and its value decreases with increase in loop diameter. With increase in heater inlet temperature the threshold heater outlet temperature at

which lower threshold of instability is observed also increases and is not always near the pseudo-critical temperature. Therefore, it can be concluded stability threshold of SPNCL is not confined to the near peak region of the steady state mass flow rate versus power curve.

The results of NOLSTA and SUCLIN are matching qualitatively, but quantitatively there is a difference. Both the codes predict lower and upper threshold of instability, but unstable zone predicted by non-linear analysis is larger. This can be attributed to differences in the linear and non-linear analysis as specified below

i) All the fluid properties are perturbed in non-linear analysis, whereas only enthalpy and specific volume perturbation is considered in linear stability analysis.
ii) Friction factor perturbation is not considered in linear stability analysis whereas non-linear analysis accounts for it.
iii) The perturbation induced in specific volume due to perturbation in enthalpy has been considered, whereas perturbation in specific volume due to perturbation in pressure has been neglected in linear analysis, whereas non-linear analysis accounts for both.

BARC also participated in the blind benchmark exercise coordinated by the University of Pisa in the frame of the IAEA Coordinated Research Programme (CRP) on Heat Transfer Behavior and Thermo-hydraulics Codes Testing for SCWR. The addressed problem involved a circular pipe with uniform heating along the axis and geometrical configuration corresponding to a SCWR-sub-channel. Eight institutes from different countries participated in the benchmark exercise. Like SUCLIN code predictions, codes used by other participants also showed some deviation from the reference data generated by University of PISA, however, all submissions confirmed the following findings

- Increase in outlet throttling results in increase in unstable zone of heated channels (a well-known fact for two phase flow in heated channels);
- The presence of oscillating as well as excursive instabilities, the latter occurring at relatively low inlet temperature, in regions that would be hopefully of little interest to nuclear reactor operation;
- The general shape of the stability boundary in the N_{TPC}-N_{SPC} plane.

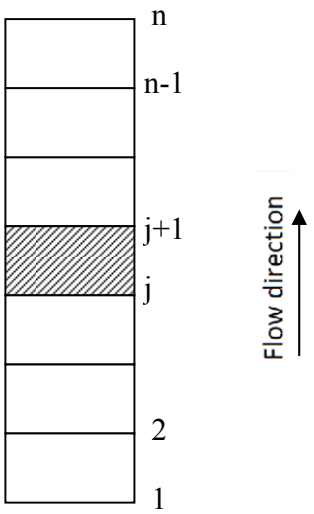

Figure 3-1: Spatial grids and control volumes along the loop flow direction

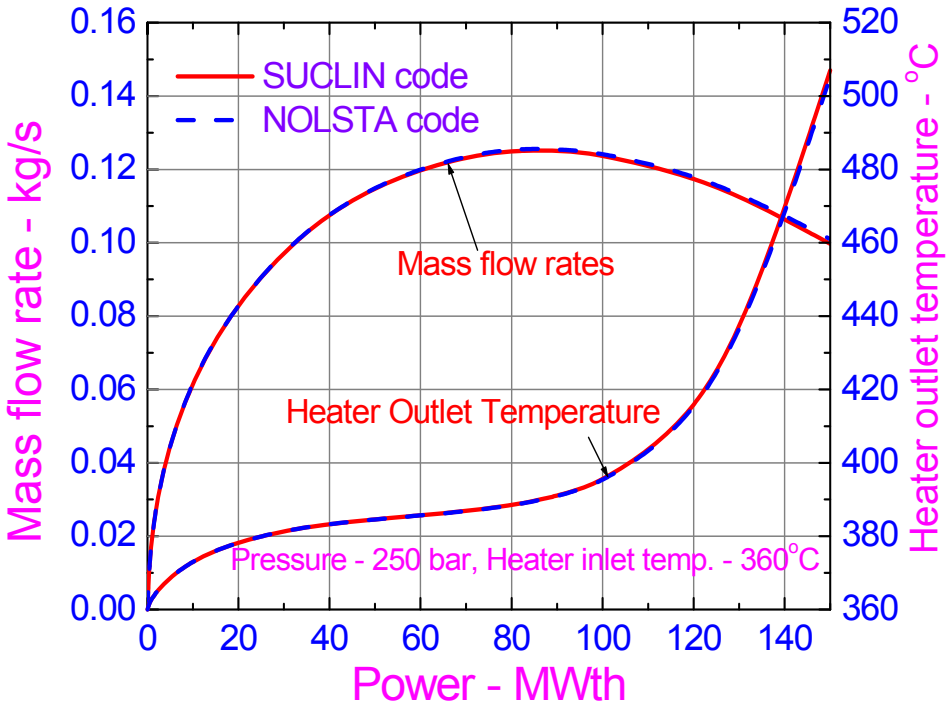

Figure 3-2: Steady state results comparison for 13.88 mm ID loop by SUCLIN and NOLSTA codes

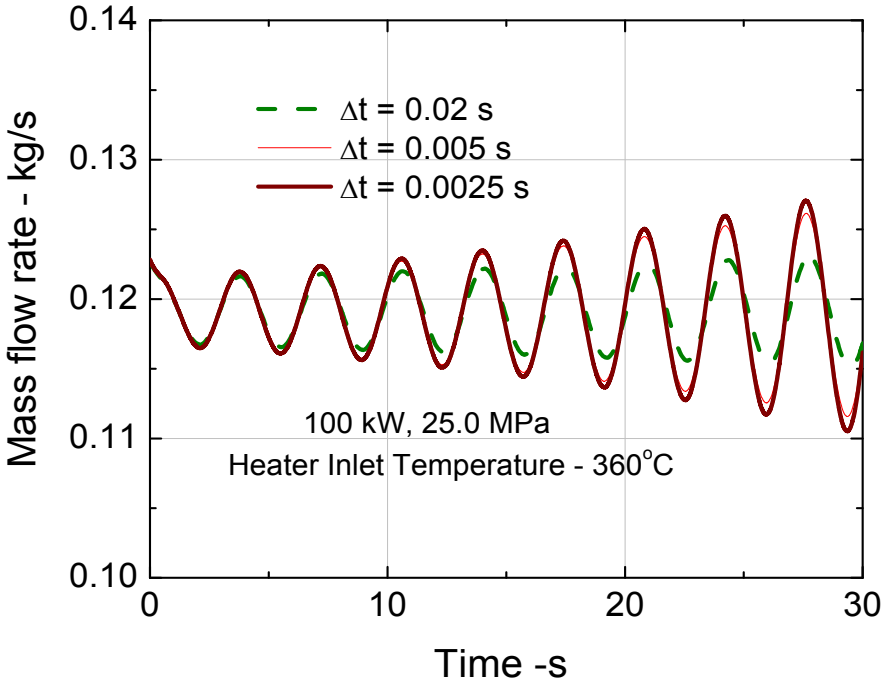

Figure 3-3: Time step sensitivity study on stability behavior of open SPNCL

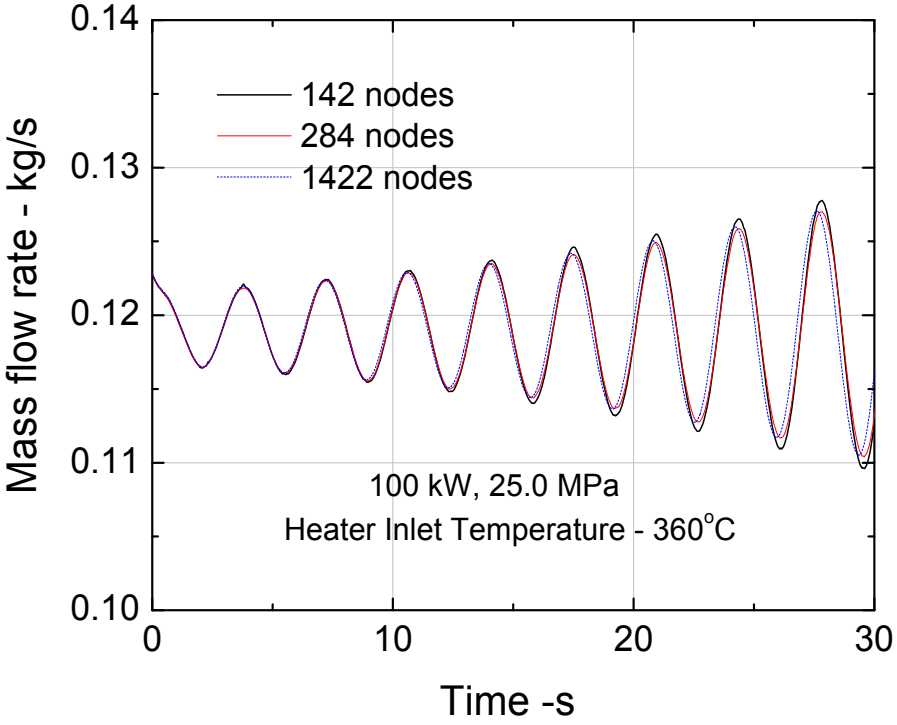

Figure 3-4: Nodes number sensitivity study on stability behavior of open SPNCL

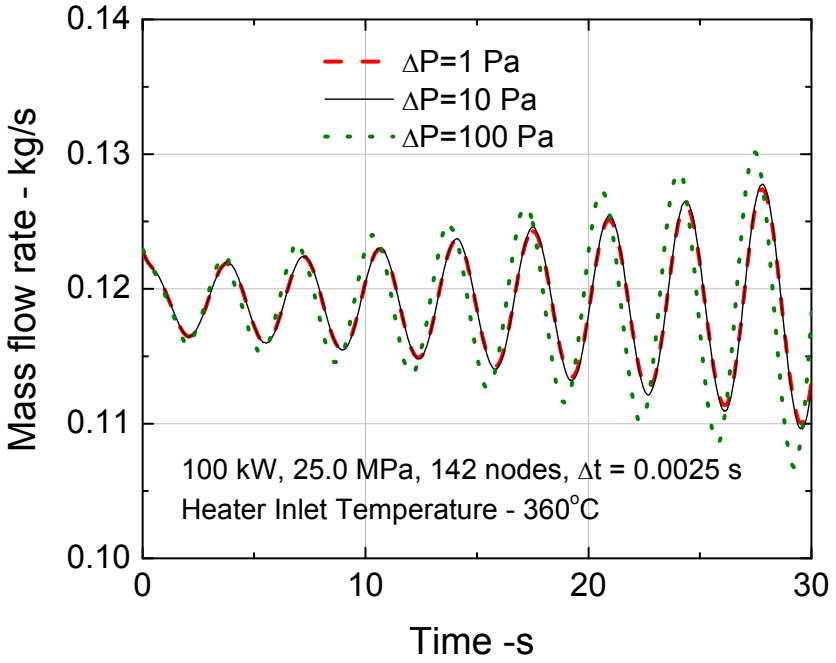

Figure 3-5: Effect of pressure closure convergence criterion on stability behavior of open SPNCL

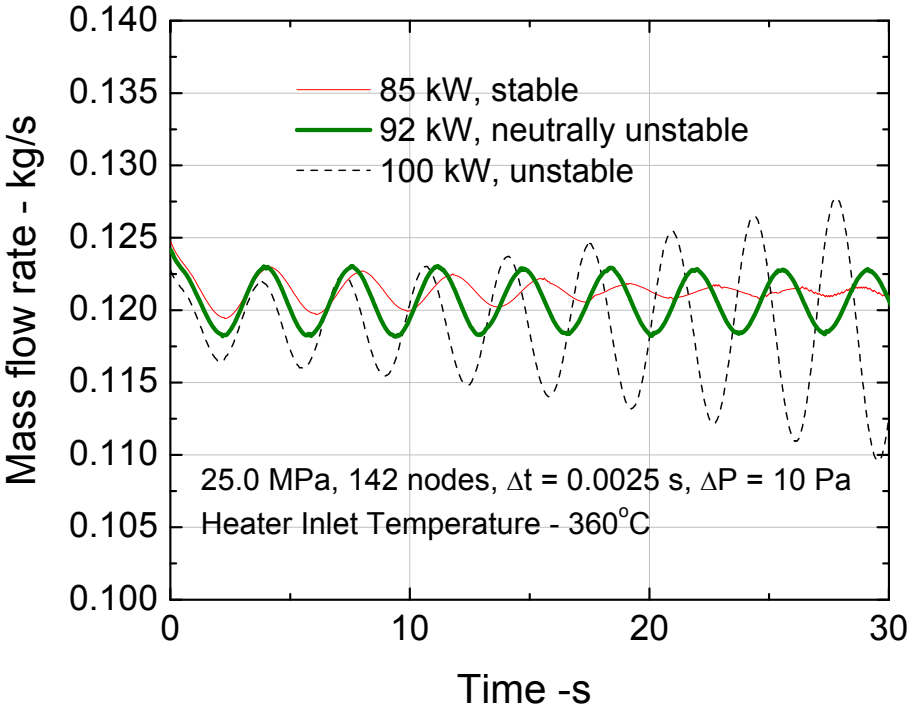

Figure3-6: Stable, unstable and neutrally stable operating conditions for open SPNCL

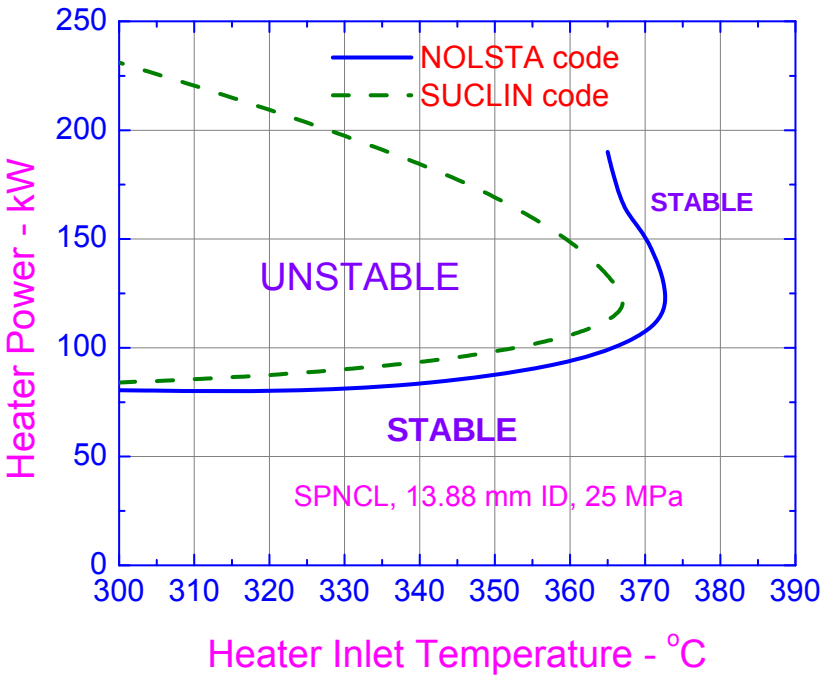

(a)

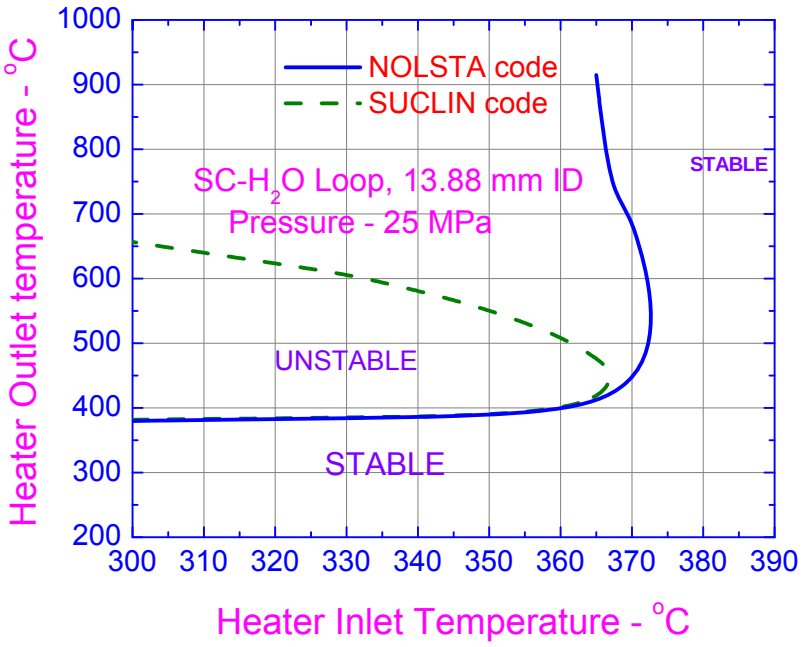

(b)

Figure 3-7: Stability maps comparison using SUCLIN and NOLSTA codes for open SPNCL (13.88mm ID loop).

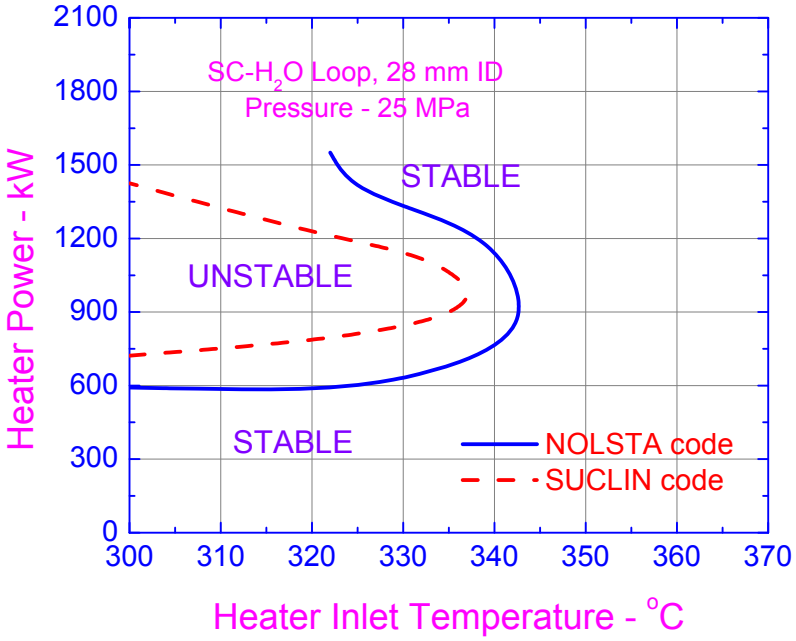

(a)

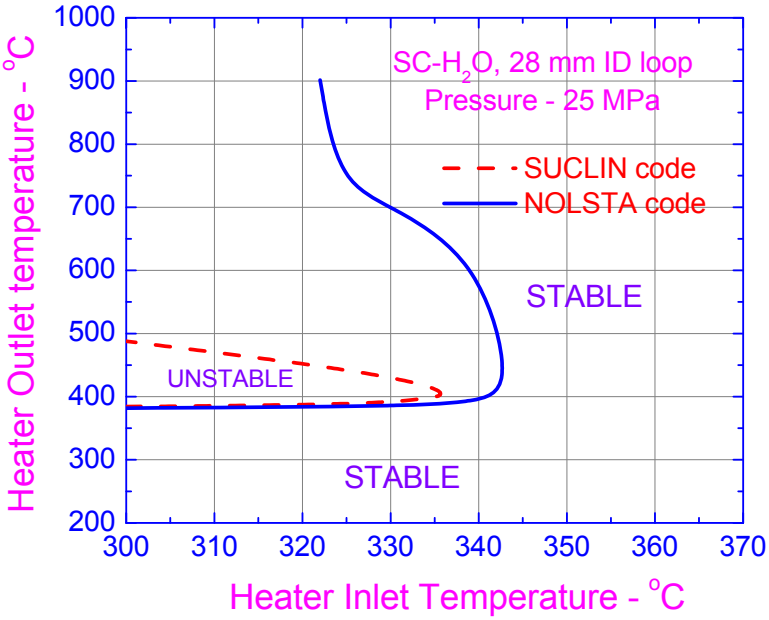

(b)

Figure 3-8: Stability maps comparison using SUCLIN and NOLSTA codes for 28 mm ID loop.

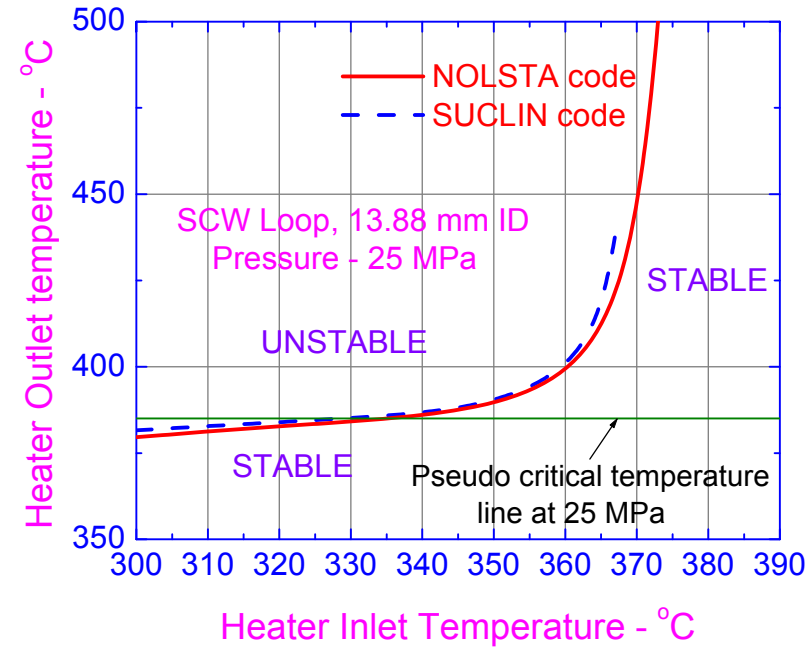

(a)

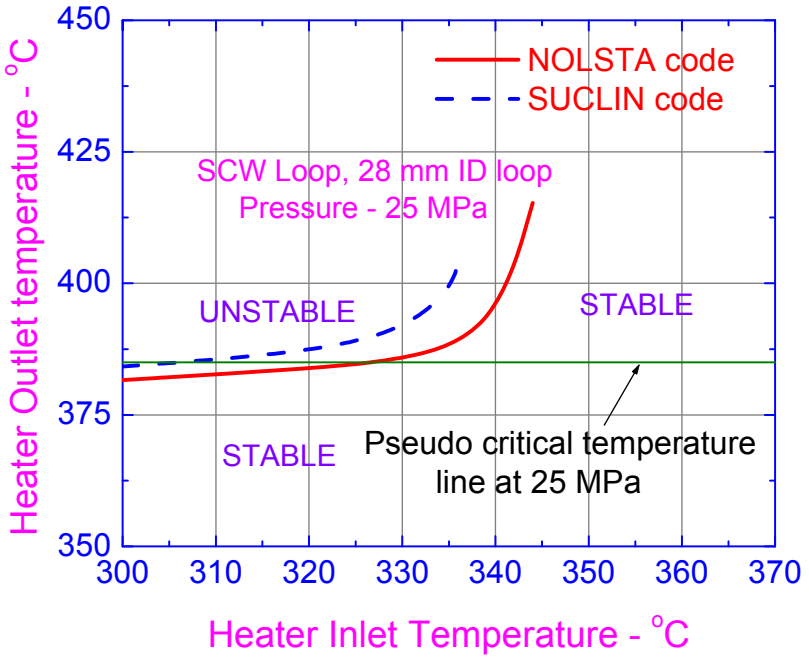

(b)

Figure 3-9: Lower threshold of instability predicted by SUCLIN and NOLSTA codes for 13.88 mm and 28mm ID loops shown in detail

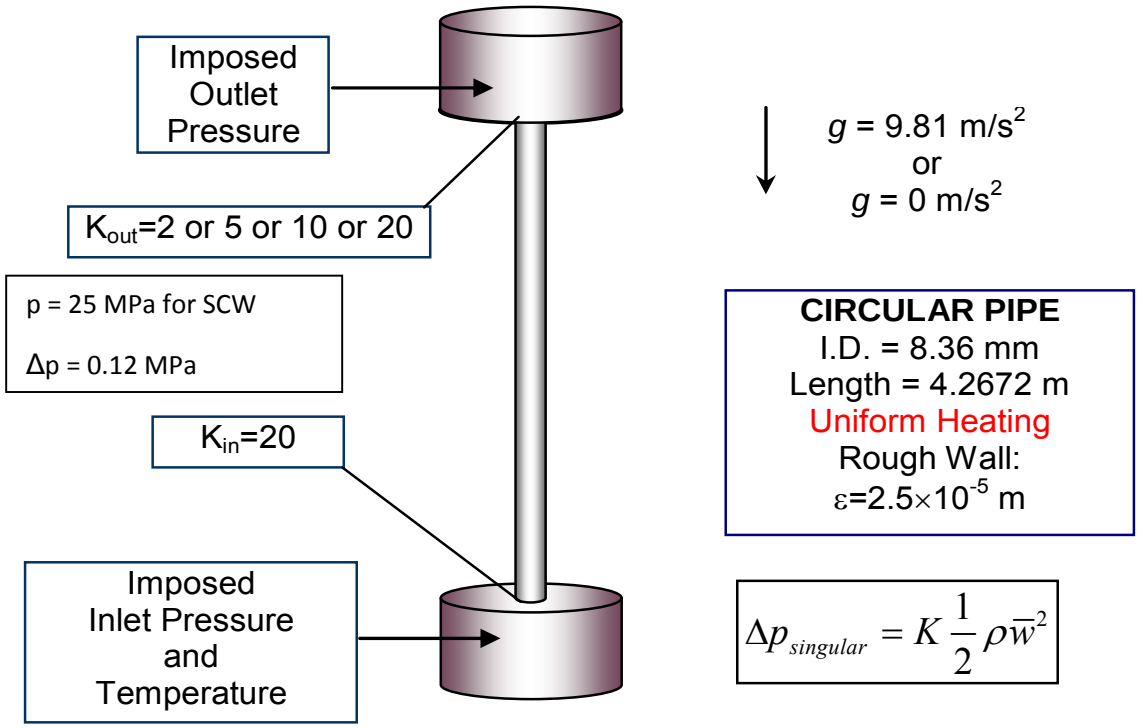

Figure 3-10: Reference geometrical configuration for flow stability benchmark under IAEA Coordinated Research Programme (CRP).

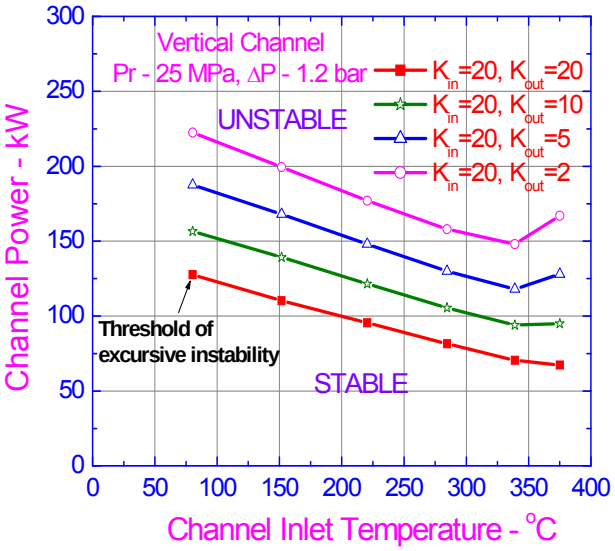

(a)

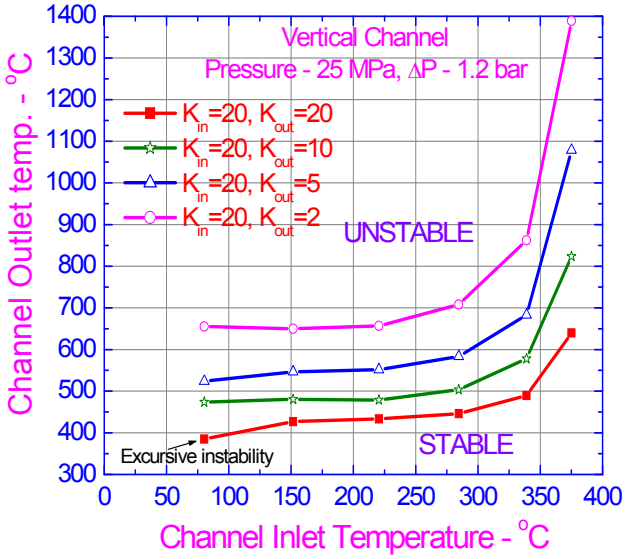

(b)

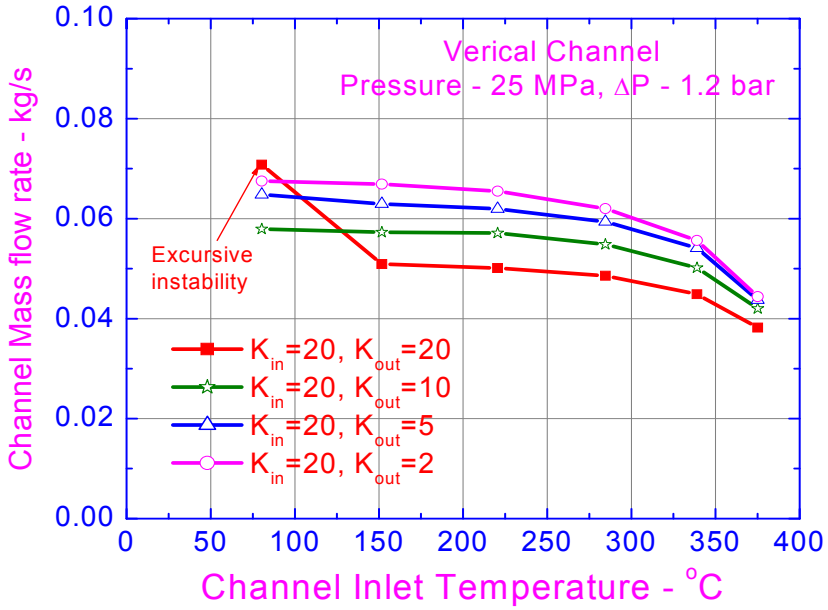

(c)

Figure 3-11: Dimensional parameters corresponding to threshold of oscillatory/ excursive instability for IAEA bench mark exercise.

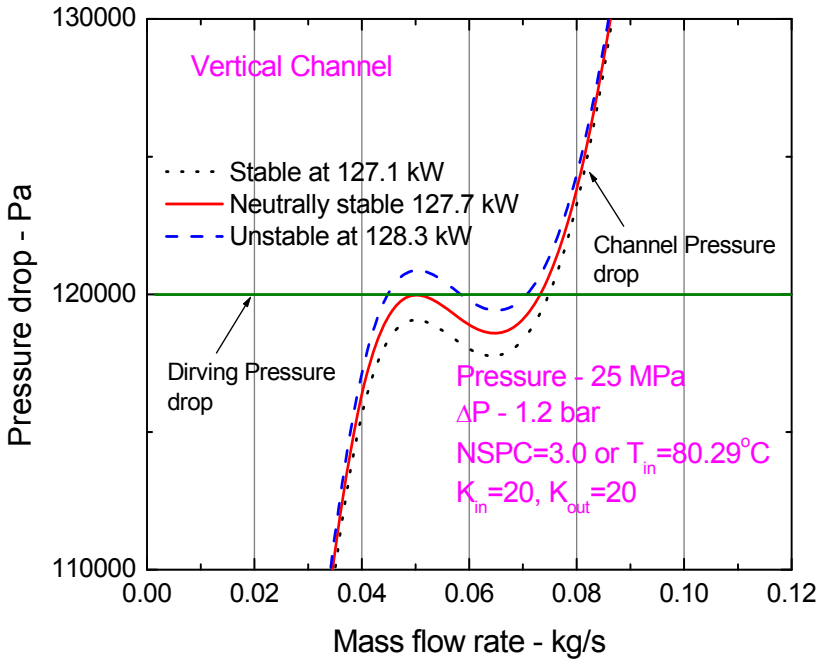

(a)

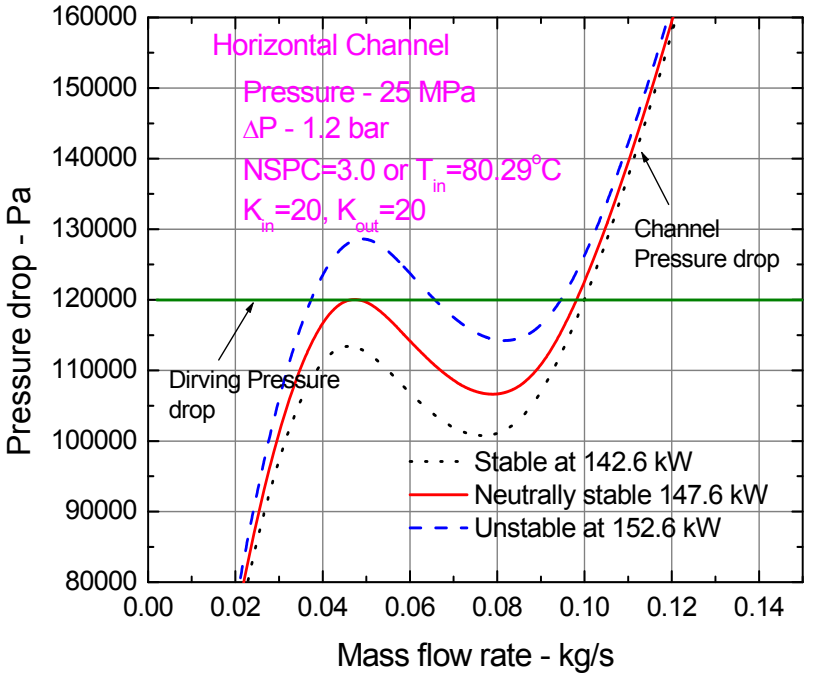

(b)

Figure 3-12: Threshold of Ledinegg/ excursive instability for IAEA bench mark exercise.

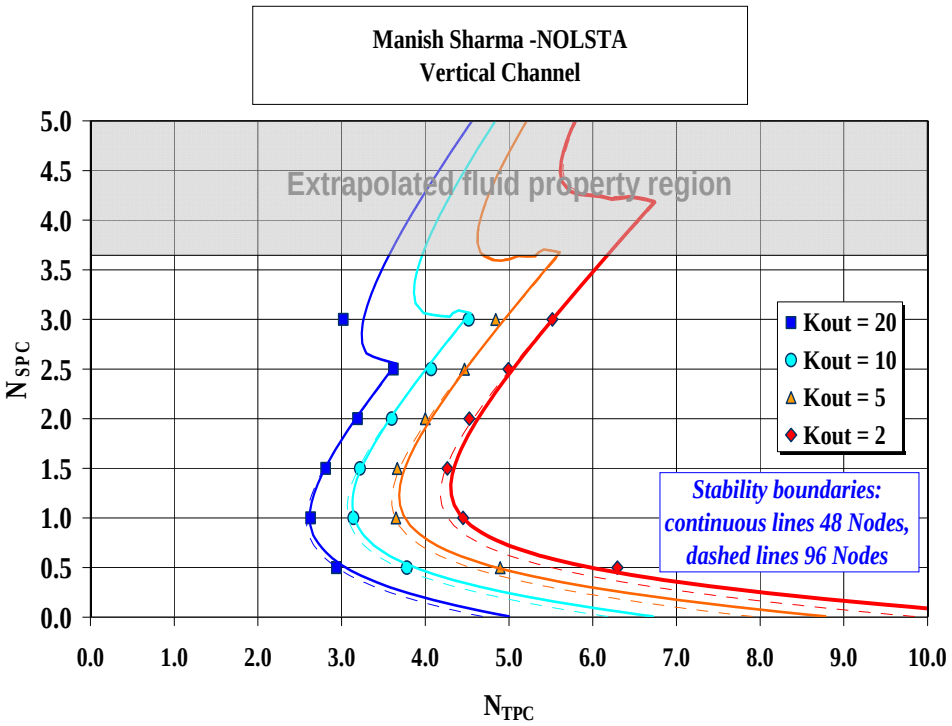

Figure 3-13: Comparison of the stability boundaries identified by NOLSTA code for water and vertical channel with the reference stability boundaries

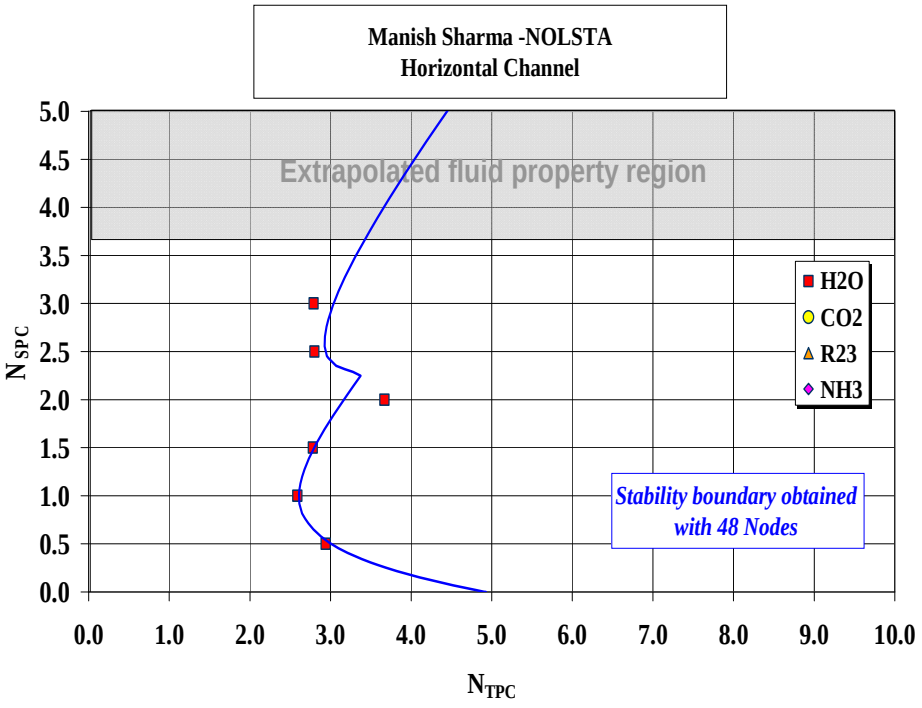

Figure 3-14: Comparison of the stability boundaries identified by NOLSTA code for water and horizontal channel with the reference stability boundaries for $K_{out} = 20$

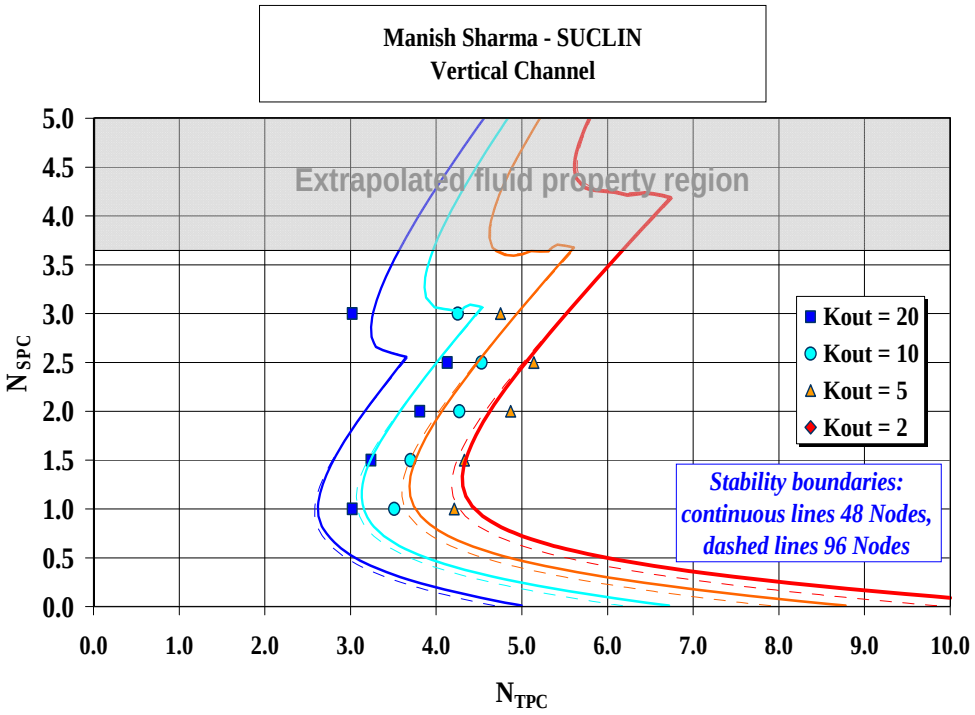

Figure 3-15: Comparison of the stability boundaries identified by the SUCLIN code for water and vertical channel with the reference stability boundaries

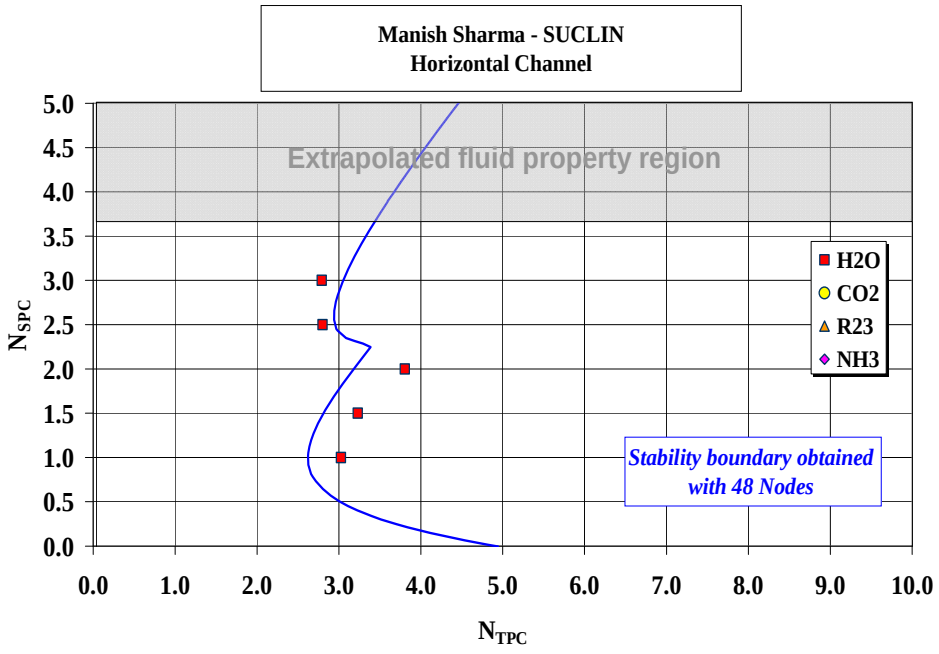

Figure 3-16: Comparison of the stability boundaries identified by the SUCLIN code for water and horizontal channel with the reference stability boundaries

Chapter 4

Steady state behavior of natural circulation loops operating with carbon dioxide at supercritical pressures for open and closed loop boundary conditions

4.1 Introduction

The literature reveals only very few experimental studies on natural circulation with supercritical carbon dioxide (SC-CO_2). Adelt and Mikielewicz (1981) performed studies on 4m high loop with carbon dioxide (CO_2). As the fluid was heated through pseudo-critical point pressure oscillations were observed for a particular test but the study mainly focused upon heat transfer rather than stability. Lomperski et al. (2004) have reported experiments in a two meter high natural circulation loop with carbon dioxide at supercritical pressure. The loop was operated in a base case configuration that maximized flow rates and in a second configuration having an orifice in the hot leg. No flow instabilities were observed in these tests as the fluid was heated through thermodynamic pseudo-critical point. Yoshikawa et al. (2005) have studied the performance of a closed natural circulation loop operating with supercritical CO_2. The performance of the loop was determined by measuring flow velocities of CO_2 which could be correlated to Grashof number, Prandtl number and dimensionless effective density difference. No flow instability has been reported during the experiments. To gain an insight in to steady state, flow stability and heat transfer behavior of natural circulation with supercritical fluids, a Supercritical Pressure Natural Circulation Loop (SPNCL) has been set up and operated in Bhabha Atomic Research Centre (BARC), India. The experiments were conducted with carbon dioxide at supercritical pressures. Carbon dioxide can be considered as a good simulant fluid for

water at supercritical conditions because of analogous change of properties particularly density and viscosity across the pseudocritical point as shown in Figure 4-1a & 4-1b. The computer code NOLSTA desribed in Chapter 3, for steady state and stability analysis of an open loop natural circulation with SCW as working fluid has been modified to carry out analysis of closed loop thermosyphon as well. Moreover, supercritical CO_2 properties obtained from National Institute of Standards and Technology (NIST) database (http://webbook.nist.gov/chemistry/fluid/) were also incorporated in the code.

4.2 The experimental loop

The test facility is a uniform diameter (13.88 mm ID & 21.34 mm OD) rectangular loop named Supercritical Pressure Natural Circulation Loop (SPNCL) with different orientations of heater and cooler, which can operate with either of the two fluids (i.e. supercritical water or supercritical carbon dioxide). The design pressure and temperature of the Test facility is 30 MPa & 450 ^{o}C respectively. The loop material of construction is SS-347. The loop has been operated with carbon dioxide at supercritical pressure (7.7 – 9 MPa). A photograph and schematic of the loop showing the as fabricated length scales is given in Figure 4-2a and Figure 4-2b. The loop can operate with different orientations of heater and cooler (e.g. Horizontal Heater Horizontal Cooler (HHHC), Horizontal Heater Vertical Cooler (HHVC), Vertical Heater Horizontal Cooler (VHHC) and Vertical Heater Vertical Cooler (VHVC)), to study the effect of orientation on natural circulation behavior at supercritical conditions. Heating is achieved by uniformly winding nichrome wire over a layer of fiber glass insulation. The coolers are tube in tube type with carbon dioxide flowing in the inner tube and chilled water (at 9 – 12^{o} C) flowing in the outer annular tube (77.9 mm ID).The loop had a pressurizer connected at the bottom horizontal

leg which takes care of the thermal expansion besides accommodating the cover gas helium above the carbon dioxide. The safety devices of the loop (i.e. two rupture discs, RD1 & RD2) were installed on top of the pressurizer. The entire loop was insulated with three inches of ceramic mat (k=0.06 W/(m K)).

The loop is instrumented with K-type thermocouples to measure the primary fluid and secondary fluid temperatures. Primary fluid temperatures at each location is measured as the average value indicated by two thermocouples inserted diametrically opposite at r/2 from the inside wall whereas secondary fluid temperatures are measured by a single thermocouple located at the tube center. The system pressure is measured with the help of Kellar make pressure transducers. The pressure drop across the bottom horizontal tube and the level in the pressurizer were measured with the help of two differential pressure transmitters. The power of each heater was measured with a Wattmeter. The secondary coolant flow rate or chilled water flow rate is measured with the help of three parallel turbine flow meters each having a range of 0-100 lpm. The accuracy of the thermocouples were within ± 0.5 ^{0}C. The accuracy of the pressure and differential pressure measurements were respectively ± 0.03 MPa and ± 0.18 mm H_2O column. The accuracy of the secondary flow as well as power measurement is ± 0.5 % of the reading.

Before operation with supercritical CO_2 the loop was flushed repeatedly with CO_2 at low pressure including all impulse, drain and vent lines. Subsequently the loop was filled with CO_2 in gaseous form at 5.5 MPa (saturation temp 18.2 ^{o}C) and then both horizontal and vertical coolers were supplied with chilled water (9-12 ^{o}C) flowing on secondary side which resulted in condensation of carbon dioxide. During condensation loop pressure may fall and more CO_2 will be admitted

from the cylinder. This process of filling and condensation will continue till there is no fall in loop pressure. Now, helium was filled on top of pressurizer at desired operating pressure (e.g. 7.7 – 9 MPa). Due to large density difference between CO_2 and Helium i.e. 744.3 kg/m^3 and 13.7 kg/m^3 respectively at 9 MPa/ 30^{o}C, the two fluids are not expected to mix and a level will be formed in the pressurizer. Once the required supercritical pressure was achieved, the helium cylinder was isolated and heater power was switched on and adjusted to the required value. Sufficient time was allowed to achieve the steady state.

4.3 Steady state natural circulation flow analysis with supercritical CO_2 operation

4.3.1 Natural circulation flow analysis of an open loop

First of all code (NOLSTA) has been validated for open loop analysis with experimental data for Supercritical CO_2 available in literature. Lomperski et al. (2004) have reported experimental natural circulation data for carbon dioxide at supercritical pressure for constant heater inlet temperature irrespective of power. The loop orientation is HHHC having ID of 14 mm and height of 2 m. The code predicts the steady state mass flow rate and heater outlet temperature appreciably well as shown in Figure 4-3. A grid size of 0.01 m was used to generate the steady state results. The predicted mass flow rates deviate within -13% to +10% of the experimental flow rates, whereas the predicted heater outlet temperatures differ from -2.5% to +8.5% of the experimental values.

A parametric study has been carried out to study the effect of diameter, orientation, pressure and heater inlet temperature on steady state behaviour of SPNCL of BARC (considering it as an open loop) operating with carbon dioxide at supercritical pressures. A grid size of 0.01 m is used to

generate the steady state results. The steady state characteristics have been predicted for various loop diameters (i.e. 7 mm, 13.88 mm, 20.7 mm and 28 mm) for HHHC orientation with SC-CO_2 (Figure 4-4). The steady state characteristics indicate that with initial increase in power the loop mass flow rate increases due to increase in buoyancy force caused by the increase in density difference between cold leg (having sub-critical carbon dioxide) and hot leg (having supercritical carbon dioxide).

Subsequently, flow decreases with power due to increased frictional pressure drop as can be explained by Figure 4-5. The frictional pressure drop in hot leg represented by inverse of density in hot leg shows an increasing slope whereas buoyancy represented by density difference between hot and cold leg shows a reducing slope with increase in power. This indicates that after certain power the frictional pressure drop will start over-riding the buoyancy head and supercritical natural circulation system will start exhibiting reduction in flow with increase in power. The mass flow rate increases with increase in loop diameter because of reduced frictional resistance. The peak mass flow rates for 7 mm, 13.88 mm, 20.7 mm and 28 mm diameter loops with supercritical carbon dioxide operation at 9 MPa pressure are observed at heater outlet temperature of 50.9^{o}C, 51^{o}C, 49.75^{o}C and 49.47^{o}C respectively (pseudo-critical temperature of CO_2 at 9 MPa is 40^{o}C).

The effect of orientation on steady state mass flow rate for open loop is shown in Figure 4-6. The maximum mass flow rate is achieved for HHHC orientation and minimum for VHVC orientation, since the elevation difference between centre line of heater and cooler is 4.1 m (maximum) and 1.45 m (minimum) for HHHC and VHVC orientation respectively. The elevation difference between centre line of heater and cooler for VHHC orientation (2.8 m) and HHVC orientation

(2.75m) is almost same, but the mass flow rates observed in friction dominant regime for VHHC orientation are much higher than HHVC orientation. This is due to smaller length of supercritical leg or hot leg (e.g. 3.1 m) for VHHC orientation as compared to length of supercritical leg for HHVC orientation (e.g. 8.755 m) for the direction of flow shown in Figure 4-2b, which leads to lower frictional resistance and higher mass flow rate in VHHC orientation.

The mass flow rate increases with pressure at high powers in friction dominant regime just as in two-phase NC systems as shown in Figure 4-7. The steady state natural circulation mass flow rate reduces significantly when heater inlet temperature exceeds the pseudo-critical temperature (e.g. 37^{o}C to 43^{o}C) as shown in Figure 4-8. This is attributed to the reduction in the density difference between hot leg and cold-leg resulting in reduced buoyancy head (as can be observed from Figure 4-1a) and as both the legs become supercritical the frictional resistance increases substantially resulting in large reduction in flow on increasing heater inlet temperature from 37 ^{o}C to 43^{o}C.

4.3.2 Steady state natural circulation flow analysis of closed loop SPNCL

In a closed loop the coolant mass flow rate on secondary side of cooler (e.g. chilled water in SPNCL) is kept constant as heater power is increased. The heater inlet temperature is not fixed and increases with increase in heater power. For analysis of closed loop, the rate of heat rejection in the cooler is evaluated based on calculation of overall heat transfer coefficient for cooler and temperature difference between primary and secondary fluid. In this case, the operating pressure of the loop, coolant mass flow rate & inlet temperature for secondary side of cooler and the

heater power are specified along with the entire geometry of the loop (i.e. hydraulic diameter, flow area and length of each pipe).

The SPNCL of BARC is actually a closed loop where heater inlet temperature is not controlled and only chilled water mass flow rate and inlet temperature on secondary side of cooler is maintained constant. During experiments chilled water temperature shows maximum temperature rise of 1^{o}C.

The governing equations for its analysis remain same as described in sections 3.2.1, 3.2.2 & 3.2.3 of Chapter 3. The procedure to achieve steady state mass flow rate is explained below:

(i) Assume an inlet temperature to heater and calculate the steady state mass flow rate of SPNCL for a given power by assuming total heat rejection in cooler or considering open loop configuration.

(ii) Now taking this flow rate and temperature distribution on primary side of cooler evaluate UA_{htr} × LMTD for cooler.

(iii) If UA_{htr} × LMTD < Power given to heater then increase heater inlet temperature else reduce heater inlet temperature. The iterations converge if UA_{htr} × LMTD is within 99.9% of the power given to heater.

$$\frac{1}{UA_{htr}} = \frac{1}{h_i A_{htri}} + \frac{\ln(d_o/d_i)}{2\pi L k_w} + \frac{1}{h_o A_{htro}} \tag{4.1}$$

$$LMTD = \frac{\Delta T_{out} - \Delta T_{in}}{\ln\left(\frac{\Delta T_{out}}{\Delta T_{in}}\right)} \tag{4.2}$$

where, ΔT_{in} is temperature difference between primary and secondary fluid at inlet of cooler and ΔT_{out} is temperature difference between primary and secondary fluid at outlet of cooler.

To calculate UA_{htr}, the evaluation of inside primary heat transfer coefficient (h_i) and outside secondary heat transfer coefficient (h_o) for cooler is required. The flow on secondary side of cooler is annular as well as thermally and hydro-dynamically developing. For secondary developing laminar flow (i.e. $Re < 2000$), the Nusselt number ($Nu_m = hD/k$) was evaluated based on solution of Navier-Stokes equation for the specific geometry and boundary conditions of the cooler. The values of the same at various Reynolds number are given in Table 4-1. For secondary annular fully developed turbulent flow (i.e. $Re > 5000$) the values of Nusselt number (given in Table 4-1) were taken from Rohsenow & Hartnett (2000). A correction needs to be applied to these values for thermally and hydro dynamically developing turbulent flow as given below

$$\frac{Nu_m}{Nu_\infty} = 1 + \frac{C}{L/D} \quad \text{, where } C = 6.0 \text{ for contraction/ expansion at the entrance.} \qquad (4.3)$$

Table 4-1: Nusselt number evaluation for secondary side flow

	Nusselt number for thermally and hydrodynamically developing annular laminar flow (Nu_m)			Nusselt number for fully developed annular turbulent flow (Nu_∞)	
Prandtl Number	Re = 1000 (developing)	Re = 1500 (developing)	Re = 2000 (developing)	Re = 5000 (developed)	Re = 10000 (developed)
3	-	-	-	46 (39.7)	77.4 (66.8)
9.6	18.69*	22.33*	25.5*	65.8 (58.1)	117.6 (103..8)
10	-	-	-	67 (59.2)	120 (106)

* Nu_m values are for $r = d_i/d_o = 0.274$

Nu_∞ values inside ( ) are for $r = 0.5$ and Nu_∞ values outside ( ) are for $r = 0.2$

For the transition region (i.e. 2000 < *Re* < 5000) linear interpolation is used between *Nu* values computed for thermally and hydro dynamically developing flows at *Re* = 2000 and *Re* = 5000 respectively.

Considering various empirical correlations available in literature for heat transfer to supercritical fluids, inside heat transfer coefficient was calculated using different correlations proposed by Bringer and Smith (1957), Jackson (2002), Swenson et al. (1965) and Shitsman (1959).

Experiments have been conducted in SPNCL with carbon dioxide for different orientations of heater and cooler and steady state data have been compared with predictions of NOLSTA code. All the experimental steady state data for supercritical carbon dioxide has been given in detail in Appendix-I for reference. The elbow loss coefficient has been taken to be 2.5 each (total 4 elbows) for predictions. The higher value of elbow loss coefficient can be justified based on local losses of two blind crosses (one upstream and one downstream of each elbow for temperature and pressure measurement of primary fluid) which have been added to the local loss coefficient of each elbow. The steady state mass flow rate for experimental conditions has been obtained by energy balance as shown below

$$w_{ss} = Q/ (i_{out} - i_{in}) \quad (4.4)$$

Enthalpy at heater outlet (i_{out}) can be calculated from heater outlet temperature and operating pressure measured experimentally and enthalpy at heater inlet (i_{in}) can be calculated from heater inlet temperature and operating pressure measured experimentally. The comparison of experimental data with code results for HHHC orientation is shown in figure 4-9a & 4-9b.

It can be observed from figure 4-9b that experimental heater inlet temperature is not constant and is increasing with power. The temperature difference between heater inlet and outlet is reducing as we are approaching the pseudo-critical temperature (37.9^{o}C for 8.6 MPa) because as one approaches the pseudo-critical temperature the specific heat (c_p) of fluid increases and is maximum at pseudo-critical temperature but as the fluid temperature is increased beyond pseudo-critical point the c_p value again starts reducing (see figure 4-10) resulting in increased temperature difference. The steady state mass flow rate increases till the heater inlet temperature reaches pseudo-critical temperature at 1400 W. As the power is increased beyond 1400 W, both hot and cold leg becomes supercritical and there is a sudden reduction in experimental flow due to increased frictional resistance which is similar to the observation of effect of heater inlet temperature on steady state behavior of open loop (figure 4-8). Moreover the volumetric expansion coefficient is also maximum near the pseudo-critical temperature which coincides with maximum flow rate near pseudo-critical temperature (see figure 4-10). The NOLSTA code predicts the experimental mass flow rates and heater inlet/ outlet temperatures very closely by using Bringer Smith correlation (1957) for calculating primary side heat transfer coefficient for cooler, whereas Jackson correlation (2002) shows much sharper reduction in flow rate beyond pseudo-critical temperature associated with a much steeper increase in heater inlet/ outlet temperature (see Appendix-III for the various heat transfer correlations referred in the thesis). Both the correlations are giving good match for experimental data below pseudo-critical temperature (i.e. below 1400 W), but beyond 1400 W Jackson correlation deviates largely from experimental data. Similarly, Shitsman correlation (1959) shows sharp reduction in flow associated with sharp increase in heater inlet/ outlet temperatures (see figures 4-11a & 4-11b) beyond the pseudo-critical temperature whereas Swenson correlation (1965) shows a smooth

reduction in flow rate. Hence, heat transfer characteristics of the cooler play an important role on steady state natural circulation characteristics of a closed loop thermo-syphon with supercritical fluids. Both Bringer Smith and Swenson correlation calculate thermal conductivity of fluid (required for calculating Prandtl number as well as Nusselt number) at wall temperatures/ pseudo-critical temperature (for bulk fluid temperature exceeding pseudo-critical temperature) instead of bulk fluid temperature which prevents sharp reduction of heat transfer coefficient and steep rise of steady state bulk fluid heater inlet/ outlet temperature beyond pseudo-critical temperature. Hence sharp reduction of flow is not observed for these two correlations beyond the pseudo-critical temperature similar to what has been observed in experiments.

Bringer Smith correlation (1957) also gives good match for experimental data for HHVC orientation as shown in figure 4-12a & 4-12b, whereas Jackson correlation (2002) again shows a sharp reduction in flow beyond pseudo-critical temperature. The maximum error associated with experimental mass flow measurement (which is a derived quantity) is ± 30% for the loop operation near the pseudo-critical region, since the bulk fluid temperature difference across the heater section is much less near the pseudo-critical region, whereas the error is much less away from the pseudo-critical region. However, the mass flow rates predicted by NOLSTA code are within $\pm$15% of the experimental values.

4.4 Experimental steady state heat transfer coefficient for carbon dioxide and comparison with various correlations

4.4.1 Determination of heater heat transfer coefficient experimentally

The SPNCL also has a provision for measurement of local heat transfer coefficient along the heater length, by thermocouples brazed on outside heater surface at six equidistant locations

along the heater length as shown in figure 4-13. The heat transfer coefficient along the heater length is estimated from the measured outside surface temperature (T_{wo} *i.e. T3-T14*) of heater pipe wall. At each location temperature is measured at two diametrically opposite positions (i.e. T3 & T4). Then, the steady state inside wall surface temperature of heater (T_{wi}) is estimated by a conduction analysis.

$$T_{wi} = T_{wo} - \frac{Q \ln\left(\frac{r_o}{r_i}\right)}{2\pi k L_h} \tag{4.5}$$

Inlet and outlet fluid temperatures (T_{in} and T_{out} respectively) of heater are measured by using two thermocouples (T1 & T2 and T15 & T16 respectively) as shown in figure 4-13. The bulk fluid enthalpy at the corresponding axial location along heater length were obtained by the linear interpolation of enthalpies at inlet and outlet of heater test section

$$i_b = i_{in} + \frac{x(i_{out} - i_{in})_h}{L_h} \tag{4.6}$$

From the local bulk fluid enthalpy, local fluid bulk temperature can be calculated. From local bulk temperature, inside heater wall temperature and heat input, the local inside heat transfer coefficient (h_i) can be estimated as given below:-

$$h_i = \frac{Q}{A_{htri}\left(T_{wi} - T_b\right)} \tag{4.7}$$

Uniform heat flux is assumed through out the heated length and A_{htri} is the inside heat transfer area of the heater tube.

It may be noted that at a single power of operation in SPNCL, a complete temperature range of bulk fluid (i.e. from sub-critical to supercritical) is not covered from heater inlet to heater outlet.

Hence, the local heat transfer coefficient along horizontal heater length (HHHC orientation) has been determined for different operating powers corresponding to sub-critical, pseudo-critical and supercritical range of operation as shown in figures 4-14a, 4-14b& 4-14c respectively. For the horizontal heater, there are six thermocouples on the top and six at the bottom of the heater surface, hence two heat transfer coefficients are determined. At the entrance region the top heat transfer coefficient is higher but as the flow gets thermally developed the bottom heat transfer coefficient becomes larger since buoyancy forces may assist the heat transfer from bottom surface of the tube. This is in agreement with experiments conducted for horizontal flow of carbon dioxide at supercritical and sub-critical pressures, Adebiyi and Hall (1976). They also found non-uniform cross-section temperature profile for horizontal flow and confirmed the effect of buoyancy forces by comparison with buoyancy free data.

Since the most correlations available in literature do not account for top and bottom heat transfer for horizontal flow, the average of top and bottom heat transfer coefficient has been taken. The average of top and bottom heat transfer coefficient is not varying significantly with the bulk carbon dioxide temperature along the length of horizontal heater test section for the sub-critical, pseudo-critical and supercritical range of operation. More over, no deterioration in heat transfer has been observed during current range of operation of SPNCL due to lower heat flux. Hence, it is worth while to plot average heat transfer coefficient versus average bulk fluid temperature across heater section corresponding to various operating powers. The maximum error associated with measurement of heat transfer coefficient is ± 15%.

4.4.2 Comparison of heat transfer data with various empirical correlations

The experimentally determined heat transfer coefficients for horizontal heater were compared with predictions of various correlations available in literature as shown in figures 4-15a, 4-15b & 4-15c. Jackson (2002), Shitsman (1954) and Bishop (1964) correlations are closer to experimental heat transfer results in the sub-critical, pseudo-critical and supercritical region of loop operation.

However, Bringer Smith (1957) is found to deviate as much as 130% in the pseudo-critical region of loop operation. Hence, for loop specific condition it is quite apparent that for evaluating heater inside heat transfer coefficient the thermal conductivity of fluid (required for calculating Prandtl number as well as Nusselt number) should be evaluated at the bulk fluid temperature, whereas for cooler inside heat transfer coefficient the thermal conductivity should be evaluated at the wall temperature/ pseudo-critical temperature for bulk fluid temperature exceeding pseudo-critical temperature.

4.5 Conclusions

The peak of the steady state mass flow rate versus power curve for supercritical carbon dioxide natural circulation is obtained at heater outlet temperature near the pseudo-critical value for open as well as closed loop boundary conditions. A change in loop diameter does not significantly affect the heater outlet temperature at which peak steady state flow rate is achieved. If the heater inlet temperature increases beyond the pseudo-critical temperature the steady state natural circulation mass flow rate reduces significantly for closed as well as open loop. The steady state natural circulation mass flow rate increases with increase in pressure at higher powers in the

friction dominant region just like two phase natural circulation loops. The HHHC orientation gives maximum and VHVC orientation gives minimum flow. For the same elevation difference VHHC orientation gives higher flow as compared to HHVC orientation. The steady state mass flow rate versus heater power characteristics for open and closed loop are slightly different. In a closed loop a larger reduction in flow is observed after a particular power when both hot and cold legs become supercritical, where as gradual flow reduction is observed for open loop with constant heater inlet temperature.

NOLSTA code predicts the steady state natural circulation mass flow rates of closed as well as open loop operating with supercritical carbon dioxide appreciably well ($\pm$ 15%). For closed loop, the steady state behavior of loop is found to be very sensitive to the empirical heat transfer correlation used for cooler primary side. The heat transfer correlations evaluating thermal conductivity at the bulk fluid temperature are showing very sharp reduction in flow after a particular power (when both cold leg and hot leg temperatures exceed the pseudo-critical temperature) which is accompanied with a steeper rise in heater inlet and outlet temperatures. However, the correlations evaluating thermal conductivity at wall temperatures/ pseudo-critical temperature for bulk fluid temperature exceeding pseudo-critical temperature (i.e. Bringer Smith, 1957) give a smoother reduction in flow similar to that observed in the experiments. For loop specific operating conditions it can be indirectly concluded that for evaluating heater inside heat transfer coefficient the thermal conductivity of fluid (required for calculating Nusselt number and Prandtl number) should be evaluated at the bulk fluid temperature, whereas for cooler inside heat transfer coefficient the thermal conductivity should be evaluated at the wall temperature/ pseudo-critical temperature for bulk fluid temperature exceeding pseudo-critical temperature.

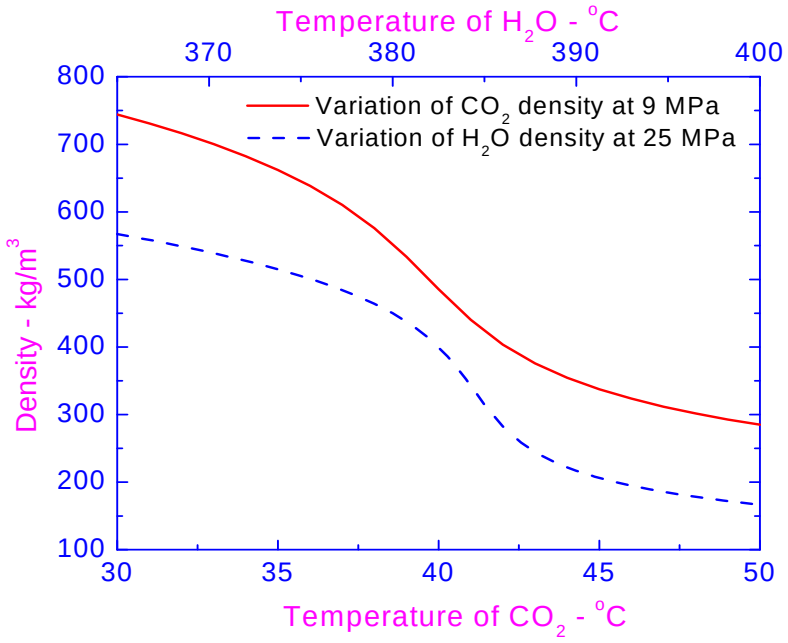

(a)

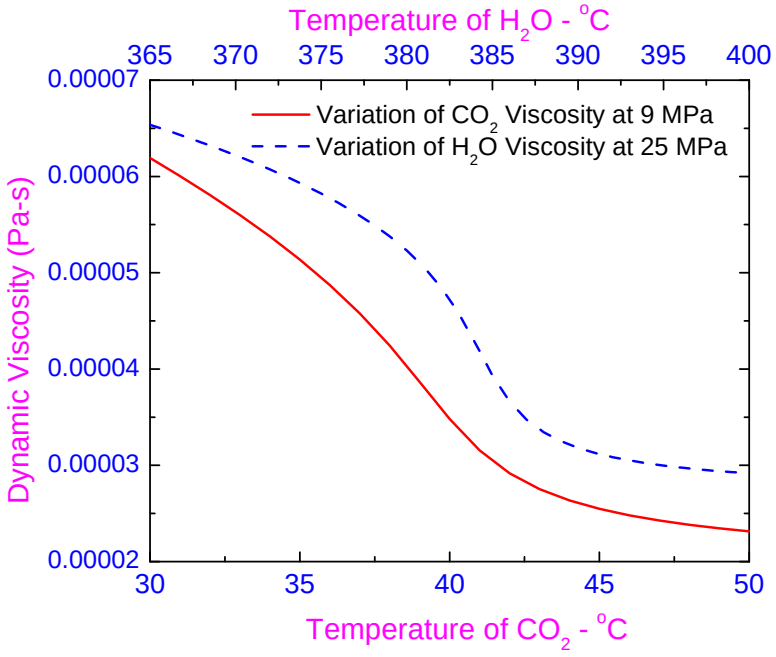

(b)

Figure 4-1: Comparison of water and carbon dioxide properties at supercritical conditions

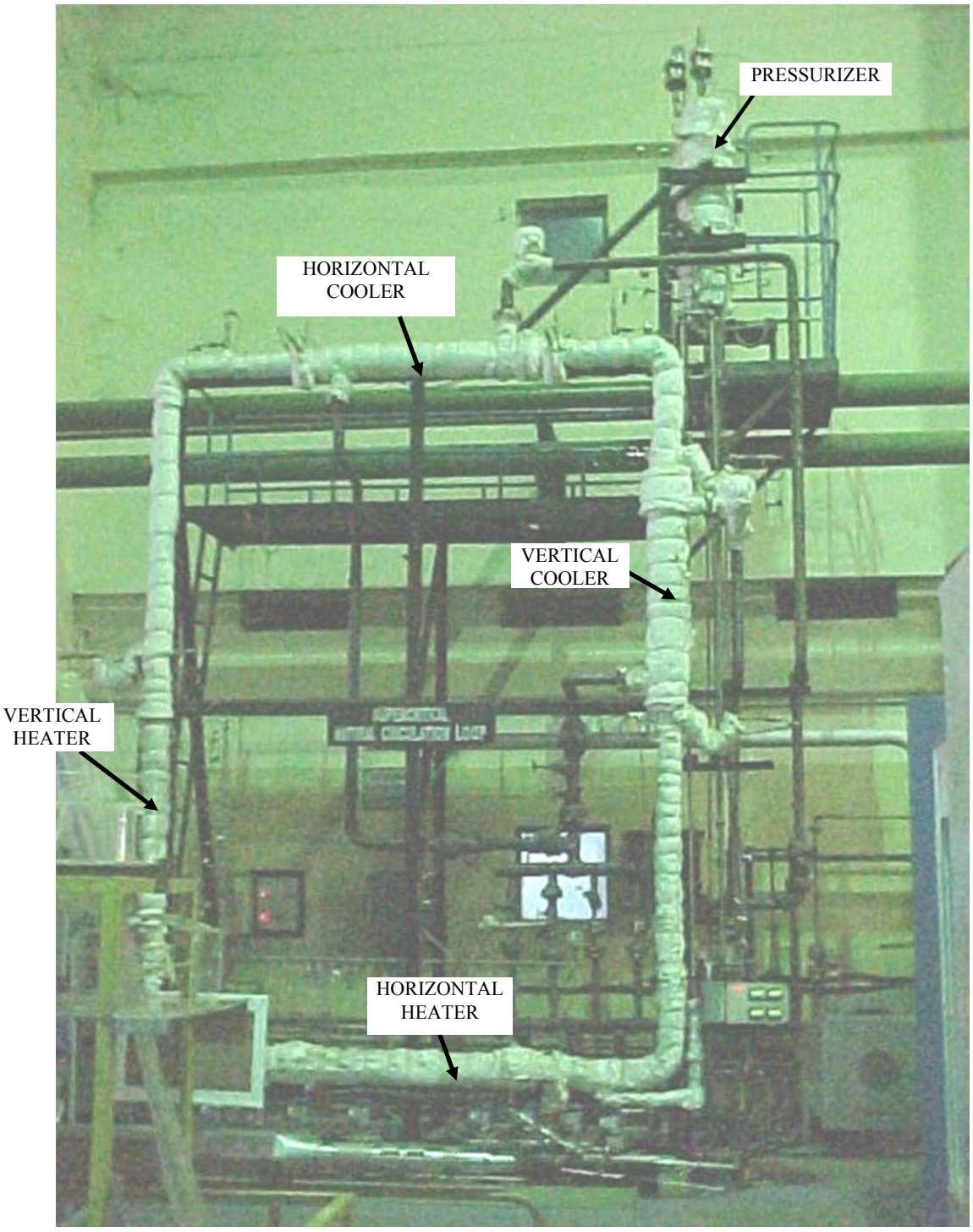

Figure 4-2a: Photograph of Supercritical Pressure Natural Circulation Loop (SPNCL).

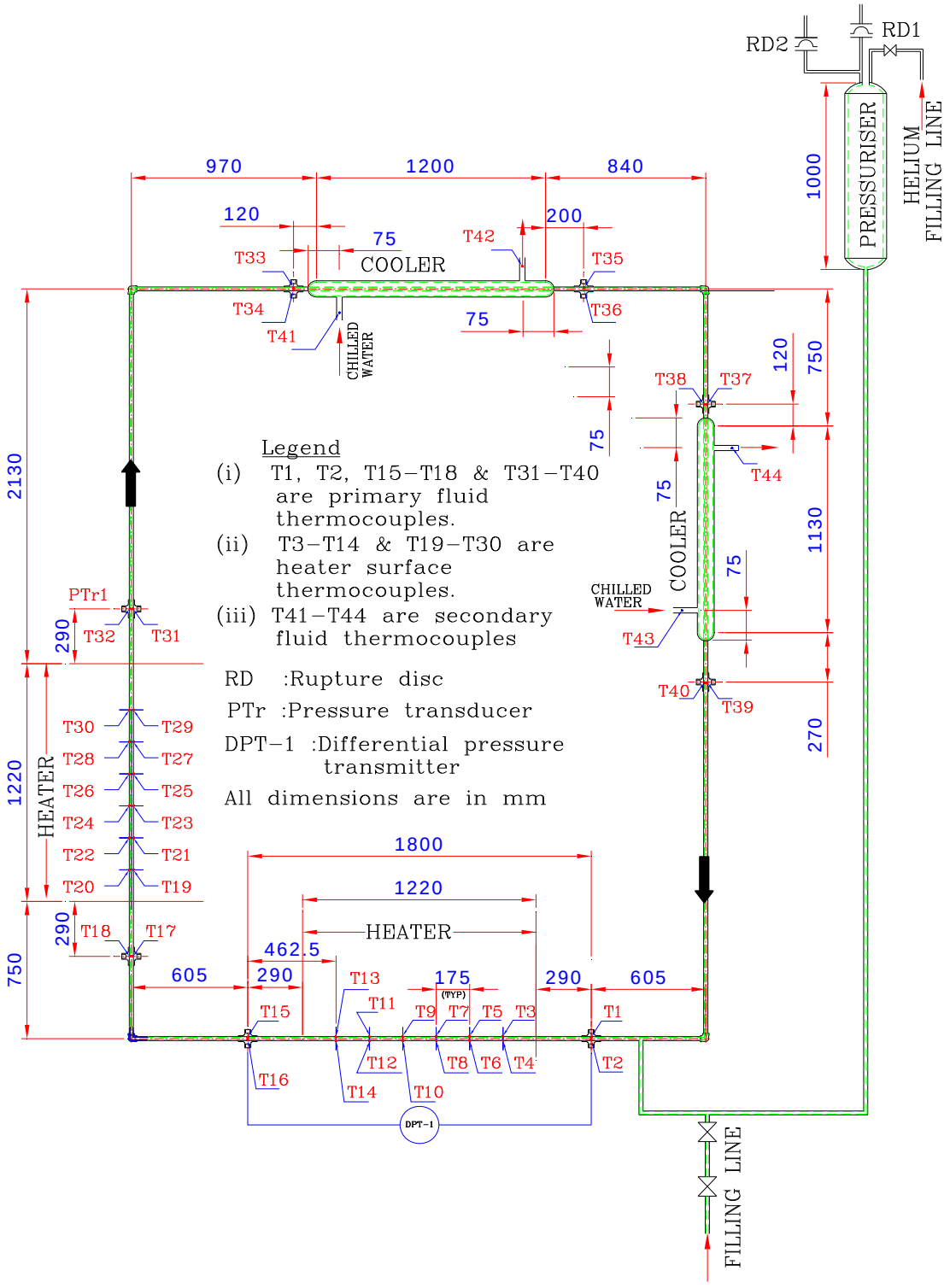

Figure. 4-2b: Schematic of Supercritical Pressure Natural Circulation Loop (SPNCL)

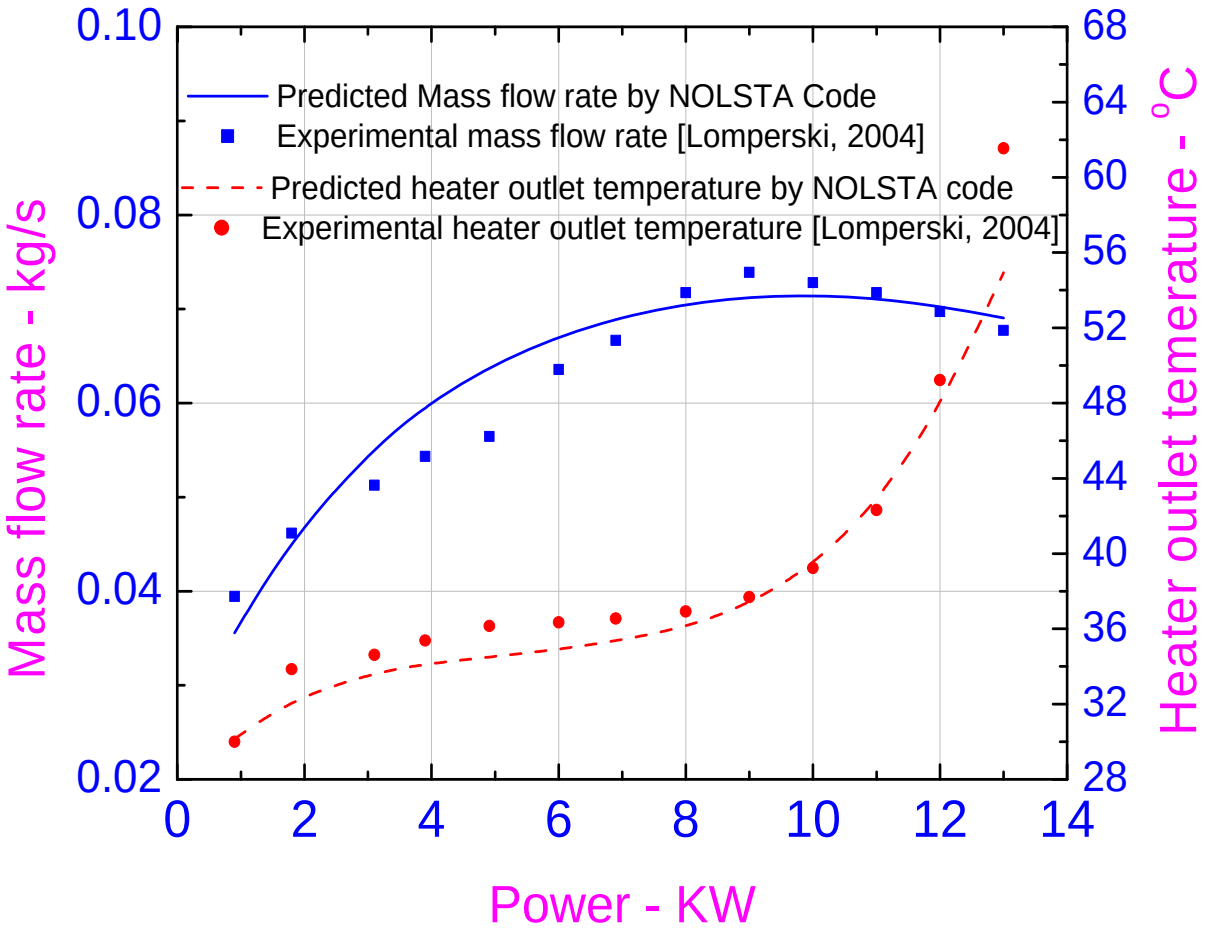

Figure 4-3: Comparison of experimental data with theoretical predictions for Lomperski's loop at 8 MPa and 24°C heater inlet temperature

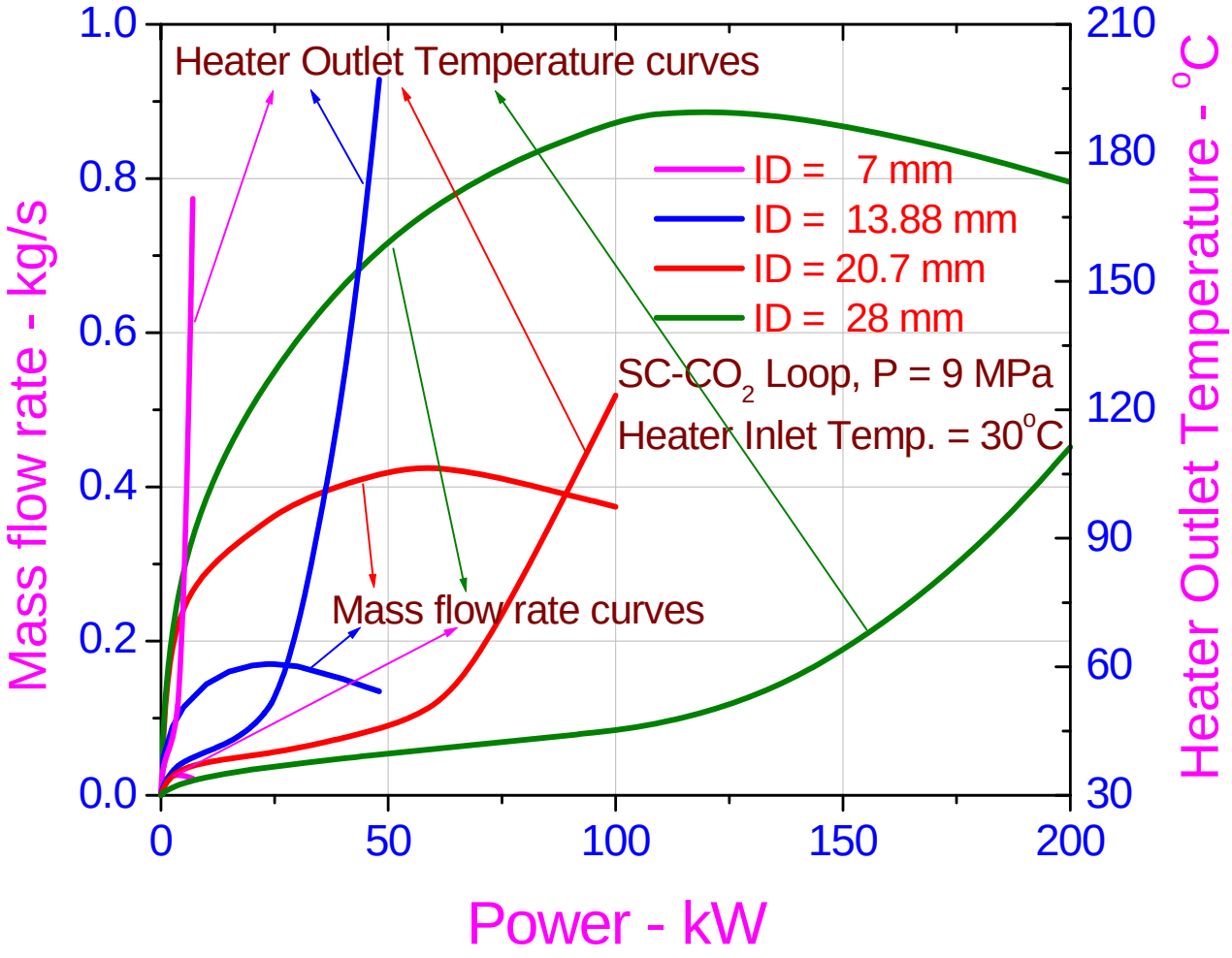

Figure 4-4: Effect of diameter on steady state behaviour of open SPNCL operating with SC-CO_2 at 9 MPa and 30°C heater inlet temperature (HHHC orientation).

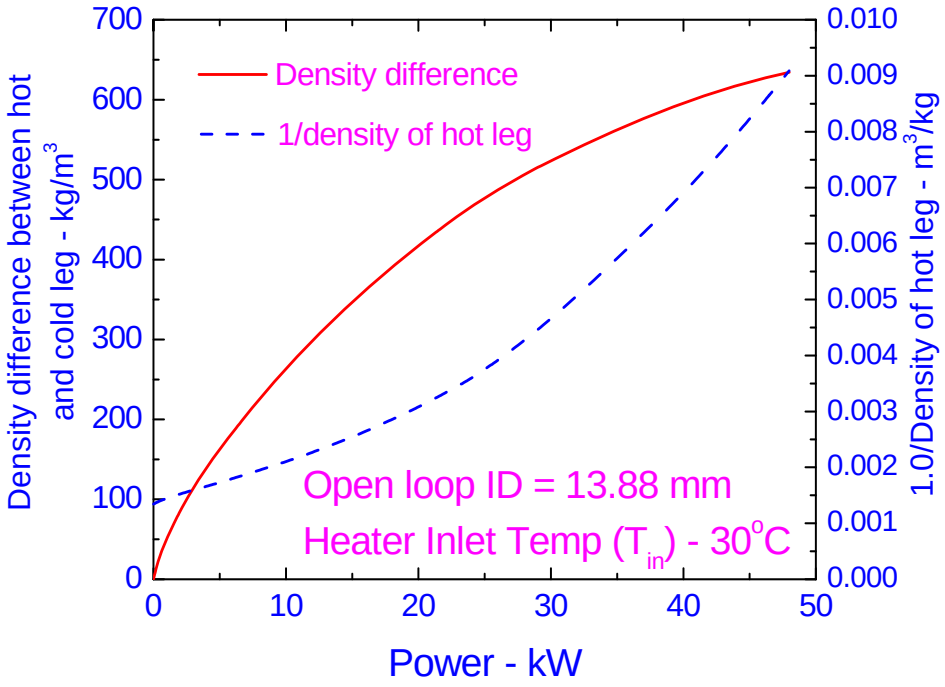

Figure 4-5: Variation of buoyancy and frictional forces with power for open SPNCL operating with SC-CO_2 at 9 MPa/ 30°C heater inlet temperature (HHHC orientation).

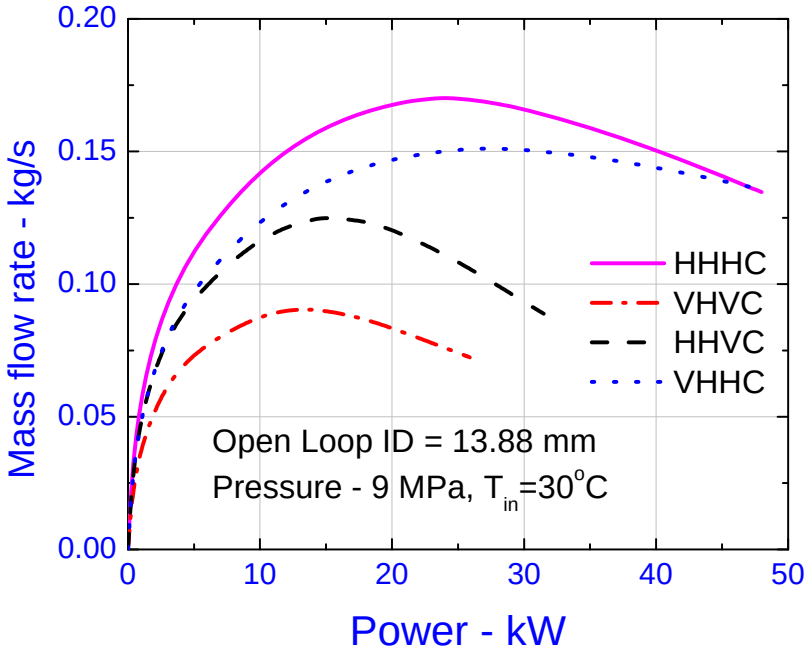

Figure 4-6: Effect of orientation on steady state mass flow rate of open SPNCL operating with SC-CO_2

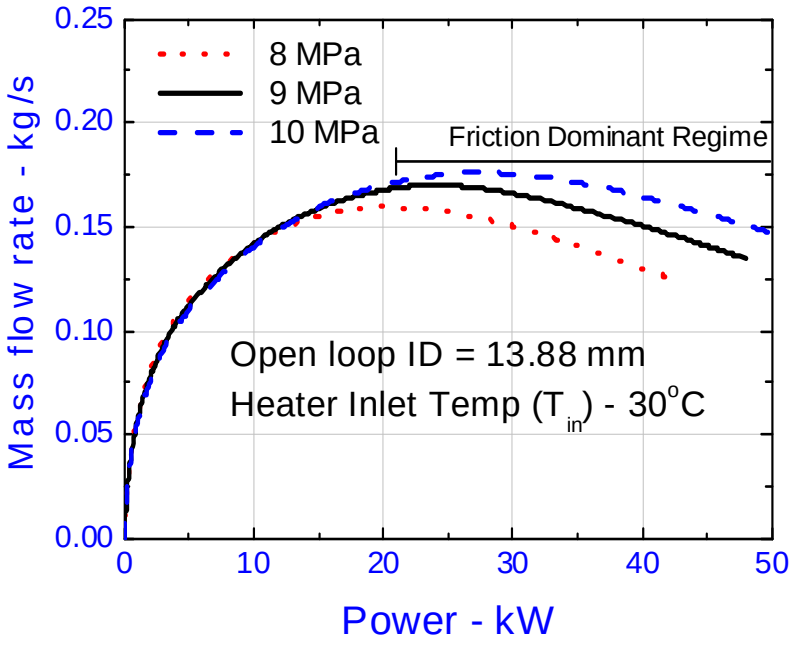

Figure 4-7: Effect of pressure on steady state mass flow rate of open SPNCL operating with SC-CO_2 (HHHC orientation)

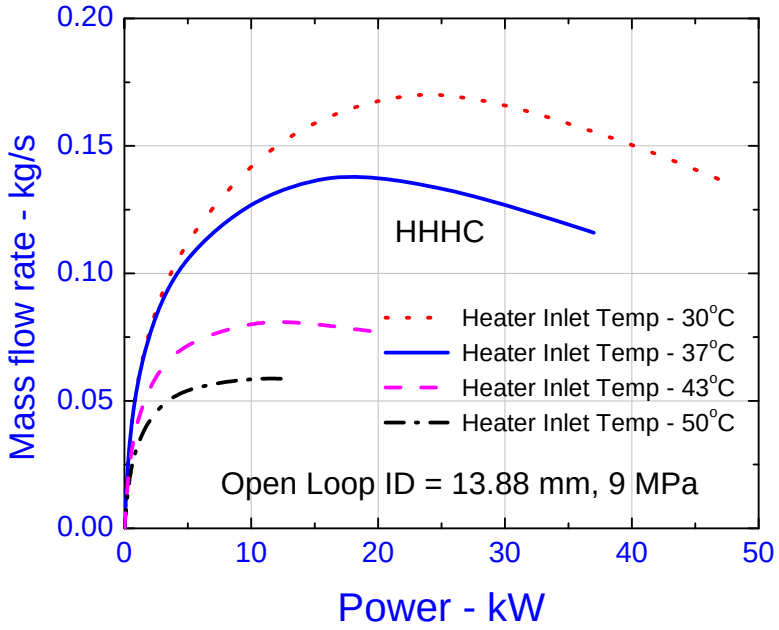

Figure 4-8: Effect of heater inlet temperature on steady state mass flow rate of open SPNCL operating with SC-CO_2 (HHHC orientation).

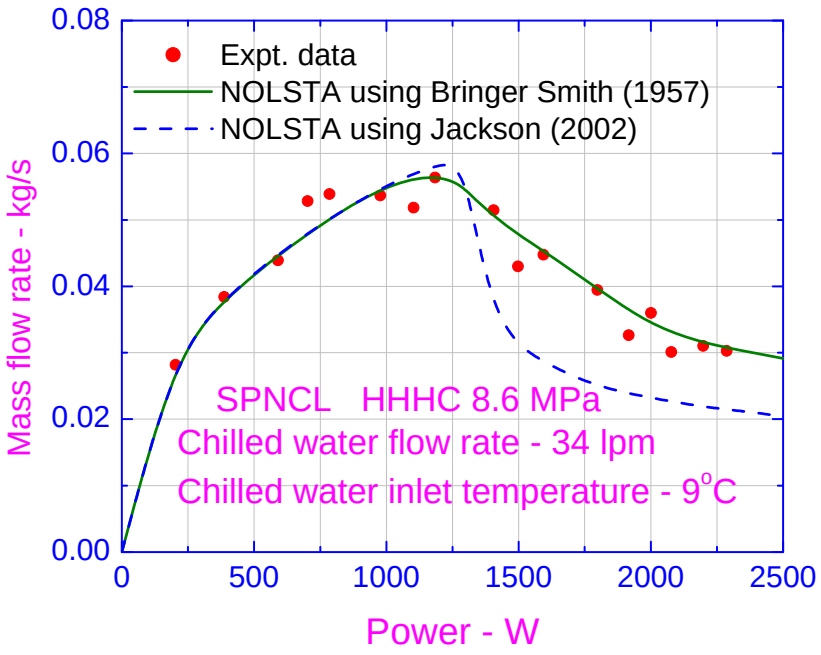

Figure 4-9a: Comparison of experimental and predicted mass flow rate for SPNCL operating with SC-CO_2 for HHHC orientation at 8.6 MPa.

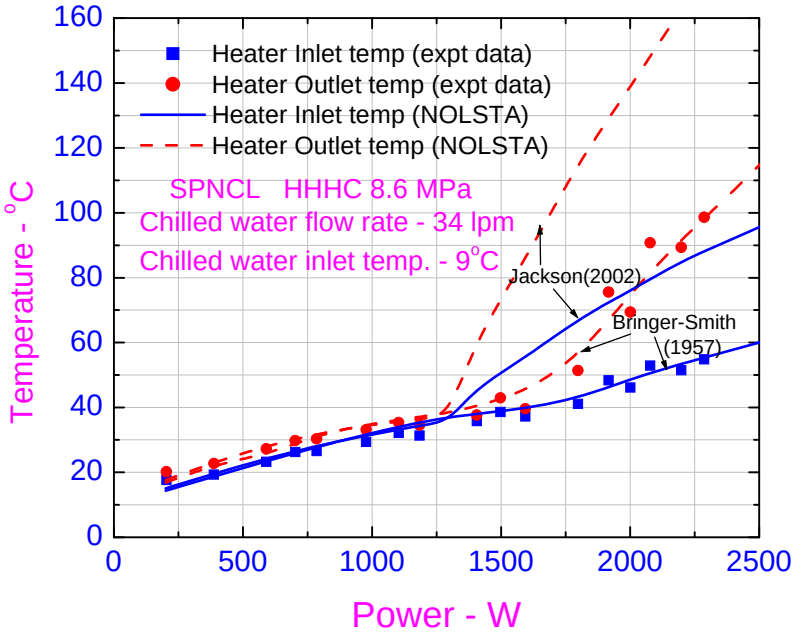

Figure 4-9b: Comparison of experimental and predicted heater inlet and outlet temperature for SPNCL operating with SC-CO_2 for HHHC orientation at 8.6 MPa.

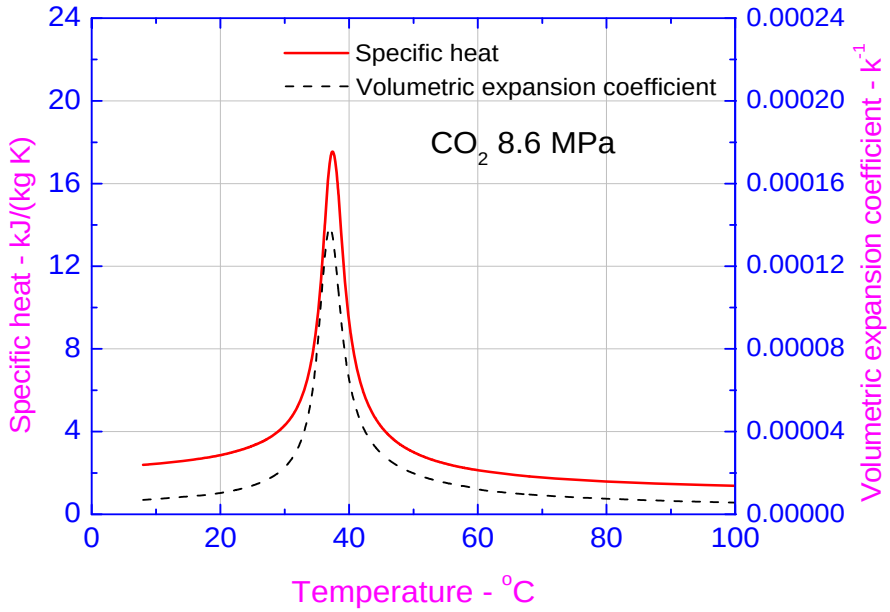

Figure 4-10: Variation of specific heat/ volumetric expansion coefficient of carbon dioxide with temperature at 8.6 MPa pressure

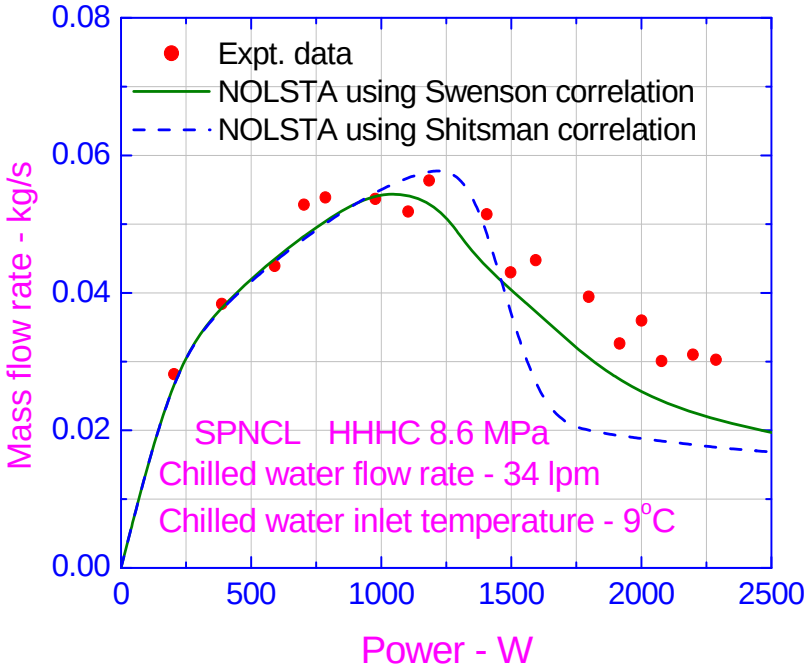

Figure 4-11a: Comparison of experimental and predicted mass flow rate for SPNCL operating with SC-CO_2 for HHHC orientation at 8.6 MPa.

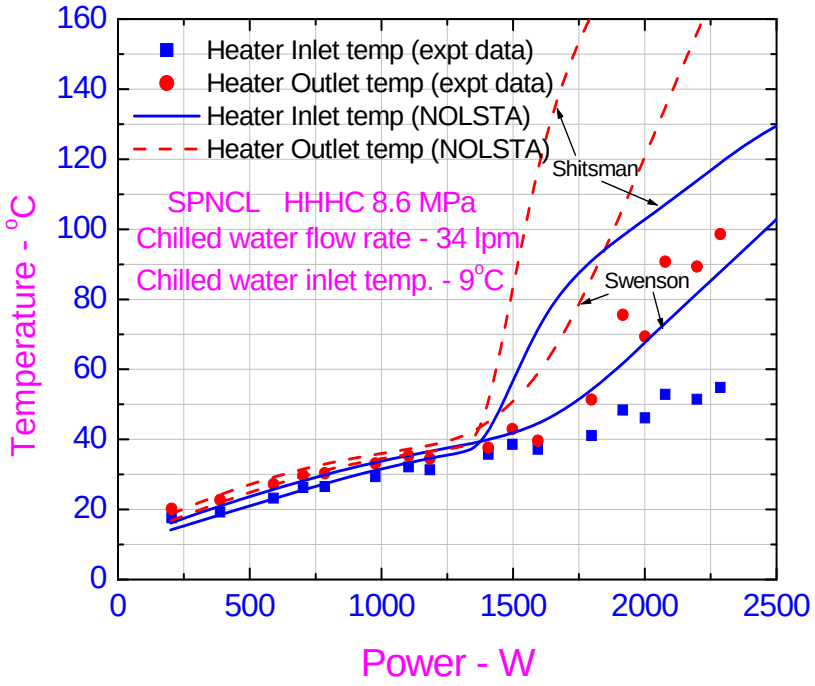

Figure 4-11b: Comparison of experimental and predicted heater inlet and outlet temperature for SPNCL operating with SC-CO_2 for HHHC orientation at 8.6 MPa.

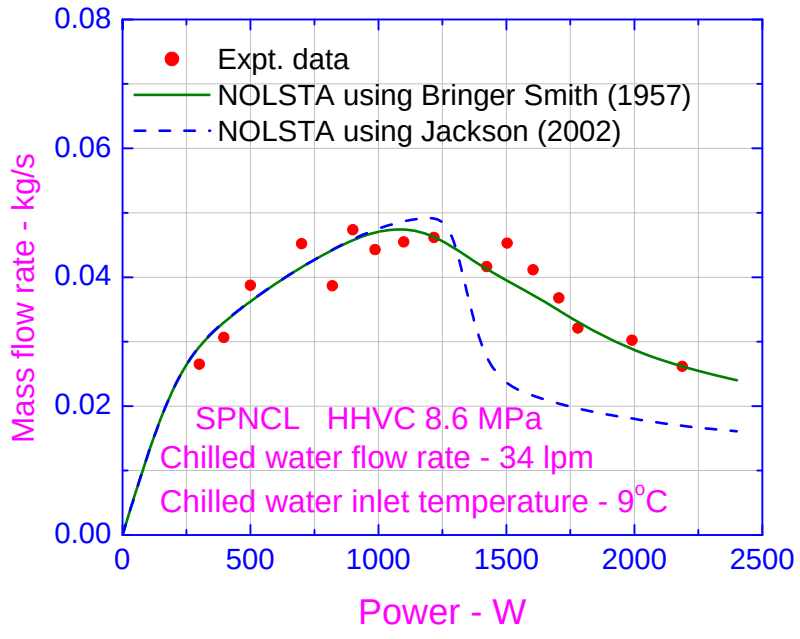

Figure 4-12a: Comparison of experimental and predicted mass flow rate for SPNCL operating with SC-CO_2 for HHVC orientation at 8.6 MPa.

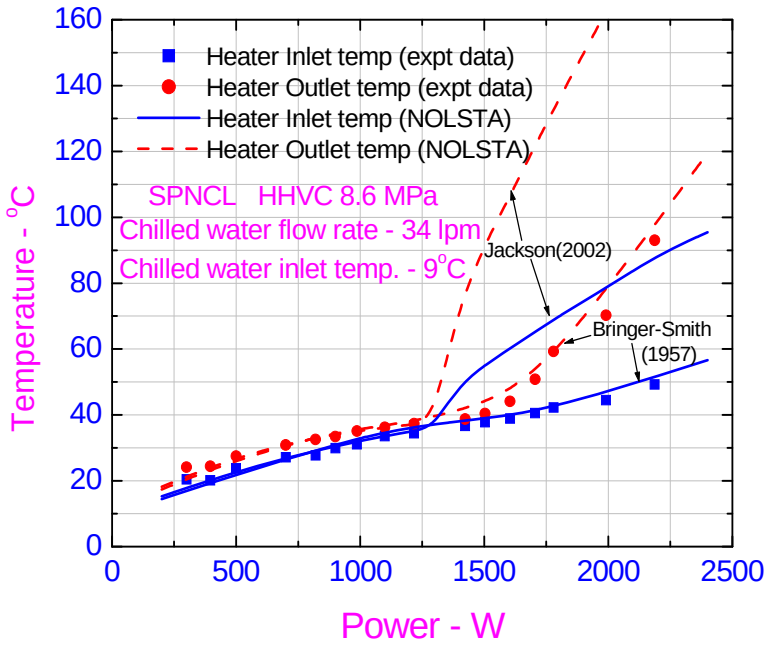

Figure 4-12b: Comparison of experimental and predicted heater inlet and outlet temperature for SPNCL operating with SC-CO_2 for HHVC orientation at 8.6 MPa.

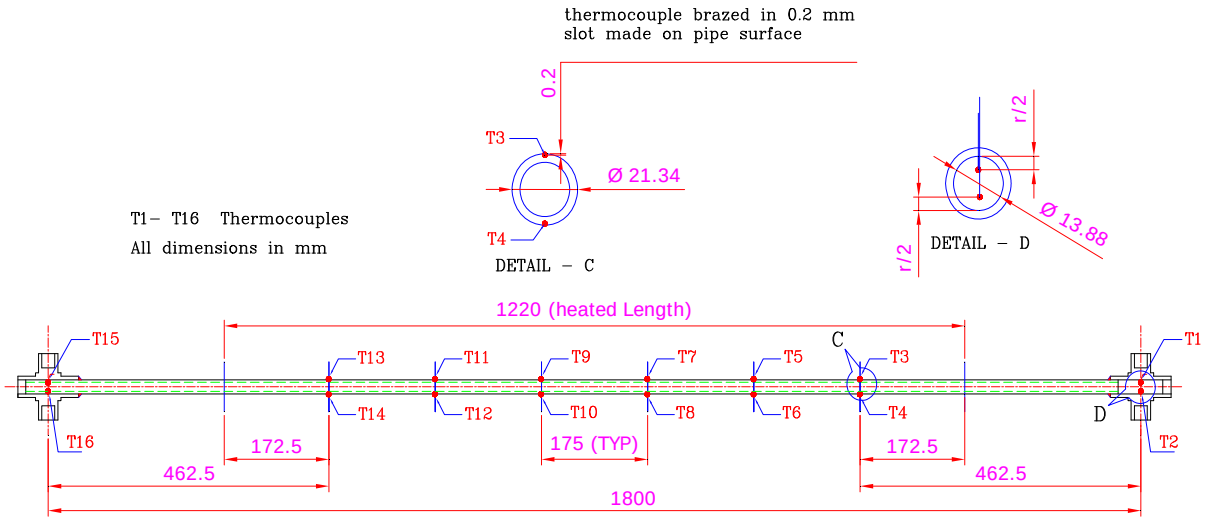

Figure 4-13: Instrumentation for measuring heat transfer coefficient in heater test section of SPNCL operating with SC-CO_2

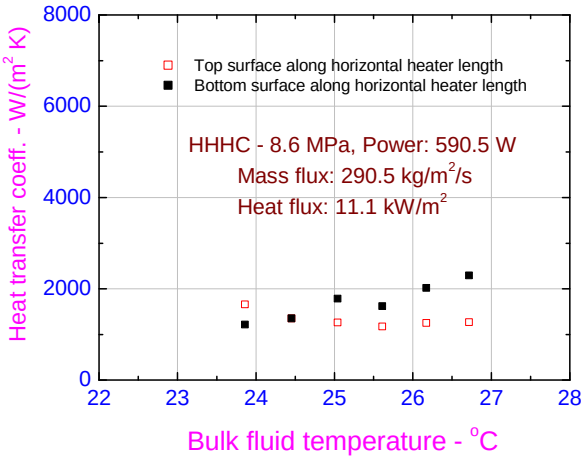

(a) Sub-critical

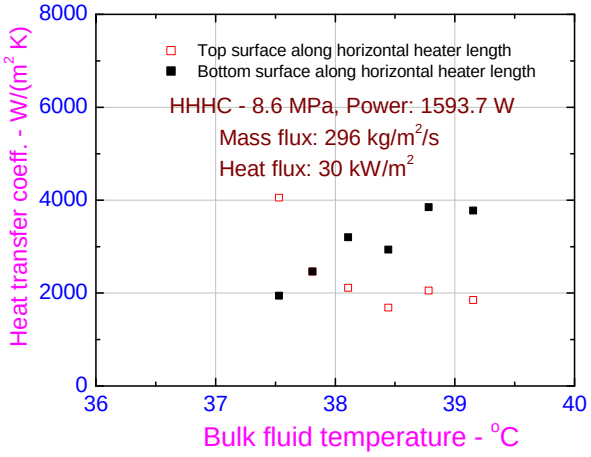

(b) Pseudo-critical

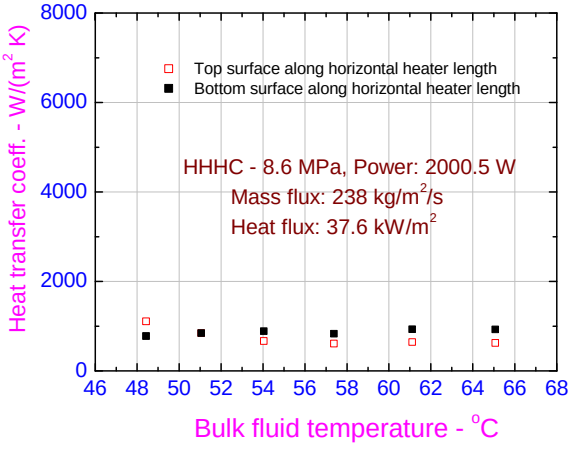

(c) Supercritical

Figure 4-14: Variation of heat transfer coefficient along horizontal heater length during sub-critical, pseudo-critical and supercritical operating temperature range of SC-CO_2

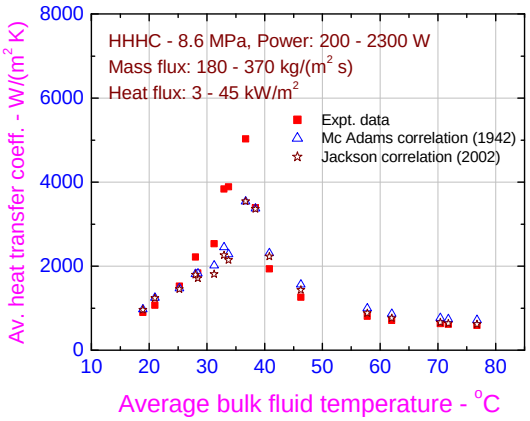

(a)

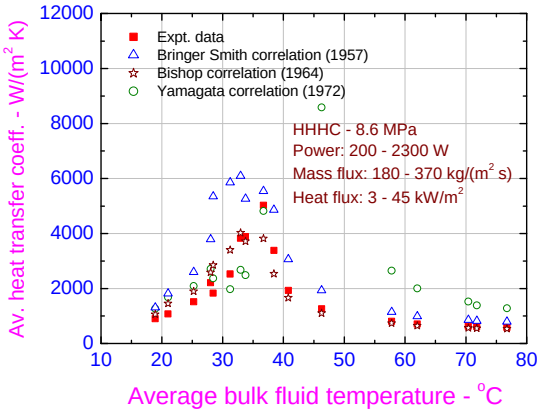

(b)

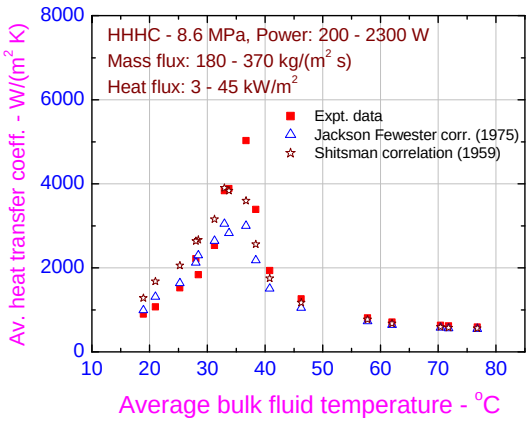

(c)

Figure 4-15: Comparison of experimental heat transfer coefficient for horizontal heater measured in SPNCL with various correlations

Chapter 5

Stability behavior of natural circulation loops operating with carbon dioxide at supercritical pressures for open and closed loop boundary conditions

5.1 Introduction

The literature reveals only very few experimental studies on natural circulation instability with supercritical fluids. Harden and Boggs (1964) conducted studies on Freon loop near critical region. High and low frequency oscillations were observed when bulk fluid temperature approached pseudo-critical temperature. Adelt and Mikielewicz (1981) performed studies on 4m high loop with carbon dioxide (CO_2). As the fluid was heated through pseudo-critical point pressure oscillations were observed for a particular test but the study mainly focused upon heat transfer rather than stability. Lomperski et al. (2004) have reported experiments in a two meter high natural circulation loop with carbon dioxide at supercritical pressure. The loop was operated in a base case configuration that maximized flow rates and in a second configuration having an orifice in the hot leg. No flow instabilities were observed in these tests as the fluid was heated through thermodynamic pseudo-critical point. Yoshikawa et al. (2005) have studied the performance of a closed natural circulation loop operating with supercritical CO_2. The performance of the loop was determined by measuring flow velocities of CO_2 which could be correlated to Grashof number, Prandtl number and dimensionless effective density difference. No flow instability has been reported during the experiments. In a very recent study, T'Joen and Rhode (2012) conducted stability experiments with artificial neutronic feedback in scaled natural circulation driven HPLWR (High Performance Light Water Reactor) facility named Delight

maintaining the inlet temperature constant (i.e. with open loop boundary conditions). They used Freon R23 at 5.7 MPa as the scaling fluid. The decay ratios and frequencies of the riser inlet temperature oscillations were measured. They found that for a single inlet temperature the system undergoes two transitions as the power is increased. At low power the system is stable and becomes unstable as the power is increased, but on further increasing the power the system stabilizes. They also found a threshold inlet temperature above which no instability is observed. Xiong et al. (2012) have carried out experiments on flow instability in two parallel channels with supercritical water. They did a parametric study which shows that flow becomes more stable by increasing the pressure or decreasing the inlet temperature in the range of experiments conducted. Clearly the literature as well as the understanding of instability phenomenon with supercritical fluids is very less. Hence, more experiments were conducted in SPNCL with supercritical carbon dioxide as operating fluid to gain an insight in to its stability behavior

5.2 Stability experiments for natural circulation with supercritical carbon dioxide

5.2.1 Stability experiments and analysis for an open loop

First of all NOLSTA code has been validated for open loop analysis with experimental data for Supercritical CO_2 available in literature. Lomperski et al. (2004) have reported experimental natural circulation data for carbon dioxide at supercritical pressure for constant heater inlet temperature irrespective of power. The loop orientation is HHHC having ID of 14 mm and height of 2 m. NOLSTA code predicted the steady state characteristics of the loop appreciably well as described in Chapter 4, section 4.3.1. The code predicts the threshold of instability as 7.5 kW for Lomperski's loop (see figure 5-1), whereas no instability has been observed during

experiments. This deviation from experimental values can be overcome by considering thermal capacitance of pipe wall which will be addressed later in the section 5.3.2.

5.2.2 Stability experiments for closed loop SPNCL

5.2.2.1 Time series of loop oscillatory behaviour

No flow instability was observed during experiments conducted in SPNCL with higher secondary side flow rate i.e. 34 lpm (Chapter 4, section 4.3.2). Extensive natural circulation experiments were conducted in the test facility with supercritical carbon dioxide as working fluid to observe instability. The instability has been observed for HHHC orientation only (all other orientations were found to be stable) and with lower secondary side flow rate i.e. 10-15 lpm. Typical instability has been observed at an operating pressure of 9.1 MPa and 10.1 lpm secondary flow as shown in figure 5-2a, 5-2b & 5-2c. It shows the transient from 700 W to 500 W to 300 W. Figure 5-2a shows the pressure drop across the horizontal heater section which shows development of instability during power reduction from 700 W to 500 W, whereas instability dies out on further reduction of power to 300 W. The instability is observed at 500 W with heater inlet temperature of ~27.1^{o}C and heater outlet temperature varying from 37-44.6^{o}C as can be seen from figure 5-2b. Figure 5-2c shows the heater outlet temperature oscillations of equal amplitude in more detail. With 15 lpm secondary flow the instability is observed at 800 W for 9.1 MPa pressure as shown in figure 5-3a, 5-3b & 5-3c. It shows the transient from 600 W to 800 W to 1000 W. Figure 5-3a shows the pressure drop across the horizontal heater section which shows development of instability during power rise from 600 W to 800 W, whereas instability dies out on further increase of power to 1000 W. The instability is observed at 800 W

with heater inlet temperature of ~31^{o}C and heater outlet temperature varying from 35-43^{o}C as can be seen from figure 5-3b. The heater outlet temperature oscillations are having consecutive larger and smaller peak (figure 5-3c) indicating near period doubling as compared to single peak oscillation observed at 500 W (figure 5-2c). A similar type of instability is observed during power transient from 925 W to 700 W to 500 W as shown in figure 5-4a, 5-4b & 5-4c. The instability is observed at 700 W with heater inlet temperature of ~31^{o}C and heater outlet temperature varying from 34-45^{o}C as can be seen from figure 5-4b. The loop is however stable at 925 W and 500 W. Figure 5-4c also shows repetitive large and small peak in heater outlet temperature oscillations indicating near period doubling as compared to single peak oscillation observed at 500 W (figure 5-2c).

The instability has also been obtained during power step down from 1900 W to 300 W at 7.7 MPa and secondary flow rate of 10 lpm as shown in figure 5-5a, 5-5b & 5-5c. The instability has also been obtained during start-up at 700 W at 8.1 MPa and secondary side flow rate of 10 lpm as shown in figure 5-6a & 5-6b. The instability dies out on further increasing power to 1100 W. Figure 5-6b shows uniform amplitude oscillations at 700 W. The operating conditions, time period and amplitude of oscillations obtained during experimentation have been reported in Table 5-1. In all cases, the instability develops by the oscillation growth mechanism as proposed by Welander (1967). Instability development from steady state condition by the oscillation growth mechanism was also observed in single-phase loops, Vijayan et al. (2007).

The amount of instability data generated in the present test facility is clearly inadequate compared to the extensive instability data that exists for single-phase and two-phase loops and sometimes the instability could not be repeated during the experimentation. Actually, the

instability is observed over a very narrow window of power and can be missed if the step change in power is high. However, in all the cases the instability is observed when heater inlet temperature is very near to the critical temperature (i.e. 31^{o}C for CO_2) and outlet temperature is oscillating even beyond the pseudo-critical temperature oscillating from 29-45 ^{o}C (considering complete range of instability data). Hence, instability is observed in the pseudo-critical temperature range of loop operation where the volumetric expansion coefficient of the supercritical CO_2 is very high, see figure 5-7.

Table 5-1: Observed oscillatory characteristics of natural circulation with supercritical cabon-dioxide in SPNCL

Power (W)	Pressure (MPa)	Secondary flow rate at 9^{o}C inlet temperature (lpm)	Heater Inlet temperature (^{o}C)	Range of heater outlet temperature oscillation (^{o}C)	Amplitude of pressure drop oscillation (mm of WC)	Time period of heater outlet temperature oscillation (s)	Loop circulation time of steady state calculated by NOLSTA(s)
300	7.7	10.0	28.4	29.4 – 34.5	59.7	226.9	43.4
500	9.1	10.1	27.1	37 - 44.6	27.74	36	33.4
700	9.1	15.5	31	34 - 45	47.25	70.2	28.3
700	8.1	10.0	29.4	30.3 – 33.4	38.0	30.6	22.7
800	9.1	15.0	31	35 - 43	51.29	65	25.5

5.2.2.2 Phase plots of observed oscillatory instability

The methodology of getting the phase plots from the experimental transient using momentum equation is described as follows

Momentum equation

$$\frac{1}{A}\frac{\partial w}{\partial t}+\frac{1}{A^2}\frac{\partial}{\partial x}(w^2 v)+\frac{g}{v}\cos\phi+\frac{fw^2 v}{2DA^2}+\frac{\partial p}{\partial x}=0 \qquad (5.1)$$

Integrating the momentum equation over the horizontal heater section gives

$$\frac{L'}{A}\frac{dw}{dt}+\frac{w^2}{A^2}(v_{out}-v_{in})+\frac{fw^2(v_{out}+v_{in})}{4DA^2}L'+\Delta p_h=0 \tag{5.2}$$

where, w is considered as the average fluid mass flow rate assumed uniform along the length of the heater test section. The finite difference form of the equation (5.2) can be expressed as

$$\frac{L'}{A}\frac{w^{n+1}-w^n}{\Delta t}+\left(\frac{w^{n+1}}{A}\right)^2(v_{out}^{n+1}-v_{in}^{n+1})+\frac{f^{n+1}\left(w^{n+1}\right)^2(v_{out}^{n+1}+v_{in}^{n+1})}{4DA^2}L'+\Delta p_h^{n+1}=0 \tag{5.3}$$

The steady state form of equation (5.3) can be expressed as

$$\left(\frac{w^n}{A}\right)^2(v_{out}^{n}-v_{in}^{n})+\frac{f^{n}\left(w^{n}\right)^2(v_{out}^{n}+v_{in}^{n})}{4DA^2}L'+\Delta p_h^{n}=0 \tag{5.4}$$

For phase plot equation (5.3) is used, in which experimental transient data where steady state is achieved (i.e. at a stable power) is taken as the starting point. At the stable power the current mass flow rate (w^n) is determined by equation (5.4) in which the current pressure drop (Δp_h^n) measured across the bottom horizontal heater section as well as the specific volume at inlet and outlet of heater section (i.e. v_{in} and v_{out} calculated from the measured current inlet and outlet temperatures of the heater test section) are substituted. The calculated current mass flow rate (w^n) is substituted in to equation (5.3) to determine mass flow rate (w^{n+1}) after time increment Δt (typical value of 2 s in experiments). Finally, w^{n+1} and Δp_h^{n+1} are plotted to get the phase plots, however, figures 5-8 – 5-12 show phase plots only for the duration of time where limit cycle oscillations for the unstable power have been achieved.

The phase plot corresponding to a typical one cycle oscillation observed at 500 W (figure 5-2) is a simple closed curve as shown in figure 5-8. From the time series at 800 W given in figure 5-3c, it is easily seen that a near period doubling occurs between 500 W and 800 W. In general, the period is expected to decrease with increase in power if the oscillatory mode remains the same. Switching of the oscillatory mode as shown by the phase plot of single cycle oscillation in figure 5-9 results in sudden period change. The phase plot of the time series (at 700 W, figure 5-4) also shows a switching of oscillatoy mode resulting in near period doubling, as shown in figure 5-10. Both the oscillatory modes characterized by the phase plots in Figure 5-8 and 5-10 are only nearly periodic as shown by the long duration phase plots in Figure 5-11 and 5-12 respectively.

5.3 Stability analysis by NOLSTA code

5.3.1 Analysis of SPNCL for closed loop boundary conditions

5.3.1.1 Sensitivity study

The stability analysis was carried out for HHHC orientation of SPNCL considering closed loop behaviour in which heater inlet temperature was allowed to fluctuate with time. Considering the steady state behaviour of SPNCL, Bringer Smith (1957) correlation has been used on primary side of cooler for transient predictions. However, heating heat flux is directly imposed on heater control volumes. The stability threshold for closed loop boundary conditions has been found to be sensitive to the convergence value of loop pressure closure condition, the time step and grid size considered for analysis. Hence convergence value of loop pressure closure, time step and grid size independence test was carried out for SPNCL for operation with SC-CO_2.

Effect of time step and grid size

To start with grid size of 0.01 m was considered and time steps were changed to carry out the stability analysis of SPNCL at 500 W/ 9.1 MPa and 15 lpm secondary flow. It was observed that larger time steps stabilized the predictions as shown in figure 5-13. On reducing the time step from 0.06s to 0.03s the predictions hardly change. Now considering 0.03 as the time step the grid size was reduced to 0.005 m but no change was observed in the results as shown in figure 5-14. However, increasing the grid size to 0.025m and 0.05 m only resulted in shift of oscillations. To preserve accuracy and save computational time the grid size of 0.01m was finalized. Henceforth, grid size and time step of 0.01 m and 0.03s respectively have been used for generating the stability results for SPNCL with closed loop boundary conditions.

Effect of convergence value of loop pressure closure condition

For closed loop natural circulation the pressure boundary condition to be satisfied at any time step is $\Sigma\Delta p = 0$, where $\Sigma\Delta p$ is sum of pressure drop of all the components of the loop. The solution is converged if $\left|\sum \Delta p\right| \leq convergence\ value$. The stability predictions are found to be dependent on this convergence value as shown in figure 5-15. Unrealistic oscillations are predicted for convergence value of 10 Pa, whereas similar oscillations are predicted for 1 Pa and 0.1 Pa. To save computational time, pressure boundary condition convergence value of 1 Pa has been taken for further analysis.

5.3.1.2 Stability analysis without pipe wall thermal capacitance effect

Considering above mentioned values of grid size, time step and and loop pressure closure convergence criterion a typical stable (400 W), unstable (500 W) and neutrally stable (450 W) case was obtained at 9.1 MPa and 15 lpm secondary flow as shown in figure 5-16. The complete

stability results for secondary side flow i.e. 15 lpm are shown in figure 5-17a & 5-17b. The loop is found to be stable at 400 W, becomes unstable at 500 W and continues to be unstable till 1300 W and again becomes stable at 1350 W as shown in figure 5-17a. The instability is predicted for heater inlet temperature varying from 27.8 ^{o}C to 74 ^{o}C (spread across pseudo-critical temperature of 40.5^{o}C at 9.1 MPa) as shown in figure 5-17b.

The typical unstable behaviour predicted by NOLSTA code at 800 W is shown in more detail in figure 5-18a & 5-18b. Figure 5-18a shows continuously increasing amplitude of flow oscillations up to flow reversal. Figure 5-18b shows increasing amplitude of both heater inlet and outlet temperature oscillations having time period of 18.4 s (steady state loop circulation time of 20.8 s) which indicates development of instability by Welander mechanism (Welander, 1967). The Welander mechanism of instability development by oscillation growth mechanism is observed for development of instability from steady state condition in SPNCL as shown in figures 5-2a, 5-3a, 5-4a & 5-5a. This is typical phenomenon of development of instability during single phase natural circulation at sub-critical conditions which mostly (but not always) leads to flow reversal. However, no flow reversal occurred during the experiments.

At 90 lpm of secondary side flow, the unstable zone increases (i.e. 1200 W to 3400 W) as shown in figure 5-19a. However, heater inlet temperature range over which instability is observed reduces substantially i.e. 27.3 ^{o}C to 47.3 ^{o}C also spread across the pseudo-critical temperature (figure 5-19b). At higher flow rate of 135 lpm even the power range of instability reduces i.e. 2200 W to 3500 W as shown in figure 5-20. At 2200 W which is the lower threshold of instability at 135 lpm limit cycle oscillation without flow reversal having amplitude of 11.2% of average flow is also observed. At still higher secondary flow rate of 180 lpm no instability is

observed as shown in figure 5-21. The secondary flow at which no instability is observed theoretically i.e. 180 lpm differs substantially from experimental values i.e. 34 lpm, however there is some degree of qualitative agreement.

The stability maps for closed loop SPNCL at 8.1 & 9.1 MPa for HHHC orientation are shown in figure 5-22. NOLSTA predicts a very large unstable zone but the predictions are in qualitative agreement with experimental findings i.e. instability is predicted over a range of power with lower & upper stable zones and at higher secondary flows no instability is predicted. Code predicts instability in the power range required for near pseudo-critical operation where the volumetric expansion coefficient of fluid is very high i.e. the power required making loop average temperature equal to pseudo-critical temperature has also been plotted for each pressure i.e. 8.1 MPa and 9.1 MPa in figure 5-22. One dimensional codes are known to produce larger unstable zone but thermal capacitance of pipe wall can have strong stabilizing effect on stability behavior of single phase natural circulation loops. Hence, the same has been considered in the next section.

5.3.1.3 Stability analysis with pipe wall thermal capacitance effect

One dimensional model for simulating thermal capacitance of pipe wall (value – 3.98×10^6 J/(m^3 K), for SS-347) was incorporated in NOLSTA code. For every single control volume of fluid (having faces *j* and *j*+1) there is corresponding single heat structure volume denoted by grid point *k*, at the center heat structure volume.

Energy balance equation for pipe wall:

$$C_w \frac{\partial T_w}{\partial t} = U_i A_{htri}(T_b - T_w) - U_o A_{htro}\left[T_w - \left(T_{amb} \text{ or } T_s\right)\right] + q''' A\Delta x \qquad (5\text{-}5)$$

$q''' = 0$, for cooler/ adiabatic walls in eq. (5-5)

The same has been dicretized in the following form as

$$(T_w)_k^{n+1}\left(1+\frac{U_i A_{htri}\Delta t}{C_w}+\frac{U_o A_{htro}\Delta t}{C_w}\right)= (T_w)_k^n+\frac{U_i A_{htri}\Delta t}{2C_w}\left[(T_b)_j^n+(T_b)_{j+1}^n\right] + \frac{U_o A_{htro}\Delta t}{C_w}(T_{amb}\ \text{or}\ T_s)+\frac{q''' A\Delta x\Delta t}{C_w} \quad (5\text{-}6)$$

Where

$$\frac{1}{U_i A_{htri}}=\frac{1}{h_i A_{htri}}+\frac{\ln(d_{mid}/d_i)}{2\pi k_w\Delta x}\ \&\ \frac{1}{U_o A_{htro}}=\frac{1}{h_o A_{htro}}+\frac{\ln(d_o/d_{mid})}{2\pi k_w\Delta x},\ d_{mid}=\left(\frac{d_o+d_i}{2}\right) \quad (5\text{-}7)$$

Thermal capacitance of each node length of pipe wall, $C_w = \rho_w A_w c_{pw}\Delta x$ (5-8)

As concluded in the previous chapter inside heat transfer coefficient (h_i) of cooler is estimated by Bringer Smith (1957) correlation, whereas Jackson(2002) correlation has been used to calculate inside heat transfer coefficient in heater/adiabatic pipe walls. The large instability zone as observed in the previous section (figure 5-22) vanishes all of a sudden by including pipe wall capacitance effect as shown for a most unstable case (called most unstable while considering without pipe wall thermal capacitance effect) for loop diameter of 13.88 mm at 10 lpm secondary flow, see figure 5-23. Some arbitrary changes were made to gain some insight in to stability behavior of SPNCL. Considering tolerance on thickness of ½" Sch. 80 commercial pipes available in the market (used for fabrication of SPNCL), the maximum inside diameter possible for the pipe is 14.9 mm, however instability could be obtained by only considering ID - 15.5 mm. Increasing the ID to 15.5 mm results in reduction in thermal capacitance of the pipe wall by 18%. Local losses were also not considered for the calculations. All these modifications may not be appropriate but gives some relevant results. Consideration of ID – 15.5 mm gives limit cycle oscillations without flow reversal (amplitude of the oscillation is 11.9%) and on increasing the

ID to 16.5 mm makes the loop more unstable as shown in figure 5-23. Another important thing is that this limit cycle oscillation for ID 15.5 mm case is just a neutrally stable case because increasing the loop power by $\pm$ 25 W makes the loop stable as shown in figure 5-24. However, the amplitude of limit cycle oscillations is very high (11.9%) as compared to amplitude of just 1.5% neutrally stable case obtained without pipe wall effect, see figure 5-16.

Instability was missed several times during experimentation also because it is just the neutrally stable case and requires very narrow adjustment of power to get instability. If ½" Sch. 40 pipe would have been used for fabrication of SPNCL flow reversal as well as larger unstable zone could have been achieved (see the flow reversal case for ID 15.8mm loop case) as shown in figure 5-25. The loop is predicted to be stable for higher secondary flows i.e. 34 lpm as shown in figure 5-26 which is in agreement with experimental data.

Moreover interaction of the fluid with heat structures can also affect the stability behavior of the loop. The same can be studied in more detail by 3D-CFD code.

5.3.2 Analysis for open loop with wall thermal capacitance effect

The results for stability analysis of Lomperski's loop without considering pipe wall were presented in section 5.2.1 which indicated threshold of instability as 7.5 kW, however no instability was observed in experiments. Considering strong damping effect of pipe wall thermal capacitance on stability behaviour for closed loop boundary conditions, effect of the same was also studied for open loop boundary condition in Lomperski's loop. As expected the instability threshold was pushed from 7.5 kW to 14.7 kW as shown in figure 5-27. Since the experimental graphs available in (Lomperski et al., 2004) are only up to 13 kW power, it shows that stability

threshold is pushed beyond the range of experiments conducted on the loop and explains the reason for non-observance of instability in the loop.

Hence, thermal capacitance of pipe walls should be definitely considered for stability analysis of natural circulation at supercritical conditions unlike two phase natural circulation case. In two phase natural circulation case there cannot be any energy interaction between two phase fluid and adiabatic heat structure as both will always be at same temperature during the transient. Any perturbation in two phase flow will give rise to a perturbation in two phase fluid enthalpy and void fraction/ density, but perturbation in enthalpy will not give rise to any perturbation in two phase fluid temperature and so there cannot be any thermal interaction with the wall. However, perturbation in supercritical fluid flow will give rise to perturbation in enthalpy/ density and perturbation in enthalpy will also give rise to perturbation in supercritical fluid temperature and hence thermal interaction with the wall becomes possible.

5.4 Conclusions

During experimentation with carbon dioxide, instability has been observed for a very narrow window of power for HHHC orientation only and that too at lower secondary side chilled water flow rate i.e. 10-15 lpm. The instability in the loop was observed in the pseudo-critical temperature range of operation where the volumetric expansion coefficient of the fluid is the highest. For closed loop boundary conditions, NOLSTA code (without considering pipe wall thermal capacitance effect) predicts instability over a large range of power bounded by lower & upper stable zones. Moreover, the instability is predicted even for very high secondary flows i.e. 135 lpm unlike experimental data where no instability was observed at 34 lpm secondary flow. However no instability was predicted at 180 lpm secondary flow. The predictions are only

qualitatively matching with experimental data, hence pipe wall thermal capacitance model was incorporated in NOLSTA code. Consideration of pipe wall thermal capacitance predicts SPNCL to be completely stable, but reducing the thermal capacitance by 18% and neglecting the local losses the code is able to simulate limit cycle oscillations without flow reversal as observed during experiments. As interaction of heat structure and fluid should be modeled in greater detail, hence 3D-CFD codes may be a helpful tool in understanding the stability behavior of closed loop thermo syphon with supercritical fluids.

The modified NOLSTA code with pipe wall effect was also used for studying stability behavior for an open loop i.e. Lomperski's loop. The consideration of pipe wall thermal capacitance pushed stability threshold beyond the experimental power range and explains the reason of instability not observed during experiments. Modeling of thermal capacitance of pipe walls is strongly recommended for stability analysis of natural circulation at supercritical conditions (both open and closed loop boundary conditions) unlike two phase natural circulation flow case. In two phase natural circulation case there cannot be any energy interaction between two phase fluid and adiabatic heat structure as both will always be at same temperature during the transient. Any perturbation in two phase flow will give rise to a perturbation in two phase fluid enthalpy and void fraction/ density, but perturbation in enthalpy will not give rise to any perturbation in two phase fluid temperature and so there cannot be any thermal interaction of fluid with the wall. However, perturbation in supercritical fluid flow will give rise to perturbation in enthalpy/ density and perturbation in enthalpy will also give rise to perturbation in supercritical fluid temperature and hence thermal interaction with the wall becomes possible.

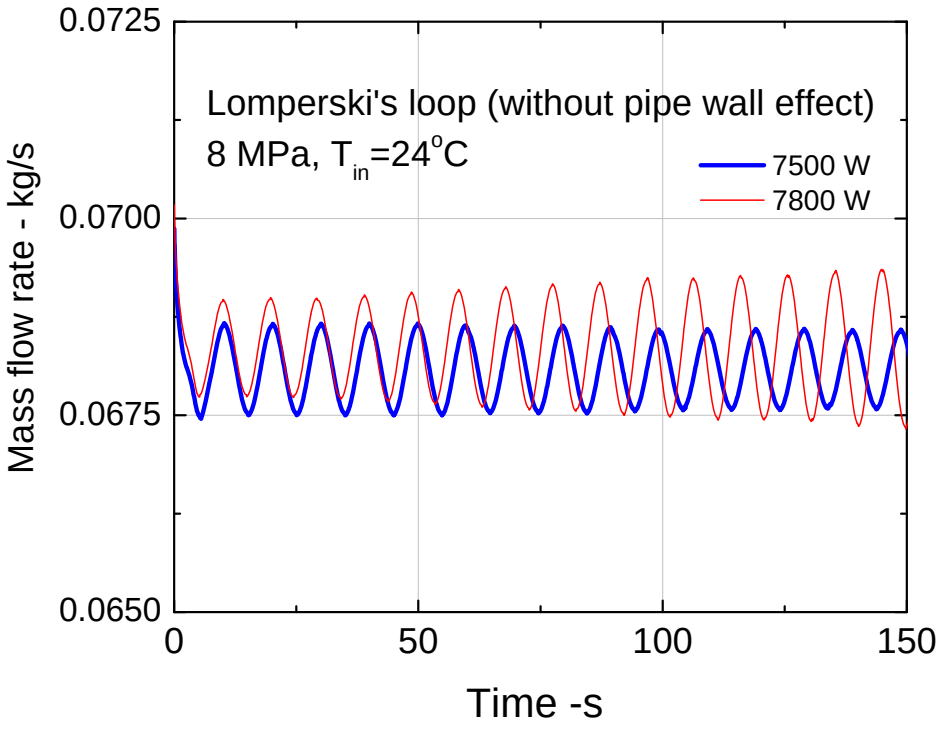

Figure 5-1: Prediction of instability for Lomperski's loop at 8 MPa and 24°C heater inlet temperature

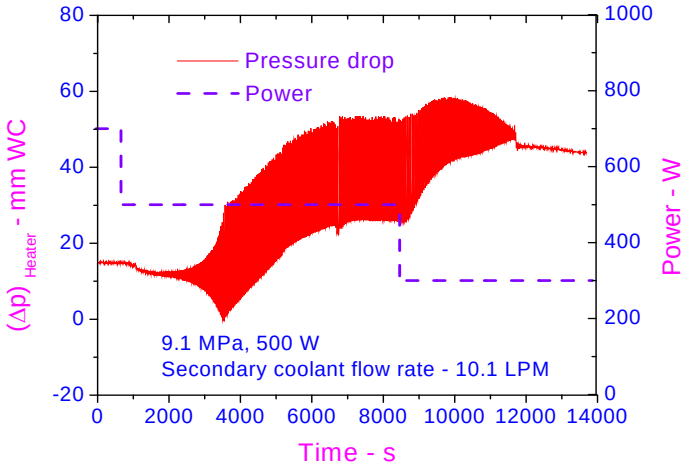

(a)

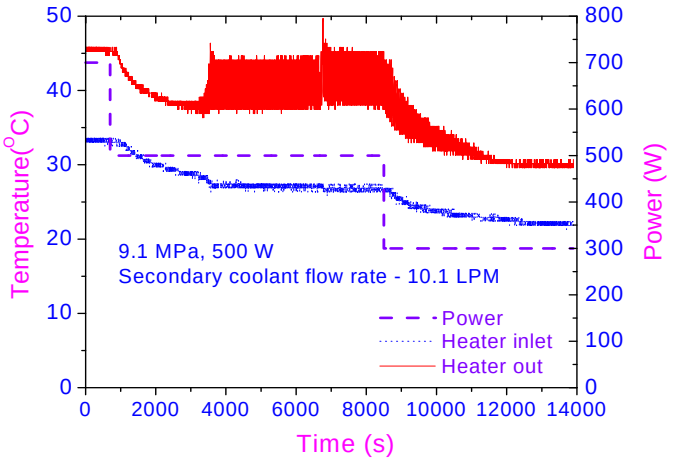

(b)

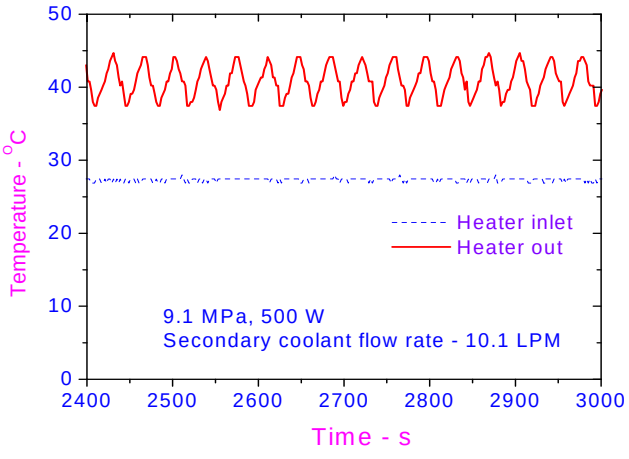

(c)

Figure 5-2: Typical unstable behavior at 500 W for HHHC orientation with SC-CO_2 operation.

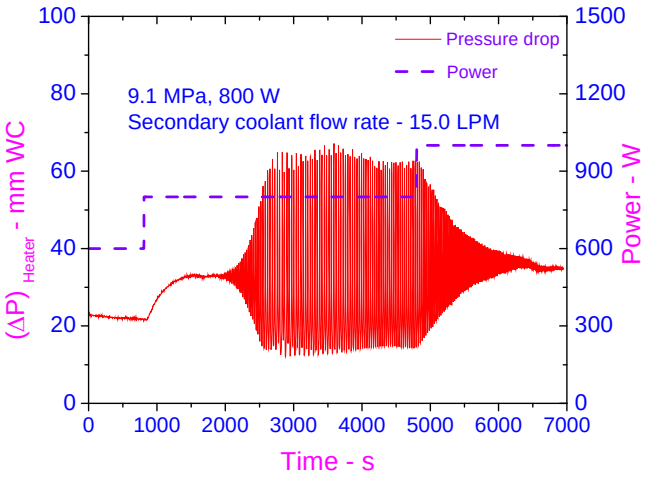

(a)

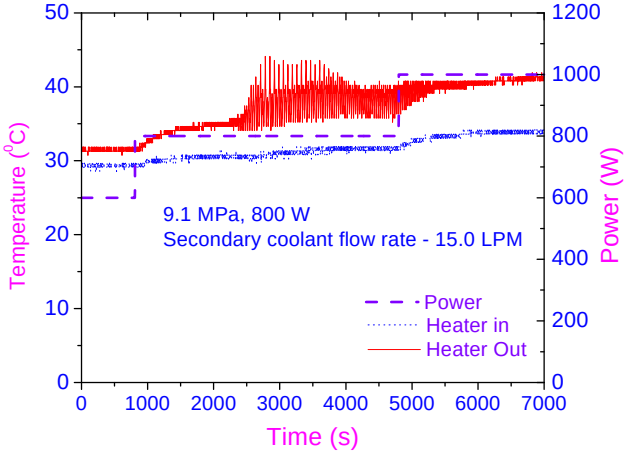

(b)

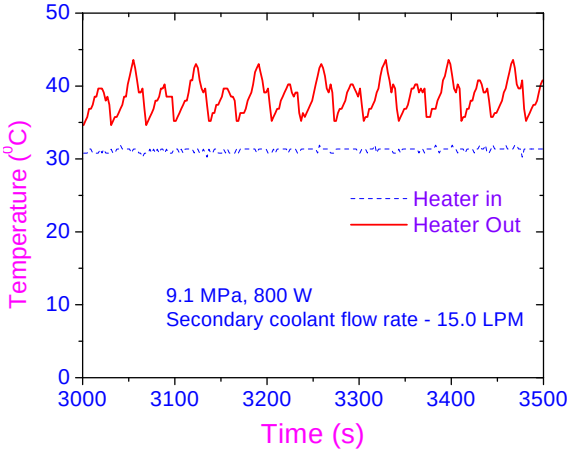

(c)

Figure 5-3: Typical unstable behavior at 800 W for HHHC orientation with SC-CO_2 operation.

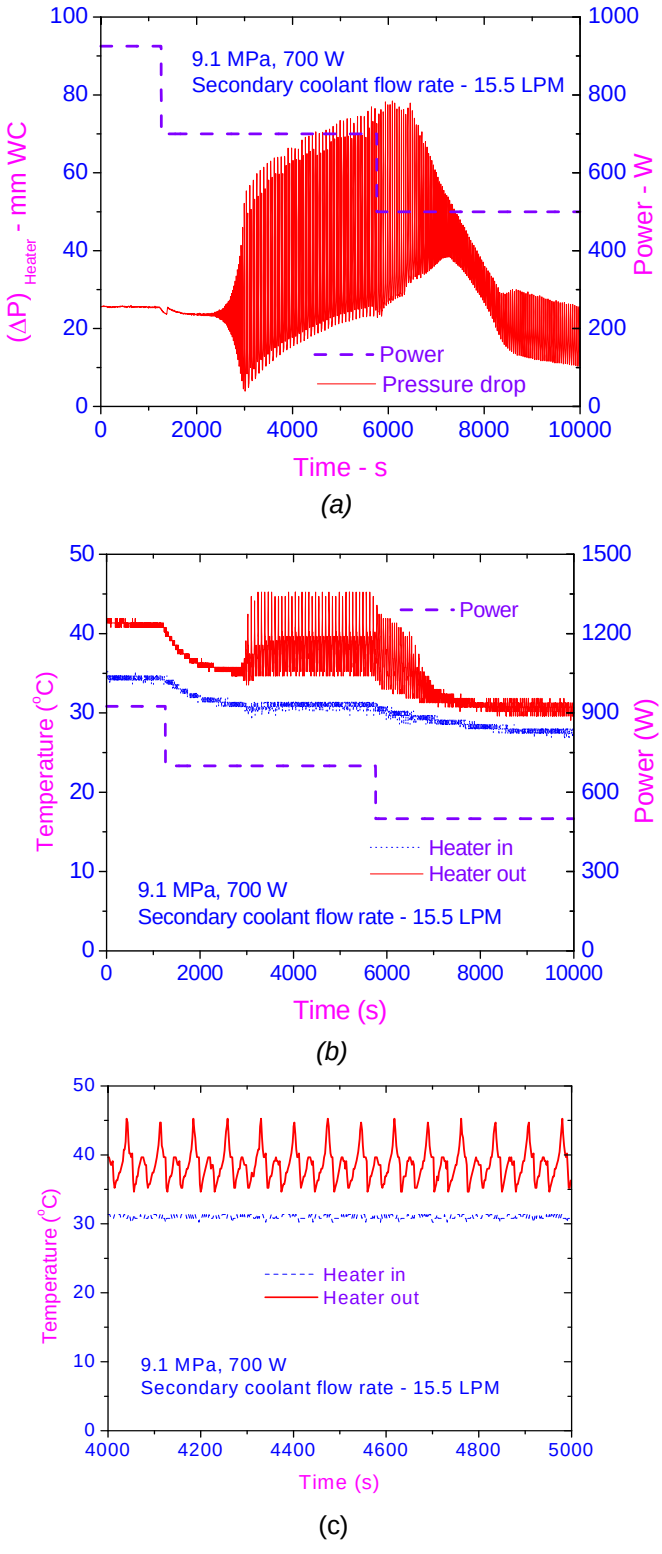

Figure 5-4: Typical unstable behavior at 700 W for HHHC orientation with SC-CO_2 operation.

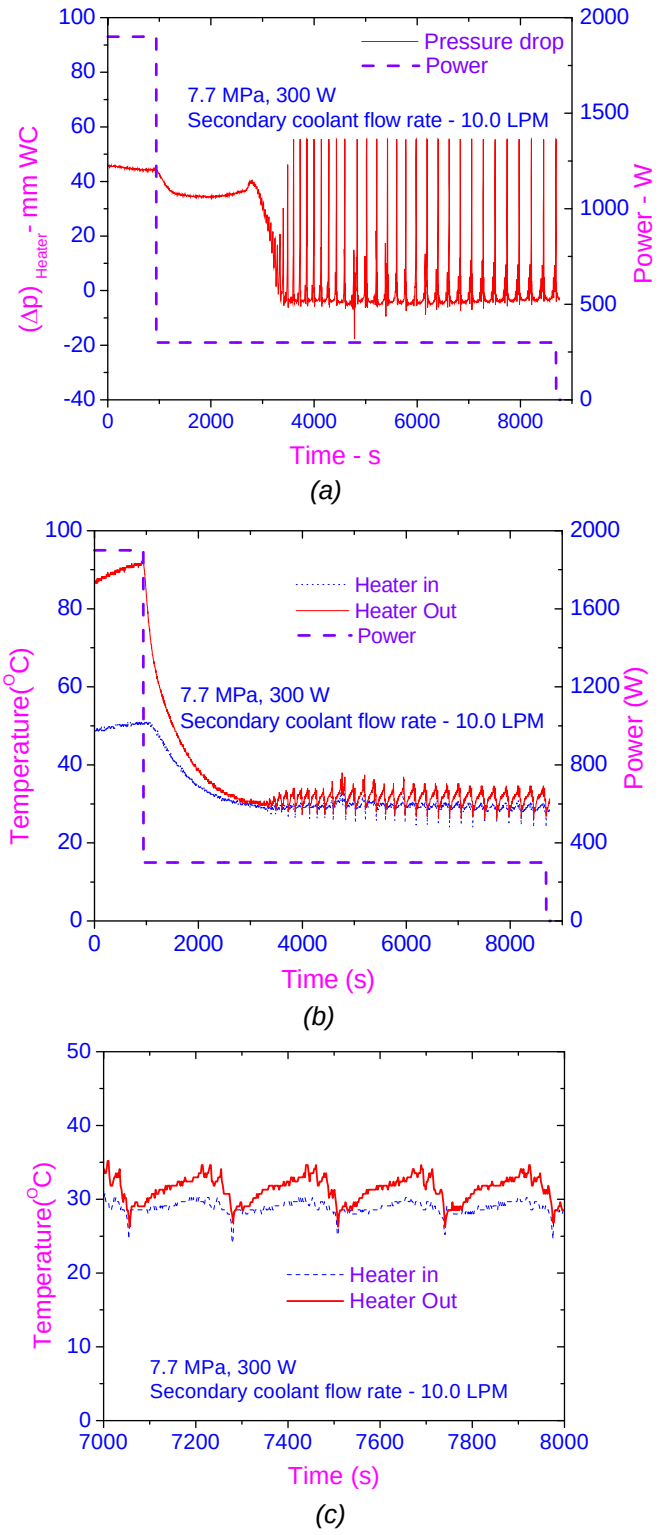

Figure 5-5: Typical unstable behavior at 300 W for HHHC orientation during power step down with SC-CO_2 operation.

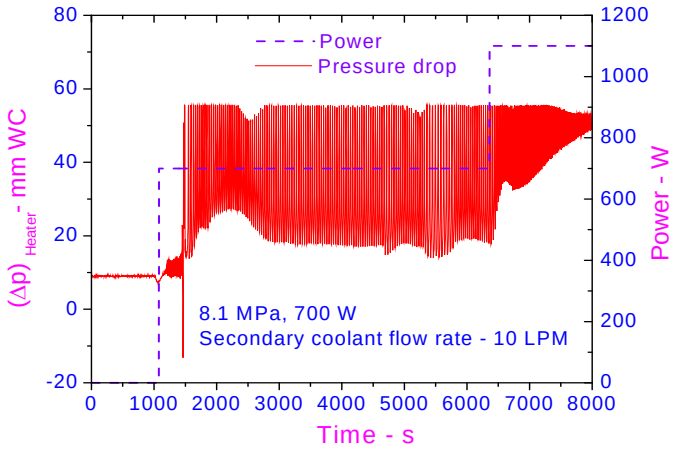

(a)

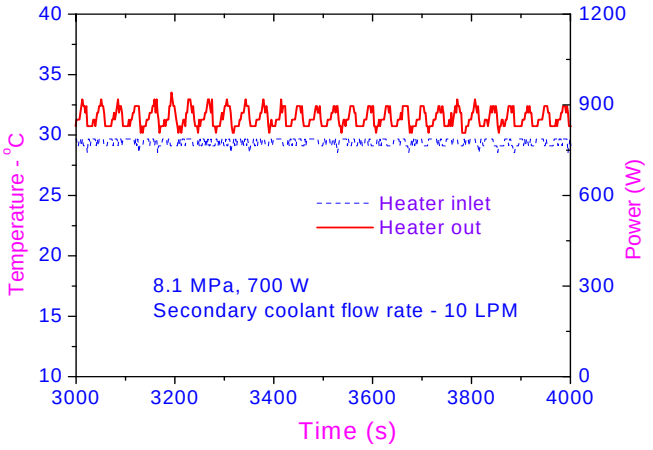

(b)

Figure 5-6: Typical unstable behavior at 700 W for HHHC orientation during power step rise with SC-CO_2 operation.

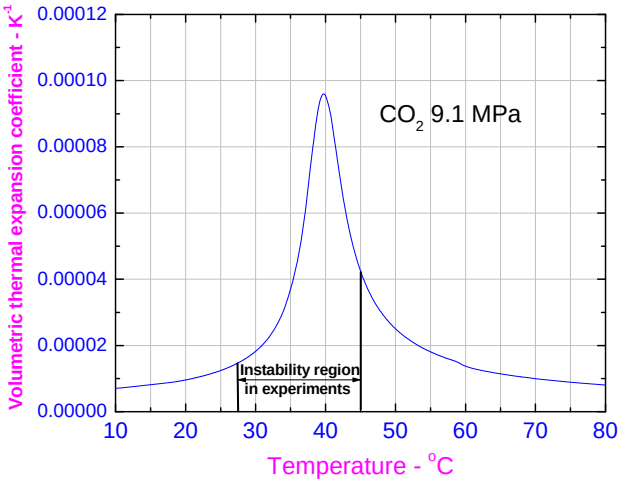

Figure 5-7: Variation of volumetric thermal expansion coefficient of carbon dioxide with temperature at 9.1 MPa pressure

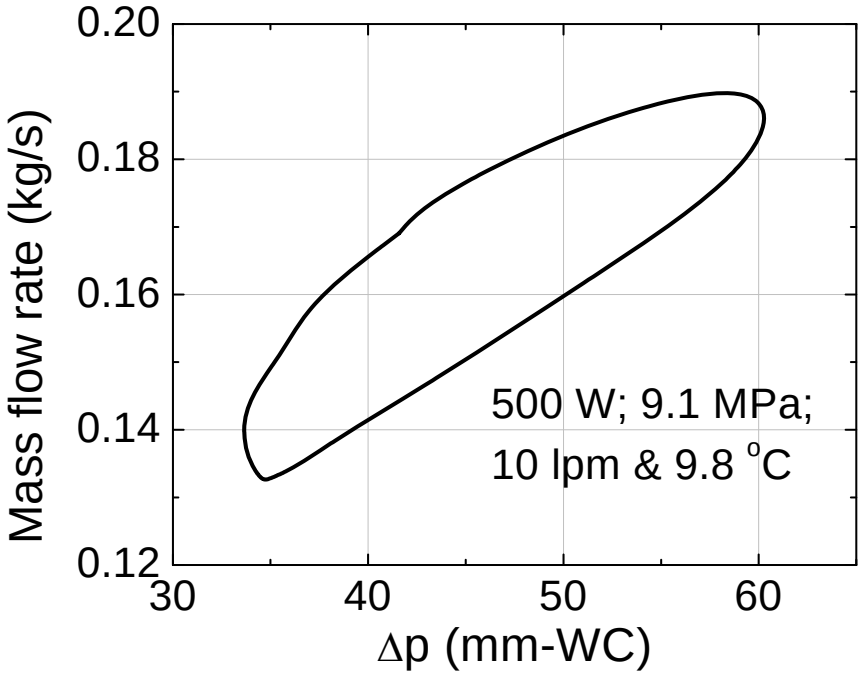

Figure 5-8: Phase plot of single cycle oscillation at 500 W corresponding to time series in figure 5-2

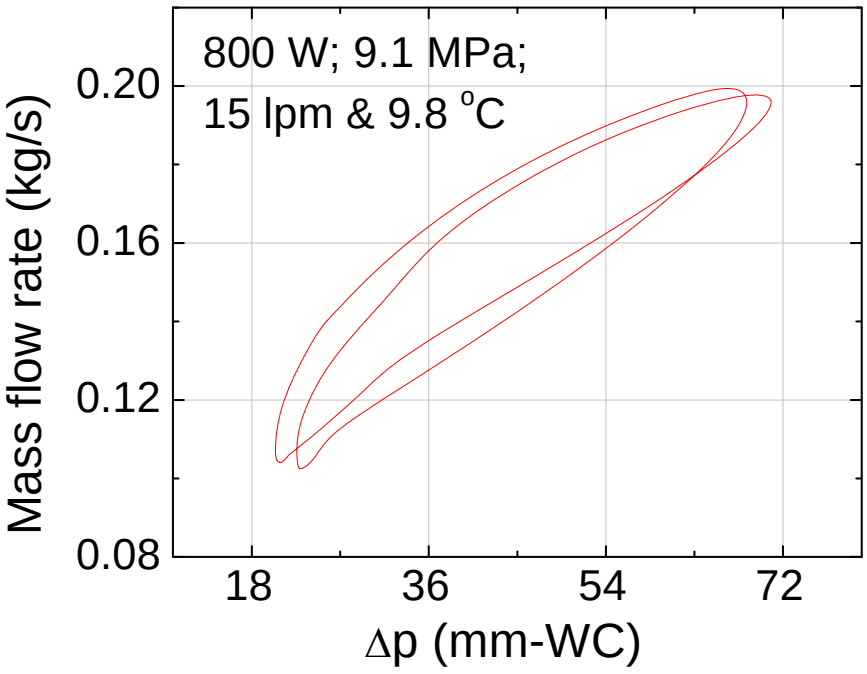

Figure 5-9: Phase plot of single cycle oscillation at 800 W corresponding to time series in figure 5-3

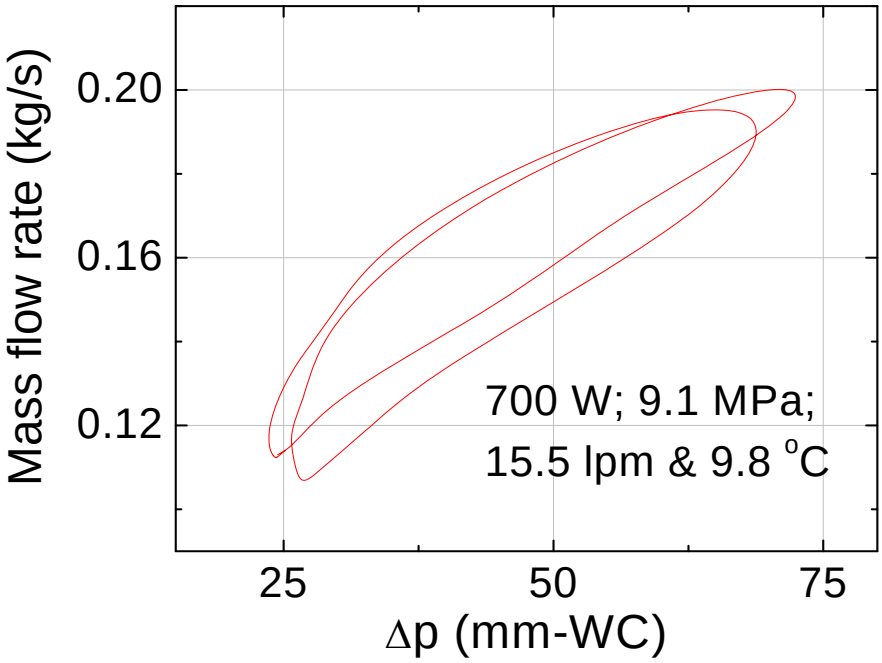

Figure 5-10: Phase plot of single cycle oscillation at 700 W corresponding to time series in figure 5-4

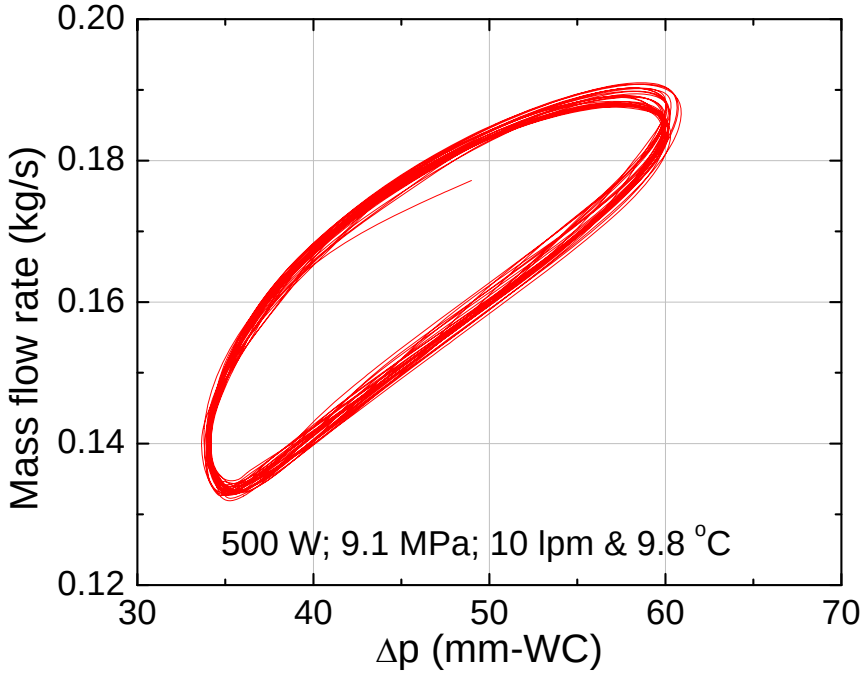

Figure 5-11: Long duration phase plot at 500 W corresponding to time series in figure 5-2

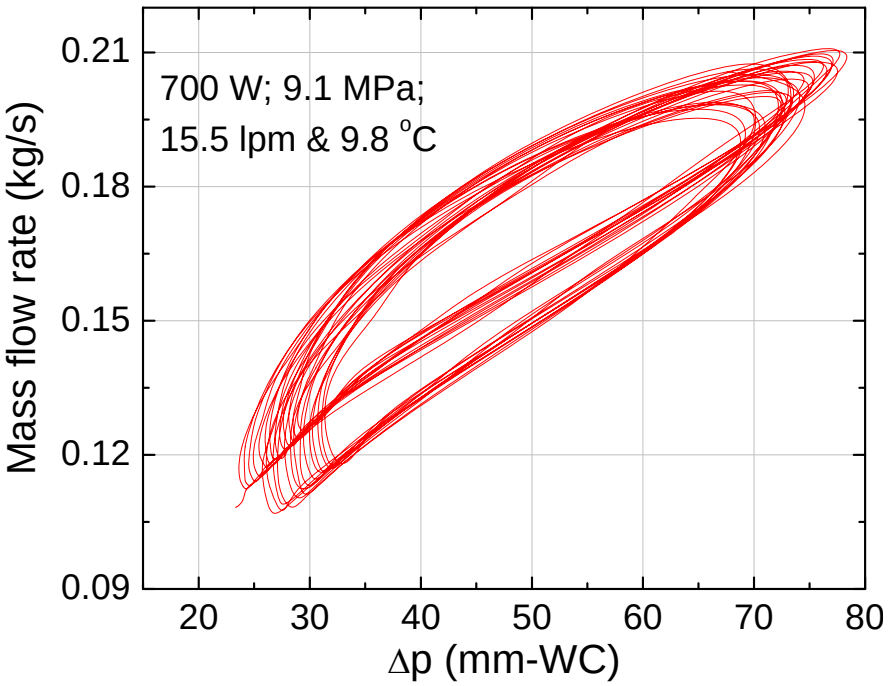

Figure 5-12: Long duration phase plot at 700 W corresponding to time series in figure 5-4

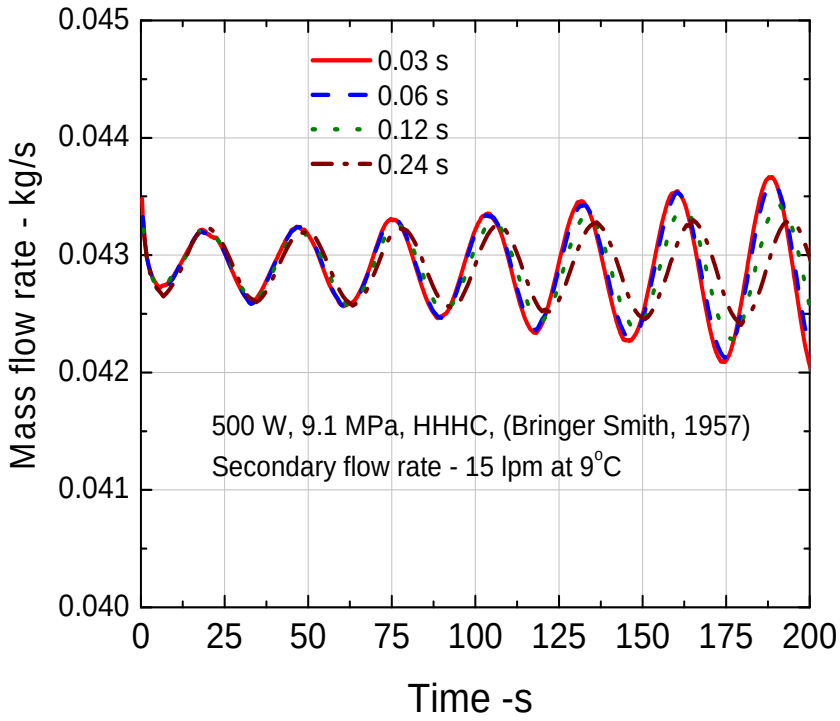

Figure 5-13: Time step sensitivity study for stability behavior of closed loop SPNCL with SC-CO_2 operation

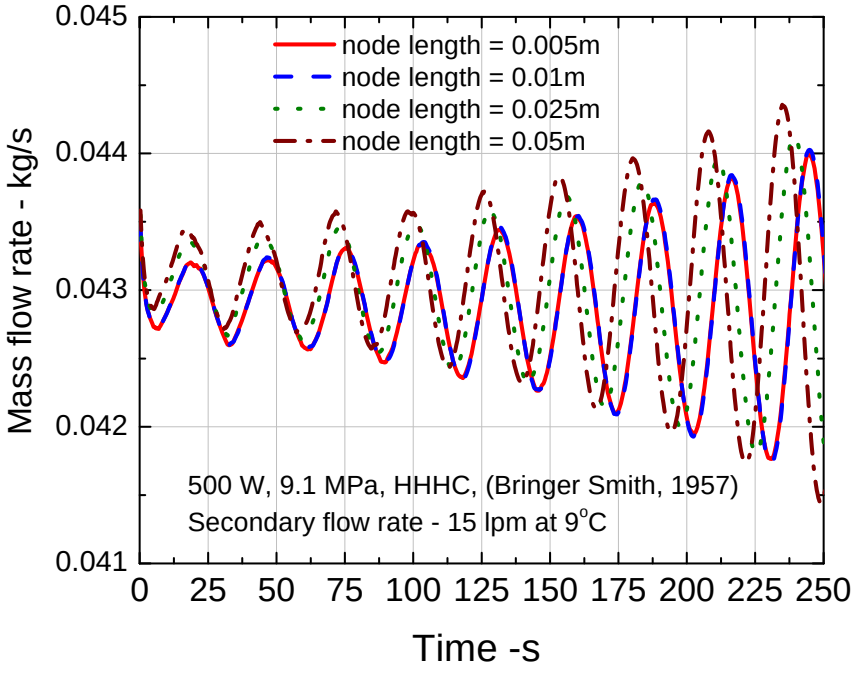

Figure 5-14: Grid size sensitivity study for stability behavior of closed loop SPNCL with SC-CO_2 operation

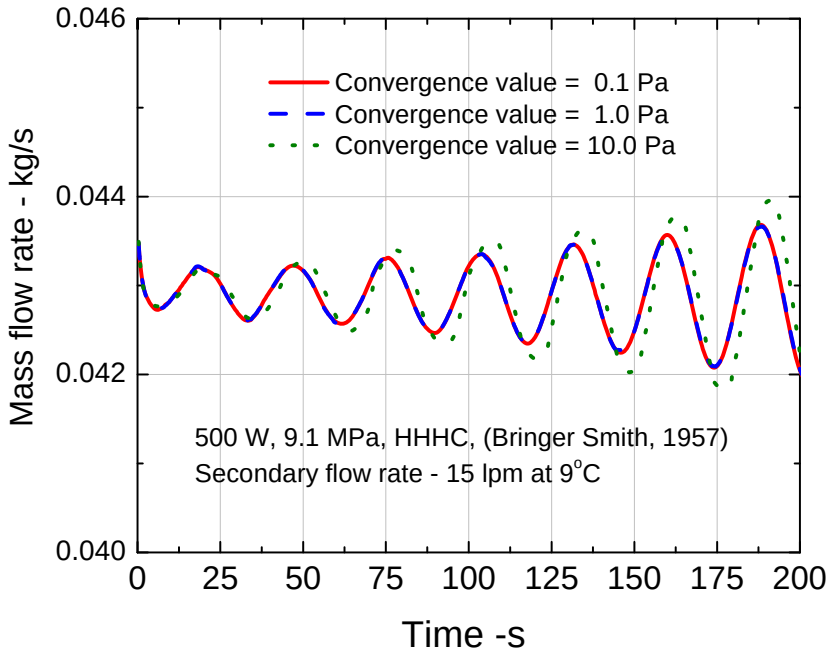

Figure 5-15: Effect of loop pressure closure convergence criterion on stability behavior of closed loop SPNCL with SC-CO_2 operation

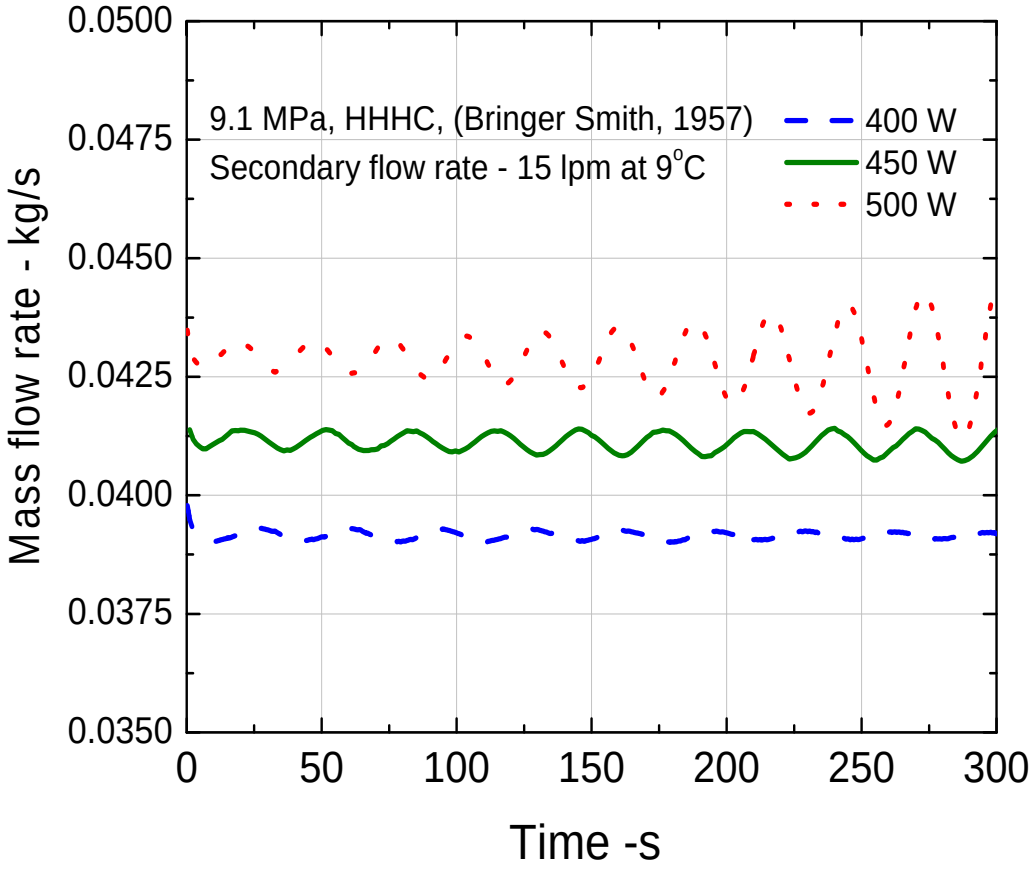

Figure 5-16: Stable, unstable and neutrally stable operating conditions for SPNCL with SC-CO_2 operation

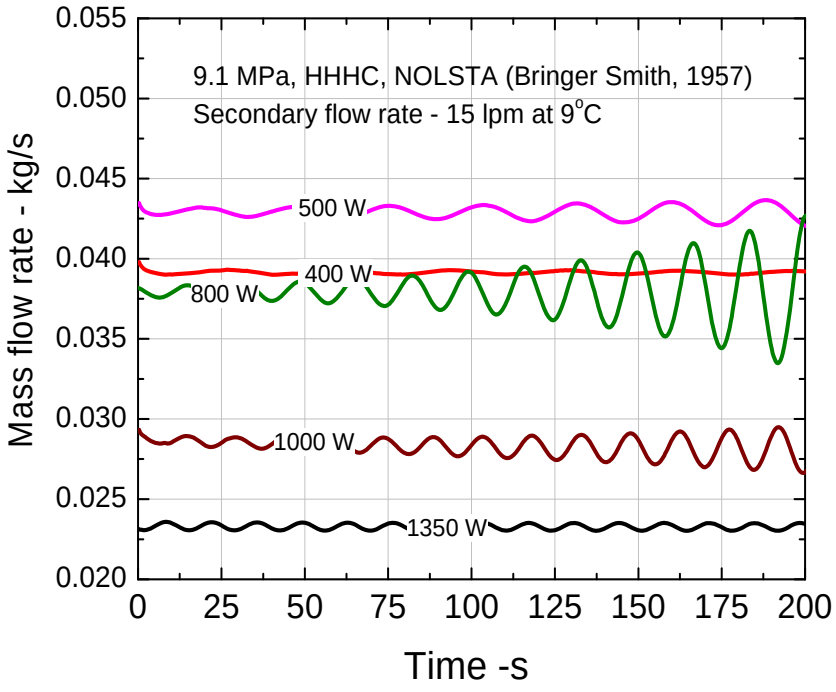

(a)

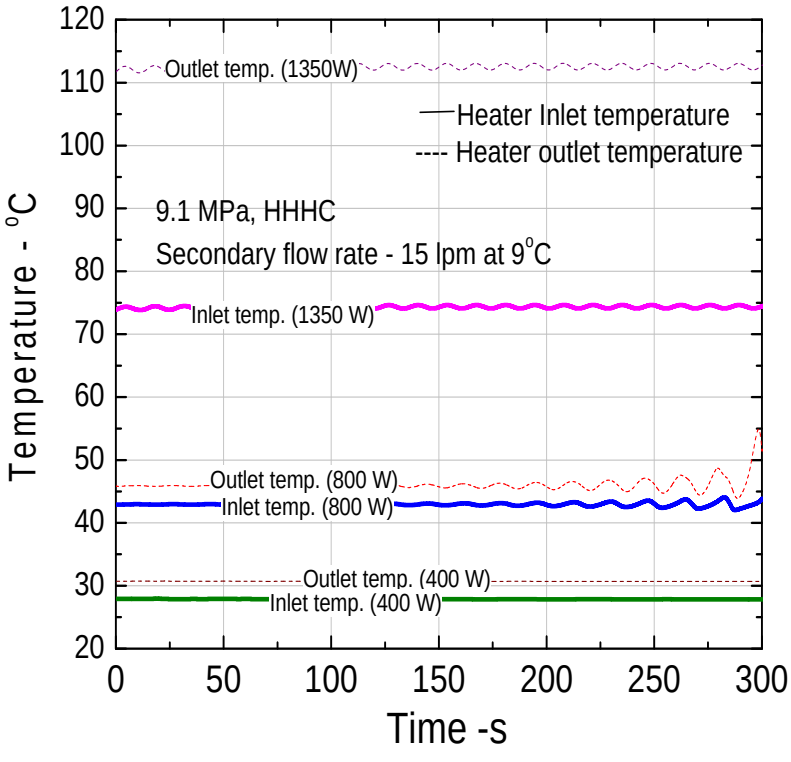

(b)

Figure 5-17: Stability predictions for closed loop SPNCL for HHHC orientation at 15 lpm.

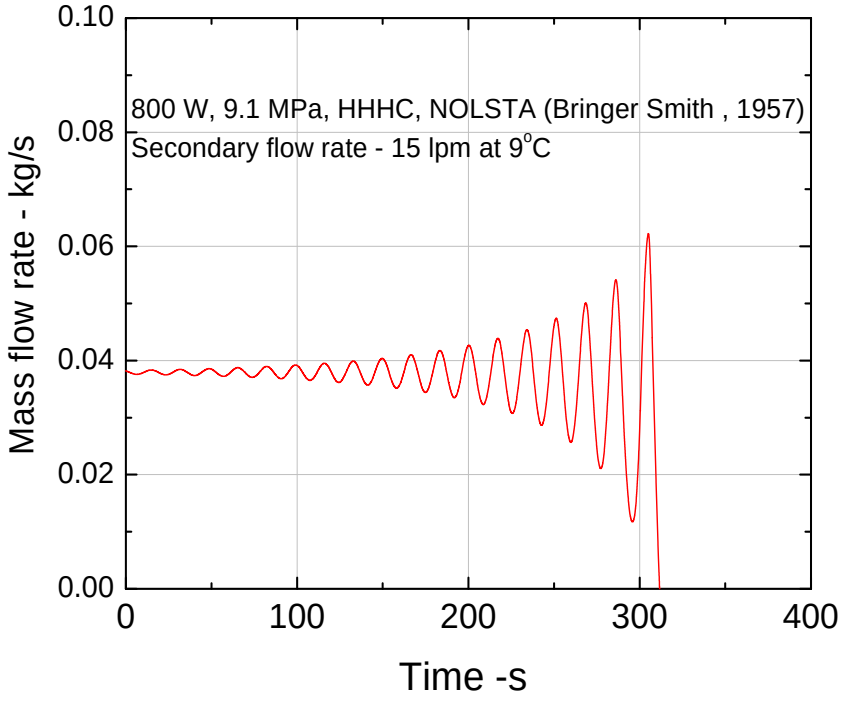

(a)

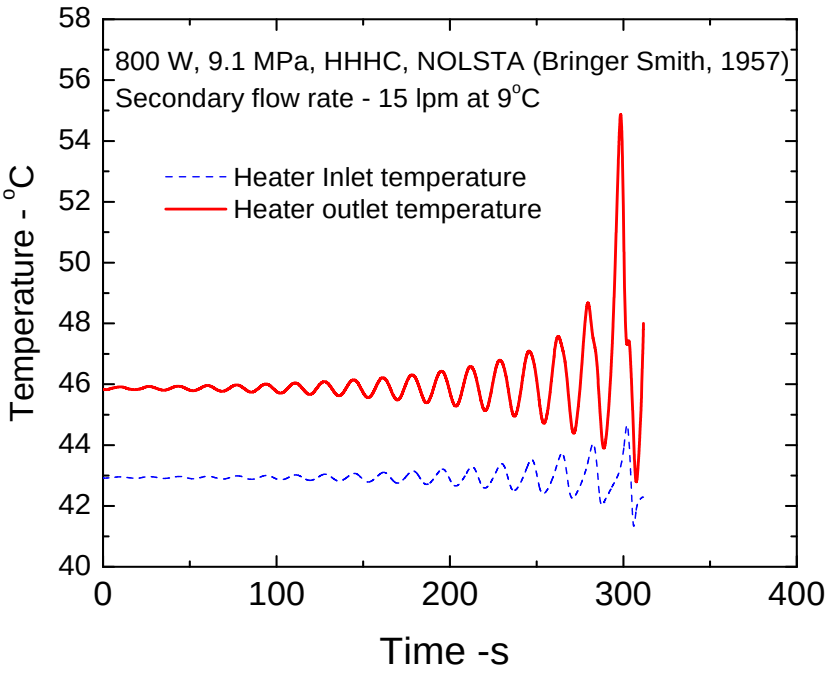

(b)

Figure 5-18: Prediction of instability at 800 W by NOLSTA code in more detail.

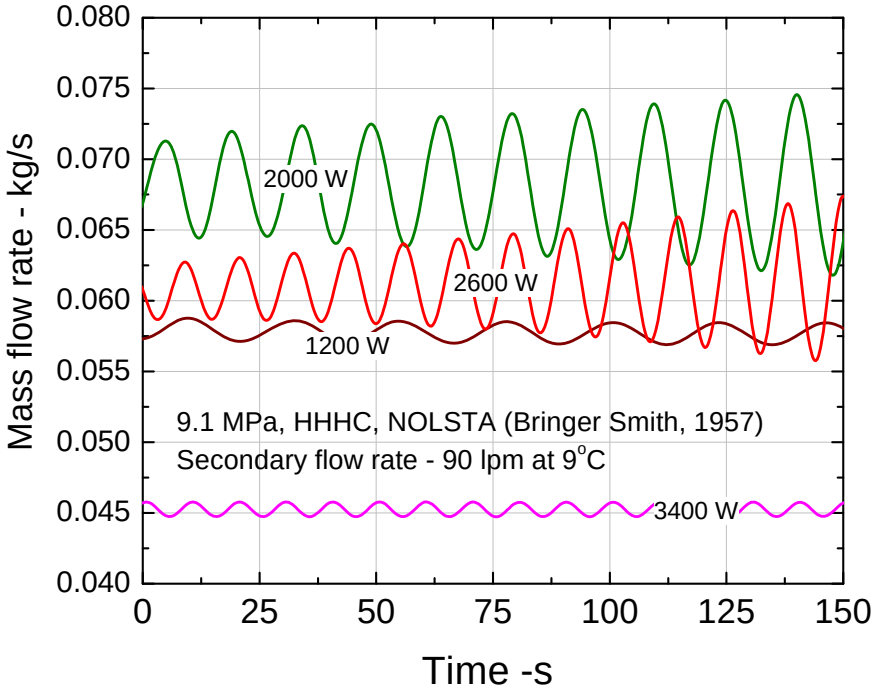

(a)

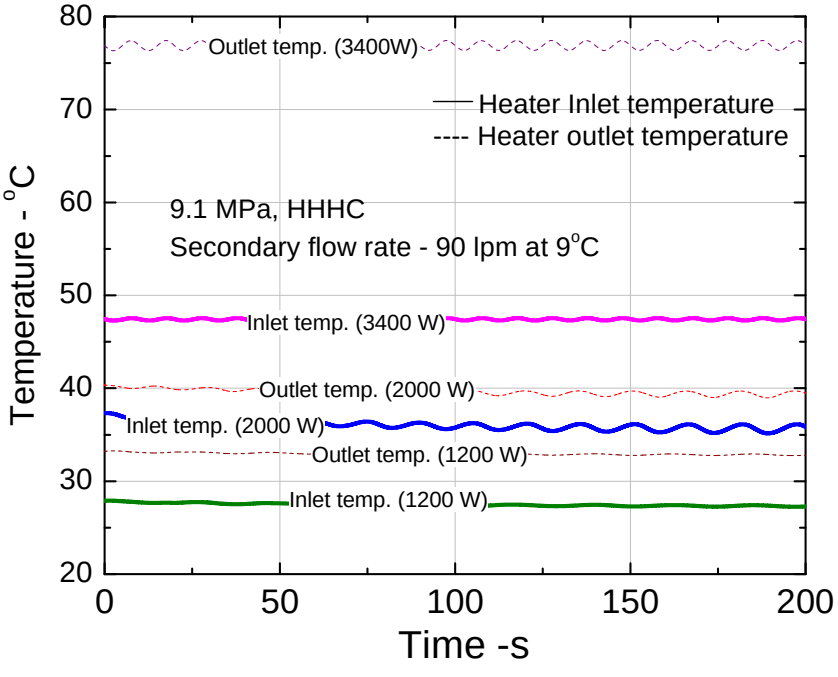

(b)

Figure 5-19: Stability predictions for closed loop SPNCL with HHHC orientation at 90 lpm.

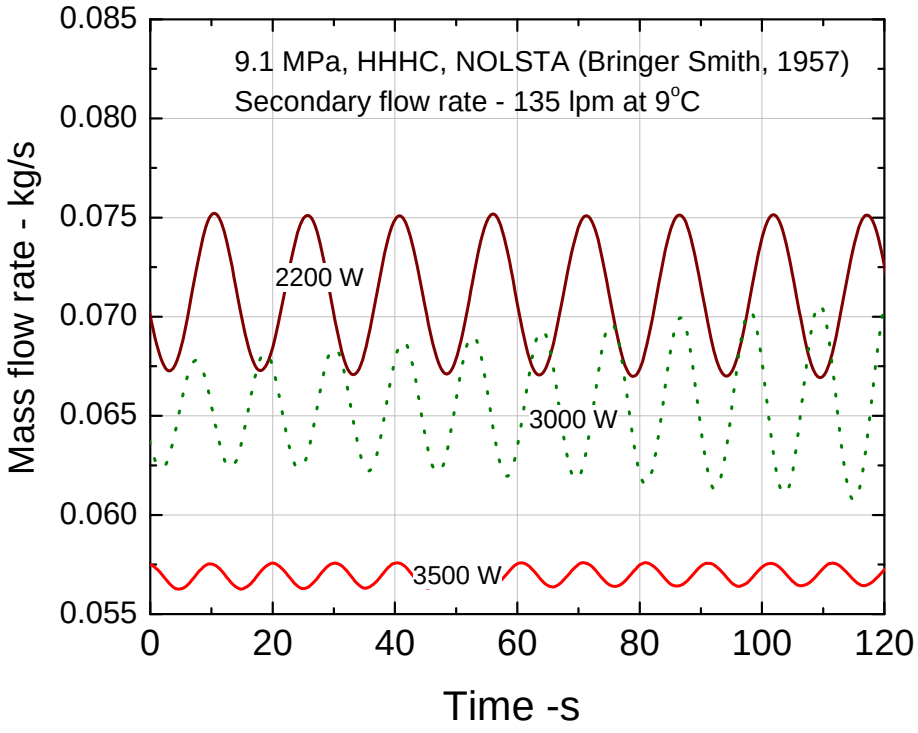

Figure 5-20: Stability predictions for SPNCL at 135 lpm

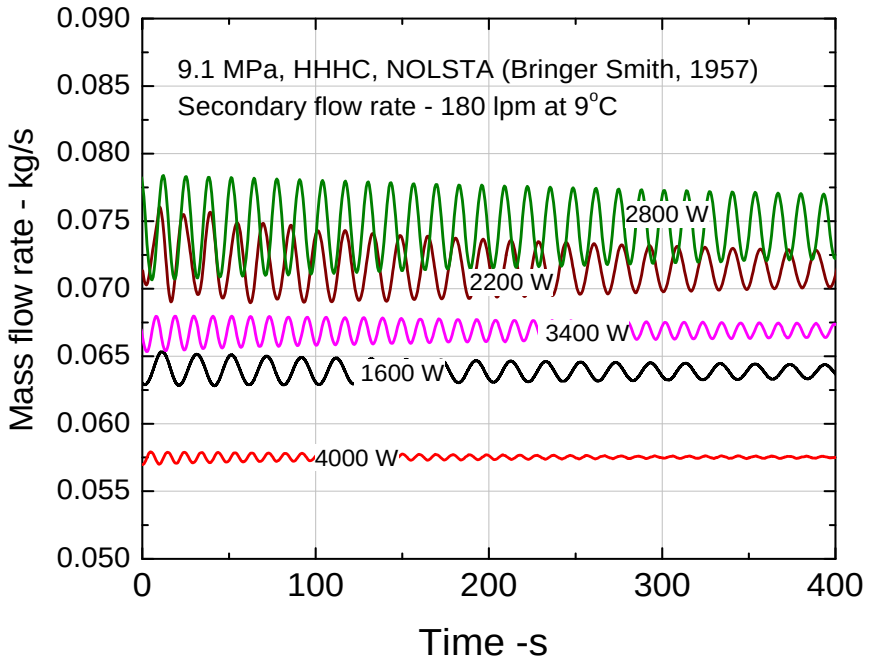

Figure 5-21: Stability predictions for SPNCL at 180 lpm

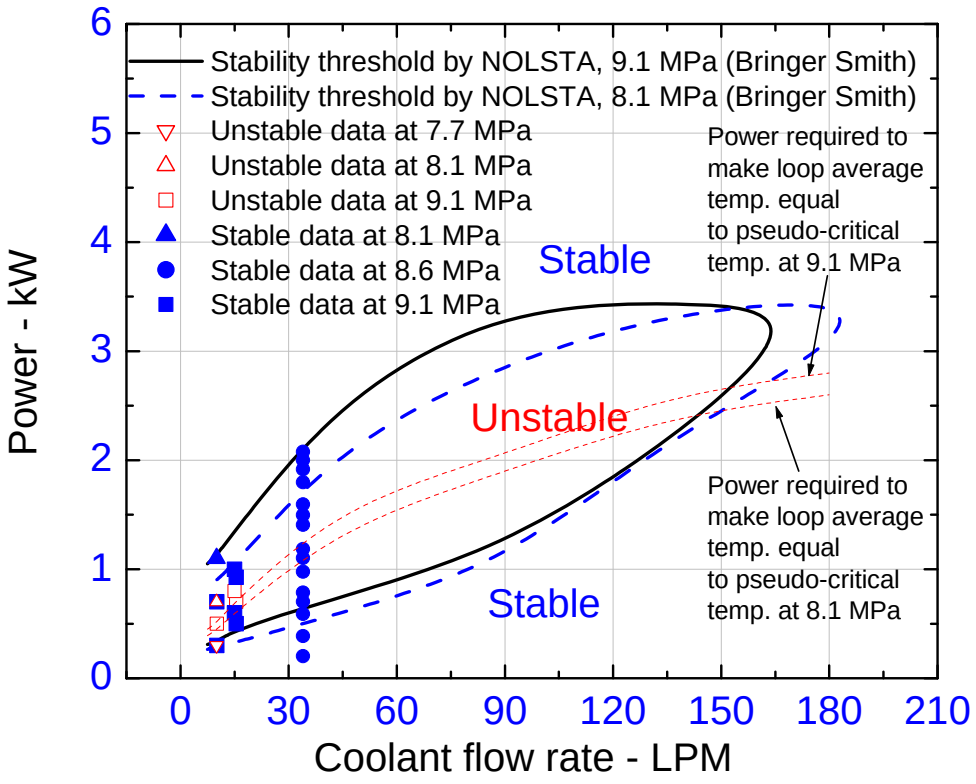

Figure 5-22: Stability maps for closed loop SPNCL with HHHC orientation at different pressures

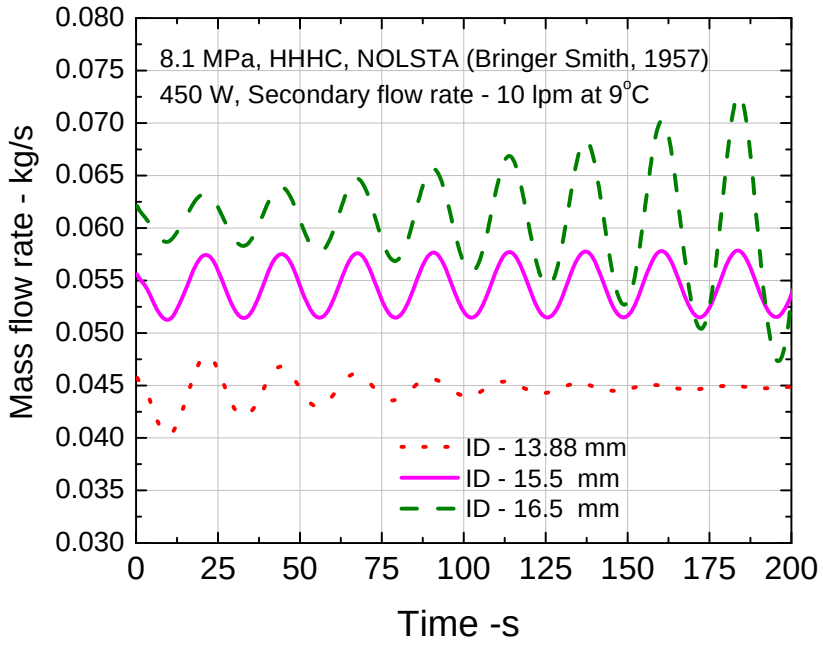

Figure 5-23: Effect of loop inside diameter on stability behavior of SPNCL

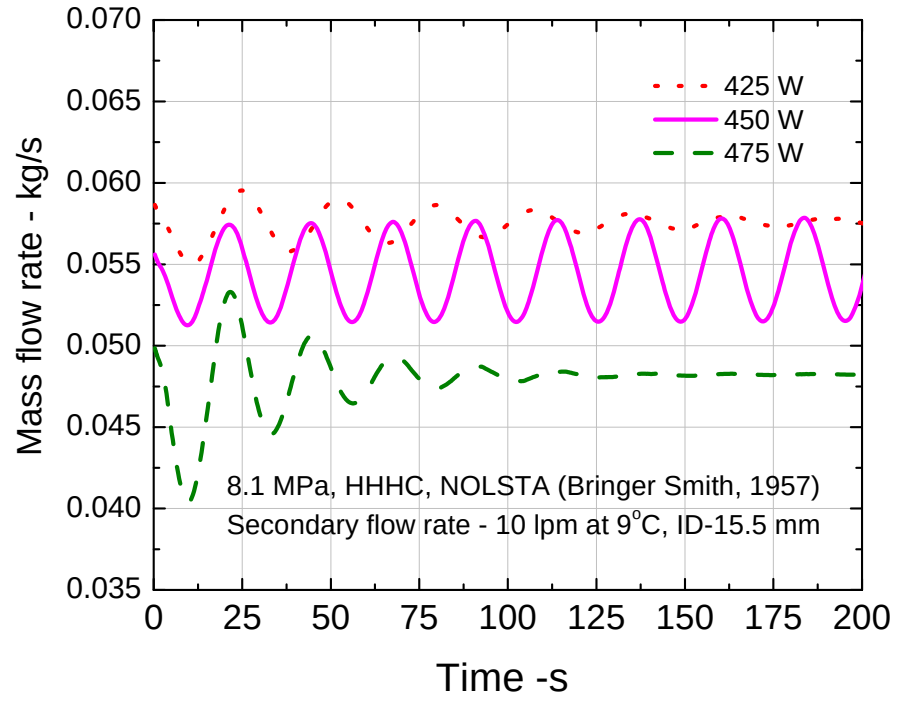

Figure 5-24: Effect of power on the limit cycle oscillations observed in SPNCL

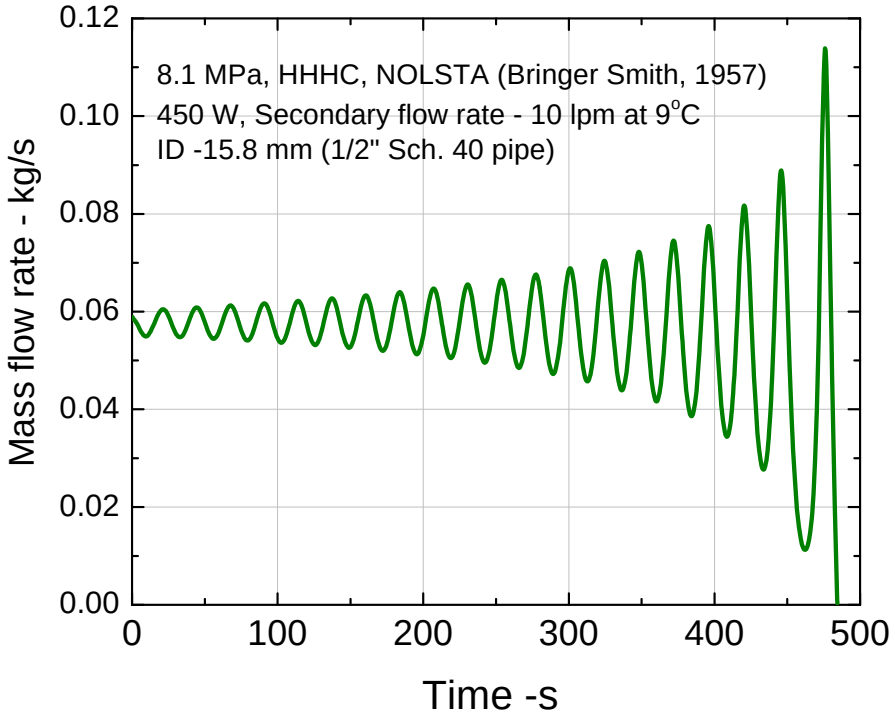

Figure 5-25: Flow reversal case obtained for ID -15.8 mm in SPNCL

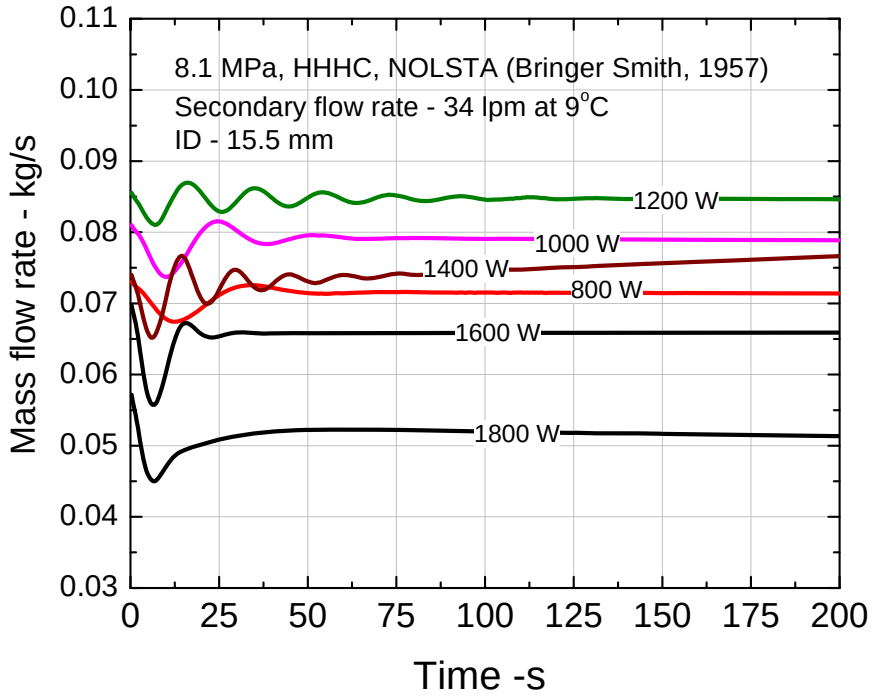

Figure 5-26: Completely stable behavior of SPNCL obtained by considering wall thermal capacitance at 34 lpm.

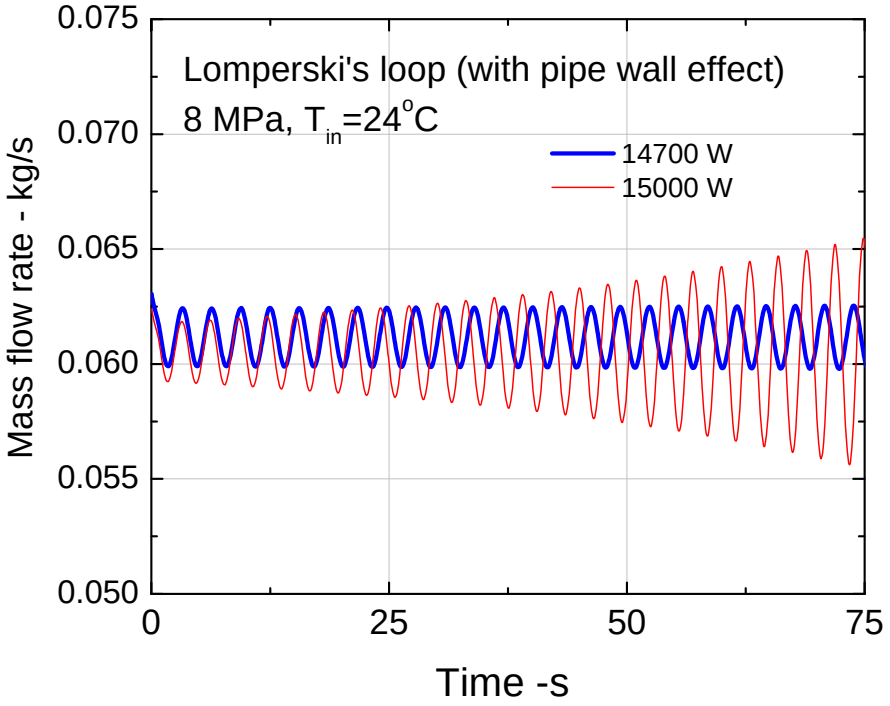

Figure 5-27: Stability threshold of Lomperski's loop after considering thermal capacitance of pipe wall.

Chapter 6

Natural convective flow and heat transfer studies for supercritical water in SPNCL

6.1 Introduction

Supercritical Pressure Natural Circulation Loop (SPNCL) was set up at Bhabha Atomic Research Centre (BARC), India to gain an insight in to steady state, flow stability and heat transfer behavior of natural circulation with supercritical fluids i.e. supercritical water and supercritical carbon dioxide. The experimental results and analysis with carbon dioxide operation were presented in chapters 4 & 5. This chapter describes the experimental results and analysis of SPNCL operating with supercritical water (SCW) in detail.

6.2 The experimental loop

6.2.1 Loop augmentation and instrumentation

After carbon dioxide experiments, SPNCL was augmented for supercritical water experiments. This involved installation of two Inconel–625 direct electrical resistance heated heater test sections (one vertical and one horizontal). The material for rest of the loop is SS-347. A new pressurizer for high pressure operation required for supercritical water conditions was designed and fabricated. The coolers are tube in tube type with SCW flowing in the inner tube and air flowing in the outer annular tube (77.9 mm ID). For this a large capacity air blower (i.e. 45,300 lpm at 20 m WC head) was installed. The loop has a pressurizer connected by U-bend at the

bottom ‘ Tee joint’ of the loop as shown in figure 6-1, which takes care of the thermal expansion besides accommodating the cover gas nitrogen above the water level in pressurizer.

An anubar was installed in the 6” blower outlet line for the air flow measurement. Besides Haskel pump was installed and connected to bottom of the pressurizer for loop pressurization to critical pressure during startup. The schematic and photographs of augmented SPNCL is shown in figure 6-1 and 6-2 respectively. A new 200 kW power supply (25 V/ 8000 A) as shown in figure 6-3 was connected to each heater test section by flexible silver coated copper busbar.

For determination of heat transfer coefficient of heater test sections, thermocouples were brazed on the outer surface of each heater test section, at thirteen different axial locations. At each location, four thermocouples were provided at 90^{o} angular interval (one each at top, bottom, side-ways) as shown in figure 6-4. The photograph of the horizontal heater test section along with brazed thermocouples is shown in figure 6-5. Increased instrumentation also necessitated the use of a new data logger. Figure 6-6 shows the photograph of control panel along with data logger.

Rest of the loop and instrumentation remains same as described in Chapter 4, section 4.2. The accuracy of the thermocouples were within ± 0.5 ^{0}C. The accuracy of the pressure and differential pressure measurements were respectively ± 0.03 MPa and ± 0.18 mm H_2O column. The accuracy of the secondary flow as well as power measurement is ± 0.5 % of the reading.

6.2.2 Experimental procedure

To achieve supercritical pressure the following operating procedure is followed

i) The loop is filled up with water to the required level in the pressurizer.

ii) Nitrogen is filled at the top of the pressurizer and the loop pressure is increased to 11 MPa.

iii) Further pressurization to 22 MPa is achieved by injecting more water at the bottom of the pressurizer with a Haskel pump which increases the water level in the pressurizer. Then the Haskel pump is isolated by closing the isolation valves V1 & V2 shown in figure 6-1.

iv) Now power is switched on and due to thermal expansion of water, the loop gets pressurized above 22.1 MPa (i.e. above the supercritical pressure).

v) To get the desired pressure, water inventory in the pressurizer is changed by either injecting water or draining water. The pressurizer leg remains cold as it is connected by a U-bend to the main loop, facilitating cold water injection in to the pressurizer without concerns of thermal stress.

6.3 Steady state experiments with supercritical water

The steady state experiments were carried out only for Horizontal Heater Horizontal Cooler (HHHC) orientation at different heater powers (1.0–8.5 kW) and loop pressures (22.1-24.1 MPa). All the experimental steady state data for supercritical water has been given in detail in Appendix-II for reference.

6.3.1 Steady state NC flow Experiments

The experimental steady state mass flow rate, heater inlet and outlet temperatures versus power for HHHC orientation with constant secondary side air flow rate are shown in Figures 6-7a & 6-7b respectively. The steady state mass flow rate is estimated by energy balance across heater test section. The temperature difference between heater inlet and outlet is reducing as we are

approaching the pseudo-critical temperature because of the increase in the specific heat (c_p) of the fluid but as the fluid temperature is increased beyond the pseudo-critical point, the c_p value again starts reducing resulting in increased temperature difference. The steady state mass flow rate increases till the heater outlet temperature reaches pseudo-critical temperature at 7 kW. As the power is increased beyond 7 kW, both hot and cold leg becomes supercritical and there is a sharp reduction in experimental flow due to increased frictional resistance. For analysis of experimental results, NOLSTA code steady state solution procedure for closed loop boundary conditions as described in Chapter 4 section 4.3.2 has been used. For steady state calculations, Bringer-Smith correlation (1957) is used for calculating primary side heat transfer coefficient of cooler where as no heat transfer correlation is used in heater (i.e. the heat flux is directly imposed on flowing fluid). The predictions are in good agreement with experimental data.

6.3.2 Steady state heat transfer experiments

The heat transfer coefficient in the heater is estimated from the measured outside surface temperature (*i.e. T3-T54*) of heater pipe at thirteen equidistant locations along the length of each heater as shown in figure 6-4. At each axial location temperature is measured at four 90^o angular locations (each at top, bottom, side-ways) and average of the four values is taken to calculate outside heater surface temperature (T_{wo}). Then, the steady state inside wall surface temperature of heater (T_{wi}) is estimated by a conduction analysis using the following equation.

$$T_{wi} = T_{wo} - \frac{q'''}{2k}\left[r_o^2 \ln\frac{r_o}{r_i} + \frac{r_i^2 - r_o^2}{2} \right] \qquad (6\text{-}1)$$

Inlet and outlet fluid temperatures of heater (T_{in} & T_{out} respectively) are measured by using average of two thermocouples each at heater inlet location (T1 & T2) and heater outlet location (T55 & T56) as shown in Figure 6-1. Corresponding to these inlet and outlet temperatures and pressure, the inlet and outlet enthalpy is obtained from steam tables. Then bulk fluid enthalpy at any location along the heater length was obtained by the linear interpolation of enthalpies at inlet and outlet locations of heater test section as given below.

$$i_b = i_{in} + \frac{x(i_{out} - i_{in})}{L_h} \tag{6-2}$$

From the local bulk fluid enthalpy, local bulk fluid temperature can be calculated from the steam table. From local bulk fluid temperature, inside heater wall temperature and heat input, the local inside heat transfer coefficient (h_i) can be estimated as given below.

$$h_i = \frac{q''' \left(r_o^2 - r_i^2\right)}{2r_i\left(T_{wi} - T_b\right)} \tag{6-3}$$

Uniform volumetric heat generation (q''') is assumed in the heater pipe wall throughout the heated length which is calculated from the ratio of measured total heater power and the volume of the heater pipe wall. It may be noted that at a single power of operation in SPNCL, a complete temperature range of bulk fluid (i.e. sub-critical to supercritical) is not covered from heater inlet to heater outlet. The heat transfer coefficient was found not to be varying significantly with the bulk water temperature along the length of heater for the sub-critical, pseudo-critical and supercritical range of operation due to moderate variation of thermodynamic and transport properties of water from inlet to outlet of heater. Moreover, no deterioration in heat transfer has been observed for the current range of operation of SPNCL as the heat flux encountered is very

low i.e. 38 – 72 kW/m^2. Hence, it is worthwhile to plot average heat transfer coefficient versus average bulk fluid temperature across heater section corresponding to various operating powers. The measured average heat transfer coefficients were compared with various heat transfer correlations available in literature for supercritical fluids (Pl. see Figure 6-8). The peak heat transfer coefficient is observed near the pseudo-critical temperature. All correlations are predicting well in the range of experiments carried out except pseudo-critical region, where only Jackson (2002) and Bringer- Smith (1957) correlations are in good agreement. Even these do not predict the peak value of heat transfer coefficient well.

6.4. Instability experiments with supercritical water

Instability has been observed over very narrow range of power i.e. 7 kW to 8.3 kW in the pseudo-critical temperature region, as was observed for instability experiments with supercritical carbon dioxdie reported previously in chapter 5. Instability was observed for experimental pressure range of 22.1 to 22.9 MPa (the pressure considered is the average of the loop pressure oscillation observed during instability). The reason of finding instability in the pseudo-critical region can be attributed to high volumetric thermal expansion coefficient for SCW and high specific heat near the pseudo-critical temperature. Figures 6-9 to 6-15 show the time series plots for different parameters during the experimental observations of instability. In all cases, the instability develops by the oscillation growth mechanism as proposed by Welander (1967) which is typical phenomenon of development of instability during single phase natural circulation at sub-critical conditions. Welander mechanism of instability can be explained as follows: Pertubation in flow will cause pockets of fluid with pertubed temperature to emerge from the heater/ cooler due to change in fluid residence time in heater/ cooler and these pockets may get

damped or amplified as a consequence of susequent passages through heater and the cooler. Instability development from steady state condition by the oscillation growth mechanism leading to repititive or near periodic flow reversals was also observed in single-phase loops at sub-critical conditions, Vijayan et al. (2007). Near periodic flow reversals are observed in all the instability experiments conducted in SPNCL with supercritical water, however, the amplitude of differential pressure (ΔP) oscillations is asymmetric with larger amplitude in the positive side. No flow reversal was observed for instability experiments conducted with supercritical carbon dioxide (chapter 5). Figure 6-9 shows the instability observed at 7.5 kW (by step rise of power from stable flow power of 7 kW, not shown in figure for clarity) which starts developing at 1350 s (see DPT1 in Figure 6-9) with corresponding heater inlet temperature and pressure of 378.6 ^{o}C & 22.45 MPa respectively (pseudo-critical temperature of water at 22.45 MPa is 375.55 ^{o}C). The oscillations in heater inlet/outlet temperature and pressure become visible a bit late i.e. at 2000 s & 1750 s respectively. The loop pressure is also found oscillating with amplitude of 3 bar approx. whereas no pessure oscillations were observed with supercritical carbon dioxide. This may be due to larger volume of pressurizer (30 liters) in case of experiments with carbon dioxide however lesser pressurizer volume of only 15 liters is available for experiments with supercritical water.

Similar instability is observed at 7.5 kW (Figure 6-10), which starts developing at heater inlet temperature and loop pressure of 379.6 ^{o}C & 22.5 MPa. Flow oscillations grow leading to near periodic flow reversals with almost similar peaks on the positive and negative side. When power is further increased to 8 kW the heater inlet and outlet temperatures increase much beyond the pseudo-critical region leading to stabilization of flow. Figure 6-11 shows similar instability at 7.5

kW which develops at loop pressure of 22.5 MPa and heater inlet temperature of 380 ^{o}C. The instability remains sustained during power step down to 7 kW shown in detail in figure 6-12.

Figure 6-13 shows development of instability at 7.5 kW at loop pressure of 22.7 MPa in the pseudo-critical region. The oscillations are sustained on increasing power to 8 kW showing increase in amplitude of differential pressure, temperature and pressure oscillations. On further increasing power to 8.5 kW the heater inlet/outlet temperatures increase much beyond the pseudo-critical range leading to flow stabilization. Figure 6-14 shows development of instability at 8.0 kW at loop pressure and heater inlet temperature of 22.8 MPa/ 380.5 ^{o}C.

Figure 6-15 shows effect of pressure on instability at 8.3 kW. Development of instability starts at subcritical loop pressure of 21.7 MPa and the instability is sustained at average loop pressure of 22.25 MPa. The instability finally dies out at 23.5 MPa. This may be due to reduction in volumetric thermal expansion coefficient and specific heat with pressure for supercritical fluids, see figure 6-33. The average loop temperatures are increasing with increase of loop pressure (at constant heater power) due to rise of pseudo-critical temperature with pressure.

The phase plot corresponding to a typical oscillation observed at 7.5 kW (Figure 6-10) is shown in Figure 6-16a, but a different signature is obtained for a similar pressure drop oscillation observed in the same experiment, see Figure 6-16b and the phase plot of two combined oscillations is shown in Figure 6-16c. The phase plot of a typical oscillation observed at 7 kW (Figure 6-12) is shown in Figure 6-17a. Figure 6-17b shows the phase plot of complete instability oscillations observed in the Figure 6-12. It shows a highly chaotic behavior of

oscillations. Similarly the phase plots of time series oscillations observed at 7.5 kW & 8 kW (Figure 6-13) are shown in Figures 6-18 & 6-19 respectively.

6.5 Analysis of SPNCL considering pipe wall thermal capacitance effect

In previous Chapter 5, it was found during stability analysis of SPNCL for CO_2 experiments that pipe wall thermal capacitance has a significant damping effect on stability behavior of open & closed loop natural circulation with supercritical fluids. Hence NOLSTA code using 1-D model for pipe wall thermal capacitance has been used to carry out stability analysis of SPNCL operating with supercritical water. Bringer Smith correlation (1957) is used for calculating primary side heat transfer coefficient of cooler whereas Jackson correlation (2002) is used to calculate inside heat transfer coefficient for heater/ adiabatic pipes.

6.5.1 Sensitivity study

The stability analysis of SPNCL was carried out for HHHC orientation considering closed loop boundary conditions described in Chapter 4 and stability threshold has been found to be sensitive to convergence value of loop pressure closure condition, the time step and grid size considered for analysis. Hence convergence value of loop pressure closure, time step and grid size independence test was carried out for SPNCL.

Effect of time step and grid size

To start with grid size of 0.01 m was considered and time steps were changed to carry out the stability analysis of SPNCL at 7400 W/ 22.5 MPa. It was observed that larger time steps stabilized the predictions as shown in figure 6-20. On reducing the time step from 0.03s to

0.015s the predictions hardly change. Now considering 0.015 as the time step the grid size was reduced to 0.005 m but no change was observed in the results as shown in figure 6-21. Hence to save computational time the grid size of 0.01m was finalized. Henceforth, grid size and time step of 0.01 m and 0.015s respectively have been used for generating the stability results for SPNCL with closed loop boundary conditions.

Effect of convergence value of loop pressure closure condition

For natural circulation the pressure closure condition to be satisfied at any time step is $\Sigma\Delta p = 0$. The solution is converged if $\left|\sum \Delta p\right| \leq convergence\ value$. The stability predictions are found to be dependent on this convergence value as shown in figure 6-22. Unrealistic oscillations are predicted for convergence value of 100 Pa, whereas similar oscillations are predicted for 10 Pa and 1 Pa. Convergence value of 1 Pa has been considered for further analysis.

Prediction of stable, unstable and neutrally stable conditions

Considering above mentioned values of grid size, time step and loop pressure closure convergence criterion a typical stable (7300 W), unstable (7400 W) and neutrally stable (7340 W) case was obtained at 22.5 MPa and 0.53 kg/s secondary air flow as shown in figure 6-23.

6.5.2 Stability analysis of SPNCL with pipe wall effect

As the experimental procedure for SPNCL involved only step power change, same is also considered for stability prediction using NOLSTA code using the time step, grid size and loop pressure closure convergence values as concluded in section 6.5.1. Figure 6-24a shows a stable flow behavior of the loop during power step rise from 7 kW to 7.3 kW at 22.5 MPa (pseudo-

critical temperature 375.6 ^{o}C) and figure 6-24b shows the corresponding heater inlet/ outlet temperatures (373.81 ^{o}C/ 375.5 ^{o}C respectively). However step rise in power from 7 kW to 7.4 kW makes the flow unstable as shown in figure 6-25a & 6-25b. The flow remains unstable up to 7.7 kW as shown in figure 6-26a & 6-26b. The flow again becomes stable at 7.9 kW as shown in figure 6-27a & 6-27b. Although the flow tries to become unstable at 7.9 kW near pseudo-critical temperature but instability doesn't get sufficient time to develop as fluid crosses the pseudo-critical region fast due to higher power. At further higher power of 8.2 kW the flow rate reduction curve becomes even smoother as still lesser time is available for instability to develop near pseudo-critical temperature as shown in figure 6-28a & 6-28b. Hence instability can be avoided in SPNCL by giving large step rise in power when fluid is approaching the pseudo-critical temperature.

The unstable zone reduces as the pressure increases to 23 MPa (i.e. 7.3 kW to 7.8 kW) as shown in figure 6-29. At 23.5 MPa the unstable zone further reduces from 7.4 kW to 7.6 kW as shown in figure 6-30. No instability is observed at 24 MPa as shown in figure 6-31.

The stability map of SPNCL for supercritical water operation is shown in figure 6-32. The stability map shows larger unstable zone at low pressures, smaller unstable zone at higher pressure and no instability beyond a particular pressure i.e. 23.7 MPa which is in qualitative agreement with experimental findings as all the unstable data near pseudo-critical region lies at lower pressures. The reason for this can be high volumetric expansion coefficient of water near pseudo-critical temperature at low pressure, however there is not very significant reduction in volumetric expansion coefficients with respect to enthalpy at higher pressures as shown in figure 6-33.

Volumetric expansion coefficient with respect to enthalpy (not with respect to temperature) is considered because at same power and flow, the same amount of flow perturbation will give rise to same perturbation in enthalpy (not temperature) at different pressures. Hence other reason can be the significant reduction of volumetric thermal capacitance of water with pressure near pseudo-critical temperature as shown in figure 6-33. High thermal capacitance of water at low pressures near pseudo-critical temperature makes the temperature versus enthalpy curve almost flat near pseudo-critical temperature just like two phase flows as shown in figure 6-34. Hence perturbation in enthalpy will give rise to very small perturbation in supercritical fluid temperature at low pressures near pseudo-critical temperature and so interaction of fluid with pipe wall will become very less. Since damping effect of the wall becomes negligible at low pressures near pseudo-critical temperature, instability is observed for the same. However, at high pressures the perturbation in enthalpy will give rise to sufficient perturbation in fluid temperature and significant thermal interaction of fluid with the wall becomes possible which damps the oscillations. The quantitative difference between experiments and analysis can be attributed to the actual interaction of the wall with the fluid which depends on the heat transfer coefficient between fluid and wall which can be studied in more detail by 3-D CFD codes.

Hence, scaling fluid (i.e. carbon dioxide/ Freon etc.) for instability studies of supercritical water should take care of the ratio of thermal capacitance of the wall and the fluid near pseudo-critical temperature. The comparison of volumetric thermal capacity of water and carbon dioxide near pseudo-critical temperature with pipe thermal capacity of SPNCL is shown in figure 6-35.

6.6 Conclusions

The peak of the steady state mass flow rate versus power curve for SPNCL is obtained at heater outlet temperature near the pseudo-critical value. If the heater inlet temperature increases beyond the pseudo-critical temperature the steady state natural circulation mass flow rate reduces significantly. NOLSTA code simulates the steady state behaviour of SPNCL appreciably well.

During experimentation with water, instability has been observed for a very narrow window of power for HHHC orientation i.e. 7.5 to 8.3 kW for operating pressure range of 22.1 to 22.9 MPa. The instability is observed near pseudo-critical temperature at low pressures however at high pressures no instability is observed. The mechanism of instability development is growth of small amplitude oscillations as proposed by Welander (1967). NOLSTA code also predicts instability over a very narrow range of power near pseudo-critical temperature and at pressures below 23.7 MPa which is in qualitative agreement with experimental data. The reason for the same is higher thermal capacitance of fluid near pseudo-critical temperature at low pressures which cause enthalpy perturbations to generate very small fluid temperature perturbations only and hence fluid interaction with pipe wall or damping effect of wall becomes almost negligible. Moreover, NOLSTA code also predicts that instability can be avoided even at low pressures in SPNCL by giving large step rise in power when fluid is approaching the pseudo-critical temperature. Scaling fluid for instability studies of supercritical water should take care of the ratio of thermal capacitance of the wall and the fluid near pseudo-critical temperature.

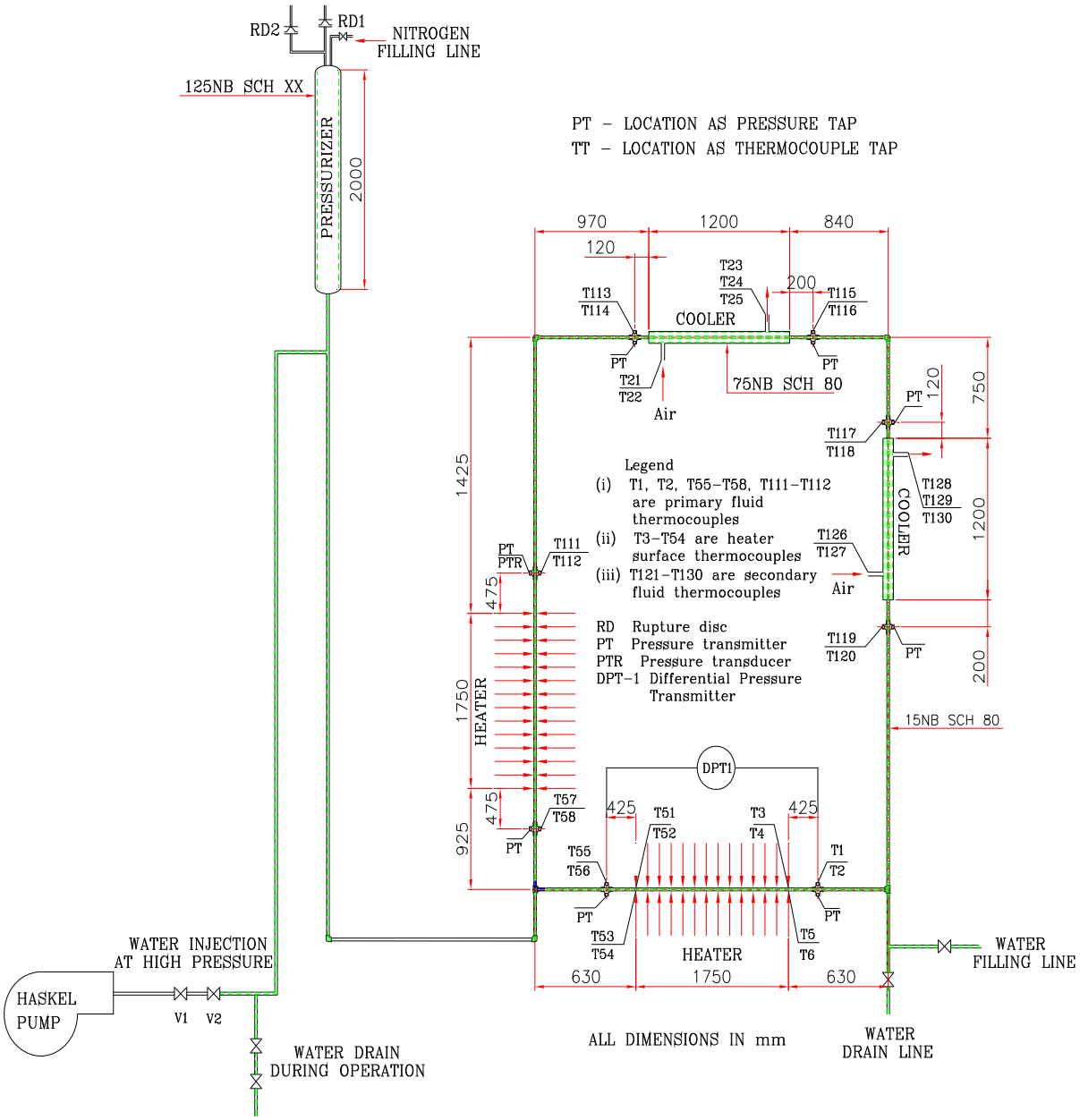

Figure 6-1: Schematic of augmented SPNCL

Figure 6-2: Photograph of augmented SPNCL

Figure 6-3: Photograph of 200 kW Power supply unit

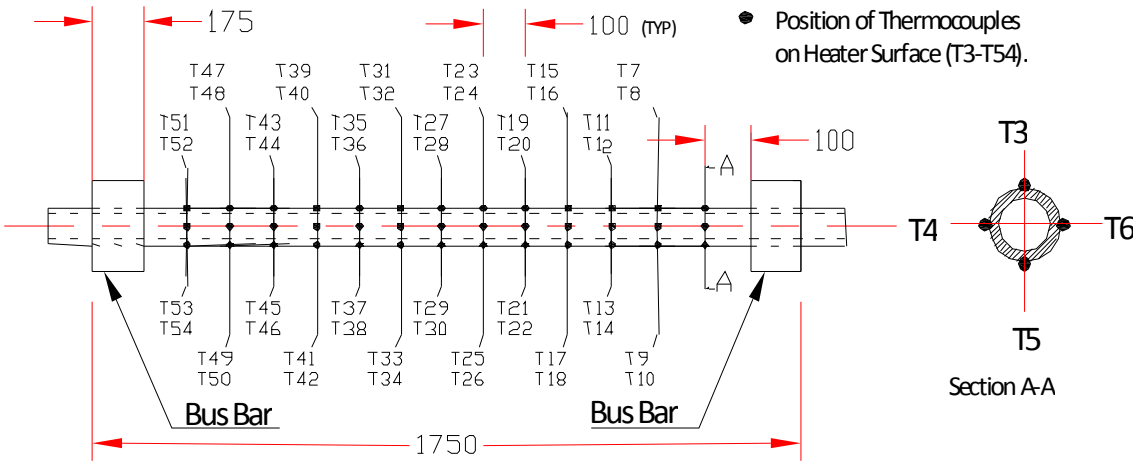

Figure 6-4: New horizontal/ vertical heater test section

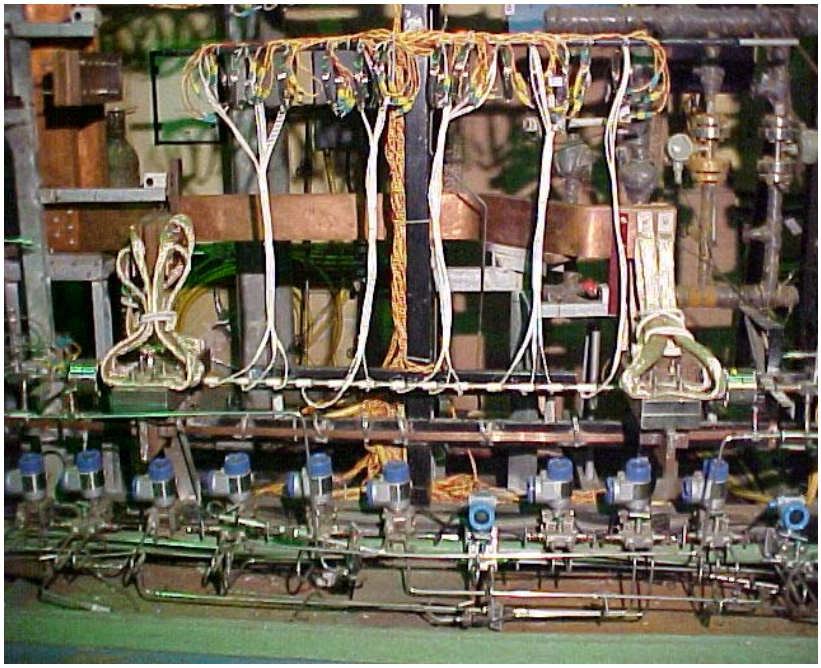

Figure 6-5: Photograph of new horizontal heater test section of SPNCL

Figure 6-6: Photograph of control panel of SPNCL

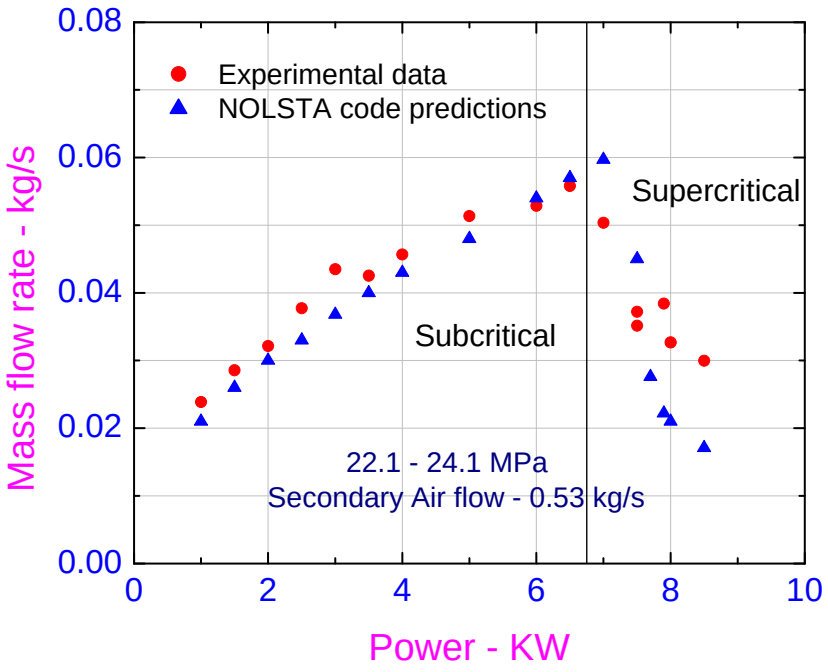

(a) Flow rate

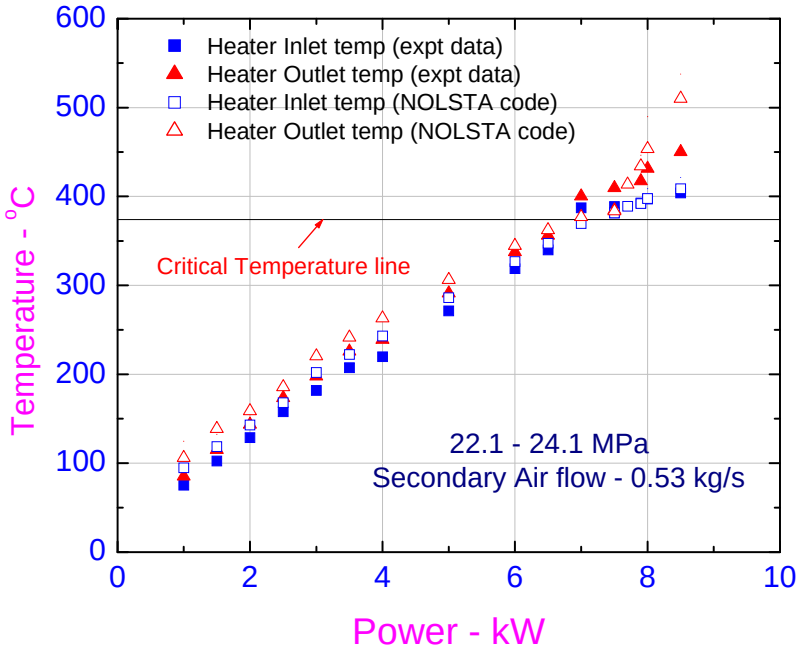

(b) Heater Inlet and outlet temperature

Figure 6-7: Measured and predicted steady state performance of SPNCL with supercritical water for HHHC orientation.

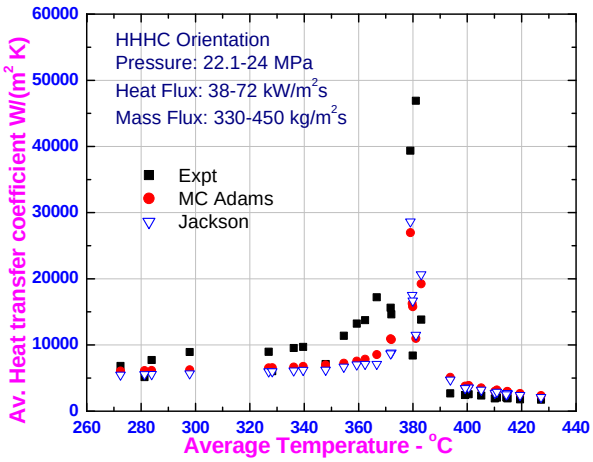

(a)

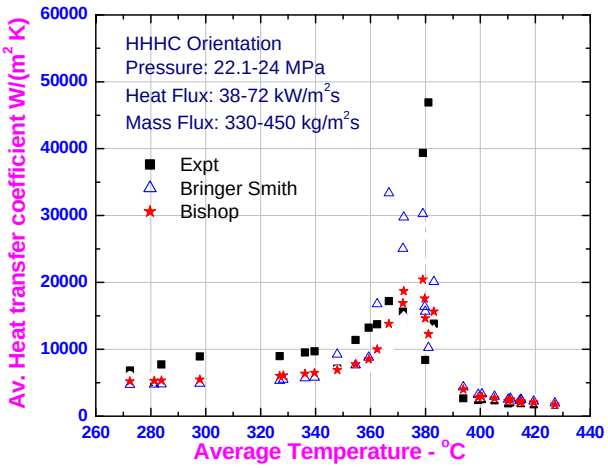

(b)

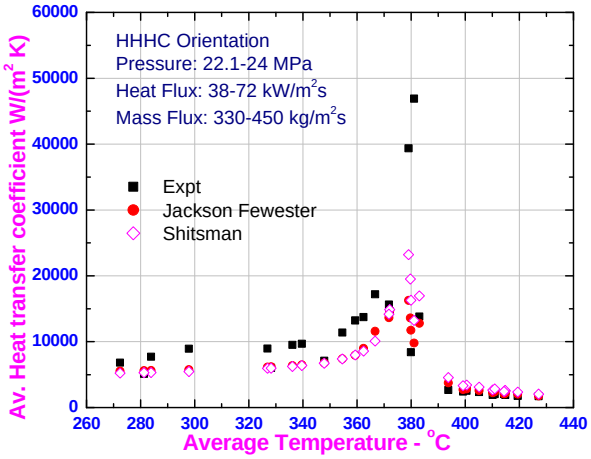

(c)

Figure 6-8: Comparison of experimental heat transfer coefficient data with various correlations for HHHC orientation of SPNCL

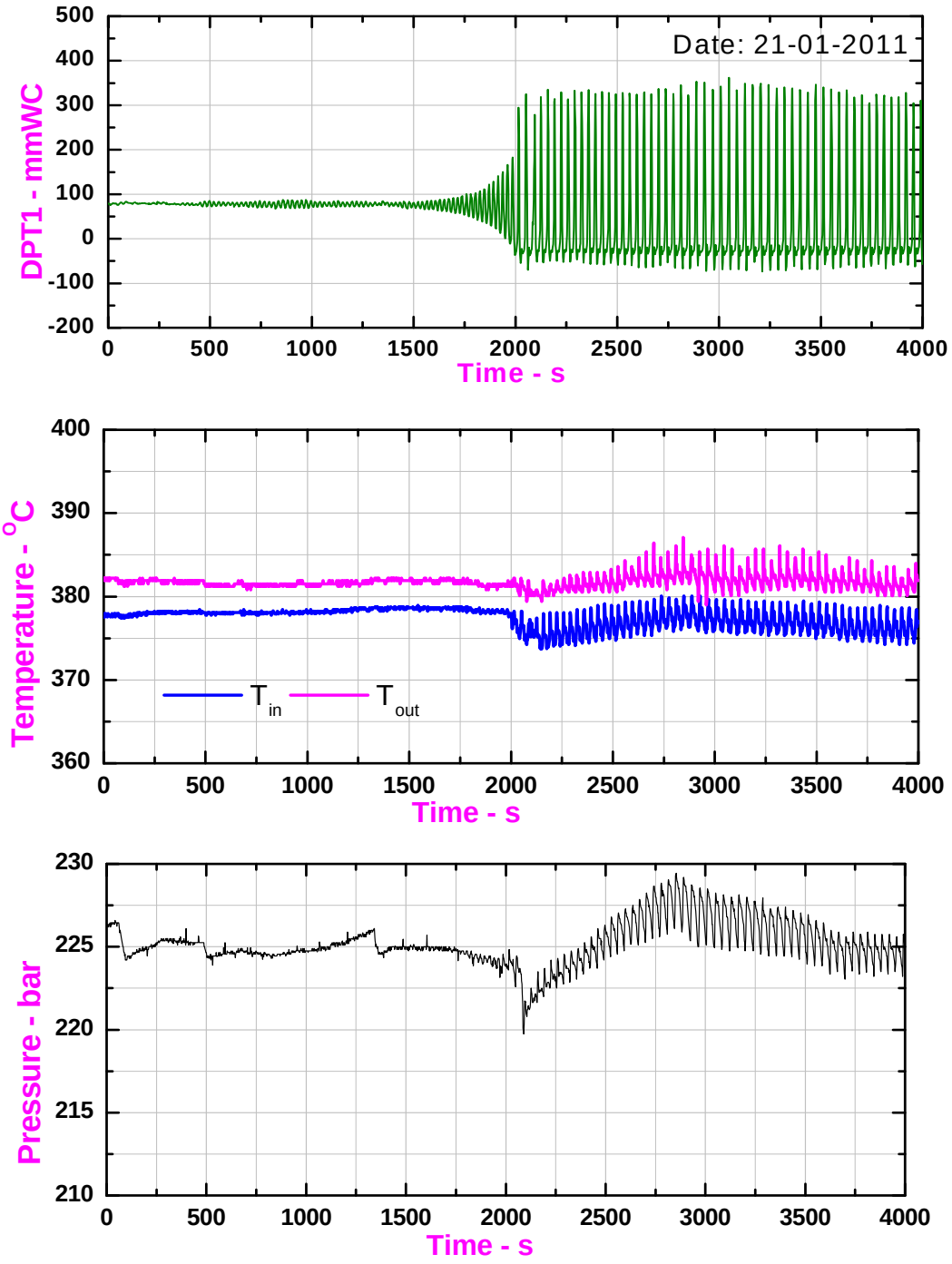

Figure 6-9: Instability observed at 7.5 kW

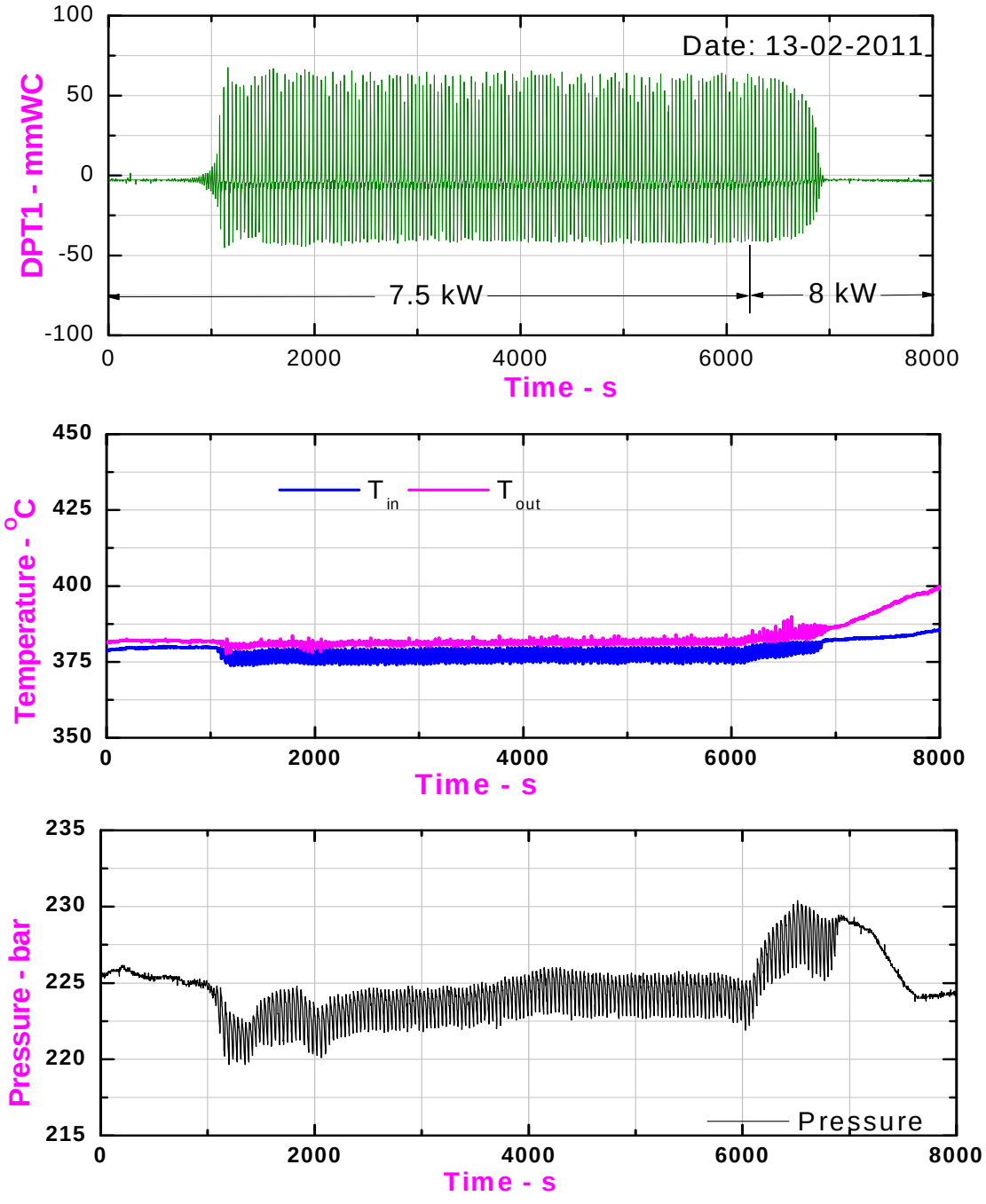

Figure 6-10: Instability observed at 7.5 kW

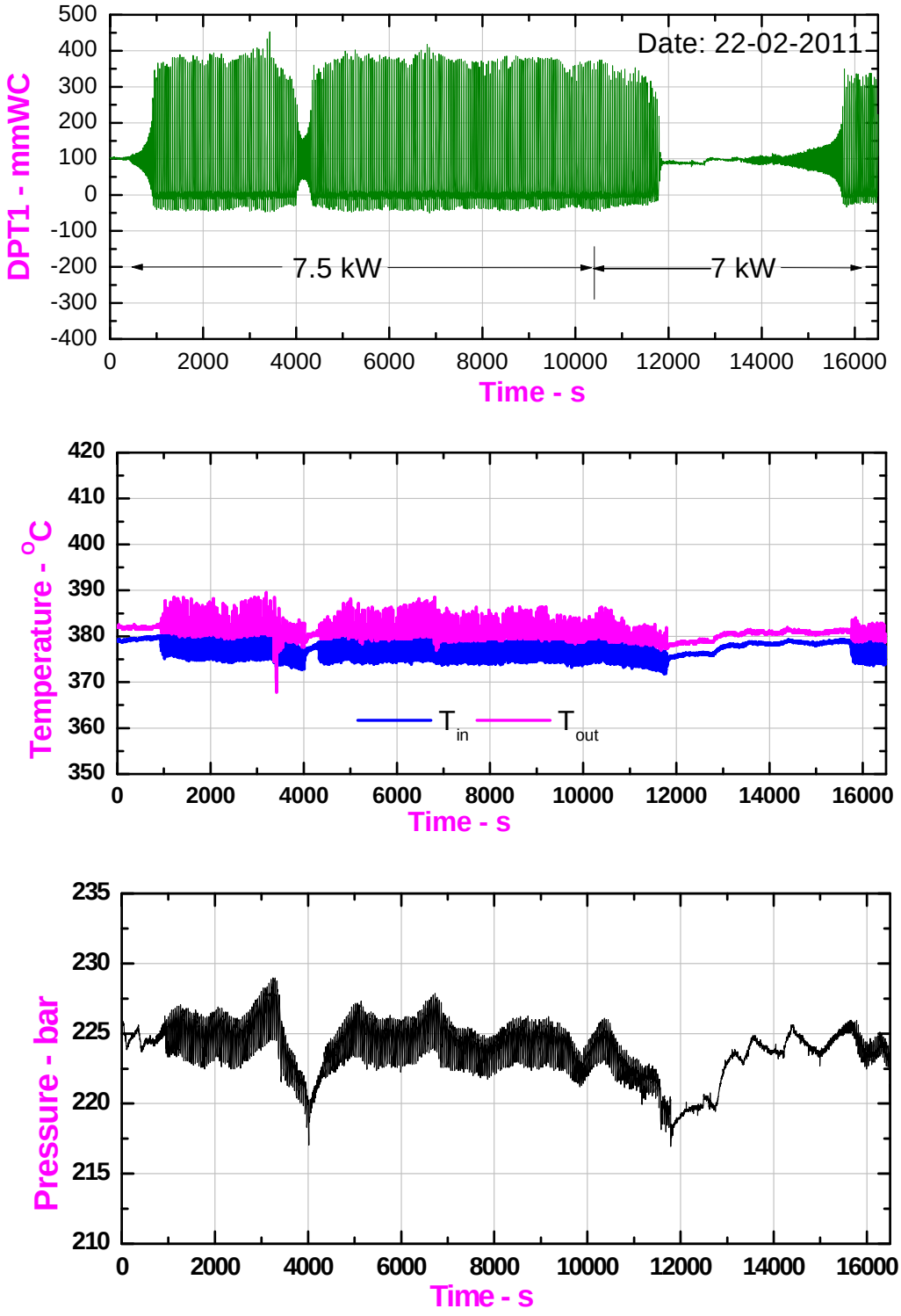

Figure 6-11: Instability during power reduction from 7.5 kW to 7.0 kW

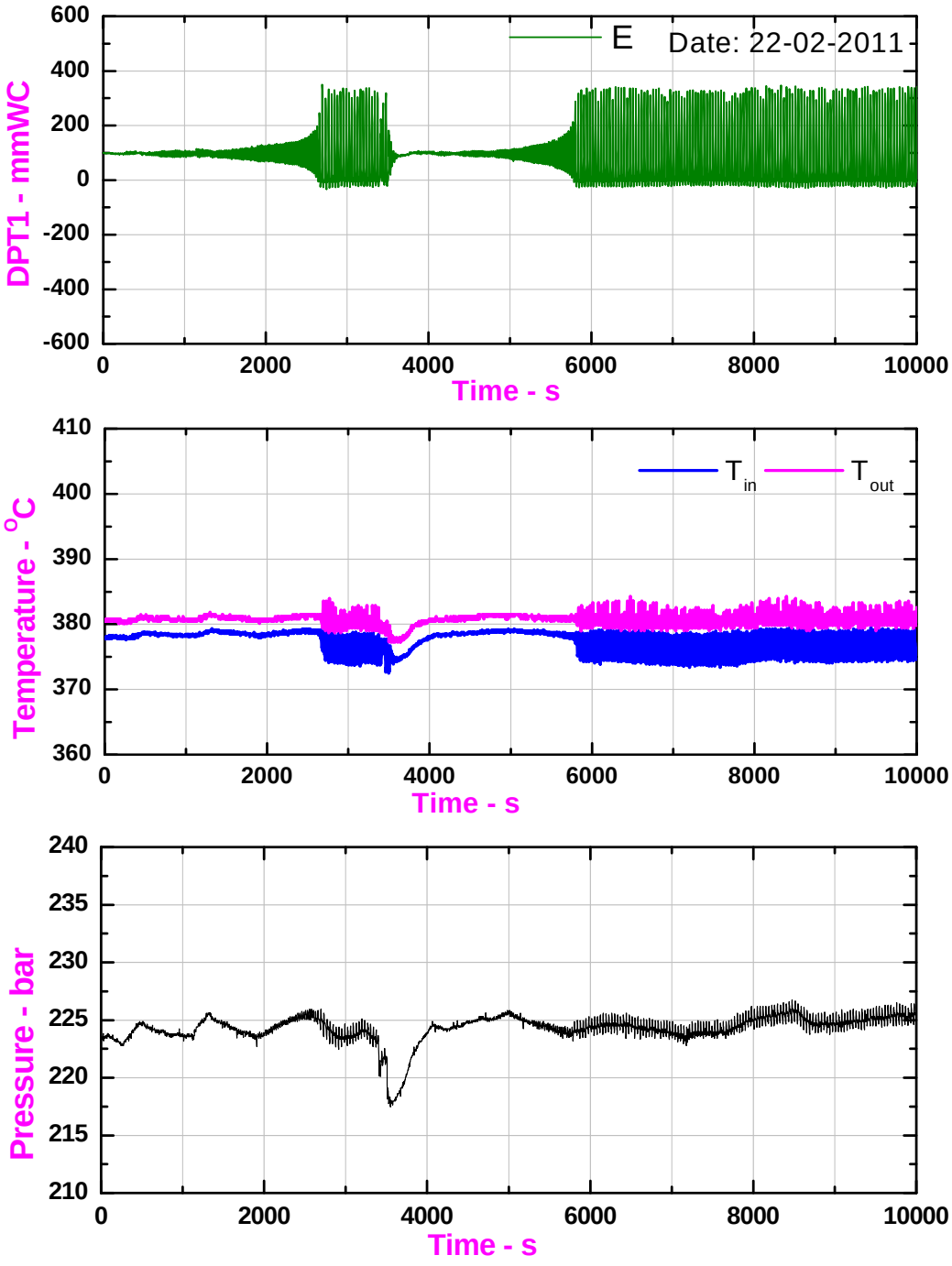

Figure 6-12: Instability observed at 7.0 kW

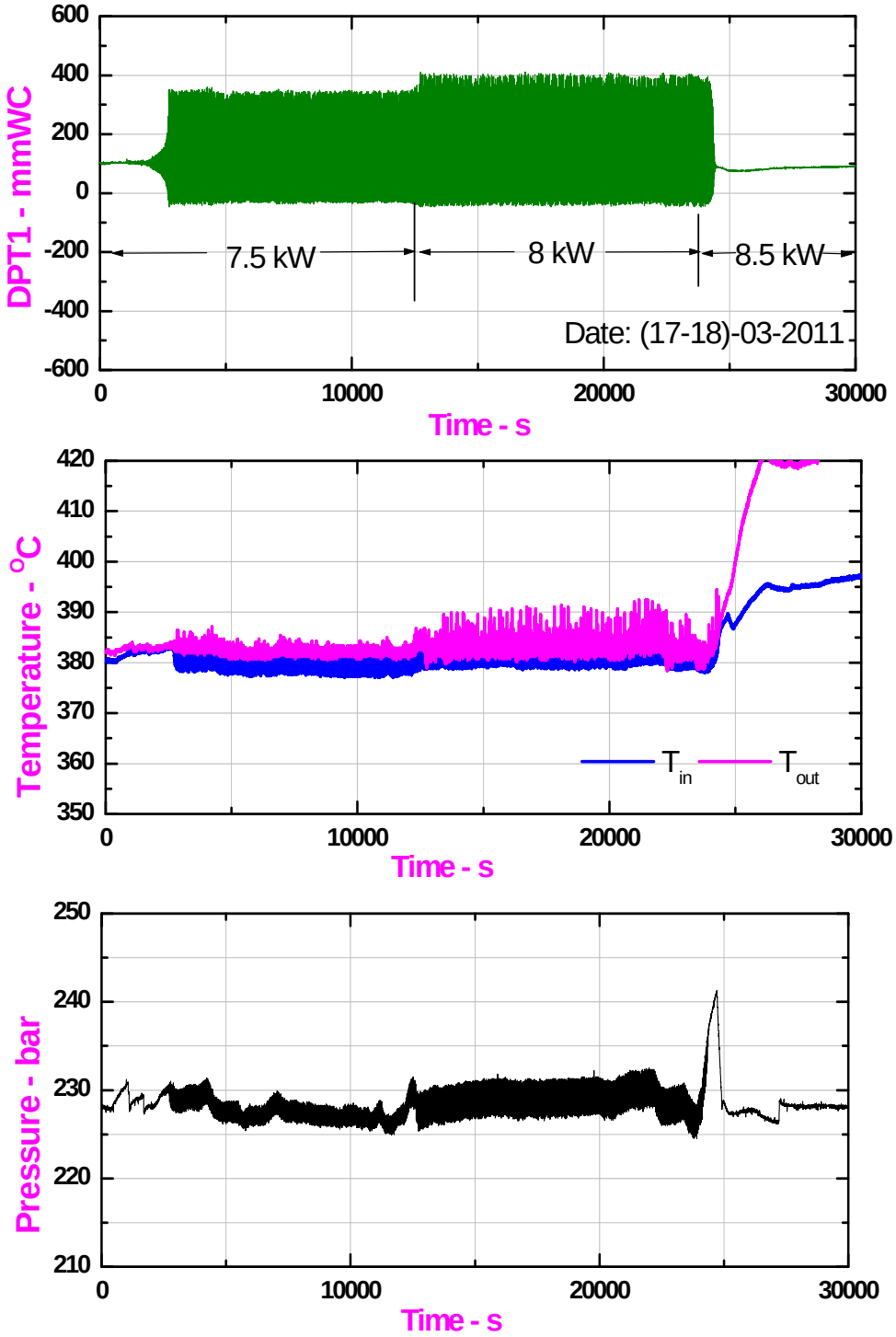

Figure 6-13: Instability during power rise from 7.5 kW to 8.0 kW

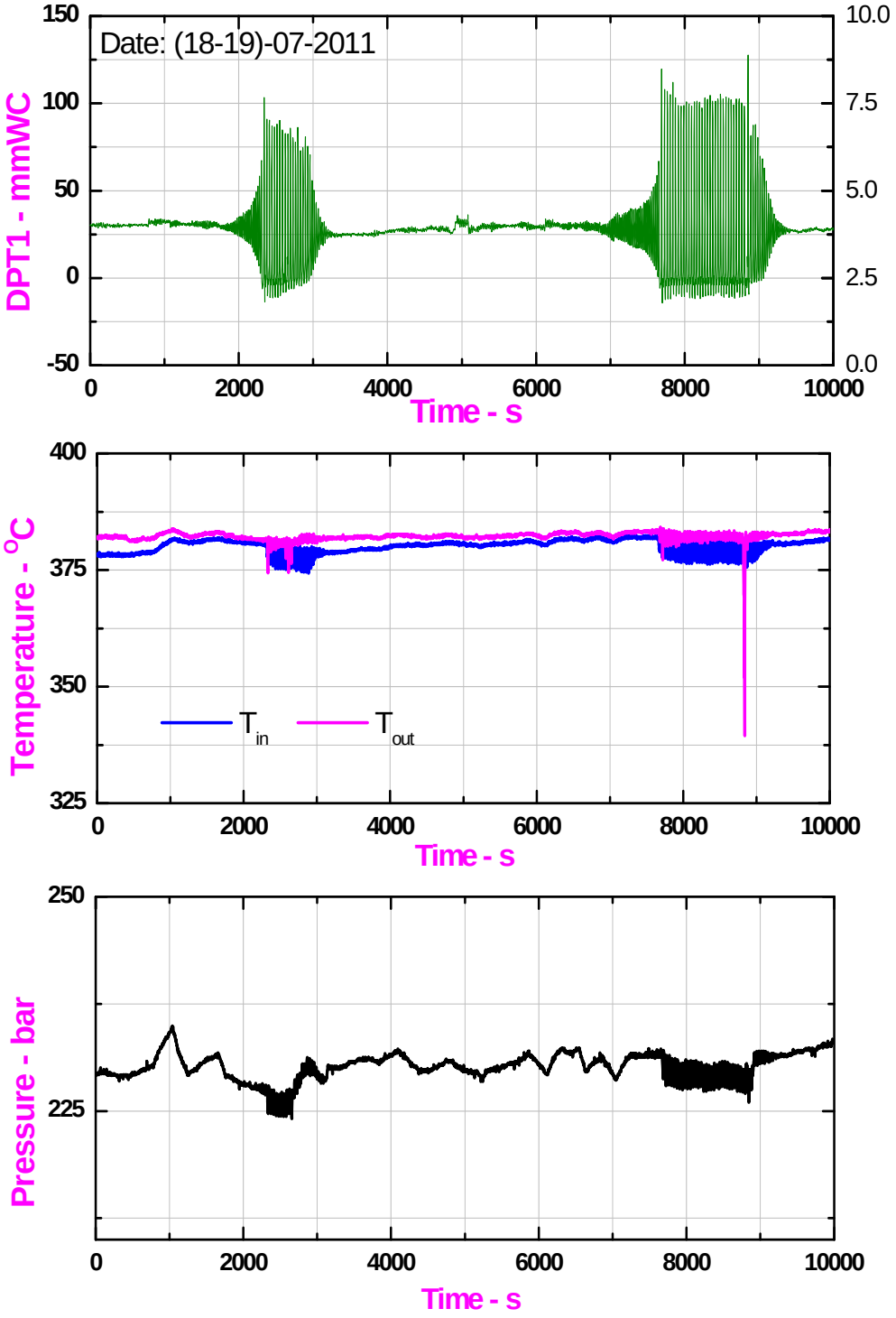

Figure 6-14: Instability observed at 8.0 kW

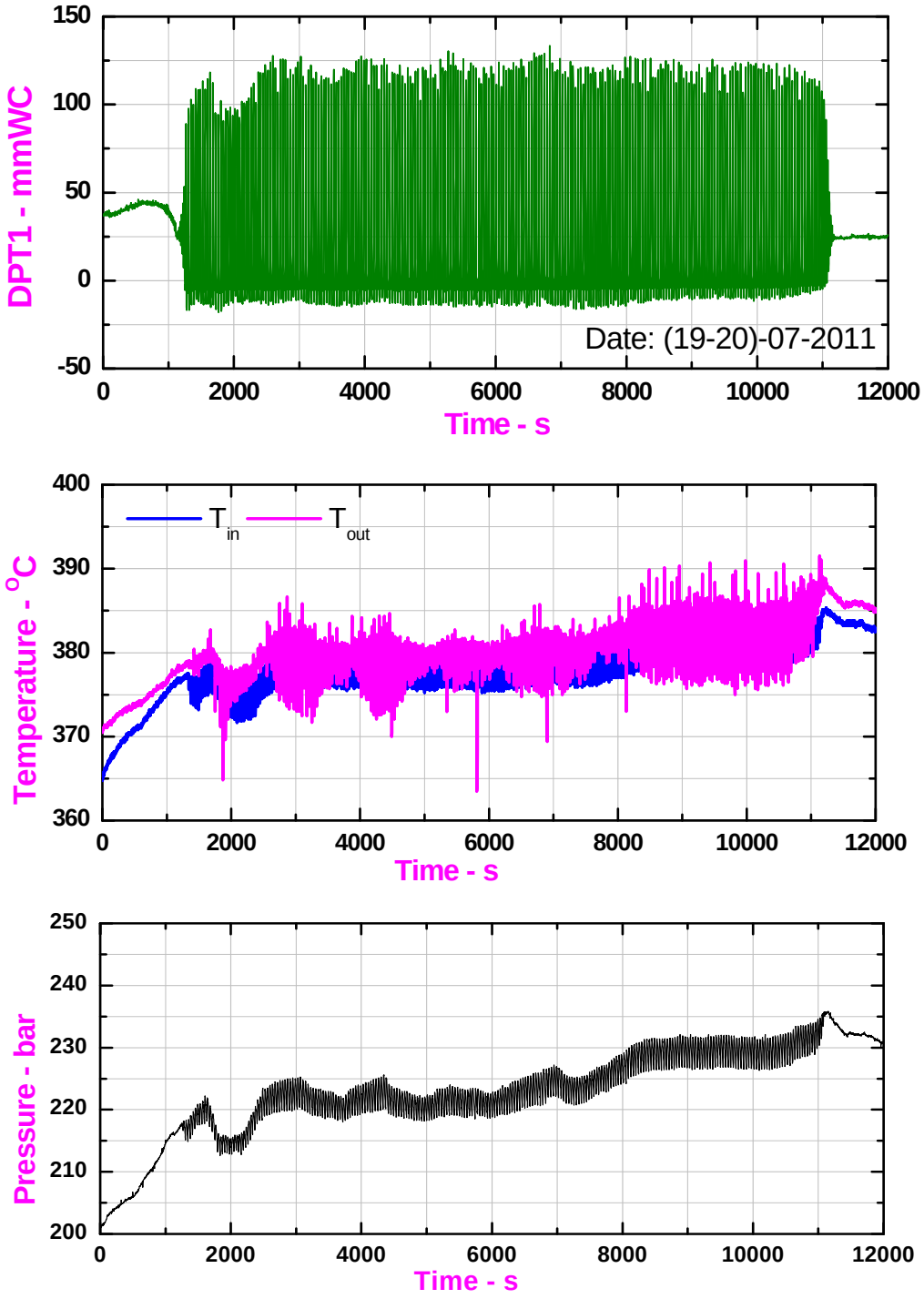

Figure 6-15: Instability observed at 8.3 kW

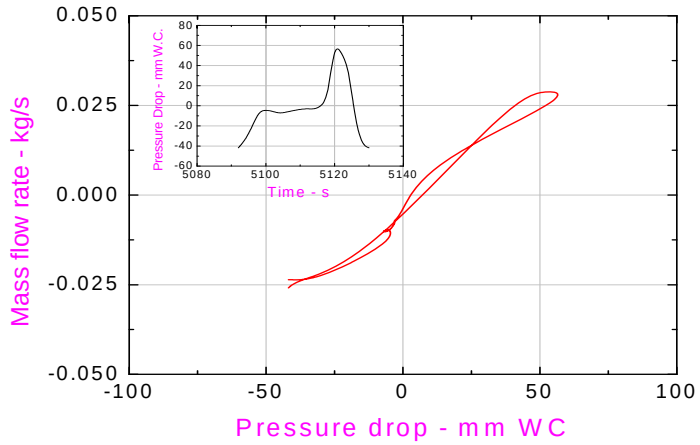

(a)

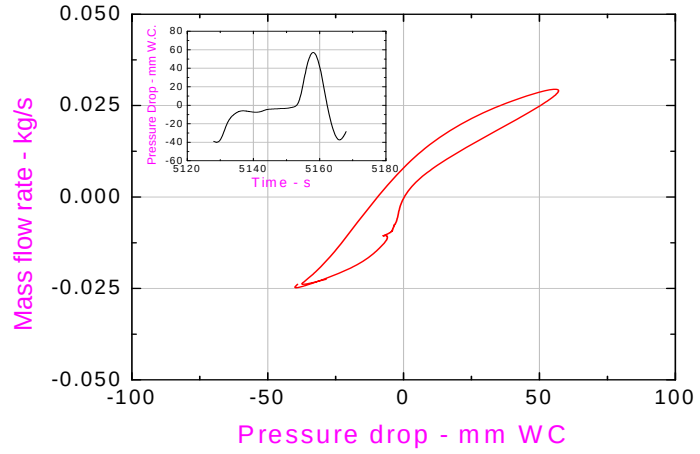

(b)

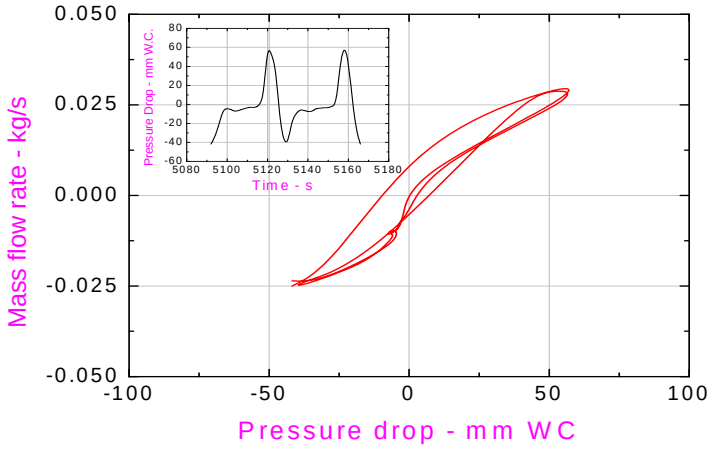

(c)

Figure 6-16: Phase plot for instability observed at 7.5 kW (figure 6-10)

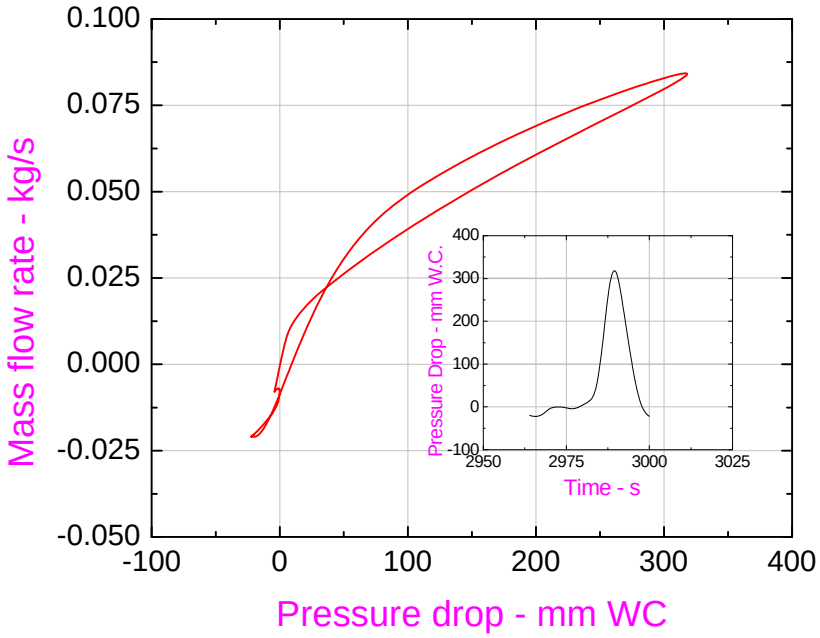

(a)

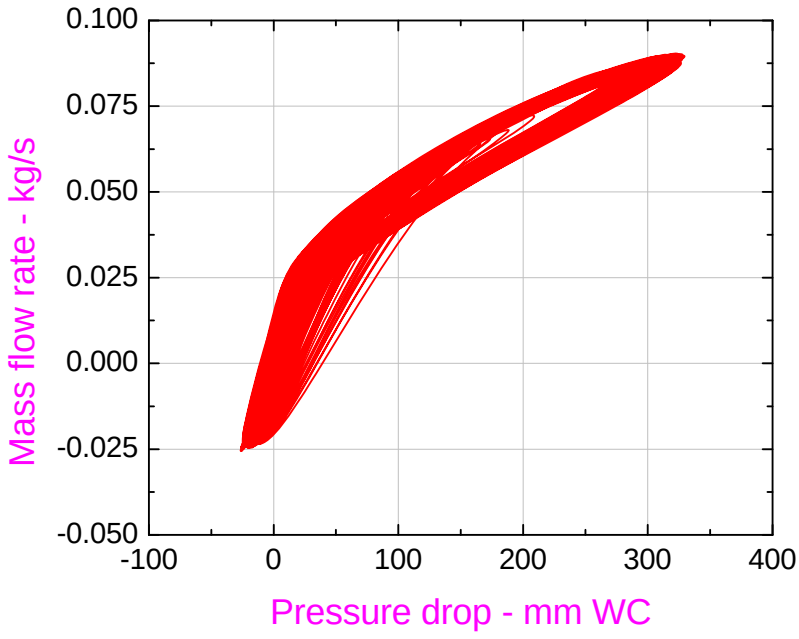

(b)

Figure 6-17: Phase plot for instability observed at 7.0 kW (figure 6-12)

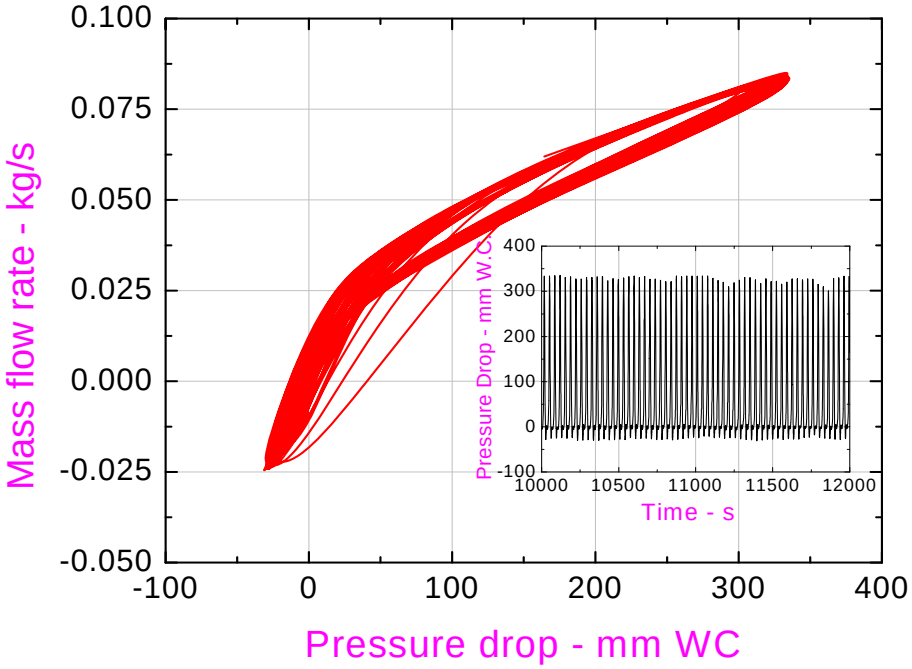

Figure 6-18: Phase plot for instability observed at 7.5 kW (figure 6-13)

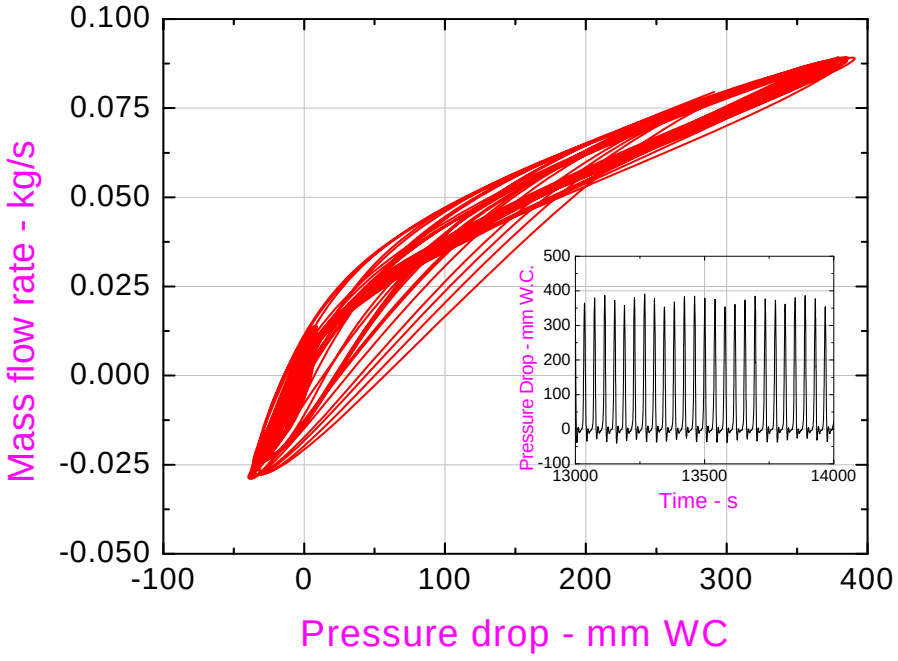

Figure 6-19: Phase plot for instability observed at 8 kW (figure 6-13)

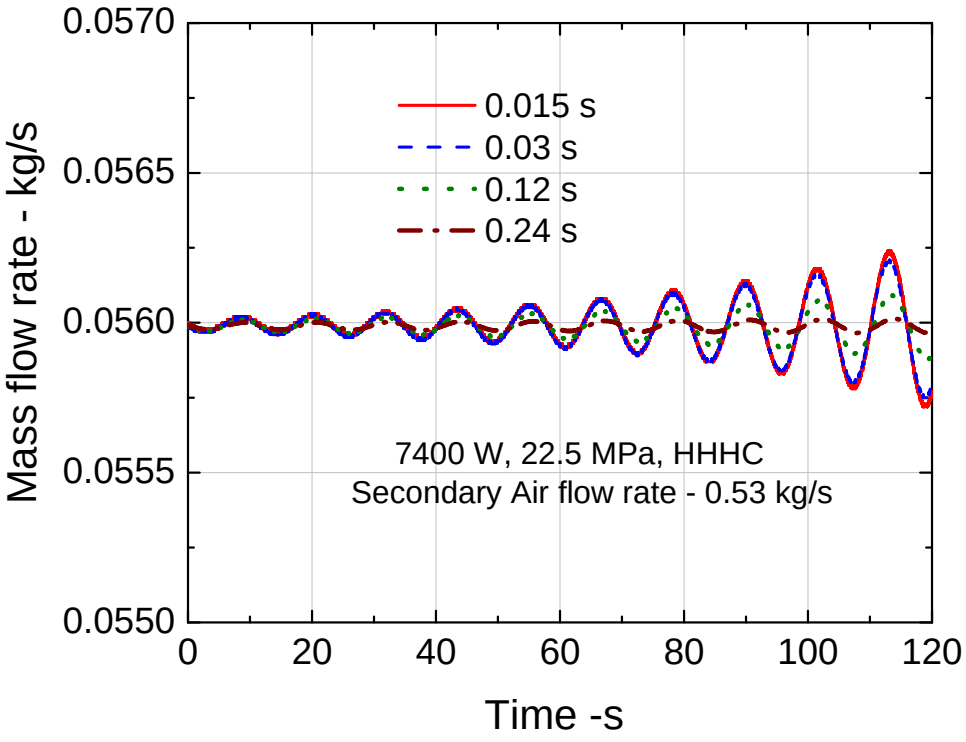

Figure 6-20: Time step sensitivity study for stability behavior of SPNCL operating with SCW

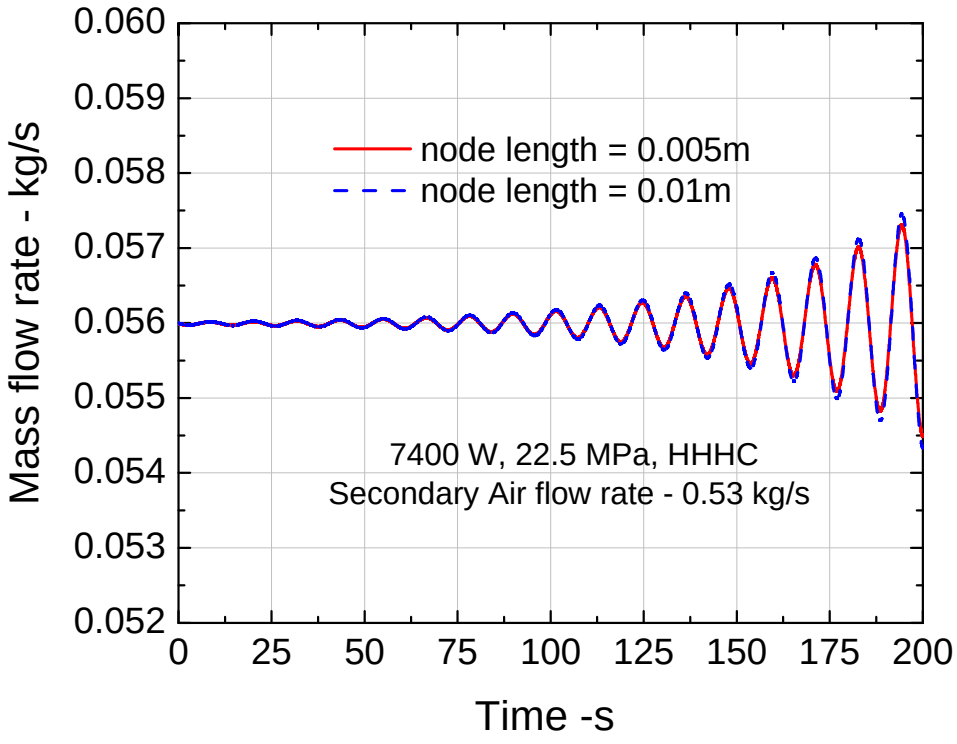

Figure 6-21: Grid size sensitivity study for stability behavior of SPNCL operating with SCW

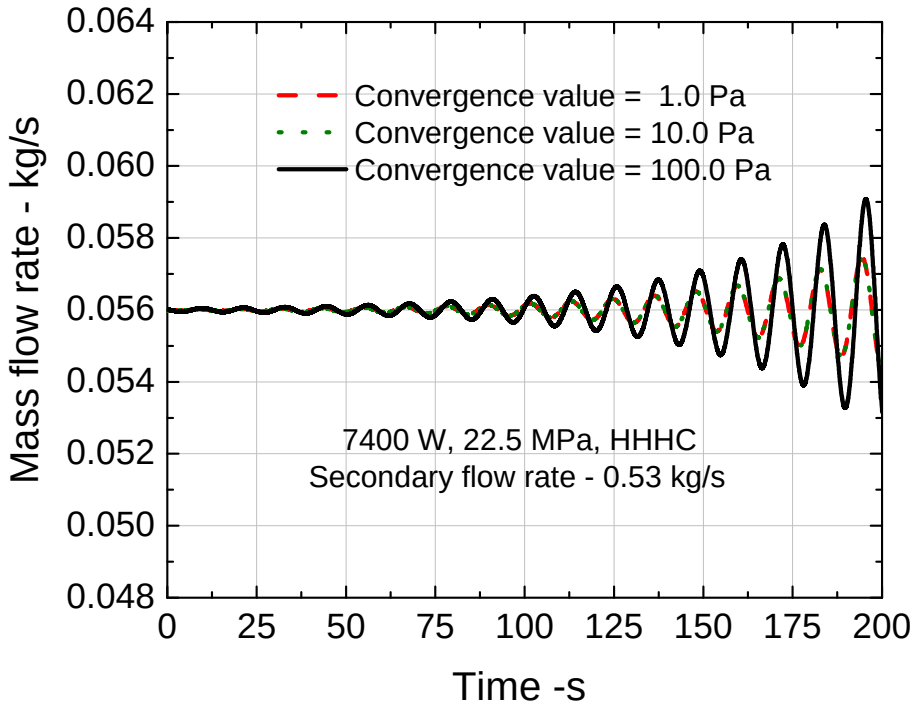

Figure 6-22: Effect of loop pressure closure convergence criterion on stability behavior of SPNCL operating with SCW

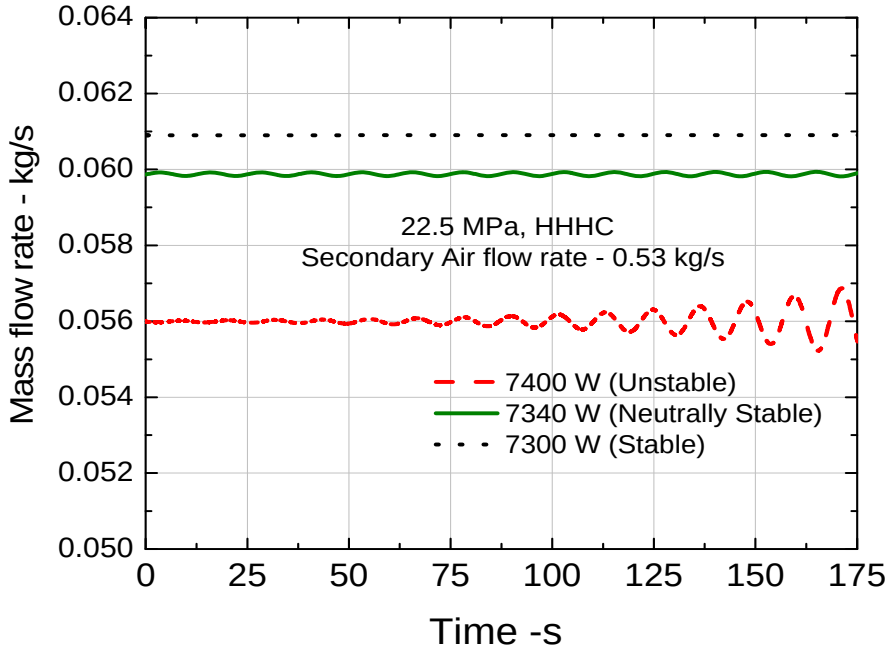

Figure 6-23: Stable, unstable and neutrally stable operating conditions for SPNCL

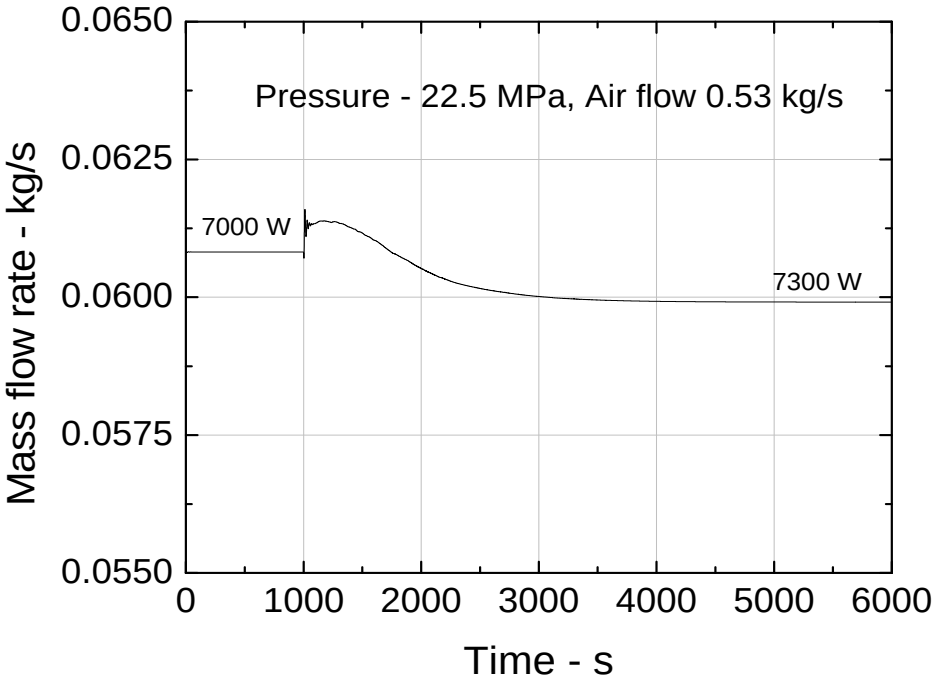

(a)

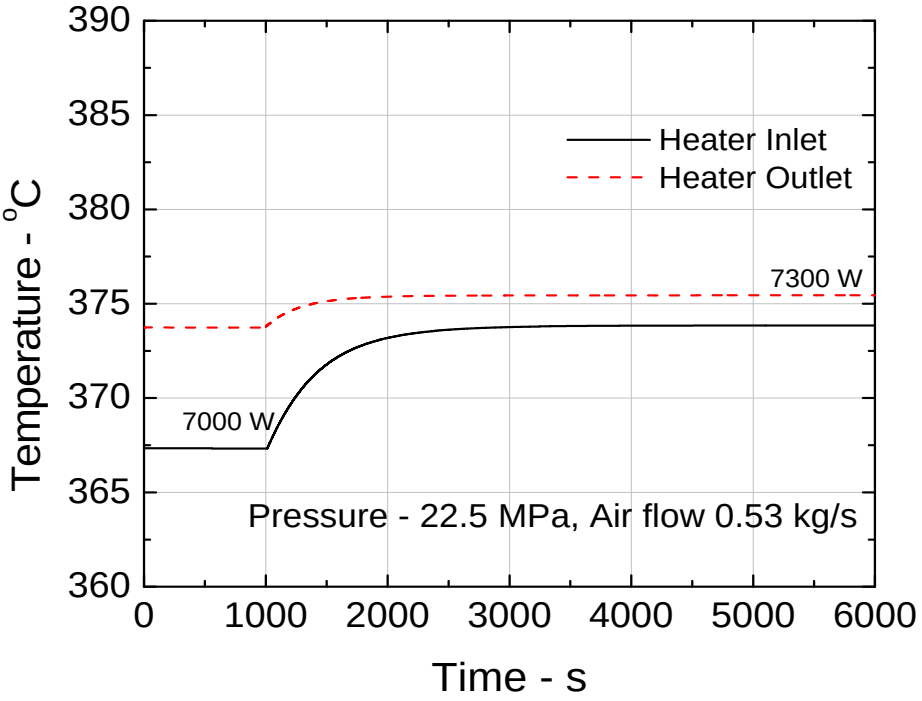

(b)

Figure 6-24: Stable behavior of SPNCL during power step up from 7 kW to 7.3 kW at 22.5 MPa

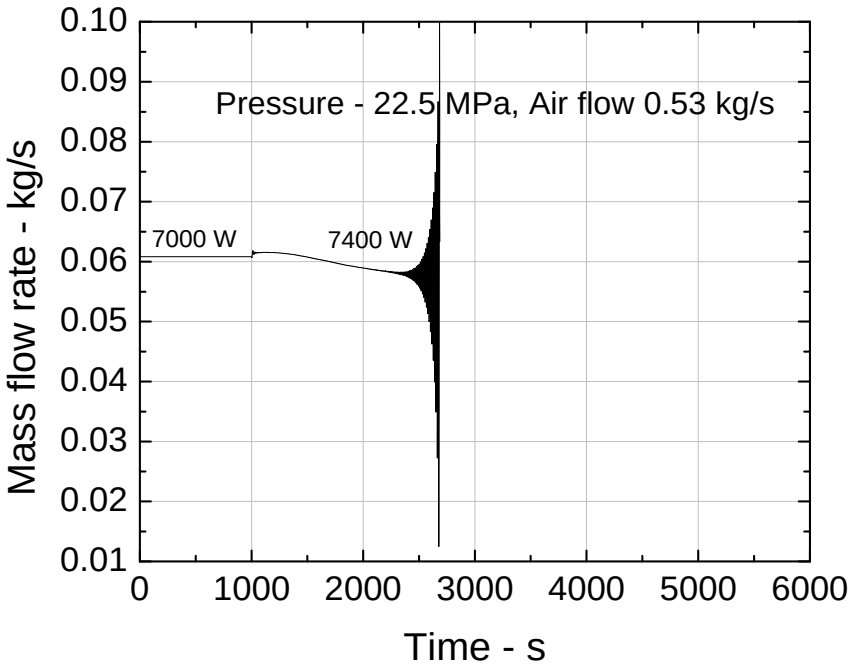

(a)

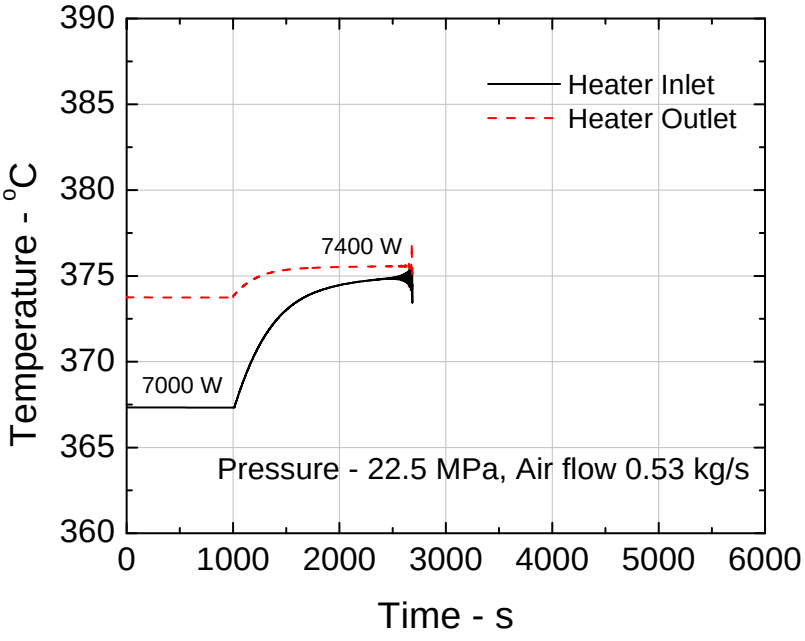

(b)

Figure 6-25: Unstable behavior of SPNCL during power step up from 7 kW to 7.4 kW at 22.5 MPa

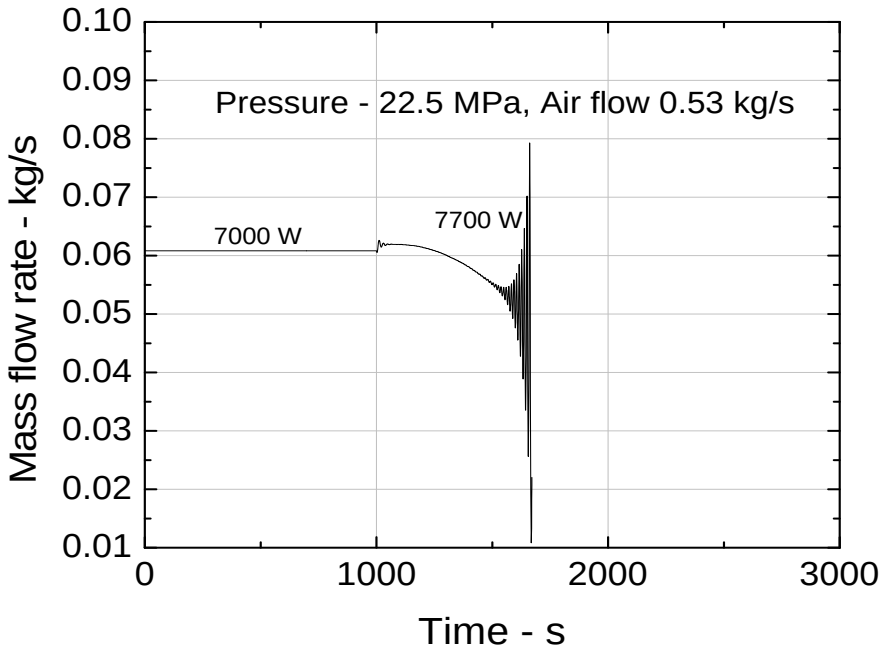

(a)

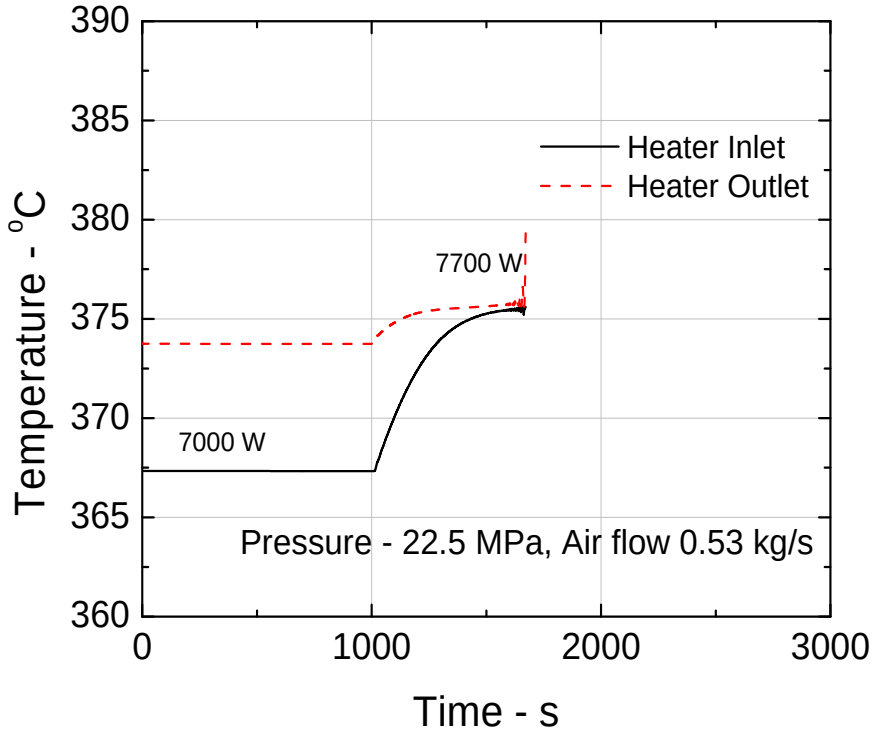

(b)

Figure 6-26: Unstable behavior of SPNCL during power step up from 7 kW to 7.7 kW at 22.5 MPa

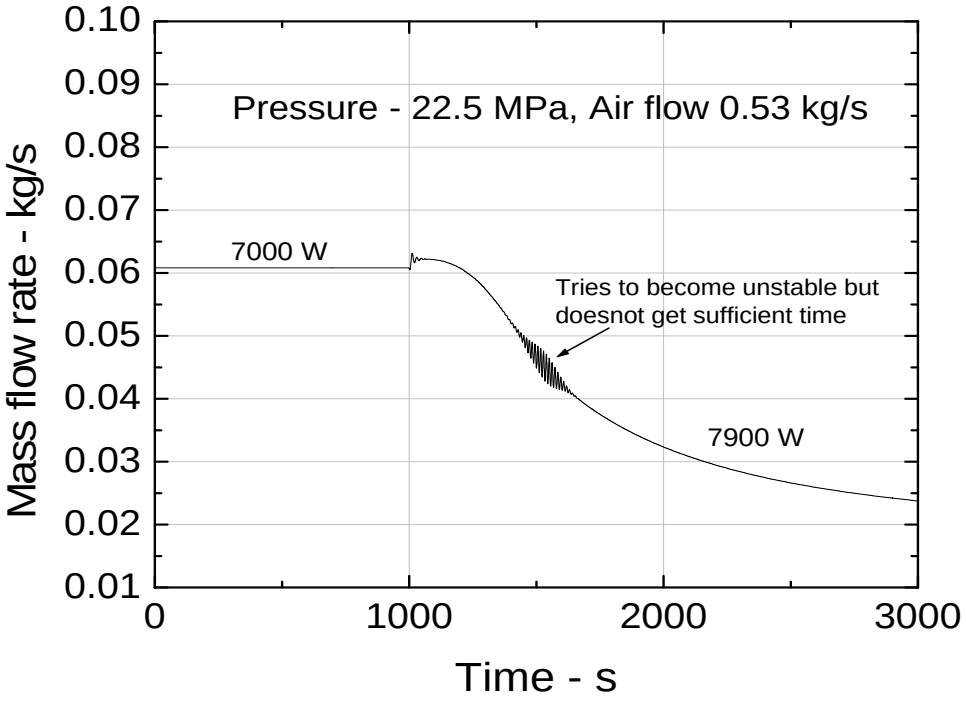

(a)

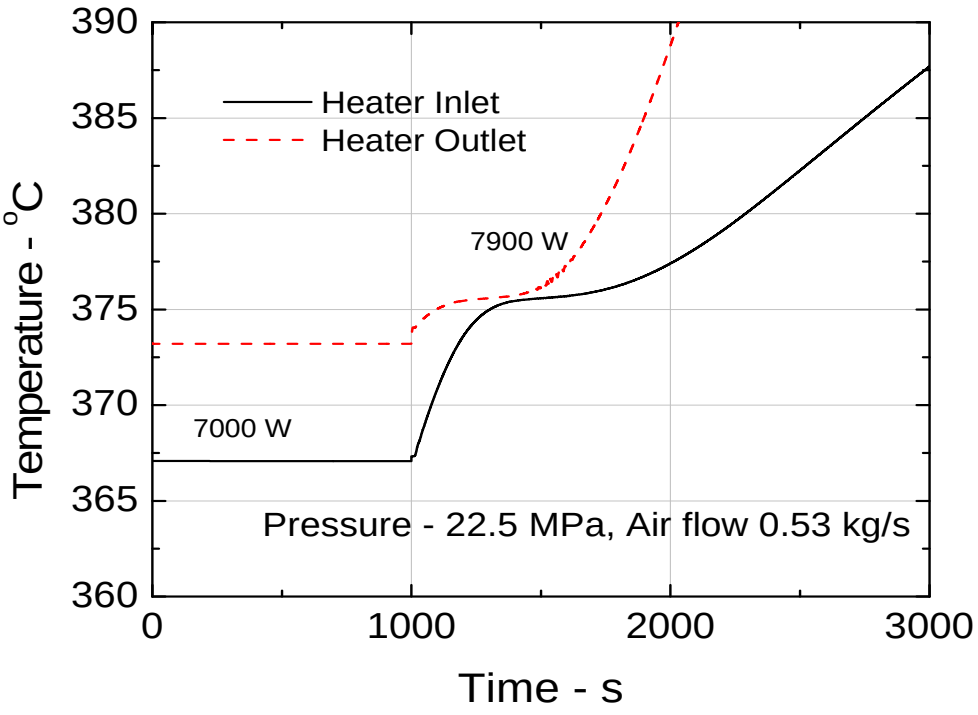

(b)

Figure 6-27: Stable behavior of SPNCL during power step up from 7 kW to 7.9 kW at 22.5 MPa

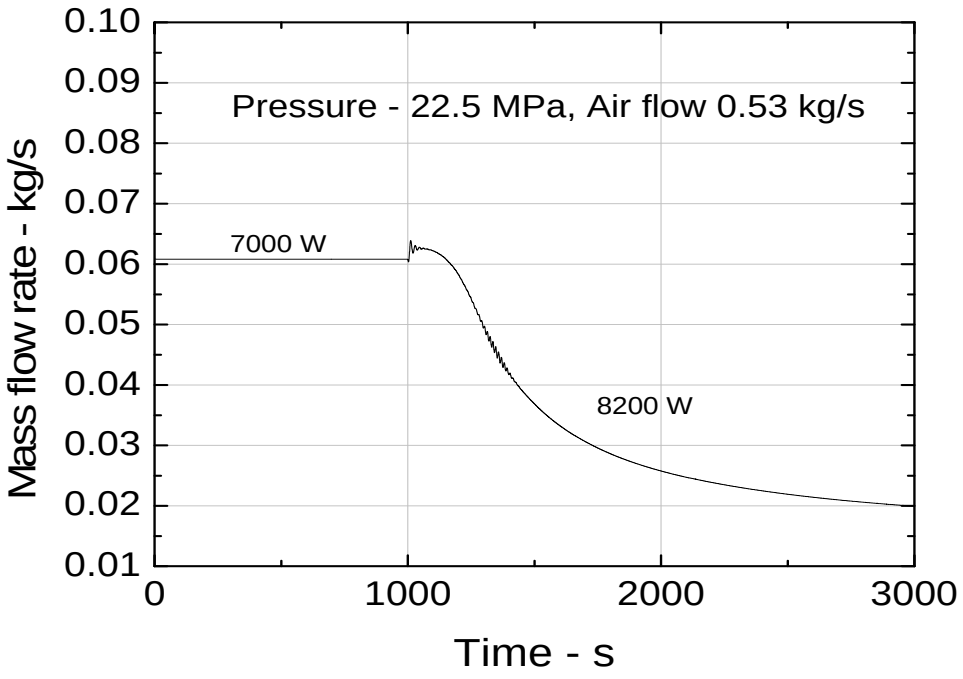

(a)

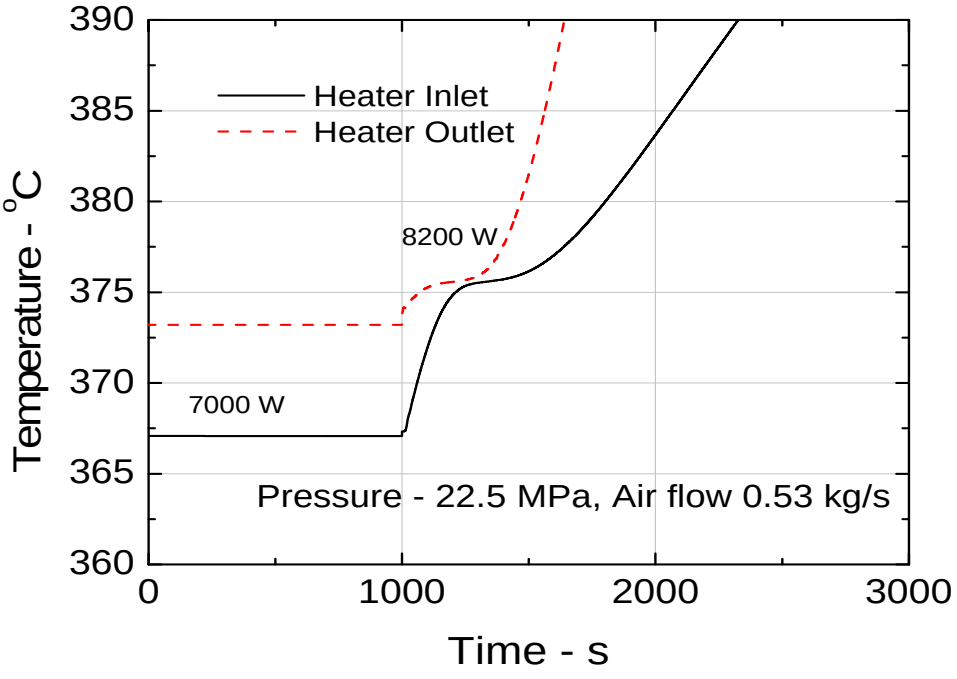

(b)

Figure 6-28: Stable behavior of SPNCL during power step up from 7 kW to 8.2 kW at 22.5 MPa

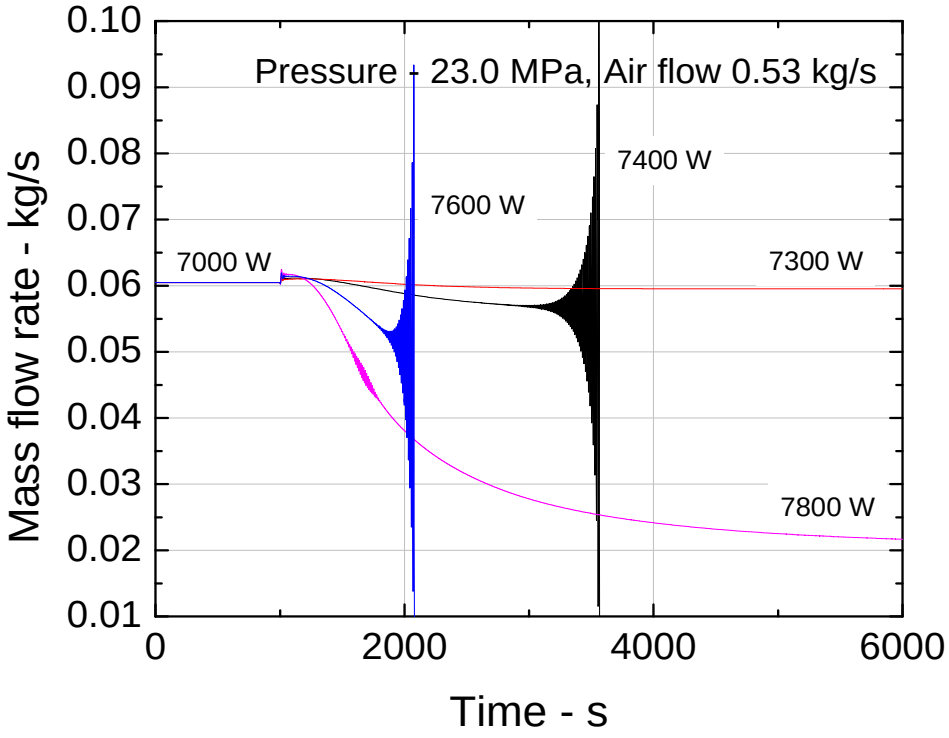

Figure 6-29: Unstable zone of SPNCL at 23 MPa

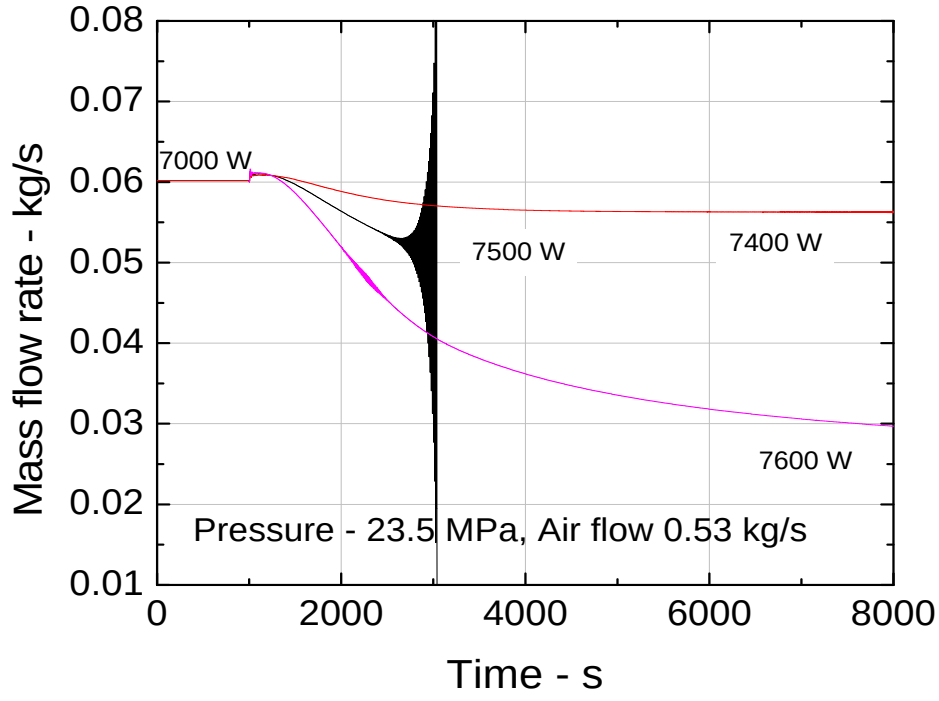

Figure 6-30: Unstable zone of SPNCL at 23.5 MPa

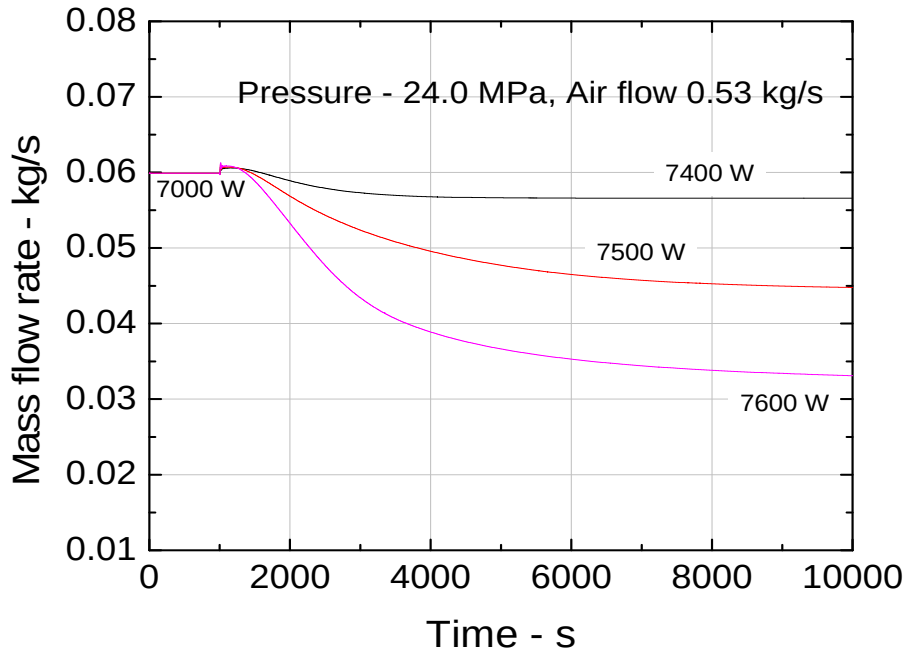

Figure 6-31: No unstable zone of SPNCL at 24.0 MPa

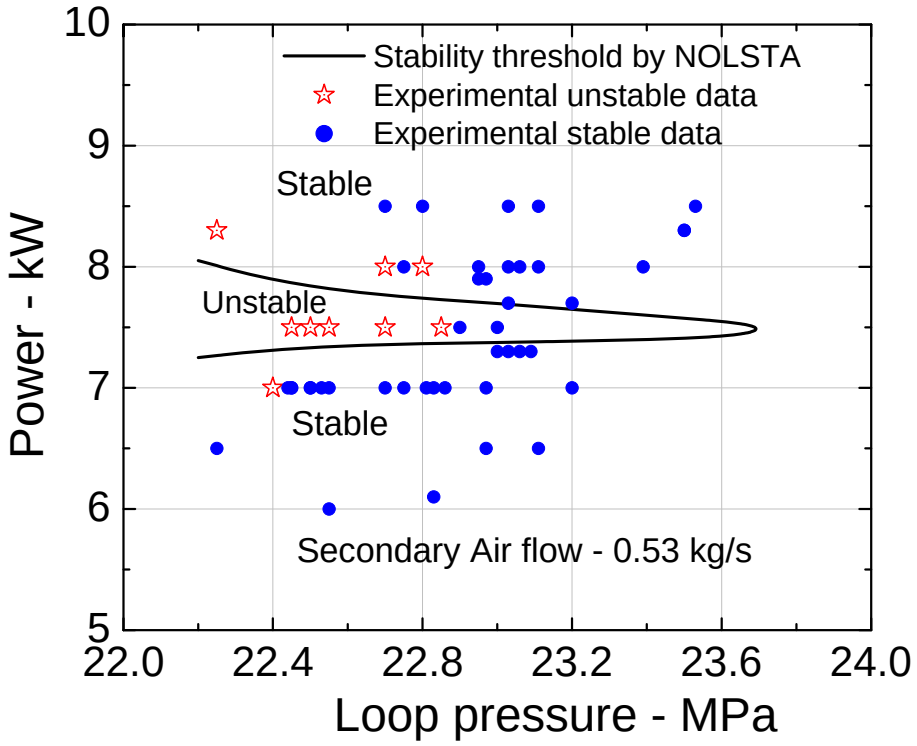

Figure 6-32: Stability map of SPNCL for operation with SCW

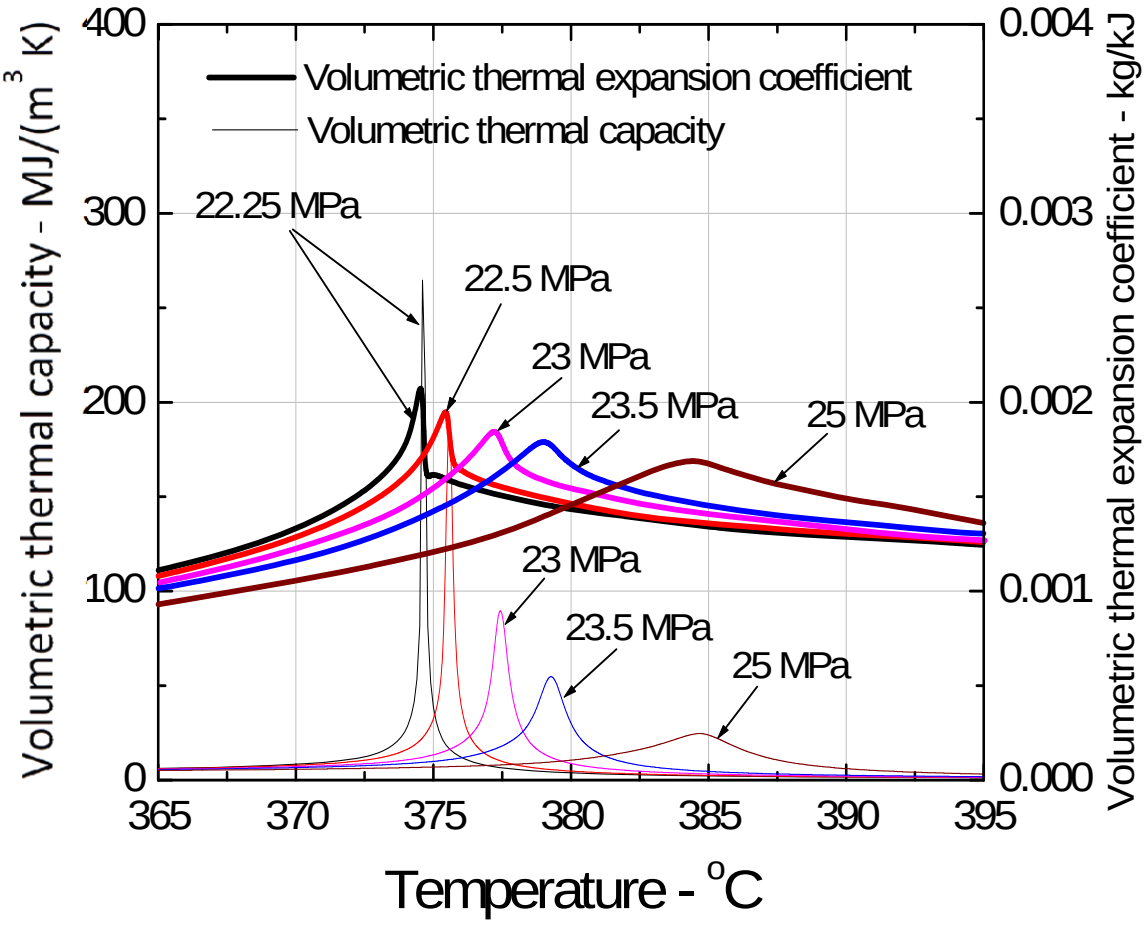

Figure 6-33: Comparison of volumetric thermal expansion coefficient and volumetric thermal capacitance of water at various pressures near pseudo-critical region

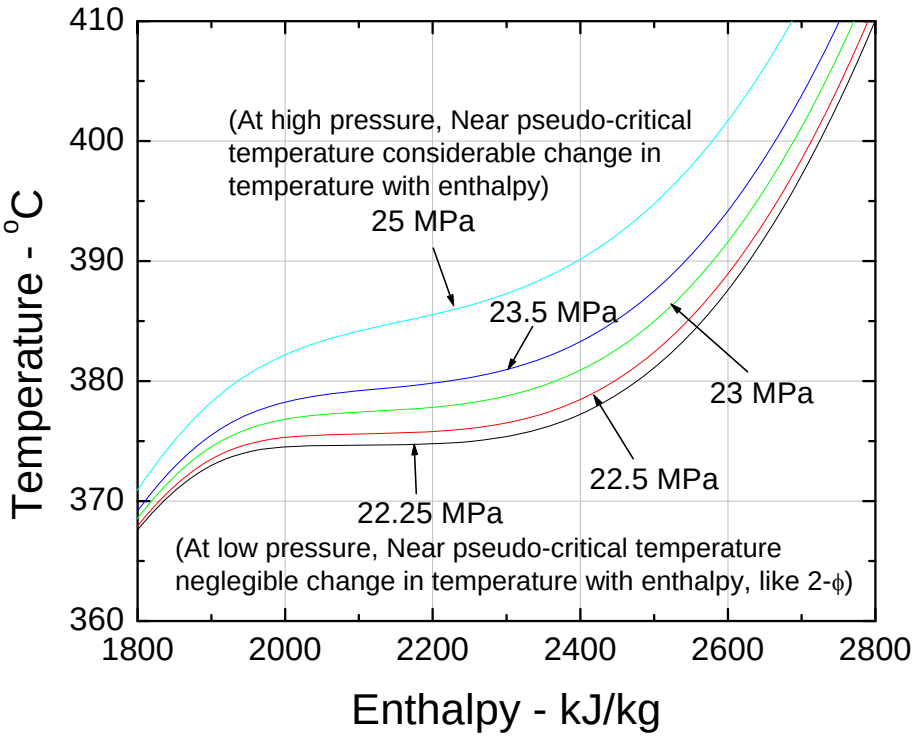

Figure 6-34: Temperature vs enthalpy curve for water at various pressures near pseudo-critical region

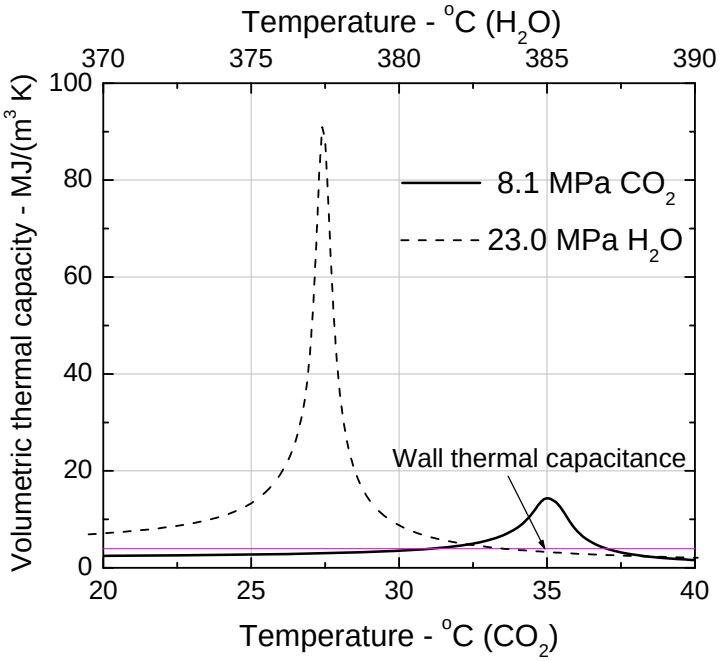

Figure 6-35: Comparison of thermal capacity of water and carbon dioxide near pseudo-critical temperature with wall thermal capacity of SPNCL

Chapter 7

Conclusions

The peak of the steady state mass flow rate versus power curve for uniform diameter supercritical water natural circulation is obtained at heater outlet temperature near the pseudo-critical value for open as well closed loop boundary conditions. For open loop, a change in loop diameter or loop height does not significantly affect the heater outlet temperature at which peak steady state flow rate is achieved. Local loss coefficient in the cold leg shifts the heater outlet temperature corresponding to peak flow much beyond the pseudo-critical temperature, whereas local loss coefficient in hot leg shifts it closer to pseudo-critical temperature for open loop. If the heater inlet temperature increases beyond the pseudo-critical temperature the steady state natural circulation mass flow rate reduces significantly for open as well as closed loop. The steady state natural circulation flow rate increases with increase in pressure at higher powers in the friction dominant region just like two phase natural circulation loops.

In all the open loops considered for linear stability analysis by SUCLIN code, it is observed that lower threshold power of instability increase only mildly whereas upper threshold of instability reduces significantly with increase in heater inlet temperature above 300^{o}C. The larger diameter loops are more unstable in terms of heater power compared to small diameter loops for supercritical water natural circulation, however smaller diameter loops are unstable over a wide range of heater outlet temperature for a fixed heater inlet temperature. Beyond a specified value of heater inlet temperature no instability is observed and its value decreases with increase in loop diameter. These

observations suggest that natural circulation systems operating with supercritical water can be designed for lower heater inlet temperatures and still not encounter instability what ever may be the power. Such systems can also take advantage of the large jump in enthalpy occurring across the pseudo-critical point. Increasing the loop height increases the SPNCL (open loop) instability. Increasing the loop pressure shifts the stability maps slightly upwards. Inducing local losses in cold leg improves the loop stability, whereas local losses in hot leg destabilize SPNCL considered as open loop which is similar to phenomenon observed in two-phase loops. For open loop, lower stability threshold deviates as much as -40% to +60% from the power corresponding to peak steady state flow in some of the cases analyzed in the thesis. Hence, it can be concluded that lower stability threshold power of SPNCL is not strictly related to the peak of the steady state mass flow rate versus power curve. Moreover, for a particular heater inlet temperature the steady state mass flow rate peak may exist but instability may be altogether absent for that heater inlet temperature as can be observed for larger diameter loops.

The non-linear stability analysis code (NOLSTA) also confirms findings of linear stability code (SUCLIN) for open loop that larger diameter loops are more unstable in terms of heater power compared to small diameter loops and beyond a specified value of heater inlet temperature no instability is observed and its value decreases with increase in loop diameter. With increase in heater inlet temperature the threshold heater outlet temperature at which instability is observed also increases and is not always near the pseudo-critical temperature. Therefore, it can be concluded stability threshold of SPNCL (open loop) is not confined to the near peak region of the steady state mass flow rate versus power curve.

BARC also participated in the blind benchmark exercise coordinated by the University of Pisa in the frame of the IAEA Coordinated Research Programme (CRP) on Heat Transfer Behavior and Thermo-hydraulics Codes Testing for SCWR. The addressed problem involved a circular pipe with uniform heating along the axis and geometrical configuration corresponding to a SCWR-sub-channel. Eight institutes from different countries participated in the benchmark exercise. Like SUCLIN code predictions, codes used by other participants also showed some deviation from the reference data generated by University of PISA, however, all submissions confirmed the following findings

- Increase in outlet throttling results in increase in unstable zone of heated channels (a well-known fact for two phase flow in heated channels);
- The presence of oscillating as well as excursive instabilities, the latter occurring at relatively low inlet temperature, in regions that would be hopefully of little interest to nuclear reactor operation;
- The general shape of the stability boundary in the N_{TPC}-N_{SPC} plane.

The results of NOLSTA and SUCLIN are matching qualitatively, but quantitatively there is a difference. Both the codes predict lower and upper threshold of instability, but unstable zone predicted by non-linear analysis is larger. This can be attributed to differences in the linear and non-linear analysis specified below

i) All the fluid properties are perturbed in non-linear analysis, whereas only enthalpy and specific volume perturbation is considered in linear stability analysis.
ii) Friction factor perturbation is not considered in linear stability analysis whereas non-linear analysis accounts for it.

iii) The perturbation induced in specific volume due to perturbation in enthalpy has been considered, whereas perturbation in specific volume due to perturbation in pressure has been neglected in linear analysis, whereas non-linear analysis accounts for both.

NOLSTA code predicts the steady state natural circulation mass flow rates of closed as well as open loop operating with supercritical carbon dioxide appreciably well (± 15%). For closed loop, the steady behavior of loop is found to be very sensitive to the empirical heat transfer correlation used for cooler primary side. The heat transfer correlations evaluating thermal conductivity at the bulk fluid temperature are showing very sharp reduction in flow after a particular power (when both cold leg and hot leg temperatures exceed the pseudo-critical temperature) which is accompanied with a steeper rise in heater inlet and outlet temperatures. However, the correlations evaluating thermal conductivity at wall temperatures/ pseudo-critical temperature for bulk fluid temperature exceeding pseudo-critical temperature (i.e. Bringer Smith, 1957) give a smoother reduction in flow similar to that observed in the experiments. For loop specific operating conditions it can be indirectly concluded that for evaluating heater inside heat transfer coefficient the thermal conductivity of fluid (required for calculating Nusselt number & Prandtl number) should be evaluated at the bulk fluid temperature, whereas for cooler inside heat transfer coefficient the thermal conductivity should be evaluated at the wall temperature/ pseudo-critical temperature for bulk fluid temperature exceeding pseudo-critical temperature. However, observed difference in heat transfer behavior of supercritical fluids under heating and cooling boundary conditions needs to be independently confirmed by other experiments as well.

During experimentation with carbon dioxide in SPNCL, instability has been observed for a very narrow window of power for HHHC orientation only and that too at lower secondary side chilled water flow rate of 10-15 lpm. The instability in the loop was observed in the pseudo-critical temperature range of operation where the volumetric expansion coefficient of the fluid is the highest. For closed loop boundary conditions, NOLSTA code (without considering pipe wall thermal capacitance effect) predicts instability over a large range of power bounded by lower & upper stable zones. Moreover, the instability is predicted even for very high secondary flows i.e. 135 lpm unlike experimental data where no instability was observed at 34 lpm secondary flow. However no instability was predicted at 180 lpm secondary flow. The predictions are only qualitatively matching with experimental data, hence pipe wall thermal capacitance model was incorporated in NOLSTA code. Consideration of pipe wall thermal capacitance predicts SPNCL to be completely stable, but reducing the thermal capacitance by 18% and neglecting the local losses the code is able to simulate limit cycle oscillations without flow reversal as observed during experiments. As interaction of heat structure and fluid should be modelled in greater detail, hence 3D-CFD codes may be a helpful tool in understanding the stability behavior of closed loop thermosyphon with supercritical fluids.

The modified NOLSTA code with pipe wall effect was also used for studying stability behavior of an open loop i.e. Lomperski's loop. The consideration of pipe wall pushed stability threshold beyond the experimental power range and explains the reason of instability not observed during experiments. Modelling of thermal capacitance of pipe

walls is strongly recommended for stability analysis of natural circulation at supercritical conditions (both open and closed loop boundary conditions) unlike two phase natural circulation flow case. In two phase natural circulation case there cannot be any energy interaction between two phase fluid and adiabatic heat structure as both will always be at same temperature during the transient. Any perturbation in two phase flow will give rise to a perturbation in two phase fluid enthalpy and void fraction/ density, but perturbation in enthalpy will not give rise to any perturbation in two phase fluid temperature and so there cannot be any thermal interaction of fluid with the wall. However, perturbation in supercritical fluid flow will give rise to perturbation in enthalpy/ density and perturbation in enthalpy will also give rise to perturbation in supercritical fluid temperature and hence thermal interaction with the wall becomes possible.

The peak of the steady state mass flow rate versus power curve for closed loop SPNCL operating with supercritical water is also obtained at heater outlet temperature near the pseudo-critical value. If the heater inlet temperature increases beyond the pseudo-critical temperature the steady state natural circulation mass flow rate reduces significantly. NOLSTA code also simulates the steady state behaviour of SPNCL operating with supercritical water appreciably well.

During experimentation with supercritical water, again instability has been observed for a very narrow window of power for HHHC orientation i.e. 7.5 to 8.3 kW for operating pressure range of 22.1 to 22.9 MPa. The instability is observed near pseudo-critical temperature at low pressures however at high pressures no instability is observed. The

mechanism of instability development is growth of small amplitude oscillations as proposed by Welander (1967). NOLSTA code also predicts instability over a very narrow range of power near pseudo-critical temperature and at pressures below 23.7 MPa which is in qualitative agreement with experimental data. The reason for the same is higher thermal capacitance of fluid near pseudo-critical temperature at low pressures which cause enthalpy perturbations to generate very small fluid temperature perturbations only and hence fluid interaction with pipe wall or damping effect of wall becomes almost negligible. Moreover, NOLSTA code also predicts that instability can be avoided even at low pressures in SPNCL by giving large step rise in power when fluid is approaching the pseudo-critical temperature. Scaling fluid for instability studies of supercritical water should take care of the ratio of thermal capacitance of the wall and the fluid near pseudo-critical temperature.

Although the amount of experimental instability data generated in the present test facility is clearly insufficient as compared to extensive instability data available for single phase and two-phase loops but has definitely helped to gain an insight in to instability phenomenon with supercritical fluids.

Appendix-1: Steady state natural circulation data with supercritical CO_2

Steady state natural circulation data generated with CO_2 given in tables A1-1, A1-2, are generated respectively for the HHHC and HHVC orientations.

Table A1-1 Steady state data for HHHC orientation (clockwise flow) with supercritical CO_2

Sr. No.	Power (W)	PTr-1 (bar)	T1 (°C)	T2 (°C)	T3 (°C)	T4 (°C)	T5 (°C)	T6 (°C)	T7 (°C)	T8 (°C)	T9 (°C)	T10 (°C)	T11 (°C)	T12 (°C)	T13 (°C)	T14 (°C)	T15 (°C)	T16 (°C)	T17 (°C)	T18 (°C)	T-33 (°C)	T-34 (°C)	T-35 (°C)	T-36 (°C)	T-37 (°C)	T-38 (°C)	T-41 (°C)	T-42 (°C)	LPM$	Mass* flow rate
1	203.7	84.7	17.4	17.9	22.5	23.3	23.7	faulty	24.7	23.3	24.7	23.9	25.5	24.1	25.2	23.5	20.3	20.1	20.2	20.2	21.4	21.5	17.3	18.1	17.5	17.2	9.2	10.0	37.0	0.02818
2	387.9	84.7	19.0	19.6	27.0	28.9	28.6	faulty	30.3	28.3	31.5	29.5	31.6	28.6	31.4	28.6	23.2	22.4	22.5	23.0	24.2	24.1	19.6	20.3	19.7	19.9	8.8	9.7	37.0	0.03841
3	590.5	85.0	23.0	23.5	32.6	35.0	34.7	faulty	35.9	33.3	37.1	34.5	37.1	33.7	37.5	33.6	26.5	26.8	27.0	27.5	27.6	27.9	23.5	24.3	23.5	23.2	9.0	9.8	37.0	0.04393
4	785.3	85.3	26.3	26.8	37.1	39.4	39.1	faulty	40.9	37.2	42.2	39.5	41.6	38.2	42.0	38.7	29.9	30.2	30.4	30.3	30.9	30.6	26.3	28.2	27.0	27.0	8.7	9.7	37.0	0.05388
5	977.5	85.3	29.1	29.6	39.9	42.7	42.4	faulty	44.3	40.0	45.5	42.3	44.9	40.4	44.8	40.9	32.8	32.4	32.6	33.7	34.3	34.2	29.1	31.6	30.1	30.1	8.8	9.5	37.0	0.05367
6	1184.0	84.7	31.4	31.3	41.0	43.8	43.0	faulty	45.4	41.7	46.7	43.4	45.4	41.5	46.5	42.0	33.9	34.1	34.3	34.8	34.9	34.9	30.8	32.8	31.6	31.4	8.9	9.7	37.0	0.05635
7	1406.2	85.6	35.8	35.8	44.9	51.0	47.4	faulty	48.8	46.1	49.5	46.2	49.3	45.5	49.3	45.4	37.8	36.9	37.7	37.6	38.2	38.4	35.8	37.3	36.4	36.6	9.0	9.9	35.5	0.05144
8	1103.0	86.3	31.9	32.4	41.0	44.9	43.5	faulty	44.9	41.7	46.1	42.9	45.4	42.1	45.9	42.0	35.0	34.6	34.9	35.9	35.4	35.6	32.5	33.9	32.8	32.7	8.9	9.7	35.5	0.05183
9	702.9	84.7	26.3	26.3	34.3	37.7	36.3	faulty	37.6	35.6	38.8	36.7	38.2	35.4	38.7	35.9	29.4	29.1	29.8	29.7	30.4	30.2	26.9	27.1	26.9	27.1	9.3	10.0	34.80	0.05284
10	1593.7	85.1	37.0	37.5	48.9	56.0	53.4	faulty	55.5	49.4	59.0	52.3	56.5	50.5	58.3	51.0	39.0	39.1	39.4	39.8	40.5	40.6	37.5	39.0	38.0	37.8	9.0	10.0	36.00	0.04476
11	1798.0	85.8	40.9	41.4	65.7	77.7	75.4	faulty	84.7	73.3	91.1	77.4	90.3	75.8	94.1	78.4	49.1	49.2	51.2	51.6	51.7	51.4	40.8	42.3	41.9	41.7	9.0	10.0	34.80	0.03944
12	2000.5	84.7	45.9	46.4	89.3	103.7	102.4	faulty	117.2	103.3	125.9	109.7	126.3	108.4	132.2	112.6	63.2	65.9	69.2	69.6	69.2	69.0	44.8	46.9	46.1	45.7	9.1	10.1	33.50	0.03599
13	2197.7	85.0	50.9	52.0	114.6	132.0	130.5	faulty	150.3	133.3	159.7	142.0	160.7	140.9	168.1	146.8	80.7	84.4	88.9	89.8	87.1	87.2	49.8	51.9	51.8	51.4	9.0	11.0	34.70	0.03104
14	2287.0	85.3	54.9	54.8	126.4	145.4	143.2	faulty	164.8	148.3	175.4	156.4	175.6	155.5	183.8	161.9	89.2	93.3	98.5	98.8	96.1	96.3	52.6	54.8	55.4	55.8	9.2	10.4	33.00	0.03028
15	2077.1	85.0	52.6	53.1	114.0	130.9	128.3	faulty	149.7	133.9	159.1	142.0	159.6	140.4	166.4	146.8	82.4	85.5	90.6	90.9	89.4	89.7	50.9	52.5	53.5	53.0	9.5	11.2	35.40	0.03009
16	1916.1	85.0	48.2	48.6	96.1	111.0	109.6	faulty	126.1	112.2	134.4	118.6	134.6	116.8	140.6	122.1	69.4	72.1	75.4	75.8	75.3	75.2	47.0	49.1	49.1	48.9	9.5	10.9	34.20	0.03265
17	1497.7	84.4	38.6	38.6	52.8	60.5	59.5	faulty	64.5	56.7	68.0	59.0	68.1	58.4	70.6	59.4	41.2	41.3	42.8	43.2	43.3	43.5	38.6	39.5	39.0	39.1	9.3	10.6	33.70	0.04299
18	198.6	89.8	17.4	18.4	22.5	23.9	23.7	faulty	24.7	23.9	25.3	24.5	25.5	24.5	25.2	24.6	20.3	20.1	20.8	21.3	21.4	19.5	17.3	18.6	18.6	19.6	9.5	10.2	30.0	0.02259
19	398.0	90.2	21.8	22.4	29.2	31.6	31.4	faulty	33.1	30.6	33.7	31.7	34.3	31.4	34.2	31.9	25.4	24.6	25.9	26.9	26.4	24.5	21.3	23.1	23.1	24.8	9.3	10.2	30.1	0.03024
20	597.3	90.0	24.6	25.2	34.8	37.7	37.4	faulty	38.7	36.1	39.9	37.3	40.4	37.6	39.8	37.0	28.8	28.5	30.4	30.9	29.8	28.4	25.2	26.0	26.4	28.0	9.4	10.3	30.0	0.02968
21	789.3	90.0	28.0	28.5	39.3	42.2	41.3	faulty	43.2	40.0	44.4	41.2	44.3	41.0	44.3	40.3	31.6	31.8	33.2	34.2	32.6	31.2	28.0	29.4	29.3	30.7	9.4	10.3	30.0	0.03576
22	1003.7	90.2	31.4	31.9	42.7	46.6	45.7	faulty	47.1	43.9	48.3	45.7	48.2	44.4	48.2	44.3	35.0	35.2	36.0	37.1	36.5	34.5	31.9	33.3	33.2	35.2	9.3	10.5	30.0	0.03909
23	1215.6	90.2	34.7	35.8	45.5	48.8	48.5	faulty	49.9	46.7	51.2	47.9	51.5	47.2	51.5	46.5	37.8	37.4	38.3	39.3	38.2	36.7	34.7	36.1	36.0	38.0	9.5	10.5	30.0	0.04441
24	1413.6	90.0	37.5	38.0	47.2	52.1	51.8	faulty	53.3	49.4	55.7	50.7	54.8	50.0	55.5	49.9	39.5	39.7	41.5	40.5	40.5	38.4	37.5	39.0	38.8	41.4	8.9	9.9	30.0	0.03791
25	1616.0	90.8	40.3	40.8	53.9	61.0	59.5	faulty	63.3	56.7	66.3	58.5	66.5	57.3	67.8	57.7	42.9	43.0	44.5	45.5	44.4	42.8	40.8	42.3	41.6	44.2	9.3	10.5	30.0	0.03885
26	1800.0	90.4	44.2	44.2	68.0	78.2	76.5	faulty	85.2	74.4	90.0	77.9	89.2	76.9	92.4	77.9	50.8	52.0	54.0	55.6	54.0	51.2	43.6	45.2	45.6	47.5	9.5	10.5	30.2	0.04034
27	2399.1	90.2	57.7	58.1	128.7	146.5	144.3	faulty	167.6	150.0	177.7	157.6	177.3	157.2	184.9	162.5	90.9	95.0	100.2	101.6	97.3	95.7	55.4	58.2	59.6	62.1	10.2	11.7	30.0	0.03136
28	2305.5	90.3	52.1	52.6	124.7	143.1	140.9	faulty	162.6	146.7	172.6	153.7	172.3	153.3	179.3	158.0	89.8	93.3	98.5	99.9	96.7	95.1	54.8	57.6	60.2	62.1	9.7	11.7	30.0	0.03109
29	1905.0	89.8	47.6	48.1	83.1	96.5	94.7	faulty	107.6	65.0	114.7	100.2	114.1	99.4	119.3	102.0	61.0	62.6	66.4	67.4	66.3	64.0	46.4	48.0	49.5	51.4	8.9	10.1	29.8	0.03653
30	1717.3	89.1	43.1	43.6	65.7	76.0	74.3	faulty	81.9	71.7	87.1	75.2	87.5	75.2	90.8	76.8	49.7	50.3	52.9	53.9	52.8	50.6	43.1	44.6	45.1	47.0	8.8	10.4	29.8	0.03944
31	1500.2	87.9	39.7	40.3	51.1	58.3	56.2	faulty	60.5	54.4	63.0	56.2	63.2	55.0	65.0	56.0	41.8	41.3	43.8	42.8	43.3	41.2	39.7	40.6	40.1	43.1	8.8	10.4	29.8	0.05081
32	907.8	89.1	31.9	32.4	41.6	46.0	44.0	faulty	46.0	42.8	46.7	43.4	46.5	43.2	46.5	43.1	35.0	35.2	36.0	36.5	36.0	34.5	31.3	33.3	33.2	35.2	9.4	10.6	29.6	0.03757
33	703.1	89.6	28.0	28.5	37.6	41.6	39.6	faulty	41.5	39.4	42.7	40.1	42.1	39.9	42.0	39.2	31.6	31.3	33.7	32.7	32.6	31.2	29.0	29.4	29.8	31.3	9.3	10.3	29.8	0.0353
34	491.1	89.1	23.5	24.6	31.5	34.4	33.6	faulty	34.8	33.3	36.0	34.0	36.0	33.7	36.4	33.6	27.1	26.8	28.1	28.6	28.1	26.7	23.5	24.8	25.3	26.3	9.3	10.3	29.8	0.03454
35	302.0	89.8	20.7	20.7	26.4	28.3	28.1	faulty	29.2	27.8	30.4	28.9	30.5	28.6	30.3	29.1	23.7	23.5	25.3	24.2	24.7	22.8	20.1	21.5	21.9	22.9	9.4	10.2	29.8	0.02497

Table A1-2 Steady state data for HHVC orientation with supercritical CO_2

Sr. No.	Power (W)	PTr-1 (bar)	T1 (°C)	T2 (°C)	T3 (°C)	T4 (°C)	T5 (°C)	T6 (°C)	T7 (°C)	T8 (°C)	T9 (°C)	T10 (°C)	T11 (°C)	T12 (°C)	T13 (°C)	T14 (°C)	T15 (°C)	T16 (°C)	T17 (°C)	T18 (°C)	T33 (°C)	T34 (°C)	T37 (°C)	T38 (°C)	T39 (°C)	T40 (°C)	T43 (°C)	T44 (°C)	LPM	Mass flow rate
1	395.9	85.8	19.6	20.7	30.0	28.7	30.3	faulty	32.5	29.4	33.7	30.6	34.4	30.3	34.2	31.4	23.7	24.0	24.2	24.7	25.3	25.5	25.3	25.2	19.5	20.6	8.9	9.1	34.0	0.03064
2	820.1	85.8	28.0	27.4	43.8	39.3	42.4	faulty	44.3	40.0	45.5	41.8	46.0	40.4	46.5	41.5	31.6	31.8	32.6	32.5	33.2	33.4	33.2	33.4	27.4	27.9	8.2	8.8	34.1	0.03867
3	987.2	86.1	31.2	31.7	46.6	41.6	44.6	faulty	47.1	42.2	49.5	44.0	48.8	42.7	49.3	43.7	34.4	34.6	34.9	35.3	36.0	36.5	36.0	36.2	30.8	31.4	8.8	9.1	34.5	0.04429
4	1216.9	86.5	34.9	35.4	51.0	44.4	49.0	faulty	51.6	45.6	53.4	47.3	53.2	46.0	53.8	46.5	37.3	36.9	37.1	37.6	38.2	38.7	38.3	38.2	34.8	35.4	8.6	9.0	33.5	0.04618
5	1423.5	85.3	36.4	36.9	54.4	46.6	52.3	faulty	56.1	48.3	58.5	50.1	56.0	48.8	55.5	49.3	38.4	38.0	38.8	38.7	38.8	38.6	39.4	39.6	36.9	36.4	9.1	9.5	34.0	0.04165
6	1604.2	85.3	38.6	39.1	67.7	56.7	66.1	faulty	72.9	61.1	77.6	64.0	77.6	64.0	80.7	66.1	42.3	42.5	43.9	44.3	43.9	43.8	44.4	44.8	38.6	39.2	9.6	10.4	34.2	0.04115
7	1780.0	85.3	42.0	42.5	92.1	77.5	91.4	faulty	104.3	88.9	111.9	94.1	113.0	94.9	117.7	99.7	55.3	56.4	59.1	59.5	59.6	59.8	59.6	59.9	42.0	42.5	9.7	10.2	34.7	0.03211
8	1990.9	85.6	44.2	44.7	107.6	92.7	107.9	faulty	125.0	106.1	133.8	113.0	135.2	115.7	142.3	121.0	63.2	65.9	69.8	70.7	70.3	70.2	68.6	68.5	44.8	44.6	9.1	9.7	34.0	0.03023
9	2186.7	85.6	48.7	49.8	136.5	120.2	138.2	faulty	159.8	140.0	171.5	149.2	174.0	152.7	182.1	159.1	83.0	86.0	92.9	93.2	91.1	91.5	87.8	87.9	49.3	49.7	8.9	10.0	33.9	0.02616
10	1705.0	85.3	40.3	40.8	78.8	66.9	78.2	faulty	89.1	74.4	95.6	79.1	94.2	78.0	98.6	81.8	48.0	48.6	50.6	51.1	51.2	51.5	51.2	51.6	40.9	40.7	8.9	9.3	33.8	0.03678
11	1503.4	85.2	37.5	38.0	60.5	51.1	58.4	faulty	63.9	54.4	68.0	56.2	67.0	55.0	68.9	56.6	40.1	39.7	40.5	40.4	41.0	41.0	41.6	41.9	37.5	37.9	9.1	9.7	34.0	0.04528
12	1099.2	85.3	33.6	33.5	47.7	42.7	46.3	faulty	48.8	43.3	50.6	45.1	50.4	43.8	50.4	43.7	36.1	35.2	36.0	36.5	36.5	36.9	37.7	37.7	33.0	33.7	9.0	9.3	33.5	0.04548
13	900.6	84.4	29.7	30.2	44.4	39.9	43.0	faulty	44.9	40.0	46.1	41.8	46.5	41.0	46.5	41.5	33.3	33.5	33.2	33.7	34.3	34.7	34.9	35.4	29.6	29.9	9.0	9.3	33.7	0.04735
14	700.4	84.4	26.9	27.4	39.9	36.5	39.6	faulty	40.9	38.3	42.2	39.0	42.7	38.2	42.6	38.7	30.5	30.7	30.9	30.8	32.0	32.3	32.6	32.3	26.8	26.7	9.1	9.5	34.0	0.04519
15	499.6	84.2	23.5	24.0	35.5	32.6	35.2	faulty	37.0	33.9	37.7	34.5	37.1	33.7	37.5	34.2	27.1	27.4	27.6	27.5	28.7	28.6	29.3	29.6	23.5	23.9	9.3	9.6	34.8	0.03874
16	300.0	84.7	20.2	20.7	28.9	27.5	29.2	faulty	30.3	28.3	31.5	29.0	32.1	29.2	31.9	30.3	23.7	24.0	24.2	24.1	25.3	25.6	25.9	25.7	20.7	20.3	9.2	9.5	34.0	0.02651

Appendix-2: Steady state natural circulation data with supercritical H_2O

Steady state natural circulation data generated with H_2O for the HHHC orientation is given in Table A2-1.

Table-A2-1: Steady state data for HHHC orientation with supercritical H_2O

Sl. No.	Logged Power (kW)	Flow (lpm)	DPT-1 (mmWC)	PT-1 (bar)	PTr-2 (bar)	TT-1 (^oC)	TT-2 (^oC)	TT-3 (^oC)	TT-4 (^oC)	TT-5 (^oC)	TT-6 (^oC)	TT-7 (^oC)	TT-8 (^oC)	TT-9 (^oC)	TT-10 (^oC)	TT-11 (^oC)	TT-12 (^oC)	TT-13 (^oC)	TT-14 (^oC)
1	7.0	9563.0	-3.5	224.4	223.2	363.2	359.8	388.6	388.2	388.3	385.6	389.4	387.4	387.9	388.9	394.5	388.2	384.5	386.0
2	8.0	13824.0	-133.7	233.9	232.4	402.7	401.1	499.6	472.9	460.7	472.7	489.8	467.8	455.5	470.4	488.1	464.8	447.5	461.3
3	7.5	12937.0	-135.1	230.0	229.2	396.4	395.1	488.6	461.3	449.5	461.5	479.3	467.8	444.9	459.1	478.1	455.2	438.2	451.2
4	5.0	11025.0	31.4	229.2	228.0	275.7	275.5	300.8	300.2	299.8	298.1	303.2	309.4	300.0	301.1	309.2	301.9	297.5	300.2
5	5.6	11025.0	30.7	228.1	227.1	290.1	289.5	316.0	315.1	314.7	313.5	318.7	324.8	315.6	316.5	324.6	316.6	312.2	314.9
6	6.1	10978.0	42.5	228.3	227.8	319.8	318.5	347.3	346.0	346.1	344.6	349.8	356.5	346.5	347.5	355.8	347.8	343.3	346.0
7	6.5	10932.0	48.8	229.7	228.4	332.8	331.8	361.2	357.9	360.6	358.3	363.3	370.3	360.4	361.7	369.1	361.7	356.7	359.1
8	7.0	10947.0	66.9	232.0	230.5	368.4	367.1	393.3	390.4	392.8	390.6	392.7	402.4	392.5	392.6	398.6	392.4	389.1	390.2
9	4.5	11056.0	28.6	230.0	228.8	264.9	264.0	288.6	287.6	287.4	286.1	291.0	297.3	288.2	289.3	296.7	289.7	285.3	287.6
10	7.9	10807.0	50.9	229.5	228.0	390.5	389.2	458.2	452.5	453.6	452.8	467.1	473.7	451.3	456.6	473.5	456.8	446.6	453.7
11	8.0	7682.0	28.7	231.1	230.5	377.4	377.3	398.9	395.6	398.2	395.2	399.9	394.7	397.3	397.6	405.7	395.7	394.1	395.2
12	8.0	7682.0	24.5	230.3	229.9	378.8	378.2	398.0	395.6	397.8	394.8	397.3	393.9	396.5	397.2	403.2	395.2	393.3	394.4
13	8.5	7673.0	27.6	231.1	230.5	397.7	397.5	490.8	484.3	482.6	482.7	502.5	483.8	480.1	488.8	509.7	486.3	475.2	485.2
14	8.5	7673.0	28.0	230.3	229.7	398.0	397.9	486.2	480.9	478.8	478.9	497.8	480.1	476.7	485.4	504.7	482.5	472.7	481.9
15	7.0	7620.0	23.5	229.7	228.8	353.9	353.4	380.3	378.1	379.2	377.3	382.2	377.2	379.2	380.5	387.4	377.6	375.6	377.6
16	7.0	7620.0	23.5	228.3	227.8	357.0	357.1	383.3	381.4	382.9	380.2	384.7	380.2	382.6	383.8	390.3	381.0	379.0	380.5
17	7.3	7635.0	21.6	230.0	229.7	328.0	327.7	359.7	357.3	358.9	356.2	363.7	356.8	358.5	360.4	369.5	357.9	355.0	357.8
18	7.3	7635.0	23.0	230.6	230.3	347.9	347.9	377.4	374.7	376.3	373.6	379.7	374.3	375.8	377.1	385.3	375.1	372.3	374.6
19	7.7	7635.0	25.8	230.3	229.4	361.3	361.3	389.6	387.2	388.7	385.2	390.2	386.0	387.6	388.9	395.7	386.9	384.5	386.0
20	7.7	7635.0	29.3	232.0	231.5	366.9	366.8	395.9	393.1	395.3	392.3	396.9	391.8	394.4	395.1	402.8	392.7	391.2	392.7
21	7.3	7620.0	-27.2	230.9	229.9	375.3	374.8	419.1	395.1	393.3	393.9	413.3	392.6	392.7	396.0	414.4	392.7	389.5	392.7
22	7.3	7620.0	-27.6	230.3	229.7	374.6	374.8	420.8	395.6	393.7	394.3	414.6	393.5	393.1	396.4	415.3	393.6	389.5	393.1
23	7.0	7899.0	92.7	228.6	227.1	379.3	375.2	398.3	395.0	397.0	394.3	397.8	400.3	396.8	396.8	403.6	396.6	392.9	394.0
24	7.0	7899.0	96.1	228.3	226.9	381.4	377.3	398.3	396.3	398.2	395.6	398.2	401.1	397.2	397.2	403.6	397.1	393.3	394.8
25	7.0	7712.0	66.2	228.1	227.1	399.2	394.1	472.6	465.8	462.7	464.8	481.0	474.9	463.1	470.0	491.4	472.0	460.9	469.2
26	8.0	6904.0	97.5	227.5	226.1	402.4	400.0	494.1	487.1	485.9	486.4	505.4	489.1	484.7	493.0	512.6	493.9	480.3	489.8
27	7.5	6858.0	92.7	229.5	228.2	398.9	396.2	474.3	467.9	467.3	467.7	484.0	469.1	465.6	472.9	491.0	473.3	461.3	470.1
28	1.0	25159.0	5.0	225.3	224.0	74.9	75.5	89.5	85.4	84.4	86.3	92.1	86.7	84.9	87.4	93.6	88.8	87.0	faulty
29	1.5	25035.0	5.4	225.8	224.2	102.2	102.8	121.1	116.7	115.0	117.8	123.2	117.2	115.8	118.3	126.1	119.6	117.7	faulty
30	2.0	24973.0	7.3	226.7	225.3	128.4	129.0	147.7	144.6	144.7	145.1	151.0	145.5	145.4	147.2	155.6	148.2	145.8	faulty
31	2.5	24693.0	8.1	226.9	226.3	157.8	158.0	176.0	173.8	174.9	174.2	178.7	174.7	175.8	177.3	183.5	176.4	174.8	faulty
32	3.0	24320.0	7.5	228.3	227.4	181.6	182.2	201.3	197.9	200.1	198.2	203.5	198.9	200.7	202.0	208.0	200.8	199.2	faulty
33	3.5	24413.0	10.9	229.5	228.6	207.1	207.7	230.0	227.1	229.1	227.2	232.9	228.5	229.9	231.2	238.0	230.3	227.7	faulty
34	4.0	24289.0	11.7	230.6	229.7	219.4	219.9	243.9	240.8	242.7	241.3	246.8	242.3	243.8	245.0	251.7	244.2	241.6	faulty
35	5.0	24351.0	14.6	234.8	233.8	271.2	271.7	297.9	294.6	297.3	295.2	301.1	296.9	298.3	299.8	307.1	298.1	295.8	faulty
36	6.0	24382.0	18.2	225.5	224.4	318.4	319.2	347.7	344.6	347.4	345.0	350.7	346.5	348.2	349.6	356.6	347.4	345.0	faulty
37	6.5	24320.0	20.5	231.1	230.3	339.4	340.2	368.4	365.8	368.9	366.1	371.7	367.3	369.7	370.9	377.4	368.0	366.0	faulty
38	7.5	24164.0	30.7	241.7	240.0	380.7	382.2	403.4	399.6	403.6	400.3	404.8	400.4	402.8	403.2	409.8	401.4	399.7	faulty
39	7.9	24326.0	34.7	229.7	228.0	393.6	392.0	465.4	458.8	459.8	459.0	474.7	480.3	458.5	463.7	481.0	463.6	453.4	461.3
40	8.0	24289.0	36.3	230.6	230.7	398.5	395.8	481.0	474.2	473.5	473.5	490.7	474.9	471.6	479.2	498.1	479.6	466.8	475.5
41	8.5	24235.0	40.9	235.3	233.9	405.2	402.8	508.0	500.4	498.7	499.2	520.1	502.4	497.8	506.3	528.4	507.4	492.9	503.3
42	7.5	24257.0	37.1	229.0	227.4	390.8	386.7	455.3	449.6	449.1	449.5	463.4	451.6	447.9	454.1	471.4	454.3	443.7	451.2
43	7.0	24195.0	30.2	225.3	224.9	389.2	385.4	444.3	438.8	436.7	437.9	450.3	446.6	436.1	441.5	459.0	443.0	433.2	439.8

Table-A2-1: Steady state data for HHHC orientation with supercritical H_2O (Contd.)

Sl. No.	TT-15 (°C)	TT-16 (°C)	TT-17 (°C)	TT-18 (°C)	TT-19 (°C)	TT-20 (°C)	TT-21 (°C)	TT-22 (°C)	TT-31 (°C)	TT-32 (°C)	TT-33 (°C)	TT-34 (°C)	TT-35 (°C)	TT-36 (°C)	TT-37 (°C)	TT-38 (°C)	TT-39 (°C)	TT-40 (°C)	TT-41 (°C)
1	393.4	387.1	386.6	392.7	401.1	388.7	387.9	363.4	405.0	387.0	383.7	faulty	393.7	421.7	387.9	381.7	400.8	390.1	388.9
2	476.9	458.5	449.2	464.9	476.3	459.4	451.9	457.3	460.4	445.5	434.3	faulty	467.8	473.4	438.6	440.6	464.1	445.9	438.3
3	466.8	448.9	439.4	454.3	465.7	448.5	442.1	453.2	452.5	437.1	426.7	faulty	457.3	459.8	429.3	431.6	454.4	436.7	429.4
4	308.9	301.1	300.0	306.1	315.4	303.4	301.7	305.5	304.6	301.1	296.0	faulty	311.3	329.0	303.8	300.6	316.5	307.4	304.4
5	323.8	316.2	314.8	320.9	330.2	318.0	316.2	317.6	320.4	315.8	310.8	faulty	326.4	344.7	318.6	315.0	332.1	322.5	319.6
6	355.2	347.2	346.1	352.2	361.9	349.0	347.4	342.8	351.7	346.5	341.5	faulty	357.3	376.4	349.0	345.1	363.3	353.1	350.0
7	368.7	360.7	359.2	365.7	375.0	362.3	360.6	357.1	365.0	360.4	355.0	faulty	370.7	380.2	362.1	358.3	376.4	365.7	363.1
8	397.2	390.9	391.3	396.5	405.4	392.1	392.2	378.5	392.9	391.2	387.1	faulty	397.1	407.3	390.9	384.2	405.1	393.4	391.4
9	296.6	289.3	288.2	294.3	302.7	291.2	289.8	282.0	293.3	288.4	284.2	faulty	299.6	315.5	291.6	288.3	303.8	295.6	293.0
10	477.8	458.9	450.0	466.2	489.0	463.6	454.1	458.6	460.8	448.8	436.0	faulty	489.1	491.6	463.1	467.4	497.1	475.7	463.6
11	405.8	394.4	395.2	faulty	413.1	faulty	394.6	395.9	398.5	396.9	393.3	faulty	402.4	396.3	395.9	398.3	410.8	396.7	394.7
12	402.4	394.0	394.4	faulty	408.4	faulty	393.8	401.0	396.8	396.1	392.4	faulty	399.9	395.5	395.1	397.1	405.8	395.4	393.8
13	517.6	493.4	481.8	faulty	532.1	faulty	487.3	500.7	491.1	480.3	462.3	faulty	533.6	515.3	501.8	521.2	544.8	518.7	503.4
14	512.9	489.2	478.8	faulty	526.2	faulty	483.9	503.3	488.2	477.0	459.8	faulty	528.1	511.5	498.4	517.4	539.3	514.5	500.1
15	386.7	377.6	378.3	faulty	392.8	faulty	378.0	382.7	383.5	380.5	374.7	faulty	387.3	382.4	381.2	384.5	392.7	383.2	380.7
16	388.8	380.6	381.3	faulty	395.8	faulty	381.4	381.1	387.2	383.4	377.7	faulty	389.4	384.9	383.7	387.0	396.1	385.7	383.3
17	369.3	357.9	358.1	faulty	377.6	faulty	358.5	359.8	365.9	361.1	353.3	faulty	371.5	364.6	361.8	366.9	378.8	365.6	361.8
18	385.0	374.7	375.0	faulty	392.0	faulty	375.5	376.4	381.0	377.1	371.0	faulty	385.7	379.8	377.8	382.0	391.9	380.7	377.4
19	394.8	386.4	386.4	faulty	402.1	faulty	387.0	390.8	391.4	388.9	382.7	faulty	394.0	389.6	387.9	391.2	402.4	390.4	387.9
20	402.8	392.3	393.1	faulty	411.4	faulty	393.3	397.6	397.2	394.4	389.5	faulty	401.5	394.2	393.8	396.7	412.9	395.4	393.0
21	405.0	391.1	392.3	faulty	402.1	faulty	391.6	390.0	405.6	392.3	389.5	faulty	402.0	390.8	390.9	392.9	400.3	390.4	389.6
22	405.8	391.5	392.3	faulty	402.1	faulty	392.1	394.6	406.0	701.1	389.1	faulty	402.4	391.3	390.0	392.9	400.3	390.8	390.0
23	403.5	395.1	395.1	faulty	411.7	395.8	395.6	379.7	401.3	395.0	393.0	faulty	400.8	425.1	394.7	392.9	408.9	396.4	395.2
24	403.5	395.5	395.9	faulty	411.7	396.7	396.0	391.1	402.5	395.8	393.4	faulty	400.8	425.6	395.5	393.7	406.8	396.8	395.6
25	498.2	478.2	466.9	faulty	509.6	482.9	472.0	492.6	483.3	461.1	448.6	faulty	507.1	534.8	481.3	491.3	515.2	493.4	481.4
26	520.7	500.1	487.2	faulty	535.0	506.7	494.6	502.2	495.8	481.3	466.8	faulty	538.1	566.1	509.2	525.1	549.0	526.5	511.3
27	497.3	477.8	467.3	faulty	509.2	483.3	472.8	482.9	477.9	464.0	450.7	faulty	511.3	538.2	484.7	500.3	520.3	498.8	486.0
28	95.1	92.8	87.9	91.2	97.5	90.0	87.9	91.5	100.0	92.6	89.8	faulty	101.7	93.2	90.0	91.0	103.8	94.5	91.2
29	128.2	83.6	118.7	122.9	130.9	121.3	119.1	111.2	133.8	124.2	121.4	faulty	136.8	125.3	122.1	123.1	139.2	127.2	123.7
30	157.0	57.9	147.5	152.4	161.3	150.2	148.1	135.9	164.6	153.7	151.0	faulty	167.0	154.6	151.7	152.4	169.6	157.0	152.9
31	183.7	86.5	176.6	181.6	188.3	178.7	176.7	171.2	192.9	182.3	184.7	faulty	201.7	188.4	185.1	185.3	204.2	190.6	186.6
32	207.9	61.7	201.1	206.5	213.2	203.4	201.4	198.9	218.3	207.6	204.1	faulty	220.1	207.5	204.9	204.3	221.5	209.5	206.5
33	237.6	42.4	231.6	237.7	245.7	234.3	233.0	231.2	252.1	239.6	237.4	faulty	257.3	241.8	238.3	238.0	259.1	244.4	241.1
34	252.1	55.0	246.8	253.3	261.4	249.4	247.9	247.1	268.3	254.3	252.1	faulty	272.4	256.6	252.7	252.9	275.1	259.5	255.9
35	305.9	85.7	297.9	304.9	312.9	300.4	299.6	300.8	317.9	306.1	303.2	faulty	321.3	307.4	303.8	302.7	324.9	309.9	307.0
36	355.6	99.5	347.8	354.7	362.7	349.8	348.7	355.0	366.7	354.1	351.7	faulty	370.7	355.7	352.8	350.5	373.8	358.6	355.5
37	376.0	98.3	368.0	374.5	382.1	369.5	369.1	365.5	384.6	702.7	371.1	faulty	388.3	373.9	371.4	368.2	391.1	376.2	374.1
38	406.4	76.2	401.9	407.0	413.4	401.2	401.4	402.0	410.3	406.5	400.9	faulty	413.7	401.8	400.5	394.6	416.1	403.0	402.3
39	485.9	466.5	458.0	474.6	499.1	472.8	463.0	475.4	465.0	455.2	441.5	faulty	499.2	502.2	473.7	478.1	508.0	486.2	473.8
40	505.0	484.1	473.7	491.5	519.4	491.6	479.7	500.1	483.3	469.9	455.8	faulty	519.7	552.2	491.8	506.1	530.0	507.2	492.8
41	537.6	514.8	500.3	520.2	552.3	522.2	508.7	492.6	509.6	493.5	478.1	faulty	556.9	583.9	525.6	541.9	569.2	545.0	528.2
42	476.9	457.7	448.7	464.5	488.5	463.2	453.2	464.5	470.4	448.0	434.3	faulty	486.2	503.9	460.1	464.1	494.5	471.9	461.1
43	463.8	445.9	437.3	451.4	472.9	449.0	440.0	444.3	457.1	435.8	426.3	faulty	468.6	489.5	445.4	453.4	475.5	455.1	445.5

Table-A2-1: Steady state data for HHHC orientation with supercritical H_2O (Contd.)

Sl. No.	TT-42 (°C)	TT-43 (°C)	TT-44 (°C)	TT-45 (°C)	TT-46 (°C)	TT-47 (°C)	TT-48 (°C)	TT-49 (°C)	TT-50 (°C)	TT-51 (°C)	TT-52 (°C)	TT-53 (°C)	TT-54 (°C)	TT-55 (°C)	TT-56 (°C)	TT-57 (°C)	TT-58 (°C)	TT-111 (°C)
1	390.6	404.2	390.2	389.1	391.5	faulty	392.0	387.2	390.2	404.8	390.3	388.9	380.3	370.6	faulty	372.3	372.4	364.3
2	446.3	454.9	440.9	436.1	441.9	faulty	441.3	437.4	441.8	451.7	440.8	440.9	429.0	392.1	faulty	390.2	389.8	387.4
3	437.4	446.1	432.5	428.1	433.2	faulty	433.3	429.8	433.0	442.4	433.7	433.2	421.2	387.8	faulty	387.4	387.4	383.4
4	308.7	319.5	308.2	305.2	309.6	faulty	311.2	306.7	311.3	322.4	312.4	309.8	304.3	292.2	faulty	292.3	291.9	286.7
5	323.4	335.4	323.7	320.3	324.6	faulty	325.9	321.5	326.0	337.6	327.6	324.3	319.2	306.3	faulty	305.9	306.0	300.2
6	353.8	366.9	354.2	350.1	355.3	faulty	356.2	351.4	356.2	368.5	357.5	354.0	348.1	334.7	faulty	335.0	334.4	328.9
7	366.9	380.3	366.8	363.5	368.2	faulty	369.3	364.5	368.8	381.6	370.1	366.8	360.5	347.4	faulty	347.2	346.7	341.8
8	393.5	408.8	393.2	391.2	394.0	faulty	394.5	391.9	394.4	410.3	394.5	393.6	384.5	377.6	faulty	376.1	376.6	371.6
9	296.4	306.9	296.9	293.5	297.5	faulty	299.0	294.9	299.2	309.3	300.6	297.5	292.4	281.3	faulty	280.0	280.8	275.5
10	477.6	502.3	478.2	465.0	479.3	faulty	483.8	469.4	485.0	508.3	491.0	477.0	479.0	411.7	faulty	411.5	410.9	403.7
11	398.5	409.9	396.7	394.7	397.9	faulty	faulty	394.4	396.4	396.9	faulty	395.2	407.1	381.1	faulty	381.3	380.2	376.7
12	397.6	405.7	395.8	393.5	396.7	faulty	faulty	393.1	395.1	395.6	faulty	394.4	406.7	381.5	faulty	381.7	380.2	377.8
13	522.4	548.8	521.3	505.5	523.2	faulty	faulty	511.3	529.3	537.8	faulty	520.9	552.1	430.6	faulty	433.0	431.0	418.8
14	518.2	543.0	517.2	501.7	519.1	faulty	faulty	507.5	524.3	533.2	faulty	516.6	545.5	429.9	faulty	430.6	432.3	419.4
15	384.5	394.5	383.3	380.9	384.2	faulty	faulty	380.9	383.8	384.6	faulty	382.5	392.0	365.0	faulty	364.4	365.7	361.0
16	387.5	397.8	386.2	383.4	386.7	faulty	faulty	383.5	386.3	387.6	faulty	385.1	394.4	367.8	faulty	366.9	368.5	363.2
17	367.7	382.0	366.5	362.1	367.6	faulty	faulty	363.3	367.9	370.2	faulty	365.6	387.9	344.0	faulty	345.2	343.7	338.0
18	383.3	394.0	381.2	378.4	382.2	faulty	385.0	378.4	382.2	383.8	faulty	380.8	399.3	360.8	faulty	361.9	360.5	355.4
19	392.1	405.3	390.0	387.6	390.9	faulty	393.4	387.7	390.5	391.0	faulty	389.7	406.7	371.3	faulty	371.4	372.7	366.6
20	398.0	415.3	395.8	393.0	396.7	faulty	398.9	393.1	396.0	396.9	faulty	394.4	412.0	376.2	faulty	376.0	377.5	371.6
21	393.4	395.3	390.4	390.1	390.9	faulty	faulty	389.8	389.7	390.1	faulty	391.0	405.1	370.3	faulty	370.2	369.3	367.2
22	393.0	395.3	390.0	389.7	390.5	faulty	faulty	389.8	389.7	389.7	faulty	391.0	406.3	369.2	faulty	368.6	369.9	367.2
23	397.3	410.1	396.9	394.6	397.4	faulty	397.9	393.1	396.1	406.5	395.8	394.9	383.2	381.5	faulty	382.1	383.2	374.4
24	397.3	407.6	396.5	395.0	397.8	faulty	397.9	393.5	396.5	403.9	395.8	394.9	383.6	382.6	faulty	383.2	382.5	375.5
25	494.9	522.9	497.8	483.9	499.7	faulty	505.3	490.0	506.0	527.8	512.0	498.7	497.6	422.6	faulty	424.8	422.5	411.0
26	532.5	555.1	528.0	512.8	530.1	faulty	536.0	519.1	535.8	560.7	544.4	526.7	530.2	437.1	faulty	437.1	438.2	447.6
27	506.7	525.8	500.8	487.2	503.1	faulty	507.0	490.9	506.4	530.3	513.7	497.0	499.7	423.7	faulty	423.7	424.9	433.6
28	97.1	105.7	95.1	92.2	97.0	faulty	96.4	92.7	97.8	105.2	97.3	93.6	95.8	82.3	faulty	85.0	85.6	79.8
29	130.5	141.7	127.7	124.5	130.7	faulty	129.3	125.1	131.8	141.6	130.5	126.4	128.8	114.3	faulty	114.7	115.4	109.6
30	159.6	171.5	157.4	153.9	160.2	faulty	158.7	155.1	161.5	172.0	160.8	156.6	158.2	143.5	faulty	143.0	143.9	137.7
31	194.2	206.7	191.8	188.3	194.7	faulty	193.3	192.1	198.9	211.3	198.7	194.0	195.7	176.9	faulty	173.1	173.7	169.8
32	212.8	223.5	211.0	207.6	213.0	faulty	212.2	211.9	216.5	225.2	216.4	213.2	212.7	196.6	faulty	197.6	197.9	190.6
33	248.7	262.1	246.2	241.9	248.8	faulty	248.0	243.5	249.2	260.3	248.8	245.1	244.9	226.4	faulty	226.3	225.5	219.8
34	263.5	278.0	261.3	256.6	264.2	faulty	263.6	258.3	264.8	276.8	264.8	260.9	261.8	240.5	faulty	238.8	239.3	233.3
35	314.1	329.1	311.9	308.2	315.0	faulty	314.1	309.3	314.7	326.6	315.0	311.5	315.9	290.1	faulty	291.6	290.6	283.9
36	362.7	378.2	360.5	356.0	363.3	faulty	362.5	358.2	364.2	377.3	363.8	360.4	364.2	336.2	faulty	338.2	337.1	330.6
37	380.4	394.6	377.7	374.0	380.3	faulty	379.8	378.4	383.1	395.9	383.2	380.0	382.8	356.2	faulty	355.2	356.8	352.5
38	406.6	418.4	403.6	401.7	406.1	faulty	404.6	401.5	404.4	414.9	403.7	402.1	402.8	384.6	faulty	383.9	385.3	382.9
39	488.1	512.4	488.2	475.1	490.2	faulty	494.3	480.8	496.4	519.7	502.7	489.4	491.0	418.1	faulty	417.8	417.2	410.4
40	511.8	535.0	507.9	493.5	509.3	faulty	514.1	497.6	514.0	538.7	521.7	504.2	507.9	425.1	faulty	427.0	436.0	415.5
41	549.2	574.0	546.0	530.0	548.4	faulty	554.5	536.8	554.7	580.6	564.2	544.9	549.6	445.5	faulty	454.9	445.6	431.2
42	474.2	499.0	474.8	461.6	476.0	faulty	480.0	465.2	480.8	503.2	485.9	472.3	474.9	408.2	faulty	409.5	409.8	399.7
43	456.9	482.6	458.9	447.4	460.6	faulty	463.6	450.0	464.1	484.7	467.8	456.2	454.2	399.0	faulty	399.9	400.6	394.7

Table-A2-1: Steady state data for HHHC orientation with supercritical H_2O (Contd.)

Sl. No.	TT-112 (°C)	TT-113 (°C)	TT-114 (°C)	TT-115 (°C)	TT-116 (°C)	TT-117 (°C)	TT-118 (°C)	TT-119 (°C)	TT-120 (°C)	TT-121 (°C)	TT-122 (°C)	TT-123 (°C)	Voltage (V)	Current (A)
1	366.8	363.6	367.2	360.4	faulty	360.5	362.2	360.7	359.4	45.5	42.0	85.1	4.3	1525.1
2	390.8	385.4	388.9	400.8	faulty	398.9	402.0	403.4	396.7	46.6	42.0	89.6	5.4	1580.8
3	386.3	382.1	385.5	394.1	faulty	392.7	395.2	396.6	391.2	48.3	43.1	92.5	5.1	1601.7
4	289.2	287.4	289.3	279.0	faulty	277.6	279.2	277.5	272.7	47.7	43.6	75.5	4.6	1239.6
5	303.1	300.8	302.6	293.1	faulty	290.6	292.1	291.6	286.4	48.3	44.8	78.9	4.7	1302.2
6	331.6	329.4	332.1	322.8	faulty	320.5	322.4	320.8	316.0	48.8	44.8	82.9	4.2	1420.6
7	345.0	342.3	344.9	336.3	faulty	333.4	335.2	334.3	329.8	48.3	44.2	83.4	5.2	1406.7
8	374.6	372.5	375.5	370.5	faulty	367.8	370.0	369.1	363.8	46.6	42.5	86.8	5.2	1539
9	278.0	275.6	278.2	267.8	faulty	266.3	267.4	266.3	261.7	47.2	42.5	72.7	4.4	1197.8
10	406.4	403.4	406.7	393.5	faulty	389.8	393.0	391.0	385.7	46.6	42.5	88.5	4.6	1594.7
11	380.2	377.8	380.2	379.7	faulty	377.1	380.1	378.6	377.3	50.2	50.5	92.7	4.6	1622.6
12	380.8	378.4	380.8	381.4	faulty	378.3	382.3	379.7	377.9	50.2	50.5	91.6	5.2	1615.6
13	422.0	418.2	420.9	405.6	faulty	400.3	404.2	400.0	398.0	50.2	50.5	95.5	4.9	1692.2
14	422.0	418.2	421.4	404.5	faulty	399.7	404.2	399.4	397.5	50.2	50.5	95.5	5.6	1622.6
15	362.9	361.0	363.0	358.3	faulty	354.6	358.2	355.6	354.4	50.2	50.5	89.9	4.8	1469.4
16	365.7	363.8	366.3	362.3	faulty	358.5	361.5	358.9	357.2	50.2	50.5	89.9	4.9	1497.2
17	340.6	338.5	340.2	333.5	faulty	329.7	332.9	330.2	328.1	51.5	51.8	86.5	5.1	1518.1
18	358.5	355.9	358.5	352.7	faulty	348.9	352.0	349.9	348.2	50.6	50.9	88.2	5.4	1559.9
19	369.6	367.2	369.7	366.2	faulty	362.5	365.5	362.9	361.1	51.1	51.3	90.5	4.8	1546
20	374.1	371.6	374.7	371.8	faulty	368.1	371.1	368.5	367.2	51.1	51.3	89.9	5.8	1706.1
21	370.2	366.0	368.0	376.9	faulty	374.3	377.8	376.9	375.1	51.1	51.3	92.7	5.1	1532
22	369.6	364.9	368.0	376.9	faulty	373.7	377.8	376.4	375.1	51.5	51.8	92.2	5.4	1552.9
23	377.4	374.8	378.3	375.0	faulty	374.6	376.2	375.8	375.9	44.9	42.0	86.3	5.4	1525.1
24	378.5	375.4	378.9	376.1	faulty	376.3	378.4	377.0	377.0	44.9	42.5	88.5	4.4	1539
25	414.2	407.8	411.7	398.6	faulty	396.6	398.6	396.1	395.6	38.7	36.5	113.9	4.3	1511.1
26	427.6	421.3	425.6	402.5	faulty	399.4	402.0	399.4	392.3	51.6	41.4	93.0	4.6	1643.5
27	417.6	411.8	416.1	396.9	faulty	394.9	396.9	395.5	388.5	52.2	42.5	95.3	4.4	1552.9
28	80.9	80.7	80.7	76.9	faulty	76.7	76.8	75.3	84.0	49.4	55.8	52.4	3.1	278.6
29	110.0	109.8	110.2	103.9	faulty	104.4	104.3	102.8	112.5	49.4	55.8	55.8	3.8	362.1
30	137.9	137.8	137.4	130.8	faulty	130.9	130.6	129.8	139.4	49.4	55.8	58.6	5.1	424.8
31	170.3	168.1	168.6	160.6	faulty	160.2	159.2	158.4	169.5	49.4	56.4	62.6	5.6	536.2
32	190.4	191.0	190.8	182.5	faulty	182.2	182.2	181.5	193.1	50.0	56.4	65.4	6.1	557.1
33	220.0	219.6	219.2	210.5	faulty	210.4	209.7	209.0	221.1	49.4	55.8	68.8	6.7	612.8
34	233.4	233.1	232.5	224.0	faulty	223.4	222.6	220.8	234.8	49.4	55.8	70.5	7	654.6
35	283.0	283.5	283.2	273.4	faulty	273.1	272.5	271.9	287.0	49.4	55.8	77.2	7.5	689.4
36	329.4	330.5	328.8	321.1	faulty	321.0	319.6	319.1	335.8	48.8	55.8	84.0	7.7	793.9
37	350.0	351.8	349.9	343.6	faulty	342.5	340.9	339.9	357.2	50.0	56.4	87.4	8.3	849.6
38	380.7	383.2	381.6	381.8	faulty	381.9	379.5	380.3	398.4	50.5	56.4	94.7	8.8	893.5
39	413.1	410.1	413.4	396.9	faulty	393.8	396.4	394.9	388.5	46.0	42.0	89.1	9	950.9
40	419.3	412.3	416.7	398.0	faulty	395.5	397.5	395.5	389.0	50.5	40.9	93.6	9	940.5
41	434.9	427.5	431.2	406.5	faulty	402.8	405.3	402.8	395.6	51.1	40.9	95.3	9.3	983.6
42	401.4	396.6	400.6	388.5	faulty	387.6	389.6	387.6	386.8	44.4	39.8	89.6	8.7	960.7
43	396.9	392.7	396.1	388.5	faulty	387.6	389.6	387.1	386.8	38.7	36.5	111.1	8.1	896.2

Appendix-3: Heat transfer correlations for supercritical fluids

(1) **Bishop** correlation (Bishop et al., 1964)

$$Nu_x = 0.0069\left(Re_x\right)^{0.9}\ \left(Pr'_x\right)^{0.66}\ \left(\frac{\rho_w}{\rho_b}\right)_x^{0.43}\left(1+2.4\frac{D}{x}\right) \tag{1}$$

(2) **Bringer Smith** correlation (Bringer and Smith, 1957)

$$Nu_x = C\ Re_x^{0.77}\ Pr_w^{0.55} \tag{2}$$

where C = 0.0266 for water, C = 0.0375 for carbon dioxide. Nu_x and Re_x are evaluated at T_x and temperatures T_{pc}, T_b and T_w are in ^{o}C.

$$T_x = \begin{pmatrix} \mathrm{T_b}, & \text{if } [(\mathrm{Tpc} - \mathrm{T_b})/(\mathrm{Tw} - \mathrm{T_b})\}] < 0 \\ \mathrm{T_{pc}}, & \text{if } [(\mathrm{Tpc} - \mathrm{T_b})/(\mathrm{Tw} - \mathrm{T_b})\}] \le 1.0 \\ T_w, & \text{if } [(\mathrm{Tpc} - \mathrm{T_b})/(\mathrm{Tw} - \mathrm{T_b})\}] > 1.0 \end{pmatrix} \tag{3}$$

(3) **Jackson** correlation (Jackson, 2002)

$$Nu_b = 0.0183\, Re_b^{0.82}\ Pr_b^{0.5}\left(\frac{\rho_w}{\rho_b}\right)^{0.3}\left(\frac{i_w - i_b}{T_w - T_b}\frac{1}{c_{pb}}\right)^n \tag{4}$$

where exponent n is defined as

$$n = \begin{pmatrix} 0.4, & \text{if } \ T_b < T_w < T_{pc} \text{ and } 1.2\ T_{pc} < T_b < T_w \\ 0.4 + 0.2\left(\frac{T_w}{T_{pc}} - 1\right), & \text{if } T_b < T_{pc} < T_w \\ 0.4 + 0.2\left(\frac{T_w}{T_{pc}} - 1\right)\left[1 - 5\left(\frac{T_b}{T_{pc}} - 1\right)\right], & \text{if } T_{pc} < T_b < 1.2\ T_{pc} \text{ and } T_b < T_w \end{pmatrix} \tag{5}$$

and temperatures T_{pc}, T_b and T_w are in Kelvin (K).

4) **Jackson Fewster** correlation (Jackson and Fewster, 1975)

$$Nu = 0.0183 Re_b^{0.82} Pr'^{\,0.5} \left(\frac{\rho_w}{\rho_b} \right)^{0.3} \tag{6}$$

5) **Mc Adams** correlation (Mc Adams, 1942)

$$Nu_b = 0.023 Re_b^{0.8} Pr_b^{0.4} \tag{7}$$

6) **Shitsman** correlation (Shitsman, 1974)

$$Nu_b = 0.023 Re_b^{0.8} Pr_{\min}^{0.8} \tag{8}$$

where Pr_{min} = Minimum of (Pr_b, Pr_w) (9)

(7) **Swenson** correlation (Swenson et al., 1965)

$$Nu_w = 0.00459 \left(\frac{GD}{\mu_w} \right)^{0.923} \left(\frac{i_w - i_b}{T_w - T_b} \frac{\mu_w}{k_w} \right)^{0.613} \left(\frac{\rho_w}{\rho_b} \right) \tag{10}$$

References

1) Adebiyi, G.A., Hall,W.B., Experimental investigation of heat transfer to supercritical pressure carbon dioxide in a horizontal tube, Int. J. Heat Mass Transfer 19 (7), 715–720, (1976).
2) Adelt, M., Mikielewicz, J., Heat transfer in a channel at supercritical pressure, International Journal of Heat and Mass transfer, vol. 44., pp. 1667-1674, (1981).
3) Ambrosini W., On the analogies in the dynamic behaviour of heated channels with boiling and supercritical fluids, Nuclear Engineering and Design 237, 1164–1174, (2007).
4) Ambrosini W., Quick Look Report on the Results of the Flow Stability Benchmark, IAEA Coordinated Research Programme on Heat Transfer Behavior and Thermo-hydraulics Codes Testing for SCWRs, University of Pisa, DIMNP RL 1251, May 14th (2010).
5) Ambrosini W., Ferreri J.C., Prediction of stability of one dimensional natural circulation with a low diffusion scheme, Ann. Nucl. Energy 30, 1505–1537, (2003).
6) Ambrosini, W., Sharabi, M.B., Dimensionless parameters in stability analysis of heated channels with fluids at supercritical pressures. In: 14th International Conference on Nuclear Engineering (ICONE 14). Miami, Florida, USA, July 17–20 (2006).

7) Ambrosini, W., Sharabi, M., Dimensionless parameters in stability analysis of heated channels with fluids at supercritical pressures. Nuclear Engineering and Design 238, 1917–1929, (2008).

8) Bergles, A.E., Review of instabilities in two-phase systems. In: Proc. NATO Advanced Study Institute, Istanbul, vol. 1, pp. 383e422, (1976).

9) Bernier M.A., Baliga B.R., A 1-D/2-D model and experimental results for a closed-loop thermosyphon with vertical heat transfer sections, Int. J. Heat Mass Transfer 35, 2969–2982, (1992).

10) Bishop, A.A., Sandberg, R.O., Tong, L.S., Forced convection heat transfer to water at near-critical temperatures and supercritical pressures, Report WCAP-2056, Part IV, November, Westinghouse Electric Corp., Pittsburgh, USA, (1964).

11) Boure, J.A., Bergles, A.E., Tong, L.S., Review of two phase flow instability, Nuclear Engineering and Design 26, 165-192, (1973).

12) Bringer, R.P., Smith, J.M., Heat transfer in the critical region, AIChE J. 3 (1), pp. 49–55, (1957).

13) Bushby, S.J., Dimmick, G.R., Duffey, R.B., Spinks, N.J., Burrill, K.A., Chan, P.S.W., Conceptual designs for advanced, high-temperature CANDU reactors, SCR-2000, Nov.6-8, Tokyo, (2000).

14) Chatoorgoon, V., Stability of supercritical fluid flow in a single-channel natural-convection loop, International Journal of Heat and Mass Transfer 44, 1963-1972, (2001).

15) Chatoorgoon, V., Non-dimensional parameters for static instability in supercritical heated channels, International Journal of Heat and Mass Transfer 64, 145-154, (2013).

16) Chatoorgoon, V., Voodi, A., Upadhye, P., The stability boundary for supercritical flow in natural-convection loops Part II: CO2 and H2, Nuclear Engineering and Design 235, 2581–2593, (2005).

17) Chen K., On the oscillatory instability of closed-loop thermosyphons,Trans. ASME J. Heat Transfer 107, 826–832, (1985).

18) Chen, L., Zhang, X.R., Yamaguchi, H., Liu, Z. S., Effect of heat transfer on instabilities and transitions of supercritical CO2 flow in a natural circulation loop, International Journal of Heat and Mass Transfer 53, 4101-4111, (2010).

19) Creveling H.F., De Paz, Baladi J.Y., R.J. Schoenhals, Stability characteristics of a single-phase free convection loop, J. Fluid Mech. 67, 65–84, (1975).

20) Dang C. and Hihara E., Numerical study on in-tube laminar heat transfer of supercritical fluids, Applied thermal engineering 30, 1567-1573, (2010).

21) Dittus, F.W., Boelter, L.M.K., Heat Transfer in Automobile Radiators of the Tubular Type, University of California Publications in English, Berkeley, vol. 2, pp. 443–461, (1930).

22) Dogan, T., Kakac, S., Veziroglu, T.N., Analysis of forced-convection boiling flow instabilities in a single- channel upflow system, Int. J. Heat and fluid flow 4, 145, (1983).

23) Driscoll, M.J., Hejzlar, P. 300 MWe Supercritical CO2 plant layout and design, Report No: MIT-GFR-014, MIT Nuclear Engineering Department, June, (2004).

24) Duffey R.B. and Pioro I.L., Experimental heat transfer of supercritical carbon dioxide flowing inside channels (Survey), Nucl. Eng. Design, 235 (8), 913, (2005).

25) Fewster, J., Jackson, J.D., Experiments on supercritical pressure convective heat transfer having relevance to SCWR, Proceedings of the International Congress on Advances in Nuclear Power Plants (ICAPP'04), 13–17 June, Pittsburgh, USA. Paper 4342, (2004).

26) Fukuda, K., Kobori, T., Classification of two-phase flow stability by density wave oscillation model. Journal of Nuclear Science and Technology 16, 95-108, (1979).

27) Gorman M., Widmann P.J., Robbins K.A., Nonlinear dynamics of a convection loop: a quantitative comparison of experiment with theory, Physica D 19, 255–267, (1986).

28) Haar, L., Gallagher, J.S., Kell, G.S., NBC/NRC steam tables, Hemisphere, N.Y., (1984).

29) Harden, D., Boggs, J., Transient flow characteristics of a natural circulation loop operated in the critical region, Proc. Heat transf. Fluid mech. Inst., 38, (1964).

30) Heusener, G., Muller, U., Schulenberg, T., Squarer, D., 2000, A European development program for a high performance light water reactor (HPLWR), SCR-2000, Nov.6-8, Tokyo, Paper 102, (2000).

31) Ho C.J., Chiou S.P., Hu C.S., Heat transfer characteristics of a rectangular natural circulation loop containing water near its density extreme, Int. J. Heat Mass Transfer 40, 3553–3558, (1997).

32) Holman J.P., Boggs J.H, Heat transfer to freon 12 near the critical state in a natural circulation loop, J. Heat Transfer 82, 221–226, (1960).

33) Hou, D., Lin, M., Liu, P., Yang, Y., Stability analysis of parallel-channel systems with forced flows under supercritical pressure, Annals of Nuclear Energy 38, 2386–2396, (2011).

34) Huang B.J., Zelaya R., Heat transfer behaviour of a rectangular thermosyphon loop, J. Heat Transfer 110, 487–493, (1988).

35) Ishiwatari, Y., Oka, Y., Yamada, K., Japanese R&D Projects on Pressure-Vessel Type SCWR, Proc. of 4th Int. Symposium on SCWR, Heidelberg, Germany, March, (2009).

36) Ishii, M., Zuber, N., Thermally induced flow instabilities in two-phase mixtures. In: 4th International Heat Transfer Conference, Paris, (1970).

37) Jackson, J.D., Consideration of the heat transfer properties of supercritical pressure water in connection with the cooling of advanced nuclear reactors, Proceedings of the 13th Pacific Basin Nuclear Conference, Shenzhen City, China, 21–25, October, (2002).

38) Jackson, J.D., Lutterodt, K.E., Weinberg, R., Experimental studies of buoyancy-influenced convective heat transfer in heated vertical tubes at pressures just above and just below the thermodynamic critical value, Proceedings of the GENES4/ANP, 15–19 September, Kyoto, Japan. Paper 1177, (2003).

39) Jain, R., Corradini, M.L., A linear stability analysis for natural-circulation loops under supercritical conditions, Nuclear Technology, Vol. 155, 312-323, (2006).

40) Jain, P.K., Rizwan-uddin, Numerical analysis of supercritical flow instabilities in a natural circulation loop, Nuclear Engineering and Design 238, 1947-1957, (2008).

41) Keller J.B., Periodic oscillations in a model of thermal convection J. Fluid Mech. 26, 599–606, (1966).

42) Kitoh, K., Koshizuka, S., Oka, Y., Refinement of transient criteria and safety analysis for a high-temperature reactor cooled by supercritical water, Nuclear Technology 135, 252-264, (2001).

43) Kyung I.S., Lee S.Y., Experimental observations on flow characteristics in an open two-phase natural circulation loop, Nuclear Engineering and Design, Vol. 150, Issue 1, p. 163-176, September, (1994).

44) Lomperski, S., Cho, D., Jain, R., Corradini, M.L., Stability of a natural circulation loop with a fluid heated through the thermodynamic pseudo-critical point, Proceedings of ICAPP'04, Pittsburgh, PA USA, June 13-17, Paper 4268, (2004).

45) Marcel, C.P., Rhode, M., Masson, V.P., Van der Hagen, T.H.J.J., Fluid-to-fluid modeling of supercritical water loops for stability analysis, International Journal of Heat and Mass Transfer 52, 5046-5054, (2009).

46) McAdams, W.H., Heat Transmission, 2nd edition, McGraw-Hill, New York, NY, USA, (1942).

47) Misale M., Tagliafico L., Tanda G., Experiments in a free convection rectangular loop, in: Proceedings of the Fourth International Symposium on Transport Phenomena in Heat and Mass Transfer, Sydney (Australia), 14–19, pp. 203–211, July, (1991).

48) Nayak A.K., Vijayan P.K., Saha D., Venkat Raj V., Masanori Aritomi, Linear analysis of thermo-hydraulic instabilities of the Advanced Heavy Water Reactor

(AHWR), Journal of Nuclear Science and Technology, Vol. 35, No. 11, pp. 768-778, November, (1998).

49) Oka, Y., Review of high temperature water and steam cooled reactor concepts, SCR-2000, Tokyo, Nov.6-8, (2000).

50) Oka, Y. and Koshizuka, S., Design concept of once-through cycle supercritical light water cooled reactors, SCR-2000, Tokyo, Nov.6-8, (2000).

51) Oka, Y., Koshizuka, S., Jeveremovic, T., Okano, Y., Systems Design of direct-cycle supercritical water cooled fast reactors, Nuclear Technology 109, 1-10, (1994).

52) Ortega Gomez, T., Class, A., Lahey Jr., Schulenberg, T., Stability analysis of a uniformly heated channel with supercritical water, Nuclear Engineering and Design 238, 1930-1939, (2008).

53) Pioro I. L. and Duffey R.B., Experimental heat transfer to supercritical water flowing inside channels (Survey), Nucl. Eng. Design, 235 (22), 2407-2430, (2005).

54) Rohsenow, W.M., Hartnett, J.P., Handbook of heat transfer, McGraw-Hill book company, (2000).

55) Scientech. Inc., Code structure system models and solution methods RELAP5/Mod3 Code Manual, vol. 1, The Thermal Hydraulics Group, Idaho, June, (1999).

56) Silin V.A., Voznesensky, V.A., Afrov, A.M., The light water integral reactor with natural circulation of the coolant at supercritical pressure B:500 SKDI, Nuclear Engineering and Design 144, 327-336, (1993).

57) Sharabi M.B., Ambrosini, W., He, S., Prediction of unstable behaviour in a heated channel with water at supercritical pressure by CFD models, Annals of Nuclear energy 35, 767-782, (2008).

58) Shitsman, M.W., Heat transfer to supercritical helium, carbon dioxide, and water: analysis of thermodynamic and transport properties and experimental data, Cryogenics 14 (2), 77–83, (1974).

59) Swenson, H.S., Carver, J.R., Karakala, C.R., Heat transfer to supercritical water in smooth-bore tubes. J. Heat Transfer, Trans. ASME, Ser. C 87 (4), 477–484, (1965).

60) Tian, X., Tian, W., Zhu, D., Qiu, S., Su, G., Xia, B., Flow instability analysis of supercritical water-cooled reactor CSR1000 based on frequency domain, Annals of Nuclear Energy 49 70–80, (2012).

61) T'Joen, C., Rohde, M., Experimental study of the coupled thermo-hydraulic–neutronic stability of a natural circulation HPLWR, Nuclear Engineering and Design 242, 221– 232, (2012).

62) Tom, S.K.S. and Hauptmann, E.G., The feasibility of cooling heavy water reactors with supercritical fluids, Nuclear Engineering and Design 53, 187-196, (1979).

63) Van Bragt, D.D.B, Van der Hagen, T.H.J.J., Stability of natural circulation Boiling Water Reactors: Part II – parametric study of coupled neutronic – thermal hydraulic stability, Nuclear Technology 121, 52-62, (1998).

64) Vijayan P.K., Austregesilo H., Teschendorff, V., Simulation of the unstable oscillatory behaviour of single-phase natural circulation with repetitive flow

reversals in a rectangular loop using the computer code ATHLET, Nucl. Eng. Des. 155, pp. 623–641, (1995).

65) Vijayan P.K., Nayak A.K., Pilkhwal D.S., Saha D., Venkat Raj V, Effect of loop diameter on the stability of single-phase natural circulation in rectangular loops, in: Proceedings of the 5th International Topical Meeting on Reactor Thermalhydraulics, NURETH-5, Salt Lake City, UT, vol. 1, pp. 261–267, (1992).

66) Vijayan P.K., Nayak A.K., Saha D., Gartia M.R., Effect of loop diameter on the steady state and stability behaviour of single-phase and two–phase natural circulation loops, Science and technology of nuclear installations, , Volume 2008, Article ID 672704, 17 pages, (2008).

67) Vijayan, P.K., Sharma, M., Saha, D., Steady state and stability characteristics of single-phase natural circulation in a rectangular loop with different heater and cooler orientations, Experimental Thermal and Fluid Sciences, Vol 31, Issue 8, Page 925-945, August, (2007).

68) Welander, P., On the oscillatory instability of a differentially heated loop, J. Fluid Mech., 29 17-30, (1967).

69) Xiong T., Yan X., Xiao Z., Li Y., Huang Y., Yu J., Experimental study on flow instability in parallel channels with supercritical water, Annals of Nuclear Energy 48, 60-67 (2012).

70) Yadigaroglu, G., Two-phase flow instabilities and propogation phenomena in two phase flows in nuclear reactors, Von Korman Institute of fluid dynamics lecture series, (1978).

71) Yamagata, K., Nishikawa, K., Hasegawa, S., Forced convective heat transfer to supercritical water flowing in tubes, Int. J. Heat Mass Transfer 15 (12), 2575–2593, (1972).

72) Yi, T.T, Koshizuka, S., Oka, Y., A linear stability analysis of Supercritical Water Reactors, (I) Thermal-Hydraulic Stability, Journal of Nuclear Science and Technology 41, p. 1166-1175, (2004).

73) Yoshikawa, S., Smith Jr., R.L., Inomata, H., Matsumura, Y., Arai, K., Performance of a natural circulation system for supercritical fluids. Journal of Supercritical fluids 36, 70–80, (2005).

74) Zhao, J., Saha, P., Kazimi, M.S., Stability of supercritical water-cooled reactor during steady-state and sliding pressure start-up, NURETH-11, Avignon, France, October 2-6, (2005).

75) Zuber, N., An analysis of thermally induced flow oscillation in the near-critical and supercritical thermal-dynamic region, Report no. NASA-CR-80609, General Electric Co., NY, USA, (1966).